

## ABSTRACT

Title of Document: IDENTIFYING LANDSLIDE HAZARDS IN A TROPICAL MOUNTAIN ENVIRONMENT, USING GEOMORPHOLOGIC AND PROBABILISTIC APPROACHES

José Gregorio Roa-Lobo PhD, 2007

Directed By: Prof. Michael Kearney, Department of Geography

The objective of this study is the performance, assessing, comparison and validation of a set of three landslide hazard maps: The geomorphological, the multicriteria evaluation (MCE) and the probabilistic (weights of evidence); in order to evaluate its accuracy, advantages and limitations, and finally state its reliability. These approaches were tested in a tropical mountain environment located in the central Venezuelan Andes, particularly in the Río Chama basin (2820.63 Km<sup>2</sup>), where the complexity and variety of the landscape provides a special geographical framework to address the landsliding process as natural hazard. The scale of this study is regional.

For doing this a GIS data base was built up to collect and manipulate the landslide inventory map and the cartography of the main landslide passive factors found in this study area. The landslide inventory map was generated through the manual interpretation of 300 aerial photographs and by the processing of two sets of Landsat imagery via contrast-widening color composite, given as result the outline of 493 landslide polygons. The landslide passive factors represent the physical features of the study area associated to landslide occurrences, as those found in the topographical, geological and physiographical settings. In that sense, given the main role played for a digital elevation model (DEM) as data input, a DEM for the study area was built through remotely sensed data obtained from the shuttle radar topographical mission (SRTM) and optical stereographic imagery provided by the advanced spaceborne thermal emission and reflection radiometer (ASTER) system. Because of the comparative nature of this study, these data was preliminary processed via density analysis in order to establish a common background on the landsliding process – passive factors relationship, which was used

later to set up the criteria applied in the geomorphological and multicriteria evaluation (MCE) approaches. All the three landslide hazard mapping approaches were fully benefited from the use of GIS, improving the processing and manipulation of the spatial information, even in procedures considered subjective as the geomorphological mapping, as well as in the use of non-areal statistics measures for the weights of evidence procedure where the Kappa index proved to be a useful index to assess the level of independence between factor maps.

As a way of validation, the accuracy and error rate of the three landslide hazard maps were performed by its comparison to the landslide inventory map. Hence through the use of contingency tables and the success rate curve, was concluded that although the geomorphological approach achieved a better landslide predictive power for this study area at a regional scale, the remaining procedures can play a complementary role, for example the MCE plays a crucial role in an early assessment of landslide hazard which highlights the needs and improving necessary to achieve a better probabilistic approach, which can be later incorporated in a more objective geomorphological assessment. Results also showed that any methodology can be improved and even empowered by the development of better and more integrated standards for geographical data collection rather than the simplification of them, in that sense, satellite data improves the spatial and temporal consistence of data used for landslide hazard purposes, potentially allowing the integration of useful geographical data as those Holdridge life's zones and geomorphometric generated and used in this study. Hence, further studies at regional scale must explore the remotely sensed imagery capacities for generation of data bases addressing regional susceptibility to landsliding process.

IDENTIFYING LANDSLIDE HAZARDS IN A TROPICAL MOUNTAIN  
ENVIRONMENT, USING GEOMORPHOLOGIC AND PROBABILISTIC  
APPROACHES

By

José Gregorio Roa Lobo

Dissertation submitted to the Faculty of the Graduate School of the  
University of Maryland, College Park, in partial fulfillment  
of the requirements for the degree of  
Doctor of Philosophy  
2007

Advisory Committee:  
Professor Michael Kearney, Chair  
Professor John Townshend  
Professor Samuel Goward  
Karen Prestegaard  
Luigi Boschetti

© Copyright by  
José Gregorio Roa Lobo  
2007

## Acknowledgements

To Prof. Michael Kearney and his invaluable help.

To the University of Maryland, College Park.

To the University of Los Andes, Venezuela.

To the Watson International Scholars of the Environment, Brown University.

To the International Institute for Geo-Information Science (ITC), The Netherlands.

To Prof. J. Townshend and the GLCF staff.

To Dr. Eric Vermote.

To Dr. Ulrich Kamp.

To my friends and informal supervisors: Matthew Smith, Julia Skory, Shannon Franks, Jan and Daniela Dempewolf, Svetlana Kotchenova, Diane Davies, Sunghee Kim, Jessica McCarty, Minnie Wong, Enrique Castellanos, Alexander Walzenbach.

## Table of Contents

Acknowledgements	
Table of Contents.....	iii
List of Tables.....	v
List of Figures.....	vi
Chapter 1:INTRODUCTION.....	1
Overview.....	1
Justification.....	2
Research Objectives.....	4
Outline of the thesis structure.....	5
Chapter 2: THE STUDY AREA.....	7
Geological aspects.....	8
Lithological units.....	9
Fault patterns.....	9
Geomorphological aspects.....	10
Climatic aspects.....	12
Landuse aspects.....	14
Typical expressions of landsliding processes in the area.....	16
Chapter 3: METHODOLOGY.....	19
Conceptual background definitions.....	19
Review of existing techniques to perform a landslide hazard zonation.....	20
General methodological procedure.....	22
The hazard modeling.....	25
Validation and comparison.....	25
Chapter 4: GENERATION OF THE DIGITAL ELEVATION MODEL (DEM) FROM SPACE BORNE SYSTEMS.....	26
Building the study area DEM from SRTM data and ASTER imagery.....	26
Chapter 5: LANDSLIDE DISTRIBUTION ANALYSIS. BASIC DESCRIPTIVE STATISTICS.....	30
The landslide inventory map.....	30
The contrast-widening color composite.....	31
Landslide geographical occurrence.....	33
Landsliding processes and factor/classes. Descriptive statistical .....	37
Landslide area - altitudinal ranges relationship.....	38
Landslide area - slope angle / slope shape / slope aspect relationship.....	39
Landslide area - lithology / lithology – slope relationship.....	41
Landslide area – drainage buffer / lineaments relationship.....	43
Landslide area – internal relief relationship.....	45
Landslide area – Geomorphometric classes relationship.....	46
Landslide area – Holdridge's life zone system relationship.....	47
Landslide area – Geomorphological units relationship.....	49
Landslide – Factor maps analysis by area density.....	50

Chapter 6: THE GEOMORPHOLOGICAL, MULTICRITERIA EVALUATION (MCE), AND THE PROBABILISTIC APPROACHES.....	54
The Geomorphological approach. Hierarchical structure and factors.....	54
The Terrain Mapping Complexes.....	55
The Geomorphological units. Factors.....	56
The Terrain Mapping Units (TMU).....	57
DEM and geomorphometry. An empirical procedure for Geomorphometric classification.....	59
The Terrain Mapping Subunits.....	61
Classification of the Terrain Mapping Subunits into a landslide hazard zonation map.....	64
The MCE paradigm. Justification of the MCE for this study.....	66
Integrating MCE into GIS.....	66
The Analytical Hierarchy Process (AHP).....	67
Definition of the processes involved in the landsliding process.....	68
Normalizing factor maps to criteria maps.....	69
Compensating weights via Pairwise procedure.....	70
Computing the Analytical Hierarchy matrices for the criteria maps.....	71
Data output integration and final classification and hazard maps.....	74
Probabilistic landslide hazard zonation through the Weights of Evidence model.....	77
Data entry. Test of conditional independence.....	78
Computing the weights of evidence. Selection of scenarios.....	85
Data integration, classification and interpretation.....	91
Chapter 7: SUMMARY OF THE THREE LANDSLIDE METHODOLOGIES AND CONCLUSIONS.....	96
Evaluation of the accuracy and error rate.....	99
Accuracy and error rate within landslide hazard maps.....	100
Accuracy and error rate within factor maps.....	102
Validation.....	104
Success rate curve.....	105
Correlation.....	106
Conclusions.....	109
Summary.....	112
Appendices.....	113
Bibliography.....	166

## List of Tables

Table 2.1. Lithological units in the study area.....	11
Table 3.1. Thresholds to classify the landslide hazard classes in this study .....	19
Table 3.2. Summary of the main methods for landslide hazard zonation .....	21
Table 3.3. General methodological procedure .....	22
Table 3.4. Data requirements and sources.....	23
Table 3.5. List of data input and generated in this study.....	24
Table 3.6. Proposed methodological / procedures for landslide hazard zonation.....	25
Table 5.1. Density analysis index aggregated per factor map.....	52
Table 6.1.1. TMU and TMsU structure and diagnostic factor applied.....	53
Table 6.1.2. Source data and criteria layers for terrain mapping complexes.....	55
Table 6.1.3. Source data and criteria layers for geomorphological units.....	56
Table 6.1.4. Source data and criteria layers for TMU.....	58
Table 6.1.5. Factors and criteria for geomorphometric classification.....	60
Table 6.1.6. Source data and criteria layers for TMsU.....	62
Table 6.2.1. MCE – GIS integration steps in a geographical case of study.....	66
Table 6.2.2. Factors, processes and criteria involved in the landsliding process.....	68
Table 6.2.3. Factor maps original data range and normalized values.....	69
Table 6.2.4. Pairwise comparison levels of importance.....	70
Table 6.2.5. MCE Reciprocal Matrix.....	71
Table 6.2.6. MCE Normalized Matrix.....	72
Table 6.2.7. Classifying MCE index susceptibility into landslide hazard classes.....	75
Table 6.3.1. Map comparison and possible combinations from the landslide inventory and a parameter map single class.....	77
Table 6.3.2. CHI SQUARE values contingency table.....	85
Table 6.3.3. Kappa values $\leq 0$ contingency table.....	86
Table 6.3.4. Kappa values $\leq 0.01$ contingency table.....	87
Table 6.3.5. Kappa values $\leq 0.1$ contingency table.....	88
Table 6.3.6. Weights of Evidence scenarios overall accuracy.....	89
Table 6.3.7. Classifying Weights of Evidence into landslide hazard classes.....	91
Table 6.3.8. Weights of evidence of selected classes (taken from Appendix 6.6).....	92
Table 7.1. Uncertainty and matching following the landslide hazard classes / landslide occurrences relationship.....	96
Table 7.2. Landslide hazard classes distribution over the landsliding area per methodological approach.....	99
Table 7.3. Matrix of correlative analysis of the landslide hazard zonation maps.....	107
Table 7.4. Suggested uses of different landslide hazard approaches.....	113



## List of Figures

Figure 1. Natural disasters – fatalities annual occurrence in Latin America.....	3
Figure 2.1. Relative location of the River Chama.....	7
Figure 2.2. Study area lithological units and faulting lineaments.....	10
Figure 2.3. Study area. Mean monthly rainfall distribution.....	13
Figure 2.4. Study area mean annual rainfall distribution.....	14
Figure 2.5. Study area land cover classification.....	15
Figure 4.1. Aster imagery used to build the study area DEM and GCPs.....	27
Figure 4.2. Flow chart on the study area DEM's generation.....	29
Figure 5.1. Landslide identification by contrast-widening color composite.....	32
Figure 5.2. Landslide inventory map of the study area.....	34
Figure 5.3. Cumulative landsliding area (%) by number of landslide polygons.....	34
Figure 5.4. Study area landslide concentration sections.....	37
Figure 5.5. Landsliding and total study area distribution (%) by altitude ranges.....	39
Figure 5.6. Landsliding and total study area (%) by altitude ranges and slope angle.....	39
Figure 5.7. Landsliding and total study area distribution (%) by slope angle.....	40
Figure 5.8. Landsliding and total study area distribution (%) by slope shape and angle....	40
Figure 5.9. Landsliding and total study area distribution (%) by slope aspect .....	41
Figure 5.10. Landsliding area and total study area distribution (%) by lithology class.....	42
Figure 5.11. Landsliding and total study area (%) by lithology and slope angle.....	43
Figure 5.12. Landsliding and total study area (%) by distance to drainages.....	44
Figure 5.13. Landsliding and total study area (%) by distance to lineaments.....	44
Figure 5.14. Landsliding and total study area (%) by internal relief.....	45
Figure 5.15. Landsliding and total study area (%) by geomorphometric units.....	46
Figure 5.16. Landsliding and total study area (%) by Holdridge's Life Zones.....	48
Figure 5.17. Landsliding and total study area (%) by geomorphological units.....	49
Figure 5.18. Cumulative Density analysis value per factor map classes.....	51
Figure 5.19. Distribution of the aggregated class indices per factor map.....	52
Figure 6.1.1. Landslide hazard heuristic geomorphological approach.....	54
Figure 6.1.2. Terrain mapping complexes classification.....	55
Figure 6.1.3. Geomorphological units classification.....	57
Figure 6.1.4. Terrain Mapping Units (TMU) classification.....	59
Figure 6.1.5. Geomorphometric units classification.....	61
Figure 6.1.6. Comparing ground geoforms to geomorphometric forms.....	61
Figure 6.1.7. Terrain Mapping subUnits (TMsU) classification.....	62
Figure 6.1.8. Classifying TMsU into a landslide hazard zonation map.....	63
Figure 6.1.9. Overview of La Trujillana landslide.....	64
Figure 6.2.1. MCE landslide susceptibility zonation.....	74
Figure 6.2.2. Landslides / MCE susceptibility cumulative frequency.....	76
Figure 6.3.1. Weights of evidence procedure.....	79
Figure 6.3.2. Chi square Test of conditional independence.....	82
Figure 6.3.3. Kappa index Test of conditional independence.....	83
Figure 6.3.4. Success rate curve of the suitable combinations.....	89
Figure 6.3.5. Weights of Evidence landslide hazard scenarios maps.....	91

Figure 6.3.6. Weights of Evidence landslide hazard scenarios comparison.....	93
Figure 6.3.7. Over representation in all weights of evidence combination.....	94
Figure 7.1. Uncertainty and matching in the Geomorphological hazard map.....	97
Figure 7.2. Uncertainty and matching in the MCE hazard map.....	97
Figure 7.3. Uncertainty and matching in the Weights of Evidence hazard map.....	98
Figure 7.4. Accuracy parameters by hazard map.....	100
Figure 7.5. Error for misclassification parameters.....	100
Figure 7.6. Accuracy parameters distribution by factor maps.....	102
Figure 7.7. Error rate parameters distribution by factor maps.....	102
Figure 7.8.Landslide hazard zonation maps success rate curves.....	104

# Chapter 1: Introduction

## 1.1.- Overview

Predictive modeling of landslide hazard has emerged as a major research field that has been enhanced by the use of new technological advancements such as GIS, remote sensing data and subsequent incorporation of statistical procedures applied to spatial data. Hence an increasing number of researchers and institutions are working towards the proposing and improving of new and existing modeling procedures relate to landslide hazard mapping at medium and regional scales (Brabb , 1984). However, the increasing complexity of GIS techniques requires skillful users who should be both able to fully exploit the capabilities of the system, as well as being familiar with the phenomenon or process under study (Fabbri et al., 2003). Unfortunately, this last assumption represents an emerging gap among landslide researchers, particularly in the geomorphological community.

Thus, two main approaches to landslide hazard mapping are presently used: Direct or indirect methods (Hansen, 1984; Brenning, 2005). The first consists essentially in a geomorphological mapping through which the surveyor identifies past and present landslides and makes assumptions on those sites where failures are likely to occur in the future. The second includes two rather different methods: namely, heuristic versus statistical approaches. In the heuristic, instability factors are ranked and weighted according to their assumed or expected importance in causing mass movement; in the statistical (or probabilistic), the role of each factor is determined on the basis of the observed relations with the past/present landslide distribution.

Moreover, there is no an explicit agreement on the methods for or even on the scope of producing hazard maps (Brabb, 1984; Carrara, 1989). Despite the conflicting views, all the methods proposed are founded upon a single conceptual procedure: The mapping of the landslides, the identification and mapping of a set of geographical factors (lithology, slope, land cover, etc) referred to slope instability, an estimate of the relative contribution of these factors in generating slope-failures, and the classification of the land surface into domains of different hazard degree (Varnes, 1984).

This unnecessary gap seems to be filled in the near future thanks to the present diffusion of hardware and software tools allowing earth science data to be efficiently and

cost-effectively processed (Carrara, 1989; Soeters et al., 1996; Carrara et al., 1991). Nowadays, besides a few exceptions (Wang and Unwin, 1992; van Westen, 1993; van Westen, N. Rengers and R. Soeters, 2003), this issue has not received adequate attention in the literature, hence the importance of bridging this methodological gap between the direct and indirect landslide hazard mapping framework. In this study this problem is approached through the performance, assessing, comparison and validation of a set of three landslide hazard maps, done under different approaches and procedures in order to evaluate its accuracy, advantages and limitations, and finally state its reproducibility and reliability applied on a tropical mountain environment.

### 1.2.- Justification

During the past century there has been an unprecedented increase in the number of people and the amount and value of property at risk for landslide hazard (van Westen, 1993). The relationship between these increases and the chance of landslide damage is not simply arithmetic. This is because pressure on the resources has forced people to exploit hazardous areas which are only marginally suited for the uses to which they are put (Crozier, 1986), however understanding the causes of landslides imposes a responsibility on the community to mitigate the impact of such phenomena.

In December 16, 1999 torrential flows that occurred in the north coastal range of Venezuela (State of Vargas) and were a unique event in Latin-American history, and perhaps in the world. On that day simultaneous extreme debris flows occurred in about twenty streams along fifty kilometers of a narrow coastal strip. The disaster caused losses of more than two billion US dollars and killed an estimate of 20,000 to 30,000 people. In terms of human losses this is the worst disaster in Venezuelan history and one of the worst in Latin America. (Wieczorek, et al., 2001)

Figure 1 illustrates the relationship between the annual occurrence of natural disaster events and associated fatalities in Latin America. The number of fatalities per year does not seem to follow a general pattern; on the contrary they appear to be driven by distinct disaster episodes, in terms of hazard type, magnitude, and degree of vulnerability of the affected environment. The four peak years are linked with particularly lethal events: the 1970 earthquake in Chimbote, Peru (66,800 deaths), the 1976 earthquake in Guatemala

(23,000 deaths) the 1985 volcano eruption in Nevado del Ruiz, Colombia (21,800 deaths) and the 1999 flood and landslides in Venezuela (30,000 deaths) (Charvériat, 2000).

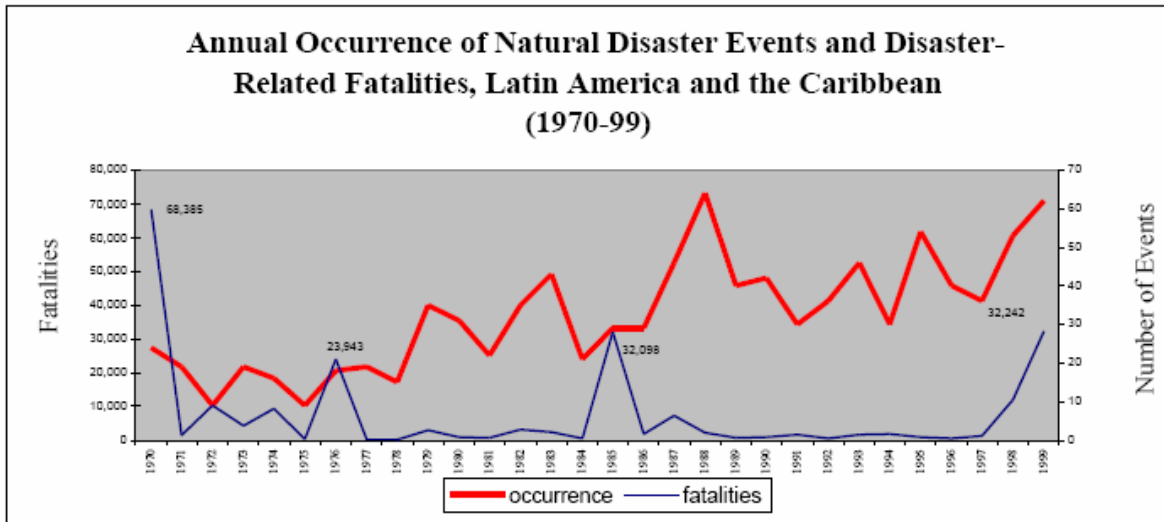


Figure 1. Natural disasters – fatalities annual occurrence in Latin America (after Charvériat, 2000)

Latin-American countries have been able to reduce loss of life from some hazards, principally through disaster preparedness and response. However, large magnitude disasters still remain hazardous due to the poor understanding of the dynamic geographical settings involved. Therefore, an important tool like that offered by natural hazard zonation mapping could open the opportunity to reduce economic and human losses through prevention and mitigation. In this regard, the most effective approach to reducing the long-term impact of natural hazards is to incorporate natural hazard assessment and mitigation activities into the process of integrated development planning and investment project formulation and implementation (Brabb, 1984). This study is part of the Venezuelan national efforts to enhance the knowledge of a major natural disaster as landsliding process is.

On the other hand, during the last thirty years a boom of methodological approaches and procedures trying to refine the best way to landslide hazard zonation has emerged (Brabb, 1984; Hansen, 1984; Varnes, 1984; Carrara, 1989 and van Westen, 1993). Many of these efforts focused in the interpretation of the landsliding process dynamic based solely on the expert experience or in advanced probabilistic techniques supported by GIS, which have been able to contribute positively with the present state of art of the field and

configuring a new challenge to research as the assessment of those approaches in terms of its accuracy and reliability.

This study is developed for a tropical mountain environment, where the multiplicity of geographical conditions is in most of the cases poorly studied. Tropical mountain environment offers a full mixture of the possible lithological, climatic and vegetation spectrum to be found on the Earth; furthermore it has been classified as a main global “hotspot” of biodiversity (Myers et al., 2000).

### 1.3.- Research objectives

Main objective of this study is the comparison, assessing and validation of three main landslide hazard mapping procedures as a way to establish a potential new procedure that takes into account the latter advances in remote sensed information suitable for the landslide hazard practice. In order to accomplish this main goal the following specific objectives are required:

- To generate accurately a landslide inventory map of the study area by the use of high resolution aerial photographs and hyperspectral information from LANDSAT imagery.
- To generate a more consistent DEM from remotely sensed data with a high level of accuracy merging and validating via ground control points the SRTM (Shuttle Radar Topography Mission) data, and the ASTER (Advanced Space borne Thermal Emission and Reflection Radiometer) stereo-image satellite data. This DEM is later used to derivate main important layers, related to topographical features, to be use in the landslide hazard modeling.
- To perform three landslide hazard scenarios, representing a gradation between the heuristic and the probabilistic approaches, these are: The Geomorphological, Multi-criteria and the Probabilistic landslide hazard zonation map.

### 1.4.- Outline of the thesis structure

This thesis is conformed by the following seven chapters:

#### CHAPTER 1. INTRODUCTION.

A briefly description on the challenges and objectives that motivated this research is offered in this chapter.

#### CHAPTER 2. THE STUDY AREA

This chapter offers a description of the main geographical settings of the study area, such as the geological, geomorphological, climatic and landcover issues. The importance of this area for a landslide hazard zonation practice is also here discussed.

### CHAPTER 3. METHODOLOGY

The purpose of this chapter is to offer a conceptual background definitions related to landslide studies as well as a succinct review of the existing techniques to assess landslide hazard. Also given that this thesis deals with the performance of three main landslide hazard approaches (the Geomorphological, the Multicriteria and the Probabilistic) under a GIS environment, a set of methodological flowcharts is offered for every procedure, as well as a general description to illustrate the phases of landslide hazard using GIS. Finally, a table pointing out the products used in this research and the generated products such as the factors maps and its classes illustrates the importance of the GIS treatment of the raw data previous incorporation of it into the landslide hazard procedures.

### CHAPTER 4. REMOTELY SENSED DATA AND IMAGERY IN LANDSLIDE HAZARD ZONATION

Although this thesis included the use of remotely sensed information obtained from different sources such as aerial photographs, LANDSAT and ASTER imagery, and SRTM data, in this chapter only the obtaining and processing of the ASTER and SRTM imagery and data are addressed since with these data were used to generate the DEM for the study area.

### CHAPTER 5. LANDSLIDE DISTRIBUTION ANALYSIS. BASIC DESCRIPTIVE STATISTICS

This chapter describes the study area landslide inventory map, how it was constructed and the role of the photo-interpretation and LANDSAT imagery played in the accuracy of this product. Following the overlaying of the landslide inventory map with the different layers representing the geographical settings of the study area, it is possible to get a statistical outline about the landsliding process / geographical factors relationship in terms of density. Finally, based in descriptive statistics a factor map analysis is offered.

## CHAPTER 6. THE GEOMORPHOLOGICAL, MULTICRITERIA (MCE) AND THE PROBABILISTIC APPROACHES

In this chapter the performance of the three proposed landslide hazard approaches is carried out. For every approach a detailed description about its data input preparation, processing and hazard modeling is described. Given the differences in the data input, treatment and hazard map generated from each of the applied approaches, the obtained landslide hazard maps are interpreted independently.

## CHAPTER 7. COMPARING THE LANDSLIDE HAZARD MAPS

An assessment of the errors and uncertainties of the derived landslide hazard maps is offered in this chapter. The landslide hazard maps are correlated with the landslide inventory map in order to calculate the uncertainty, accuracy, error rates and the success rate curve; being a statistical method used to validate the reliability of these hazard maps. To complement this comparison, a correlation index is applied to establish the level of association between the landslide hazard maps evaluated.



## Chapter 2: The study area

The study area is situated in the Venezuelan Andes, in the mountainous section of the Río Chama basin (Figure 2.1). This is situated between 8°14' to 8°53' north latitude and 70°05' to 71°35' west longitude, having a size of 2820.63 km<sup>2</sup>. It is located at the central section of the Cordillera de Mérida, which has a maximum elevation of 5007 masl (Pico Bolivar). This area is situated 650 km west from Caracas and 45 km south from Lake Maracaibo. The area has a perimeter of 301.7 km.

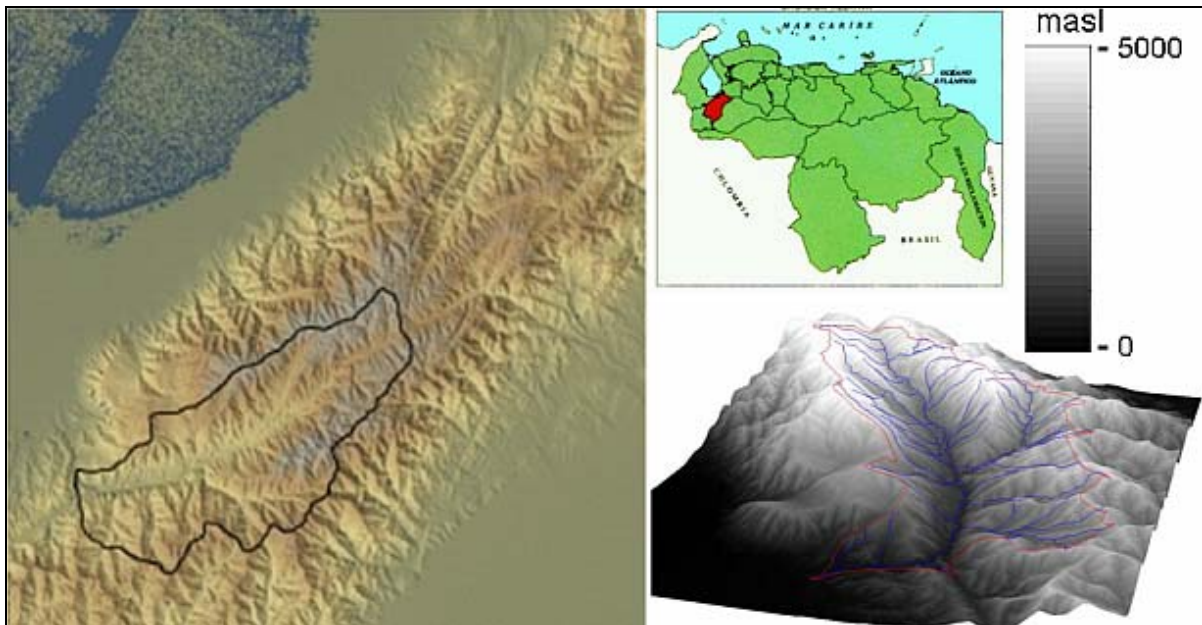


Figure 2.1 Relative location of the River Chama basin and DEM from SRTM-based data.

The Río Chama basin was chosen as the study area to test the comparative study developed in this work because of its following characteristics:

- This area is very susceptible to mass movements.
- The availability of maps, aerial photos, satellite imagery, reports and a wide range of thematic maps from different years and at different scales.

The Río Chama basin area forms the transition between the northern and southern slopes of the Mérida Andes. The climate of this region is Tropical Mountain with alpine influences because of the altitude. Annual precipitation varies between 754 mm in the driest section of the basin to almost 2000 mm in the cloudy forest area. Rainfall is seasonal, with the wet season from May to October and the dry season from November to April (MARNR, 1983). The seasonality of the rainfall in combination with the steep

slope of weathered granite outcrops and Quaternary deposits that form the valley slopes are responsible for the high number of landslides.

### 2.1 Geological aspects

The geology of the area has been widely investigated, and there are geological maps ranging in scale from 1:500000 to 1:50000, as well as a very complete description of the geological formations is found in the Stratigraphical Lexicon of Venezuela (<http://www.pdv.com/lexico/lexicohi.htm>). An overview of the geological evolution of the Cordillera de Merida can be found in La Marca (1993).

The Venezuelan Andes were formed from surrounding areas during the Paleocene, and they continued developing until the end of the Pliocene, at which time they attained their greatest height. Since the tectonic uplift was continued throughout the tertiary into the Quaternary, most of the rocks experienced an intensive regional metamorphism with local occurrences of intrusive rocks along the Boconó faulting system. Nowadays the geological constitution of the study area offers a wide-range of lithological units ranging from Precambrian age to Quaternary period geological formations and constituted mainly of quartzite schists, gneisses, limestones and isolated granitic and diabasic intrusions. Soils are predominantly inceptisols, but entisols are also common in the slopes and areas exposed to erosion (Vivas 1992). The nucleus of the Cordillera de Merida is formed by Precambrian rocks of the Sierra Nevada (PESi) group, which are intruded by acidic stocks and dikes of upper and lower Paleozoic age (PzYa1-PzYa3). These rocks are extensively covered by the metamorphic rocks representing the Tostos (Pzo1-S1- Pzo2-S2), Sabaneta (Pzc3-p3) and Mucuchachi (Pzc2-p2), geologic formations, also dated as belonging to the lower and upper Paleozoic age. Another interesting feature in the study area is that since the Pleistocene until present day large volumes of unconsolidated sediments have been deposited particularly along the main longitudinal valleys in the study area, creating in conjunction with the orogenic uplifting and river basal erosion a very complete topographical sequence of alluvial terraces dated from late Pleistocene to the Holocene (Schubert, 1980)

## 2.2 Lithological units

The lithological units map was extracted from the Venezuelan Geologic and Structural Map (Bellizia et al., 1976), (Figure 2.2), which matches the information found in the Stratigraphical Lexicon of Venezuela. The map is generalized and probably it does not show accurately the limits and contacts of the lithological units as well as the fault lines, given its 1:500000 scale. Therefore it was necessary to enhance this information by two criteria. First, in the case of lineaments, many faulting lines can be traced through information derived from the study area DEM's, as slope profile and plan curvature. These data can be use to estimate borders between metamorphic and igneous intrusive rock outcrops, as well as neotectonic traces found in Quaternary deposits. Second, estimate the limit of the sediments, the slope gradient was used as criterion assuming that continuous areas on the valley bottom with slope gradients lesser than  $12^{\circ}$  are potentially representing terraces and alluvial fans formed by unconsolidated conglomerates and Quaternary alluviums. In order to extract these areas from the DEM's study area a similar procedure as that described for Miliarexis (2001), was applied which is based in the application of a segmentation algorithm on a post processed DEM. This technique was successfully applied to extract bajadas and playas in the Death Valley, California; being later validated through LANDSAT ETM+ imagery, for a better description of this procedure a review of the website: [http://hydrogis.geology.upatras.gr/PAGE/\\_lists.htm](http://hydrogis.geology.upatras.gr/PAGE/_lists.htm) is suggested. A brief description of the lithological units found in the study area is given in Table 2.1, which is based on the official geological maps and the Stratigraphical Lexicon of Venezuela (PDVSA-Intevep, 2007).

## 2.3 Fault patterns

The Boconó fault is one of the most important fault zones in Venezuela and it is crossing the River Chama basin in a NE-SW direction. The Boconó is a spectacular NE-SW trending, dextral strike-slip fault that extends for about 700 km forming the backbone of the Venezuelan Andes (Audemard et al., 2000).

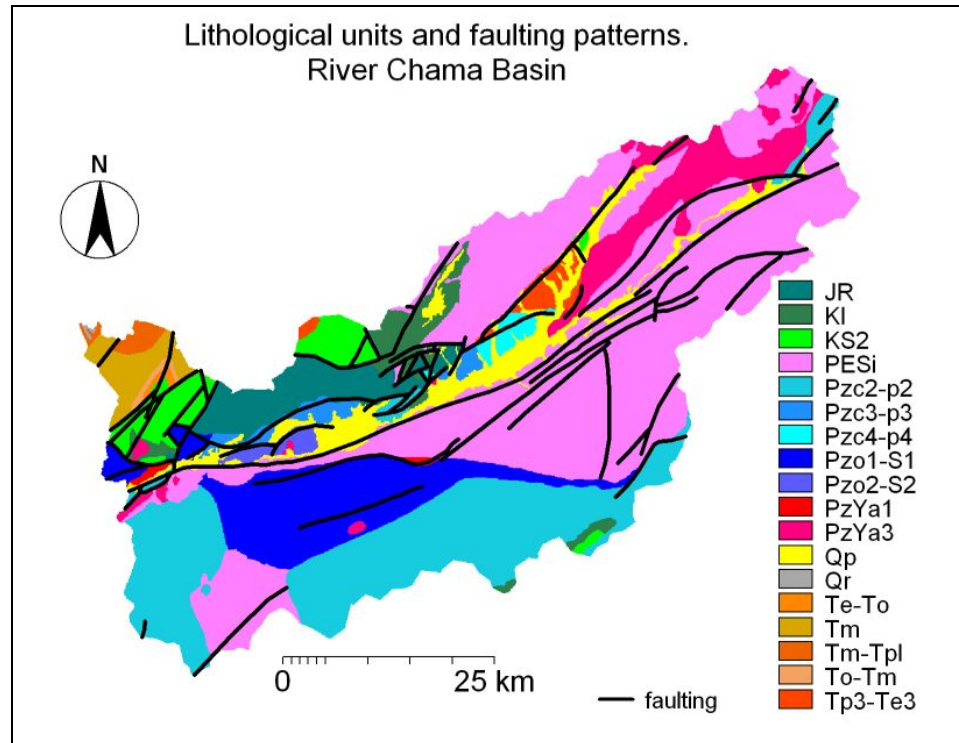


Figure 2.2. Study area lithological units and faulting lineaments

This system consists of numerous subparallel anastomosing faults with individual lengths of up to 50 Km which can be observed clear in the study area, visible in the form of fault scarp, linear longitudinal valleys and depressions as well as concentration of landslides. Although the Boconó fault is primarily a dextral strike-slip fault, a detailed study (Schubert, 1980), on neotectonic evidences, has shown the occurrence of late Cenozoic pull-apart basins, in which is easy to recognize large vertical displacements (normal faulting), pulled apart by narrow faulting segments, within a clear right-lateral displacement, which shows a clear evidence of Quaternary activity as displacing of morainic walls and alluvial fans have been observed, indicating that this fault system has been active during the Holocene.

#### 2.4 Geomorphological aspects

The River Chama basin comprises a typical tropical mountain environment, an active mountain range under wet tropical conditions, characterized by deep weathering, strong Plio-Pleistocene uplift and associated deep fluvial incision, mass movement problems and at higher elevation remnants of glacial activity. The geomorphological zonation

carried out in this analysis is based on the ITC system of geomorphological survey (Verstappen et al., 1991), and described in the section 6.2 of Chapter 6.

Table 2.1. Lithological units in the study area, colors are related to those in Figure 2.2. (Bellizzia et al., 1976 and PDVSA-Intevep, in: <http://www.pdv.com/lexico/lexicohi.htm>, last visit: Feb, 2007)

CODE	AGE	FORMATION NAME	LITHOLOGY
Qr	HOLOCENE	Alluvial deposit	Alluvion
Qp	PLEISTOCENE	Unnamed Pleistocene	Unconsolidated conglomeratic sediments
Tm-Tpl	MIOCENE-PLIOCENE	Betijoque	Massive conglomerate
Tm	MIOCENE	Isnotu	Claystone
To-Tm	OLIGOCENE-MIOCENE	Palmar	Clayey sandstone
Te-To	EOCENE-OLIGOCENE	Carbonera	Clayey sand, shales, coal seams
Tp3-Te3	PALEOCENE-EOCENE	Mucujun	Pebble to fine clayey consolidated conglomerate
KS2	UPPER CRETACEOUS	La Luna	Oil shales with intercalated limestone
KI	LOWER CRETACEOUS	Aguardiente	Siltstone shale limestone intercalated layers
JR	JURASSIC	La Quinta	Conglomeratic red sands
PzYa3	ACID INTRUSIVE UPPER Pz	Acid intrusive upper Pz	Granites, pegmatites
Pzc4-p4	CARBONIFEROUS-PERMIAN	Palmarito	Marine shales, marls, limestone
Pzc3-p3	CARBONIFEROUS- PERMIAN	Sabaneta	Meta-conglomeratic sandy matrix
Pzc2-p2	CARBONIFEROUS-PERMIC	Mucuchachi	Phyllites, shales, quartzites Meta-sands
Pzo1-S1	ORDOVICIC-SILURIC	Tostos	Phyllites, schists, shales
Pzo2-S2	ORDOVICIC-SILURIC	Tostos	Phyllites, schists, shales
PzYa1	ACID INTRUSIVE LOWER Pz	Acid intrusive lower Pz	Granites, pegmatites
PESi	UPPER PRECAMBRIAN	Sierra Nevada	Granitic gneiss, mica schists

The denudational geomorphic set, in the most extended category over the study area (74.3% of the study area), and generally the denudational processes in the study area are empowered by the steep slopes currently found on it and although some areas have been defined as stable mountains or hills, this feature is assumed given a relative stability represented particularly by a less broken topography.

It is assumed that the presence of a tectonic pull-apart basin in the Lagunillas area has facilitated a spectacular example of Quaternary accumulation process (Ferrer et al, 2005b), however given that this accretion / degradation process has been governed by the drainage dynamics, in this analysis those units comprising almost 5% of the study area is considered as of fluvial origin.

Finally and as expected from a mountain environment with active river basal erosion as well as clear neotectonic features, the study area shows along many of the drainage system and faulting lines associated cliffs and escarpments. Due to this mixed origin, this landform has the better geographical expression along the main river canyons with active basal erosion which are generally controlled by the area tectonic framework as well and where the enlarging of the escarpment walls is caused by the retrogressive erosion up the wall made by gullies and rills over a very weathered soft metamorphic lithologies in a broken topography.

### 2.5 Climatic aspects

The Intertropical Convergence (ITC), is located within a belt of 5° S to 5° N latitudes, and it moves back and forth across the equator following the sun's zenith position generating a wider belt which can include land territories until the 10° N as well as the 10° to southern latitudes. This belt of low pressure works as a net rainfall generator controlling the seasonal occurrence of the precipitations in the Venezuelan Andes. During the boreal summer the ITC moves over the northern latitudes affecting the study area for a period of time starting in April and ending in November, defining a wet season with two main precipitation peaks, the first one located in May and the second by October when many of the meteorological stations along the study area record the highest rainy events (Figure 2.3). After November when the ITC is moving towards southern latitudes, the NE trade winds blowing across the Caribbean, the Orinoco Basin, and the upper Llanos, from the northern higher pressure systems dry literally the study area until March creating the dry season. November and April could be considered as transition periods between these two atmospheric systems, which also affect temperatures particularly the daily variation, being during the rainy period less variable than during the dry period.

The mapping of the annual mean rainfall distribution was improved by the inclusion of data related to the cause/consequent factors affecting the spatial distribution of the precipitation over the study area. In that way and following Meijerink et al., (1994), the final annual rainfall distribution map is the result of the integration of the conventional linear interpolation of precipitation gauge records, rainfall-altitude relationship and vegetation response to rainfall.

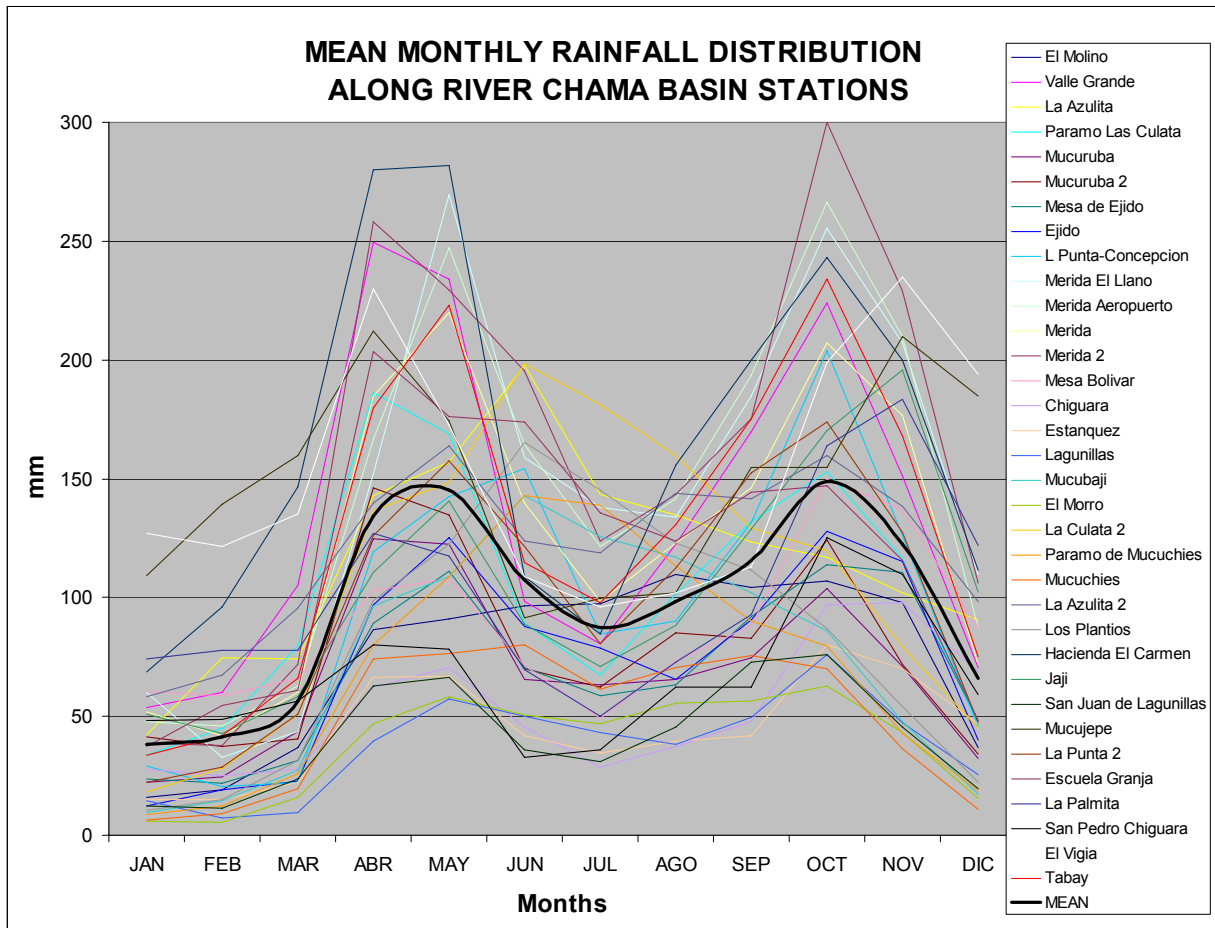


Figure 2.3. Study area. Mean monthly rainfall distribution per meteorological stations (data from MARNR, 2004 )

These additional data used were derived from the study area DEM to compute the relationship between the rainfall gauge data and altitude / altitude ranges; and from LANDSAT TM imagery which were used to generate vegetation and wetness indices as the NDVI and NDWI are, these indices were interpreted as the vegetation response to rainfall spatial distribution patterns over the study area. Figure 2.4, illustrates the procedure followed to get the mean annual rainfall map for the study area.

2.6 landuse aspects

A brief zonation of the study area land cover was obtained from a histogram classification of a NDVI product made from LANDSAT TM imagery taken during the wet season of 1998 (Figure 2.5).

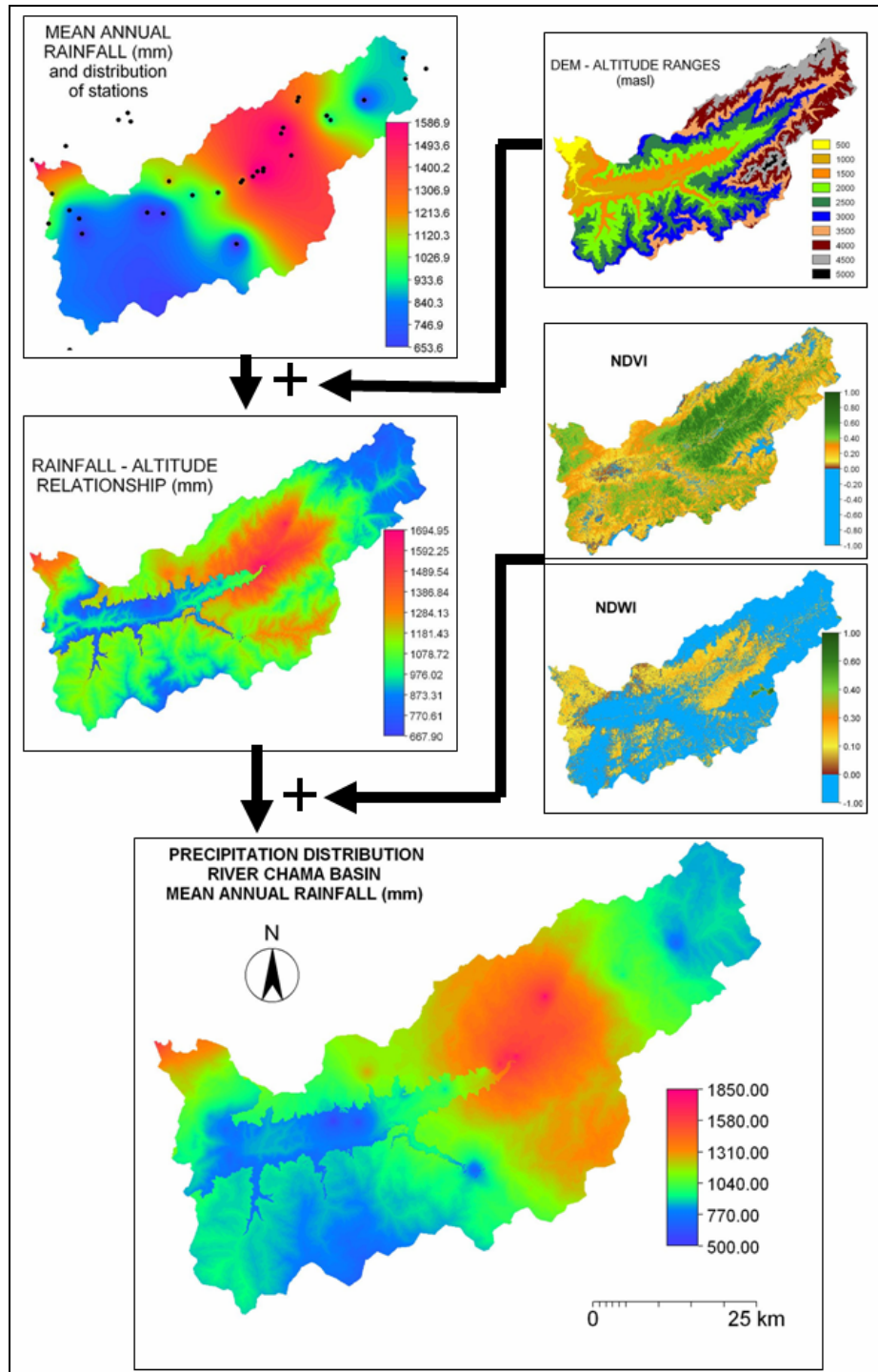


Figure 2.4. General illustration on the procedure carried out to get the mean annual rainfall distribution map of the study area.

From this zonation is clearly noticeable the presence of two main units as those are: 1) The shrublands and bare soils located at the upper part of the Río Chama Basin which represent highland grassland vegetation units as well as glacial and periglacial rock



outcrops respectively and; the semi-xenophile vegetation units located in the inner valley of the River Chama middle section. 2) The dense forest has mostly developed upstream the formed middle section, and covering the inner slopes around the study area main city. These main units could be considered the remnants of the original vegetation patterns of the study area, and their present occurrence could be explained by the extreme ecological conditions, in the case of the shrublands and bare soils, and for the presence of protected areas as the Sierra Nevada and La Culata national parks.

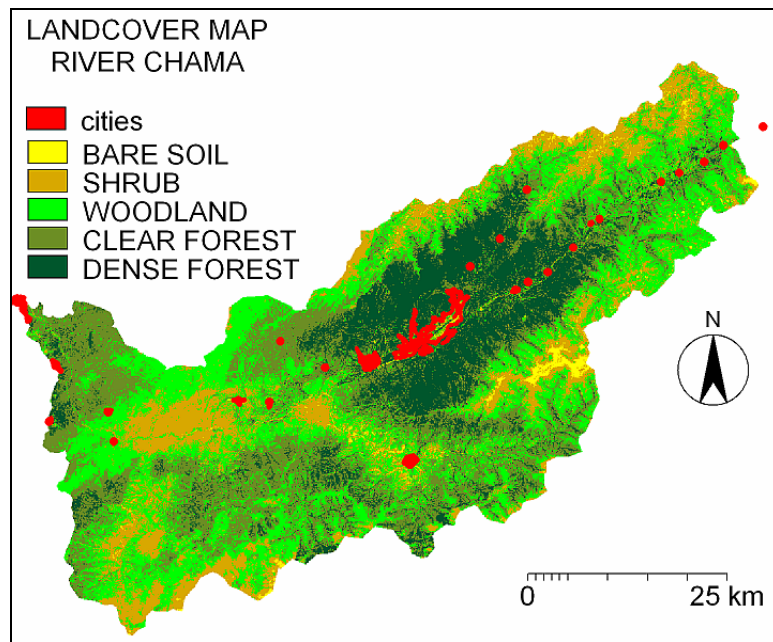


Figure 2.5. Study area land cover classification from a 1998 LANDSAT TM imagery.

Urbanization in the study area takes place in the inner valleys, particularly the River Chama valley where the urban population is mostly concentrated. Given the broken topography, towns and cities are spatially compacted whereas the reduced rural population is dispersed over the slopes and/or concentrated in linear patterns along the main roads and river valleys. Appendix 7.5 offers an approximation to the total study area population taken from the 1990 and 2000 census and expressed by the municipalities conforming or partially included in the study area, these records clearly show a low demographic dynamic in terms of population size with a highly concentration in the urban hinterlands and spatially oriented to the River Chama middle section.

This spatial distribution of population along the main valleys, illustrates its potential vulnerability to major disasters associated to landslides as the debris flows event occurred

in the neighbor River Mocotíes basin during February 2005 (Roa, 2007), where after three days of intensive rainfall a combination of simultaneous landslides and runoff discharge, generated several massive debris flows that in less than 5 hours destroyed much of the basin's main road system and other urban infrastructure, killing up to one hundred people. The River Mocotíes basin located at the southeast of the study area discharges into the River Chama lowest section and, as a part of the Cordillera de Mérida's longitudinal valley has similar geographical features to the study area here analyzed.

### 2.7 Typical expressions of landsliding processes in the area

- **Landslides caused by antropic slope alteration:** It is generally expected that the construction of a road through a mountain terrain results in the generation of mass movements. However such adjustments on the landscape are also expected to be transitory, evolving later to a stabilization (Ortigao et al., 2004). The disturbances caused by a road construction and particularly that related to excavation, slope grading and drainage concentration, typically result in a permanent focus of slope instability, particularly on the rural roads of the study area. As illustrated in Appendix 2.1, the presence of a rural road in a steeply mountain terrain seems to be linked to the surrounding landslides, which becomes sharper if considering that neither the lineament's corridor nor the softer lithologies (Fm. Aguardiente, Fm La Quinta), found in the area show even a similar level of slope instability to that found in the terrain considered to be of harder lithology (Fm. Mucuchachí), and by which was traced the rural road. Probably, the construction of this rural road increased the shear stress by the removal of slope support done during the road excavation and grading, as well as the material strength was reduced by a deliberated and not natural concentration of the drainage/runoff creating weak spots which are later susceptible to mass wasting. The increasing of shear stress and reducing of material strength have been already pointed out by Varnes and Cruden (1996), as two out of the three broad types of processes dealing with landslide process, and in this case those are associated with road construction. However, although road's net is an important factor for landslide hazard zonation however given the regional scale

considered and the difficult in mapping accurately rural roads in the study area with non-orthorectified aerial photographs, roads are not included as a factor map in this analysis.

- **Landslides caused by river basal erosion:** This kind of mass movements is typical in the River Chama middle section, where a combination of a highly weathered rocks and very steep and broken slopes, increases the erosive capacity of some permanent streams and rivers. During the Pleistocene the River Chama middle section was filled with large amounts of sediments which later and given the progressive uplift of the Cordillera de Mérida (Vivas, 1992), were incised by the drainage system creating deep canyons and escarpments which nowadays separate remnants of the original depositional surface as those present isolated mesas and terraces. Probably the capacity of incision of some rivers and streams is associated with the weakness generated by faulting lineaments as well as the rock/deposit resistance. Another important feature playing an important role in the present river incision is the highly geomorphological dynamic in this sub-area, as illustrated in Appendix 2.2, newer formation of alluvial fans can displace the river bed against more vulnerable units increasing in that way the river basal erosive capacity. As result, this section is quite susceptible to continuous mass movements which can develop into major landslides with a potential of river blocking. Already Ferrer et al., (2005a), evidences of a historic damming of the River Chama caused by landslide and occurred in this same middle section. Appendix 2.3, depict in small scale the potential of a landslide body accumulation to block a river's bed, as well as the erosive capacity of same river to incise it.

- **Landslides associated with deforestation:** Deforestation is usually linked to landsliding processes because of the alteration of an assumed former stable scheme to an instable one, however some cases report that rather than solely deforestation does not contribute to the acceleration of erosive patterns but the land management after deforestation (Gerrard and Gardner, 2002). Appendix 2.4, shows a major landslide occurring at the River Chama left slope which is clearly visible from Mérida (main city in the study area), which has been associated with a deliberated land cover change, from cloud forest to pastures as depicted in Appendix 2.5. Generally pastures include overgrazing and

overstepping as well as construction of very rudimentary path road, which in this specific case are weakening the relative slope stability and reducing its regenerating process. On the other hand, given the weathered conditions of the Sierra Nevada lithologies, where this landslide took place, once a landsliding process starts the subsequent rills and gullies process helped by the steep slopes potentially enlarge the initial affected area to a major dimension.

- **Landslides from different life zone areas:** Given the variety of ecological zones in mountain environments as those in the study area, mass wasting can develop with some particularities, Appendix 2.6 provides an example of the starting point of mass movements in the study area but under different ecological framework. The first picture from Appendix 2.6 shows how the dry ecological conditions of the River Chama middle section, combined with the subsequent high weathered soils and very steep slopes, can drive a landsliding process into a rapid event. In this case is noticeable that this landslide is quite shallow, involving only the slope's saprolite upper layer, probably under another ecological condition as that more suitable for vegetation developing, this slope failure could be naturally be revegetated and potentially reaches some degree of stability. Paradoxically with same lithology and slope gradient found in first mass movement; second picture of this Appendix 2.6, shows a vegetated hill belonging to the upper area of the River Chama basin where a potential landslide is taking place but in this case and given the grass cover, the movement becomes slow, having a high probability to reach a better stability. Also, the this second mass movement is taking place over a more developed soil profile in opposition to the less consisted saprolite found in the first mass movement, which allows a better support for vegetation develop and subsequent cohesion, both features are given by the better ecological conditions found in this part of the study area.

## Chapter 3: Methodology

### 3.1 Conceptual background definitions

The main principle used in this analysis is encompassed by the well-known and widely applied principle *"the past and present are keys to the future"*, which implies that landslides in the future will be more likely to occur under those conditions which led to past and present mass movements (Varnes, 1984; Carrara et al., 1991; 1995). As intended by van Westen et al., (1993), in this study the terms mass movement, landslide, slope movements and slope failure are used synonymously.

Landslide hazard maps to be produced in this study aim to predict where failures are most likely to occur without any clear indication of when they are likely to take place, because on a regional scale, the temporal dimension of a landsliding process depends much more on triggering mechanisms which are of climatic or geodynamic origin and therefore not easily to be linked to a geomorphological-lithological oriented model of spatial instability (Miles et al., 1999) as the approaches applied in this study. The final scale / legend to classify the final landslide hazard zonation maps in this study is structured in four hazard classes and approximately close to those defined in Kwang-Hoon et al., (2002) and described in Table 3.1.

Table 3.1. Thresholds to classify the landslide hazard classes in this study.

<b>LANDSLIDE HAZARD CLASSES</b>	<b>AREAS WITH:</b>	<b>EXPECTANCY OF BEING AFFECTED FOR A PREDICTED LANDSLIDE</b>
Low hazard	Natural resistant to landsliding processes	< 30%
Moderate hazard	Tendency to slope instability under stressed conditions	Up to 60 %
High hazard	Affected for a preliminary phase of landsliding processes	Up to 80 %
Very high hazard	Already fully affected by landsliding processes	Over 80 %

Definitions and terms for hazard, vulnerability and risk have been given by several authors, but only standard terms suggested by UNDRO (United Nations Disaster Relief Organization), Sassa (2001), and Varnes (1984) are used in this study and included in the Appendix 3.1.

### 3.2 Review of existing techniques to assess a landslide hazard zonation

An overview of various hazard zonation techniques can be found in the studies of Cotecchia (1978), Hansen (1984), Varnes (1984), Guzzetti et al., (1999), Aleotti and Chowdhury, (1999), Huabin et al., (2005), and van Westen et al., (2006). The many factors influencing the occurrence of slope instability, a large number of input parameters and techniques of analysis are required, making the landslide hazard analysis a complex practice furthermore the time and money for data collection.

Probably because of this, earlier studies were focused on deterministic evaluations on a more detailed or large scale, considering the internal friction angle, soil cohesion, layering thickness or depth of water table. A rather popular way of working out of landslide hazards under deterministic modeling are those dealing with infinite slope models, calculating safety factors from different geologic and morphometric units (Chowdhury, 1988, Duncan, 1996, Dietrich, W. and D. Montgomery, 1998). Hydrological features are also suitable to be modeled under deterministic approaches, in that way some authors have been able to simulate soil pore pressure over time together with a slope instability model and in that way quantifying the landslide susceptibility and subsequent critical thresholds (Terlien, et al., 1995; Terlien, 1998; Lin et al., 2006). Glade (1998) also defined rainfall thresholds to estimate landslide probabilities for areas where relationship between the landsliding process and magnitude/frequency of rainfall triggering events is known. However, in spite of deterministic approaches which provide a useful quantitative information on landslide hazards to be used particularly in the design of engineering works, these procedures are only suitable for small areas (van Westen et al., 2006), and not over the larger geographical variability found on a regional scale. Later development of procedures pointed out that the need for an increase in the degree of objectivity, assigning weight factors to relevant parameters or using multivariate analysis for the large data sets were obtained during the survey (Carrara et al., 1989). With the emerging of GIS, approaches to landslide hazard zonation were oriented to a more qualitative / quantitative objectivity and rapid analysis of a landslide hazard, and the classification of different approaches applied have been described mostly upon the choice of the aspect to be emphasized (i.e, method, data, work scale, etc).

Table 3.2. Summary of the main methods for landslide hazard zonation; the boxes indicate the procedures to be used in this landslide hazard zonation study.

MAIN TYPE		METODOLOGICAL APPROACH	PROCEDIMENTAL FORMS	TECHNIQUES APPLIED	AUTHORS
WHITE BOX	Geomorphologic Zonation <b>Direct Mapping</b>	- Landslide Inventory	- Inventory maps	- Data collection on landslides (field survey, photo interpretation).	-Wright et al. (1974) -Pasuto et al. (1991)
		- <b>Heuristic Approach</b>	- Landslide isophlets  (Landslide Density)	- Landslides density is calculated for circular areas.  - Provide information as landslide types and processes acting on slopes	-Pomeroy (1978), -Kienholz (1984) -Delaunay (1981) -DeGraff et al. (1988). -Leroy (1996).
GREY-WHITE BOX	Geomorphologic Zonation <b>Indirect Mapping</b>	- Geomorphic Analysis	- Geomorphological Maps  <b>-Terrain Mapping Units reclassification.</b>	- The landscape is subdivided in homogeneous areas and landslide hazard is evaluated for each of them, afterwards a hazard level is assigned in every TMU.	-Van Westen (1993) - Reichenbach (2005)
GREY BOX		- Qualitative map combinations	<b>- Multicriteria Evaluation.(MCE)</b>	- Qualitative hazard assessment by Pairwise comparison and hierarchical analysis matrix. - An experimental global prediction satellite based system.	-Roa (2007) -Brabb (1984),  -Yang et al. (2007), -Carrara et al. (1977), -Lessing (1983), -Corominas et al.(1992).
GREY BOX	Geomorphologic Zonation <b>Indirect Mapping</b>	- <b>Statistical Approach</b>	- Rainfall-Triggered landslides - Descriptive Statistics on point data. - <u>Bivariate Statistics:</u> ⇒ Susceptibility Mapping. <b>⇒ Weight of Evidence modeling method</b>	- A checklist of causal factors is associated with landslide occurrence.  - Correlation of inventory maps and factor maps with the support of bivariate statistics.	-Yin and Yan (1988), -Bonham-Carter (1994), -Van Westen (1993), -Chung and Fabbri (1999). - Carrara et al. (1978, 1990
GREY-BLACK BOX		- Bivariate statistical analysis.  - Multivariate statistical analysis	⇒ Information value method ⇒ Likelihood ratio <u>Multivariate statistics</u> ⇒ Multiple Resregion ⇒ Discriminant Funtion analysis ⇒ Artificial neural network	- Multivariate statistical analysis performed on terrain units as pixels or slope units.	1991, 1992, 1995) -Gorsevski et al. (2000, 2003) -Aleotti et al. (1996, 1998)
BLACK BOX	Logical / Deterministic Approach.	- <b>Deterministic Approach</b>	- Deterministic models in static, pseudostatic and dynamic conditions.	- Combination of geotechnical and geometrical data to evaluate stability parameters.	-Bishop (1956), -Sarma (1979), -Newmark(1965), -Terlien et al. (1998). -Miles et al. (1999)

For example, these different approaches can be classified on the basis of how the assessed area is defined (Aleotti and Chowdhury, 1999), differentiating between study areas defined by the adoption of regular grid of identical shape and size and those used in the analysis of Carrara (1983) and Anbalagan et al., (1992); the use of morphological units as those used in studies from Carrara et al., (1991) and van Westen et al., (1993); and the use of units automatically derived from overlays of each parameter map as those found in the analysis of Chung et al., (1995).

However, at present classifications of the landslide hazard zonation approaches depend more upon the data availability and methodology applied. Huabin et al., (2005), after a careful review of the methodologies for landslide hazard zonation states that the most commonly used methods are the geomorphological hazard mapping, analysis of landslide inventories, heuristic index- based methods, statistically based models and geotechnical or physically based models. Table 3.2 describes a summary of the main landslide hazard zonation procedures reviewed for this study and classified following the methodological approach, demarcating the position of the methodological procedures applied in this study.

### 3.2 General methodological procedure

The general methodological process in a hazard zonation analysis in this study is based in the recommendations given by van Westen et al., (1993), and Johnson and DeGraff (1988), and described in Table 3.3.

Table 3.3. General methodological procedure to achieve a landslide hazard zonation followed in this analysis.

<b>van Westen (1993)</b>	<b>Johnson and DeGraff (1988)</b>	<b>This analysis</b>
Preparation phase	Formulation of the investigation	Conceptualization
	Data collection	Data collection
Fieldwork Phase		
	Data interpretation	Data evaluation and analysis
Assessment Phase	Application of analysis techniques	
	Cartography of the results	Data generation



**Conceptualization:** It is contained in the research objectives and key questions intended in this landslide hazard zonation analysis and described in Chapter 1.

**Data collection:** Includes a selection of the preliminary cartographic and risk related information obtained from aerial photographs and thematic maps. Landslide hazard zonation requires information on a large series of factors, ranging from geological structure to landcover, in this study the input data is strongly conditioned to data availability. Data available for the study area are displayed in Table 3.4 and Table 3.5 described preliminary products obtained from this phase.

Table 3.4. Data requirements and sources. Abbreviations: IGN = Instituto Geográfico Nacional; MEM = Ministerio de Energía y Minas; MARNR = Ministerio del Ambiente y de Los Recursos Renovables; GLCF = Global Land Cover Facility; NASA-SDB: NASA Scientific Data Buy Program; USGS-SRTM = US Geological Service – Shuttle Radar Topographical Mission.

PRELIMINARY AVAILABLE DATA	DATA SET	TIME SPAN	SCALE / RESOLUTION	SOURCE
Aerial photographs	Missions 010493 010494	1997 – 1998 – 1999	1: 40000 1: 65000	IGN
Topographical maps	Isohipsas	1967-1974	1: 250000 1:100000	IGN
Geological maps	Lithology / structure	1967	1: 50000	MEM
Climatic data	Precipitation Temperature	1960 - current	- -	MARNR
Satellite imagery	LANDSAT ASTER SRTM	2001 2004 2000	30 m 15 m 90 m	GLCF NASA-GLCF USGS-SRTM

**Fieldwork:** The fieldwork was carried out in two dates: the first phase during July – September 2004, in order to choose the working scale, to collect the aerial photographs, GPS control points, documents and cartography of the study area, as well as the establishing of useful links with local institutions involved in natural hazards affairs. A second phase was carried out in April – June 2005, when activities were oriented to verify the photo-interpretation and other cartographic improvements such as the hydrological up dating and geological settings.

**Data evaluation and analysis:** After fieldwork a preliminary analysis is carried out, this part of the research is described in Chapter 5. This allows the processing of the data under a GIS environment, providing the researcher with a better perspective about the landsliding process in the study area, and subsequently supporting of all the decisions

related to the analysis of the interaction between factors and landslide occurrences for all the three approaches applied in this study.

Table 3.5. List of data input and subsequent data generated in this study. Abbreviations: API = Aerial photo-interpretation, DEM = Digital Elevation Model.

TYPE OF DATA	DATA LAYERS	DATA ATTRIBUTE	SIGNIFICANCE	MADE BY
GEOMORPHOLOGIC	1.- TERRAIN MAPPING UNITS.	TERRAIN MAPPING UNITS AND SUBUNITS	GEOMORPHOLOGIC PATTERNS	API + FIELDWORK
	2.- LANDSLIDE DISTRIBUTION	MASS MOVEMENTS	LANDSLIDE OCCURRENCES	API + FIELDWORK
	3.- GEOMORPHOLOGY	MAIN LANDFORMS	GEOMORPHOLOGIC SUITABILITY	API + FIELDWORK
TOPOGRAPHIC	4- DIGITAL ELEVATION MODEL	ALTITUDE CLASSES	CLIMATE, VEGETATION, POTENTIAL ENERGY	WITH GIS FROM SRTM DATA AND ASTER IMAGERY
	5.- SLOPE MAP	SLOPE ANGLE CLASSES	OVERLAND AND SUBSURFACE FLOW VELOCITY AND RUNOFF, SOIL WATER CONTENT, POTENTIAL INSTABILITY	WITH GIS FROM DEM
	6.- SLOPE ASPECT MAP	SLOPE DIRECTION CLASSES	SOLAR INSOLATION, EVAPOTRANSPIRATION, VEGETATION.	WITH GIS FROM DEM
	7.- SLOPE FORM MAP	CONCAVITIES, CONVEXITIES AND FLAT AREAS	FLOW ACCELERATION, EROSION/DEPOSIT RATE, SOIL WATER CONTENT	WITH GIS FROM DEM
	8.- INTERNAL RELIEF	RELATIVE HEIGHT DIFFERENCES	RUNOFF VELOCITY, POTENTIAL ENERGY	WITH GIS FROM DEM
	9.- GEOMORPHOMETRIC	TOPOFORMS	EROSION, ACCUMULATION PATTERNS	WITH GIS FROM DEM
GEOLOGIC	10.- LITHOLOGY MAP	LITHOLOGIES	WEAKNESS TO WEATHERING	GEOLOGY MAP + FIELDWORK
	11.- FAULTING PATTERNS	BUFFER DISTANCE	TECTONIC ENERGY, RCK WEAKNESS	GEOLOGY MAP + FIELDWORK
HIDROGRAPIC	12.- DRAINAGE	STREAM TYPE	POTENTIAL ENERGY	TOPOMAP+API
	13.- DISTANCE TO DRAINAGE	BUFFER DISTANCE	WATER CONTENT, RUNOFF CONCENTRATION	WITH GIS FROM DRAINAGE MAP
LAND COVER	14.- LANDCOVER MAP	GENERAL LANDCOVER	SOIL PROTECTION AND STABILITY	LANDSAT IMAGERY
	15.- NDVI , NWDI	VEGETATION AND MOISTURE DENSITIES	VEGETATION DENSITY AND WATER CONTENT	LANDSAT IMAGERY
BIOCLIMATIC	16.- HOLDRIDGE LIFE's ZONES	LIFE's ZONES	BIOCLIMATIC UNITS	GROUND DATA NDVI , NWDI

**Data generation:** The available data were used as a baseline to generate new data as attribute maps, statistical tables or just to improve the original data. Products from this step are the final landslide hazard zonation maps.

### 3.3 The Hazard modeling.

In a broad sense and following Brenning (2005), Aleotti et al., (1999), Soeters and Van Westen, (1996), Wieczorek (1996), Hansen (1984), and Wright et al., (1974), the cartographic representation of landslide analysis maps can be grouped in three main types as: Landslide inventory, landslide density and landslide hazard maps. Table 3.6 describes the approaches and subsequent procedures developed in this study, which represent the most connoted approaches applied in a landslide hazard zonation at a regional scale. The methodological aspects of these procedures are further developed in the incoming chapters.

Table 3.6. Proposed methodological / procedures for landslide hazard zonation.

<b>METHODOLOGICAL APPROACH</b>	<b>PROCEDURE</b>	<b>BASED IN:</b>
Geomorphological	Terrain subUnits (TMSu) reclassification	Knowledge-driven Geomorphological assessment
Mixed Knowledge / Logic Statistical	Multicriteria Evaluation (MCE)	Pairwise comparison and Analytical Hierarchy Process matrix
Probabilistic	Weights of Evidence	Bayesian statistics

### 3.4 Validation and comparison

The validation of the Geomorphological, Multicriteria and Weights of Evidence landslide hazard maps generated in this study was assessed in terms of spatial and prediction effectiveness through the Success rate curve (Zezere et al., 2004), which is performed in order to determine whether and to what extent the landslide prediction of each model computed, can be extended in space, to neighboring areas with similar geographical settings (Chung et al., 2001).

The success rate is based on the comparison between each model computed and the landslide inventory map of the study area (Zezere et al., 2004). This procedure will be used not only to interpret but to classify in a consistent way with each one of the hazard maps produced. After the classification of the three hazard maps in four hazard classes, the accuracy was evaluated by a coefficient of correlation. Validation and comparison procedures are full described in Chapter 7.

## Chapter 4. Generation of the Digital Elevation Model (DEM) from space borne systems

DEMs are increasingly used for the modeling of the landscape and surface processes (Tucker et al., 2001), important geomorphic parameters involved in hydrologic and soil-erosion processes slope and aspect, can be also calculated from a DEM (Van Westen, 1994), which are main factors in the modeling of natural hazards such as landslides.

At present time there are two main techniques to obtain DEMs from space borne sources: The first is related to the use of satellite stereo pair images from optical satellite sensors and the second depends on the use of space borne radar via synthetic aperture radar (SAR) or interferometric synthetic aperture radar (InSAR). In the case of optical satellite scanners, the generation of high-resolution imagery provides an important source of data for topographical mapping. Results have been published in peer-reviewed literature about the potential of using the Advanced Spaceborne Thermal Emission and Reflection Radiometer (ASTER); for example, Bolch & Kamp (2006) and Kamp et al., (2003) described the development of an ASTER DEM for Cerro Sillajhuay, Chile/Bolivia, and a first comparison of an ASTER DEM with and a DEM derived from contour maps (Kamp et al., 2005).

In this chapter a DEM from the study area is generated by the use of two main sources such as those provided from ASTER data (optical) and SRTM data (radar). Main idea of this procedure is to demonstrate the possibility of an integral use of remote sensing data and GPS fieldwork for the building of a DEM for geomorphological purposes. The use of ASTER imagery to generate a higher resolution DEM than based solely in SRTM data even if the final DEM was aggregated to 90m horizontal resolution, accomplished this goal, however, since ASTER imagery do not cover the whole study area, SRTM data is used to complete the remaining sections and to improve gaps related to ASTER imagery artifacts.

### *4.1 Building the study area DEM from SRTM data and ASTER imagery*

A DEM (Digital Elevation Model) for the study area was built based in ASTER and SRTM elevation data. SRTM data 90m resolution was obtained from the GLCF website and the ASTER imagery were provided by Prof. Kamp from the University of Montana. A first set of ASTER imagery was a level 1B dated from March 2003 (Figure 4.1A); with

a 15% of cloud cover, which allowed the location of the most sensitive areas of error and subsequent fieldwork to collect GCPs (Ground Control Points). The second set is dated in August 2004 (Figure 4.1B); and since it has only 5% of cloud cover, this set was used to get data for the study area DEM. Both data sets, the SRTM and the ASTER imagery, were georeferenced to the WS84 datum. Additionally, 240 GCPs (Ground Control Points) collected during the 2004 study area fieldwork and registered by the use of three hand-held GPS (Geographical Positioning System) instruments: Garmin GPSMAP 76S, Garmin eTrex Vista, and Garmin eTrex; were calibrated to the study area main geodetic point located at the pass of Pico El Aguila (4049 msnm). The mean deviation between the GPS measurements and the official altitude was 5.0 m for the Garmin GPSMAP 76S, 6.3 m for the Garmin eTrex Vista, and 5.3 m for the eTrex, resulting in an average deviation of only 5.5 m. As the fieldwork was being carried out (Kamp, 2004), found that hand-held GPS instruments allow for elevation accuracies of only a couple of meters. Thus, since the mean deviation between the three GPS instruments is 12 m, and only very occasional high deviations were measured with a maximum of 66 m.

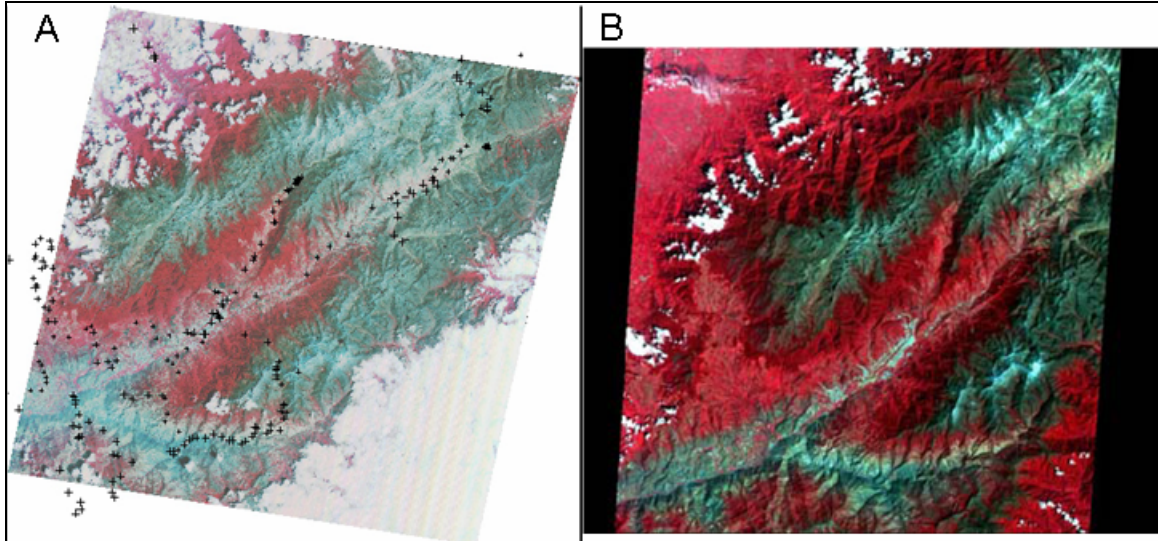


Figure 4.1. Aster imagery used to build the study area DEM. Aster scene from March 2003 (A), showing the GCPs (black dots) collected during fieldwork. These GCPs were later used in a second Aster set dated in August 2004, which because of its lower cloud coverage was chosen to generate the DEM.

These GCPs were added to the ASTER imagery and processed under the GIS Geomatica (<http://www.pcigeomatics.com>) to generate three preliminary DEMs with

different vertical resolution (low, middle and high), all of them with 15m horizontal resolution, the RMSE<sub>x,y</sub> was calculated to 7 m for channel 3N and ~17 m for channel 3B. The number of artifacts in the generated 15 m DEMs varies with the vertical resolution: in the DEM of low vertical resolution 8.8% of the area is artifacts, and this deteriorates to 13.3% in the DEM of middle vertical resolution, and to 15.2% in the DEM of high vertical resolution. Then, artifacts from the high vertical resolution were filled with data from the middle and eventually from the low vertical resolution, reducing the number of artifacts to 5.9%; remaining spots of missed data were corrected with data from the SRTM to get a seamless continuity. A DEM created from ASTER imagery can be expected to have a vertical accuracy of approximately 25 meters, although in areas with less vegetation or man made features, this can rise to approximately 11 meters (Selby, 2007).

As mentioned before, because ASTER spatial coverage does not match the total extension of the study area, SRTM data was used instead for the remaining sections of the study area, and then a linear correlation of both data sets was carried out in order to integrate them into a final DEM. For this purpose, a section located in the center of the study area (Figure 4.2), where the ASTER DEM reports a low density and size of artifacts, was chosen for this comparison, obtaining a  $y = 0.9948x$  linear function with a correlation of  $R^2 = 0.9829$ . Given the 90m SRTM DEM horizontal resolution, it was necessary to aggregate the ASTER DEM (15m horizontal resolution) also to 90m in order to match both data sets. The accomplished correlation was considered quite acceptable, and it was used to integrate the ASTER and SRTM DEMs data and subsequently to generate a 90m study area's DEM. Figure 4.2 illustrates the already described steps followed to achieve this DEM.

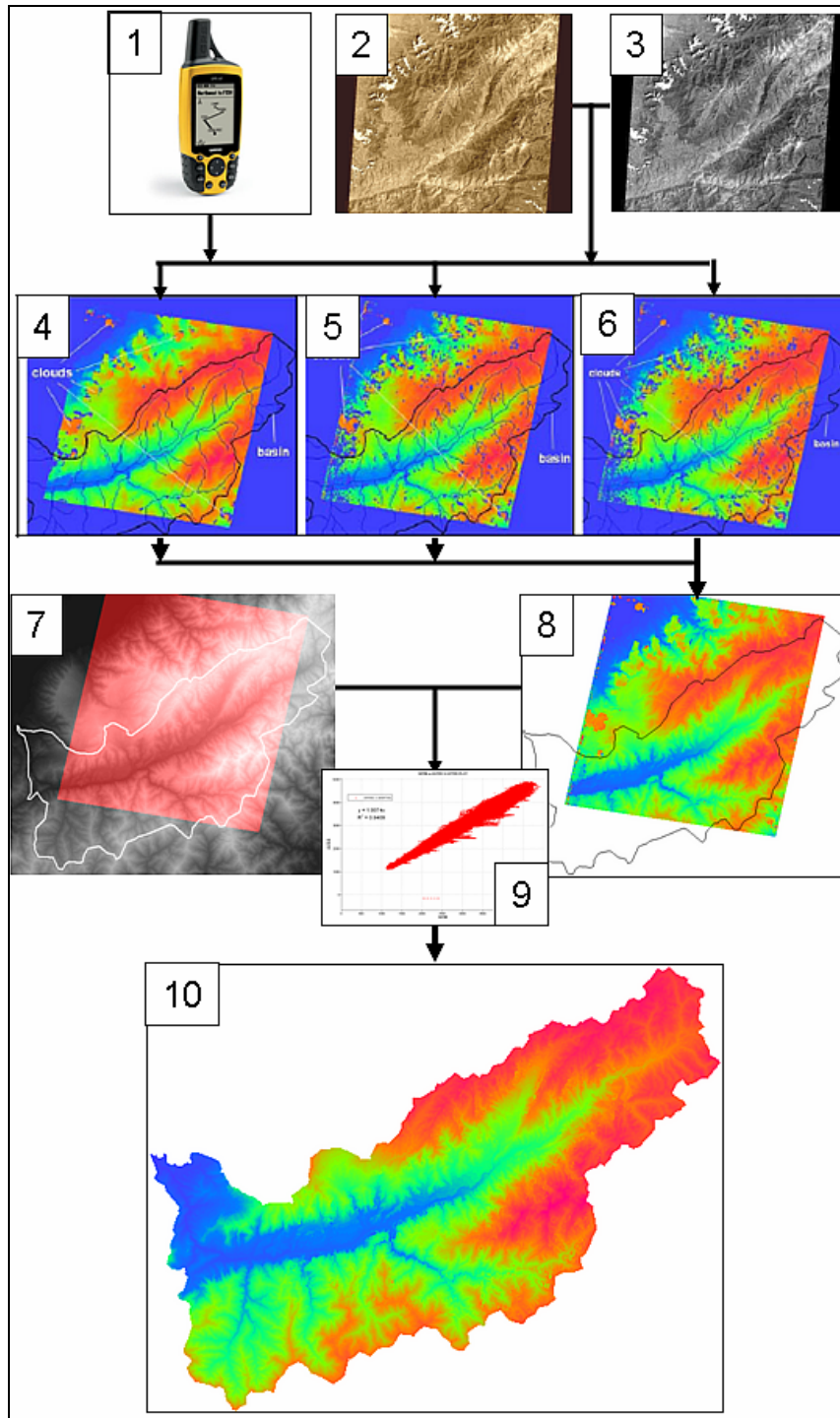


Figure 4.2. Flow chart on the study area DEM's generation: Preliminary DEM data is collected through GCPs (1); and ASTER channels 3N (2) and 3B imagery (3); which are processed to generate low (30m) (4), middle (5) and high (15m) (6) resolution DEMs. Missed pixels at the high resolution DEM (6) are filled with data from the former resolution (8); then remaining "voids" are filled with SRTM (90m) data (7). Later, ASTER DEM is correlated to the SRTM DEM (9), and the data is aggregated (from 15m to 90m resolution) and integrated into a single DEM covering the whole study area (10).

## Chapter 5: Landslide distribution analysis: descriptive statistics

### 5.1 The landslide inventory map

The USGS defines the landslide inventory map as a cartographic identification of areas that appear to have failed by landslide processes, including debris flows and cut-and-fill failures (USGS, 2006). This is a systematic mapping through various techniques (i.e., field surveys, aerial-photointerpretation, site measurements, historical records, etc.) of past and recent landslides in a region.

Practically all the existing techniques for landslide hazard zonation depend upon the accuracy and reliability of the landslide inventory map obtained from the area to be modeled. However, given that the surveying for landslides in a study area via aerial photo-interpretation, satellite imagery and even intensive fieldwork is largely based in the skills and experience of the interpreter, the construction of a landslide inventory map is still a subjective task. The size of the study area plays a decisive role in the accuracy of the landslide inventory map since the data input format are given at a regional scale which implies an absence of detail in some features, which even being recreated by other additional input, could be omitted when uploading this information into a GIS data base with a 90m pixel resolution or in the best of the cases generalized. Taking into account these assumptions, the landslide inventory map here interpreted corresponds to the visible scars and slide bodies pointed out mainly from the aerial photographs set used. Additions on mass movements not represented in this set of photos were taken from the fieldwork and the processing of a Landsat TM imagery which is explained later.

As mentioned in Chapter 3, the landslide inventory map was obtained through the interpretation of two sets of black and white aerial photographs obtained from the area during the dry season (December to March), in 1998 and 1999, at a nominal scale of 1:65000 and 1:40000 respectively. Due to the large amount of aerial photographs, together with the non availability of a faster computer processor and high storage capacity, no processing related to ortho-rectification was performed on the 300 aerial photographs. However, the a-priori knowledge of the area as well as two fieldwork experiences enables one to carry out the analysis of the aerial photographs by the use of a single mirror stereoscope. In the case of landslide inventory, this photo-interpretation was



conducted in order to identify and isolate mass movement processes which were followed by its digitizing and subsequent incorporation into the GIS data base.

### 5.2 The contrast-widening color composite

Because the study area is covered by two different temporal and path / row Landsat TM scenes (006/054 on the 08-13-1996 and 007/054 on the 09-05-1996), both were radiometrically calibrated following the standard procedure described in Chander and Markham, (2003). Landsat imagery provides an excellent basis for the transferring and digitizing of the landslides polygons because of the geographical information displayed (i.e. drainage network), and the potential to create several color composites in order to highlight a desired feature (as the isolation of landslides by the contrast-widening color composite performed in this study). Such processing is based in the use of the contrast between the object to be discriminated (landslides, scarps) and the surrounding environment. This method assumes that the bare soil exposed in a slide scarp should have a higher reflectance than the adjacent non denudated area, allowing in that way the identification and isolation of landslides. The algorithm is based in a false color composite with the NDWI (Normalized Difference Water Index) in the red channel, the NDVI (Normalized Difference Vegetation Index) in the green channel and the medium infrared band in the blue channel (Gond et al., 2004); where:

$$\begin{aligned} \text{NDWI} &= (\text{NIR}-\text{MIR})/(\text{NIR}+\text{MIR}) && \text{(Gao, 1996);} \\ \text{NDVI} &= (\text{NIR}-\text{VISred})/(\text{NIR}+ \text{VISred}) && \text{(Rouse et al., 1974),} \end{aligned}$$

With: NIR = Near infrared band  
MIR = Medium infrared band  
VISred = Visible red band

Figure 5.1, illustrates the data input and process followed in the landslide identification using aerial photo-interpretation and the contrast-widening color composite.

Although the methodological principle used over here is functional, it is necessary to point out that the method is dependable and its use in this study displayed three main gaps: 1) the existence of aerosols, clouds and shadows in the raw Landsat TM set which did not allow the discrimination of scarps in some areas; 2) the Landsat TM spatial resolution ( $\approx 30\text{m}$  pixel), increases the uncertainty in the outlining of smaller scarps,

hence the importance of the spectral information enhancing via the contrast-widening. 3) infrastructure, houses, crop fields and exposed rocks could be misinterpreted as landslide scarps because of the similar reflectance of these compared to scarps and exposed detritus from recent landslides (therefore even being considered as an useful methodological tool, any landslide inventory map generated from this procedure must be confirm with a higher spatial resolution imagery and/or fieldwork).

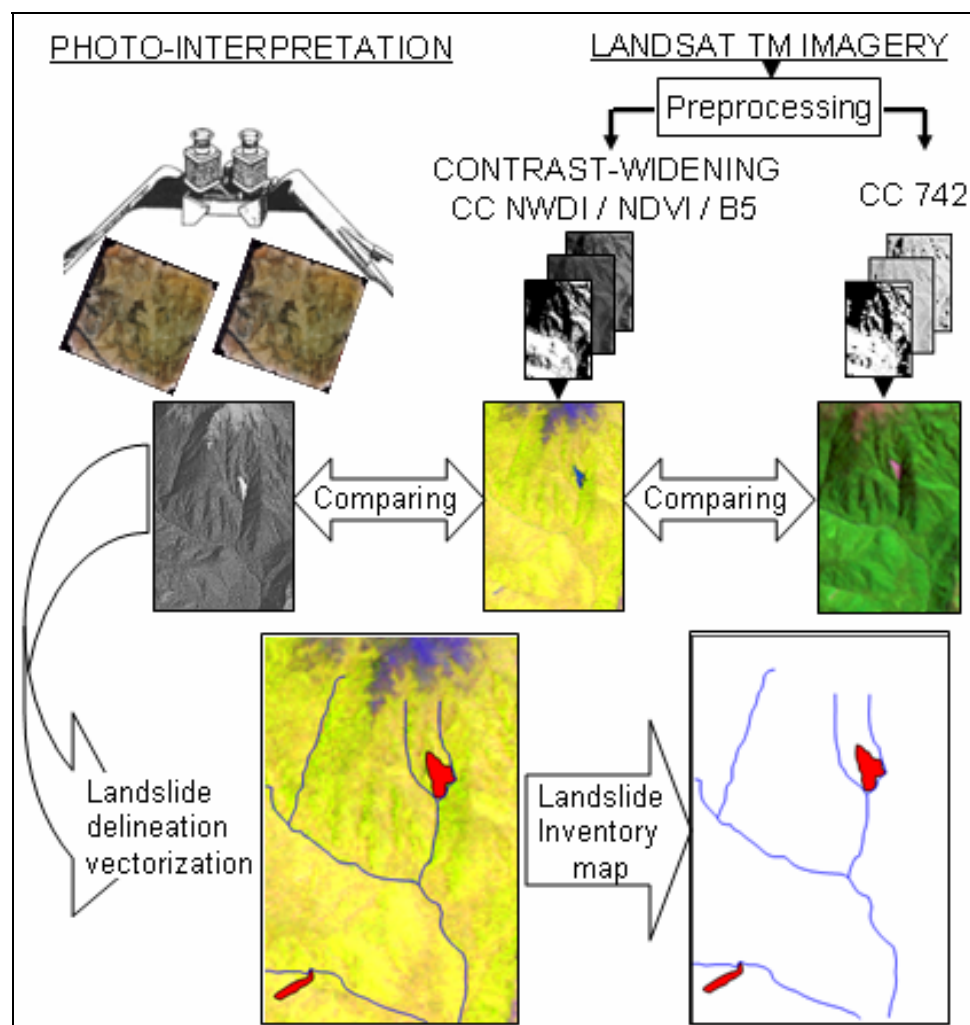


Figure 5.1. Procedure to landslide identification by aerial photo-interpretation and Landsat TM imagery contrast-widening color composite.

### 5.3 Landslide geographical occurrence

The study area covers 2893 km<sup>2</sup> (100%), although the landslide inventory map shows that only 86 km<sup>2</sup> (3%) –given the regional scale of this study– is affected by landsliding processes. These landslide processes are represented by the 493 landslide polygons outlined in the study area landslide inventory map (Figure 5.2). The landsliding process is not randomly distributed across the whole study area; actually, it is concentrated towards the southwestern sections, where also the larger landslide polygons are founded. Figure 5.2 shows an accumulated frequency analysis on the relationship between the landsliding area and the number/area of landslide polygons. The figure indicates that 50% of the total landsliding area is contained in the first 40 landslide polygons ordered by size; however, at the same time are only the 8.1% of the total landslide occurrences in the study area. This notable concentration of the total landsliding area in few landslide occurrences is confirmed when considering that 134 landslides (27.2% of the total outlined polygons), contain the 80% of the total landsliding area. At a regional scale this frequency analysis could be merely illustrative but it allows a preliminary assessment on the magnitude of the landsliding processes in the study area.

#### **Examples of mass movements**

**La Trujillana's landslide.** This is a clear translational landslide with an active retrogressive scarp which has already instabilized the rock blocks located in the upper part, causing rock fall (topple) given the extreme steep slope. Located at the lowest Chama River section, where the river valley becomes entrenching at the western part of the study area (Figure 5.4), this landslide has 750m length (from scarp to toe), and 450m in the widest section, it has a perimeter of 2526m, covering an area of 300000m<sup>2</sup>, between 500 and 1000 masl. This landsliding process occurs in a claystone with intercalated sandy layers lithology dating back from the Tertiary – Miocene period.

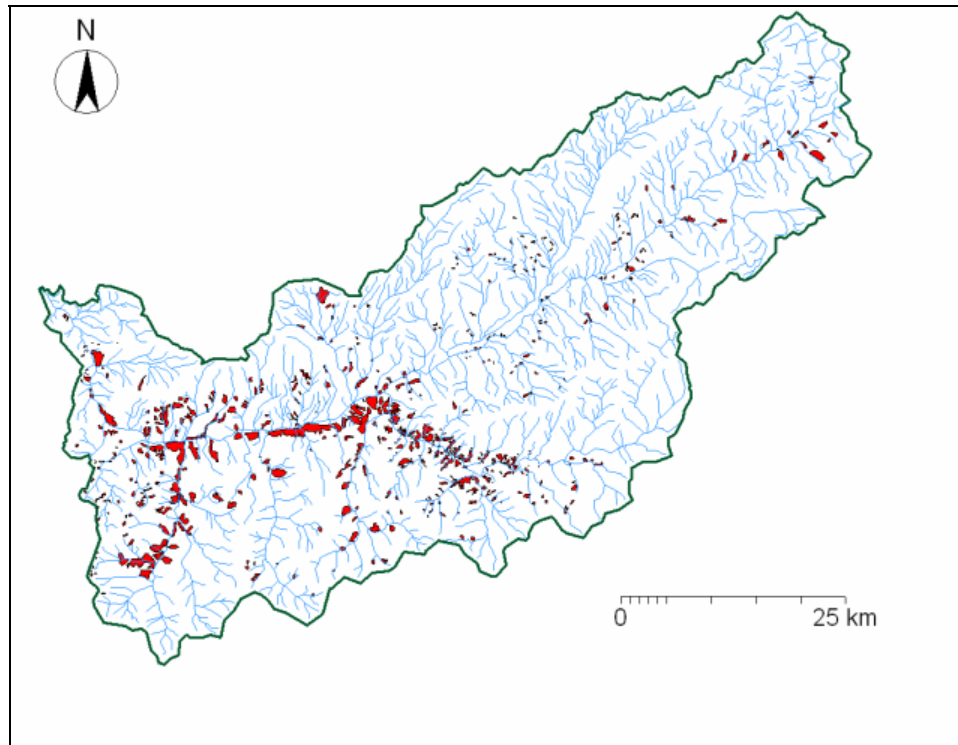


Figure 5.2. Landslide inventory map of the study area obtained from the photo-interpretation and contrast-widening procedure. Landslides (red polygons) are showed together with the drainage network.

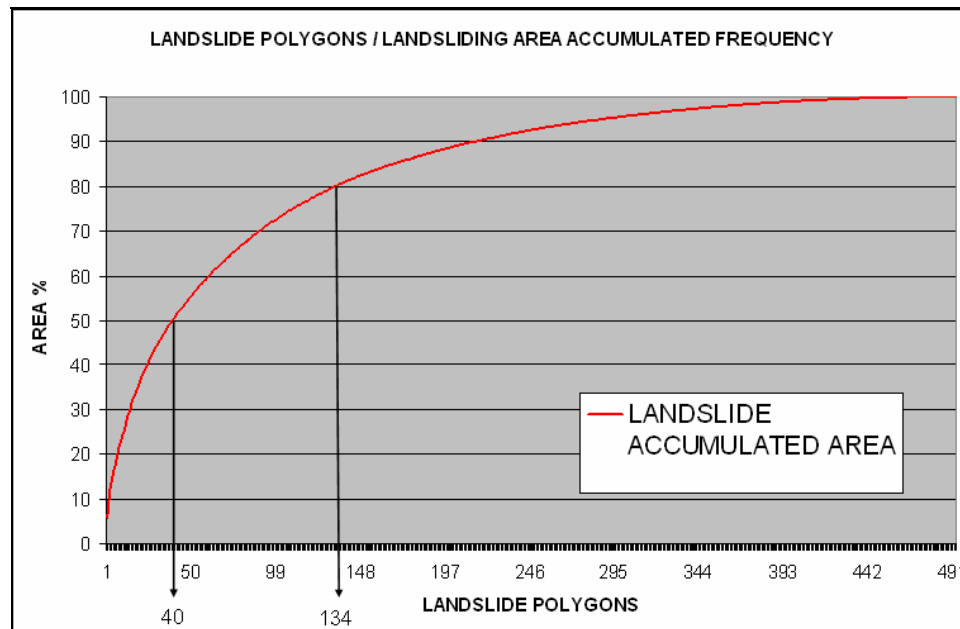


Figure 5.3. Distribution of the cumulative landsliding area (%) by number of landslide polygons. The landslide polygons have been previously arranged by area size in decreasing order, allowing the estimation of landsliding area reached at certain numbers of polygons. For example the first 40 landslide polygons contain 50% of the total landsliding area, while to reach 80% of landsliding area requires to include until 134 landslide polygons.

Despite the massive texture of the claystone, it behaves as a soft rock once weathered. Moreover, the presence of sandy layers increase the water infiltration and subsequent erosion resulting in a progressive breakdown of the all claystone structure resting position. This is particularly important, because in this landslide case, with a slope inclination at the scarp section over the  $60^\circ$ , a simple lack of cohesion in the rock structure is potentially to cause rapid mass movements. Since this landslide is rather active, all its structure (scarp, transition, body), is full denudated and bare, Although the surrounding area is covered by a compact tropical dense forest. The orientation of this landslide is mostly S – SE, which protects it from the direct impact of the humid winds entering the valley from the north. Slope and lithology have been considered the main passive factors involved in this landsliding process, but other factors as the entrenching of the relief in the area which tends to concentrate the surficial and internal drainage shall be considered as well. On the other hand, the probably use of explosives during the construction of the high way at the footslope increased the susceptibility of this slope to landsliding processes so nowadays the main risk of this landslide is the blocking of the high way connecting the two larger cities in the area (Mérida and El Vigía), event that is often during the rainy season. A ground picture of this landslide can be seen in Appendix 5.1.

**The Lagunillas's badlands.** The Lagunillas's badlands are a complex succession of mass movements promoted mainly by the steep slope and dry climate condition in the area (Appendix 5.2). The climate conditions fit into the Holdridge's life zone of subtropical dry shrubland, which in the study area is characterized by moderate to high temperatures, a very limited low density vegetation cover, and a very concentrated rainfall season. This set of bioclimatic conditions increases the weathering capacity on the area soil and rocks, resulting in an extensive layer of saprolites and highly weathered rocks. The lithological set where these landsliding processes are taken place is compounded by nominally hard igneous- metamorphic rock which as mentioned before has been highly weathered, this lithological framework is a combination of granite, gneiss and mica schist dated from the Precambrian era. The Lagunillas's bad lands, located almost in the center of the Chama River middle section southern slope at an average of

1000 masl, are mostly a system of translational retrogressive landslides, affected widely by active gullies and rills, forming a compact sliding set of 20056 m perimeter and 5040363 m<sup>2</sup> area, with more than 70° slope inclination and a N – NW average exposition. The area where these badlands occurs is practically unpopulated but crossed by important roads which are annually blocked by slides, some authors as Ferrer (1999), found historical and geomorphological evidences of damming of the Chama river caused by landslides in the area, so this could be the main risk coming from an intense mass movement activity in the badlands.

**El Palón landslide.** Because of the combination of very weathered saprolites, a more availability of water and moderate slope; this landslide behaves as a flowslide. The most representative feature of this flowslide is the spectacular accumulation body which is fan shaped and constituted by pebble, gravel, in a coarse sand matrix. This flowslide takes place at the northeast part of the study area, starting the scarps at almost 3000 masl and ending at 2500 masl, after a non linear length of almost 1000m and 400m at the widest section, having an area of 224110 m<sup>2</sup> and 2989m perimeter.

This landslide occurred over the same lithological background than the Lagunillas's badlands (granite-gneiss-mica schist, Precambrian?), and showing a similar depth in the saprolite. The flowslide began as a serie of small rotational slides that rapidly evolve into a big translational movement, rather than retrogressive this flowslide is mainly progressive forming an alluvial fan at the end of the body that nowadays is target of basal erosion from Chama River. The slopes along this flowslide are between 30° to 40° inclination and show an exposition N – NW – W. The causes of this flowslide could be associated to a loss of cohesion in the saprolite layers given a saturation of water, which created a kind of very located debris flow down stream. Given the relative moderate slope, a considerable amount of the debris generated still rests in the flowslide channel, which allows the activity of this flowslide almost every rainy season. Probably the main risk of this flowslide will that it can block and dam the Chama River becoming in a serious hazard for the communities settled down stream. A ground picture of this landslide can be seen in Appendix 5.3.

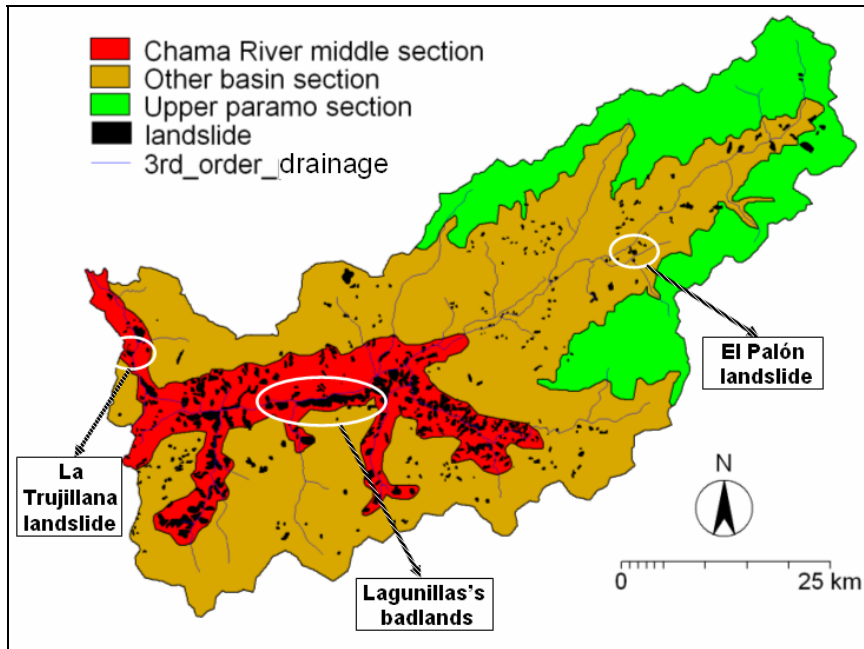


Figure 5.4. Study area map displaying delimited sub-areas based in landslide concentration patterns.

### 5.3 Landsliding processes and factor/classes. Descriptive statistical relationship

A landslide inventory map does not provide information about the causes of mass movement events, being considered as a static representation of the mass movement processes. However, its combination and comparisons with the classes derived from the factor maps available in the GIS data base provide an understanding of the relationship between related geographical variables and the landslide occurrences. This relationship is described statistically provides the researcher and decision maker with a guide to the following steps of the landslide hazard zonation process.

This preliminary statistical treatment on the landslide inventory map and factor maps / classes relationship is illustrative and only partial answers about the landslide hazard could be expected because of the descriptive nature of this distribution analysis. The relationship is based in the percentage distribution of the total landsliding area per factor map and its classes, these last features were already described in Table 3.6 from Chapter 3. The following charts display the percentage landsliding area for every factor map/class analyzed illustrated as red bars, these also include in blue lines or bars, the percentage distribution of the same classes analyzed across the whole total study area, showing the

classes distribution patterns not only from the landsliding area but also in the remainder study area not affected by landslides.

#### 5.4 Landslide area - altitudinal ranges relationship

As illustrated in Figure 5.4, the landsliding processes in the study area tend to be concentrated in certain sections or sub-areas, where the prevalence of certain factor or group of factors promotes the generation of mass movements. In that way, Figure 5.5 illustrates the distribution of the landsliding area by altitude indicating that there is a clear concentration of the landsliding processes taking place in altitude ranges from >500 masl up to 2000 masl in spite of much more of the total study area rest in areas located over 2000 masl. So from this chart (Figure 5.5), a preliminary conclusion about higher landslide susceptibility of the altitude ranges between 500 masl up to 2000 masl can be made. Nonetheless this apparent relationship between altitude and landsliding process is clearly not the only factor involved. For instance in Figure 5.6, the landsliding area is depicted according to the altitude range and slope class. Although the landslide concentration pattern previously found in the altitude range distribution still applies, slope angle classes 30° and 40° (>20° to ≤40°), seems to play a very important role in the concentration of the landsliding processes around the 500 masl up to 2000 masl altitude belt.

#### 5.5 Landslide area - slope angle / slope shape / slope aspect relationship

It is well known that in landsliding process slope plays a very crucial role (Chung et al., 2003; Coelho-Netto et al., 2006) In this study the landslide inventory map was correlated with three important slope related factor maps as those are the slope angle, slope shape and slope aspect, in order to explore the distribution of the landsliding area among the slope classes. These classes are obtained by simple interval division of the domain or range of values found in the factor map; this guarantees the common base necessary for the comparative purpose of this analysis. With respect to slope angle (Figure 5.6), it was found that classes from 30° to 40° are where the concentration of the landsliding processes occur.



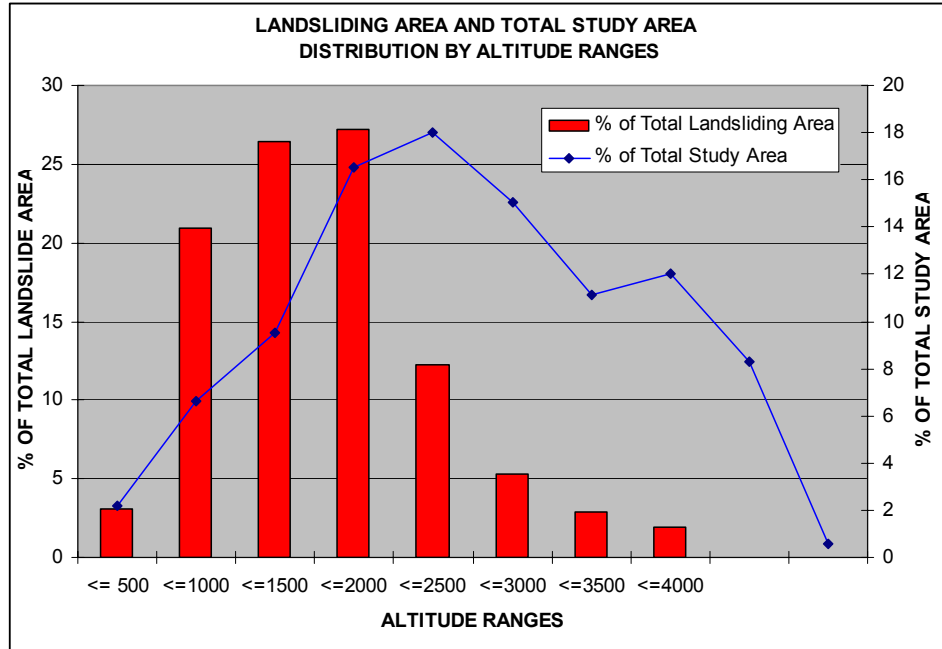


Figure 5.5. Landsliding area and total study area distribution (%) by altitude ranges.

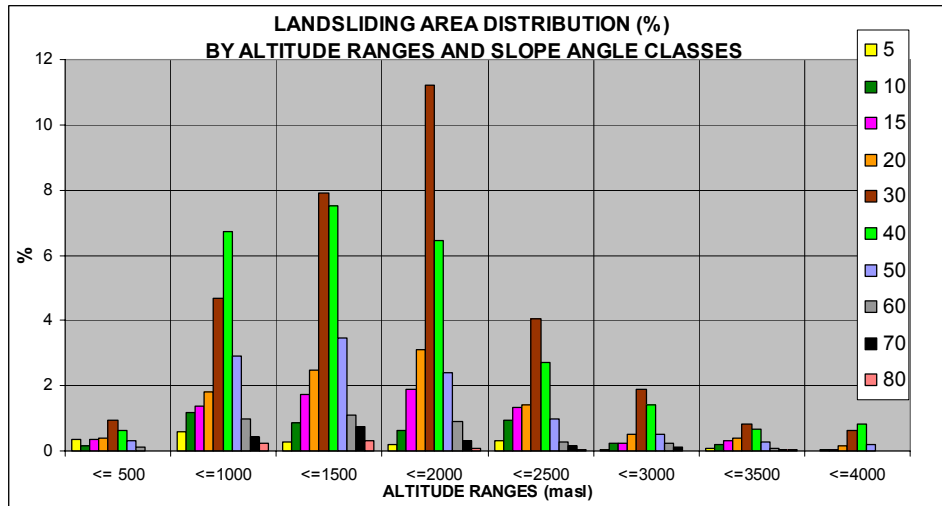


Figure 5.6. Landsliding area and total study area distribution (%) by altitude ranges and slope angle classes.

This assumption is confirmed through Figure 5.7, where the landsliding area already plotted by slope angle classes reveals the dominance of these mentioned slope classes, but is also demonstrates that the total study area displays a similar pattern in the distribution of the slope classes across it. This suggests that the slope angle is by itself not a reliable variable in the explanation of the landslide occurrences since not all the areas within the 30° to 40° slope angle classes are fully affected by landsliding processes in the study area.

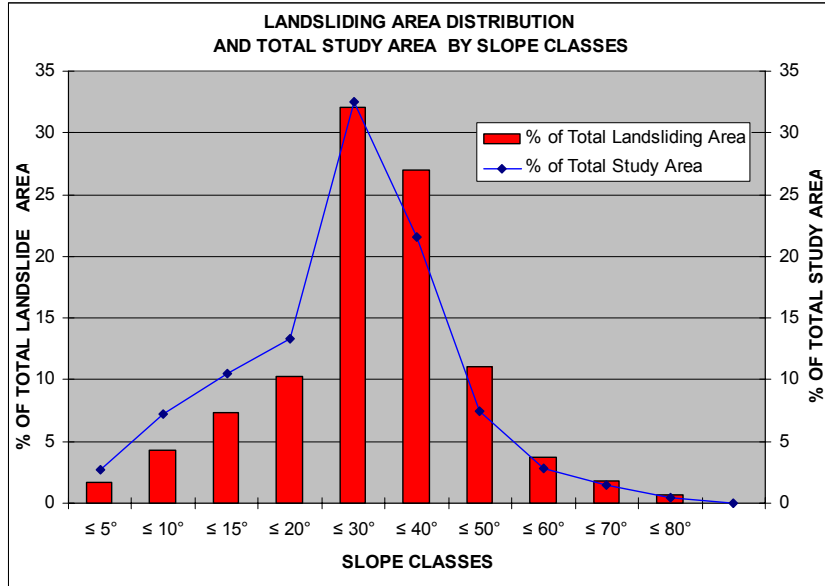


Figure 5.7. Landsliding area and total study area distribution (%) by slope angle classes.

For a better discrimination of the slope angle and shape influence on the concentration patterns of the landsliding area, a map comparison between the slope angle, shape and the landslide inventory maps was performed, and the results are shown as frequency distribution in Figure 5.8. From this chart it can be seen that straight slopes play a main role as the class which explains landsliding concentration in the 30° to 40° slope classes; in the remainder of slope angle classes all the slope shape classes –particularly the concave class– are associated to the landsliding processes.

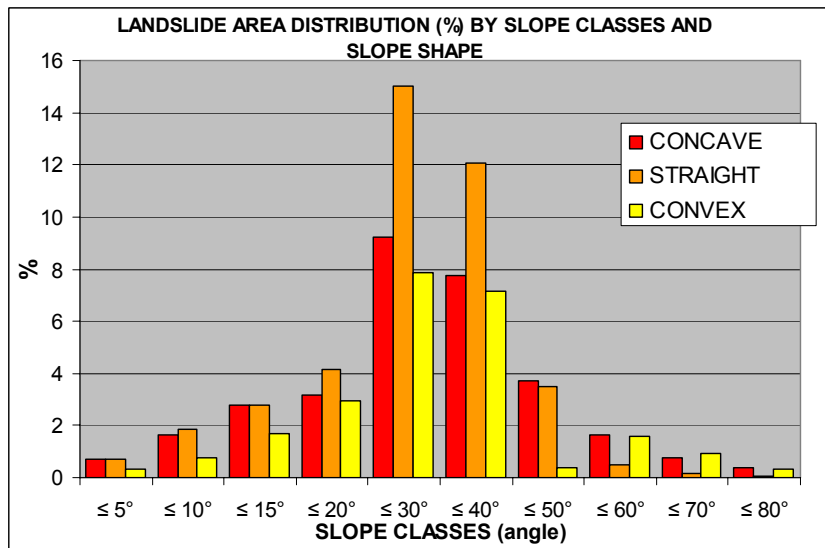


Figure 5.8. Landsliding area distribution (%) by slope shape and slope angle.

In the case of slope aspect, nine slope aspect classes were computed including the flat class and compared with the landslide inventory map. Figure 5.9, shows the slight prevalence of landslides with exposition to N, NE, and E.

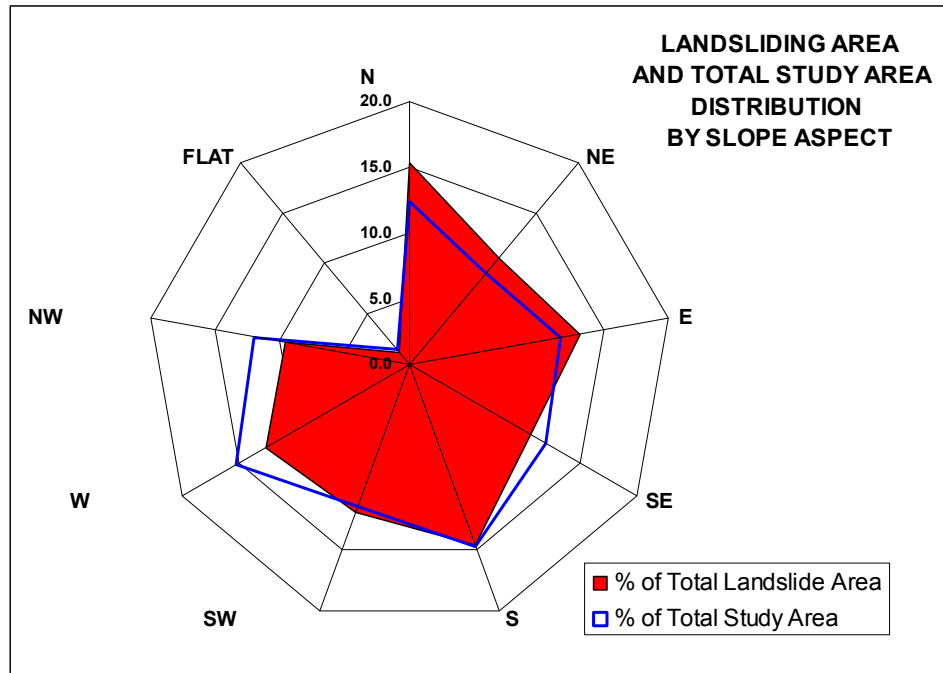


Figure 5.9. Landsliding area and total study area distribution (%) by slope aspect.

### 5.8 Landslide area - lithology / lithology – slope relationship

The propensity of the certain lithological units to be susceptible of landsliding process in the study area is associated with other factors as the topographical position, slope angle and landcover. However, it is necessary to illustrate the “performance” of lithological units in the landslide processes. For instance, Figure 5.10 indicates that most of the landslides occur over granite-gneiss-schist, phyllites-shales and, phyllites-shales- schist lithologies. All of those are hard to soft metamorphic rocks affected by intensive weathering (Ferrer and Lafaille, 2005a), and subsequently having a well developed soil-saprolite profile, which can be highly landslide prone, particularly when it is taking place on broken or steep slopes. Taking into account the spatial scope of the lithological units per landsliding area and over the total area, the best performance in terms of mass wasting resistance is illustrated by the siltstone-shale-limestone-intercalated-layers and granite-pegmatites classes.

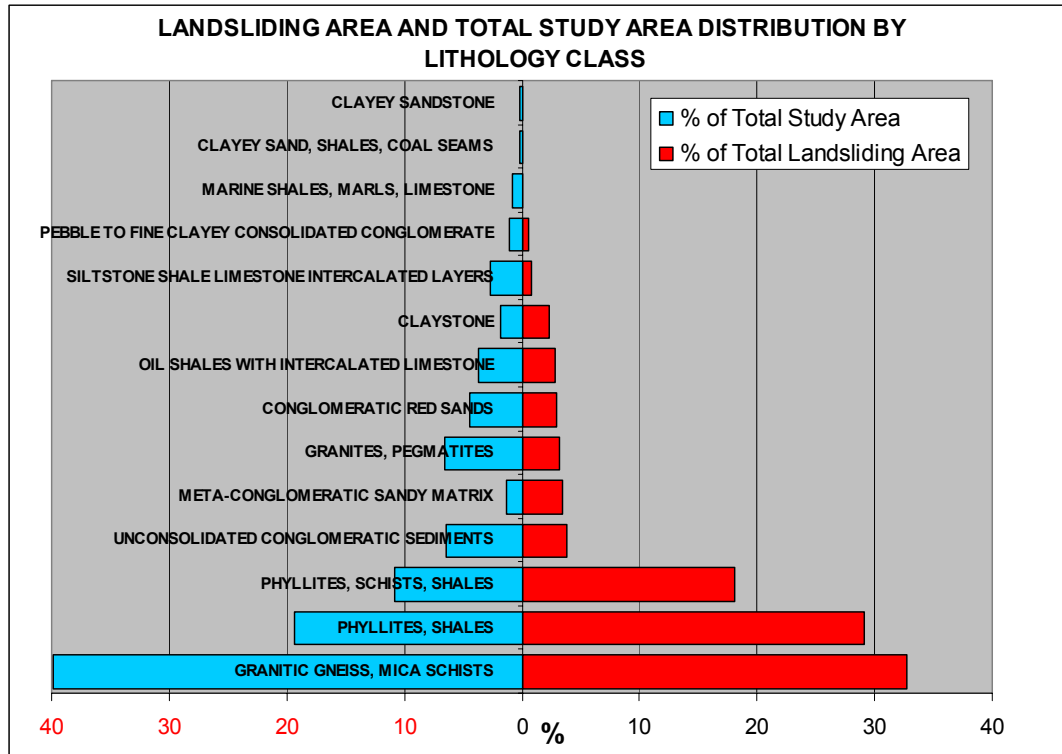


Figure 5.10. Landsliding area and total study area distribution (%) by lithology class.

The impact of the slope angle on the propensity of particular lithological classes to experience landsliding process is illustrated in Figure 5.11. The slope class of 30° — also considered in Figure 5.7, as the main influential slope class in landslide occurrences — dominates the distribution of landslides over two main lithological classes (phyllites-shales and granite-gneiss-schist), however not with respect to the remaining lithological classes. Based in the former, it is possible to state that neither the slope angle nor the lithological units can explain by either themselves or together the overall complexity of the landslide occurrences in the study area.

### 5.7 Landslide area – drainage buffer / lineaments relationship

The drainage factor map was derived from information extracted from the aerial photo-interpretation as well as from the processing of the DEM generated by the performing of the hydrological routine offered by most of the GIS packages.

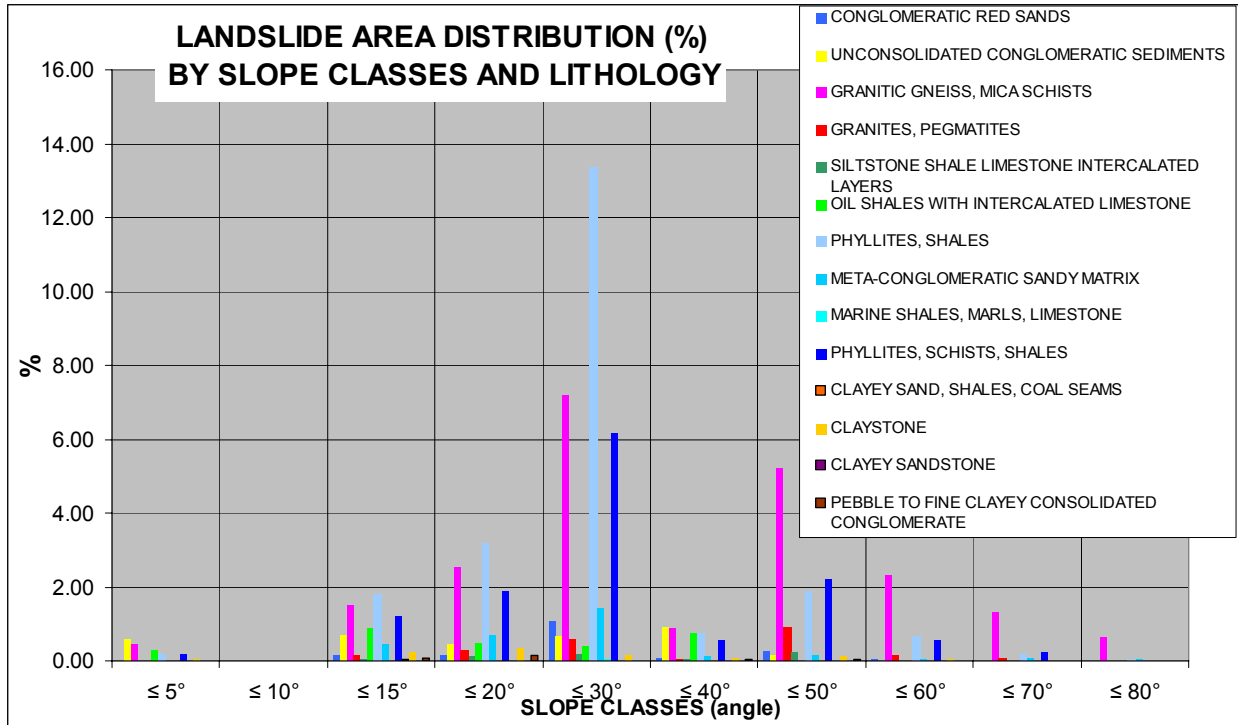


Figure 5.11. Landsliding area and percentage of total study area distribution by lithology and slope classes.

In that way the drainage net was classified in two main classes, one enclosing 3<sup>rd</sup> and higher levels order streams (following the Strahler method, (Strahler, 1997)), and the other enclosing the remaining lower streams orders. Because of the higher erosive potential of the 3<sup>rd</sup> order streams, a 90 m buffer classification was performed for these streams, while for the remaining lower stream orders — considered to have a lesser erosive potential— a 45 m buffer was assigned. From Figure 5.12 it can be observed that the <90 m river buffer class is more significant for landsliding processes given its greater capacity for basal erosion, particularly in very entrenched valleys as those found in the Chama River section where many of the landslides were identified by photo-interpretation. In the case of the landslides associated to the <45 m stream buffer class, these tend to be of a lesser magnitude and activity, many of them belongs to spontaneous slides in recently deforested areas as well as in the sub-basin’s upper zones. However, they should be considered important since they contribute not only water but sediment that clogs major watercourses.

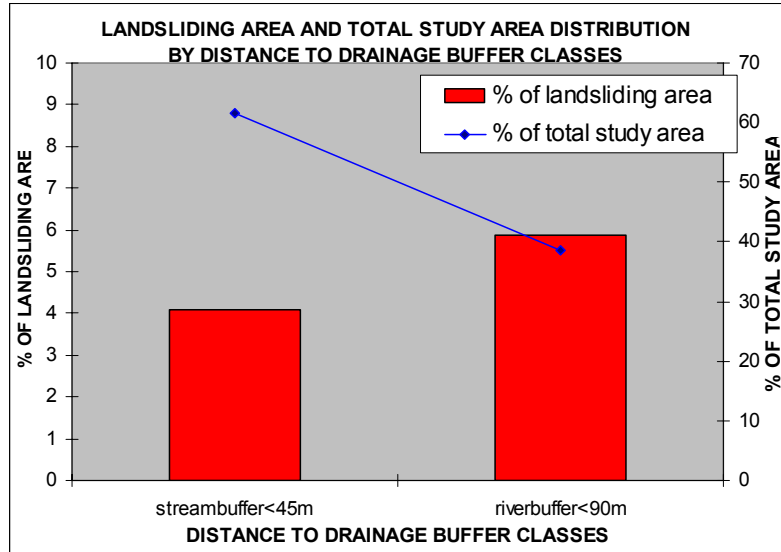


Figure 5.12. Landsliding area and total study area distribution (in %) by distance to drainages.

Also, the statistical relationship between the landslide occurrences and the structural lineaments was explored via the construction of distance buffer classes calculated on both sides of all the fault lines. No distinction in terms of fault activity or magnitude was considered. The Figure 5.13 shows the six buffer classes considered in this analysis and their distribution in the landsliding area as well as within the total study area. It can be observed that these buffer classes do not describe a relevant concentration of landsliding processes within any of them.

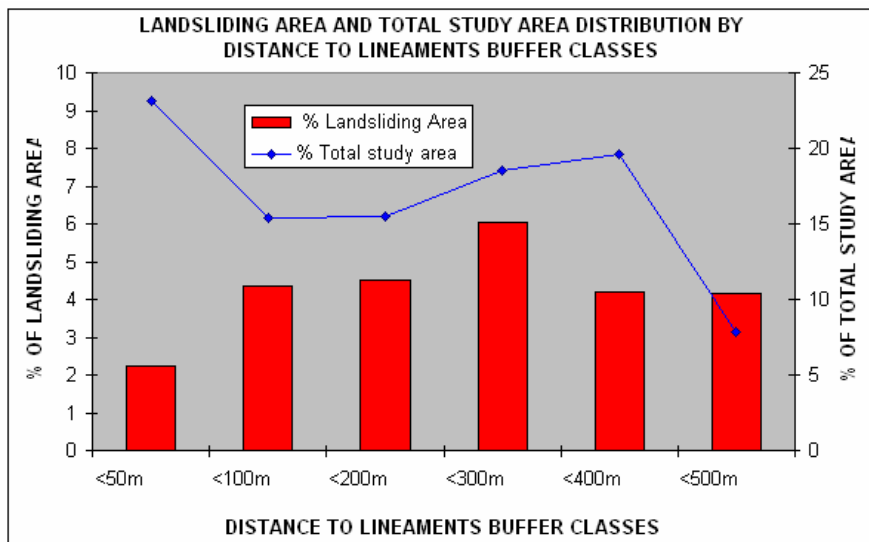


Figure 5.13. Landsliding area and total study area distribution (%) by distance to lineaments.

### 5.8 Landslide area – internal relief relationship

Most of the major landsliding processes in the study area were found in zones with high internal relief, given the general assumption that increasing internal relief can result in a more sensitivity to landslide incidences. As expected from a young mountain environment with a broken relief, most of the total area (Figure 5.14, blue line), is enclosed in higher internal relief classes. The same behavior is observed in the landsliding area distribution (red bars), particularly the concentration of landsliding process in the classes between 100 m to 200 m of internal relief, which reach a noticeable summit at the <200 m class, considering the magnitude of this class in the whole area.

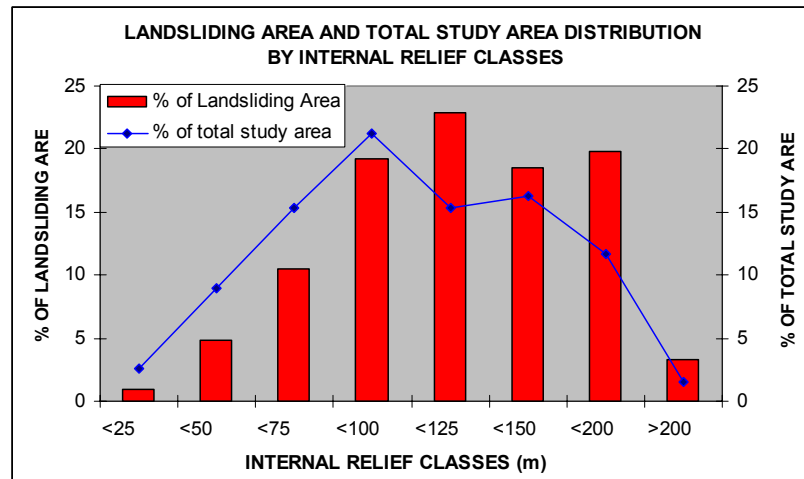


Figure 5.14. Landsliding area and total study area distribution (%) by internal relief classes.

However, it is possible to assume that not necessarily higher internal relief classes drives all landslides since the lithological resistance of some igneous-metamorphic outcrops like those found in the upper páramo section (Figure 5.5) despite being characterized very broken topography with internal relief classes over 200 m show a low density in landslides; some limestone wall and escarpments found elsewhere in the other basin section, appear to be more consolidated given the high vegetation density covering it and subsequently less prone to mass movements. A good example of the influence of internal relief as a landslide prone factor can be found in the Chama River middle section (Figure 5.5). Here the very steep slopes alongside the watercourses define large corridors of cliffs prone to rockfall and easy erosion.

5.9 Landslide area – Geomorphometric classes relationship

Geomorphometry, as stated by Evans (1981), is the measurement and analysis of the geometric characteristics found in the topography and applicable to any continuous rough surface. A better description on the building of the geomorphometric factor map for this study is displayed in Chapter 6. In this analysis a comparison to the landslide distribution map was performed in order to estimate which geomorphometric classes could be more landsliding prone. From Figure 5.15, classes representing landscape shapes as steep-slope and colluvial-slope are associated to most of the landsliding. Steep slopes are a major extensive feature in mountain environment, and generally colluvial slopes are associated with steep slopes since they occur at the transition between the steep slopes and the valleys; therefore, most of the landslides occurring at the steep slope sections will affect the colluvial slopes. Another interesting geomorphometric class affected by landslides (but more related to slope shape) is the pit class. This class that is expressed mainly by linear concavities found in the study area and it is associated also to the 90m drainage buffer class, since is at this section is where the most of the concave slope profiles are found in the study area.

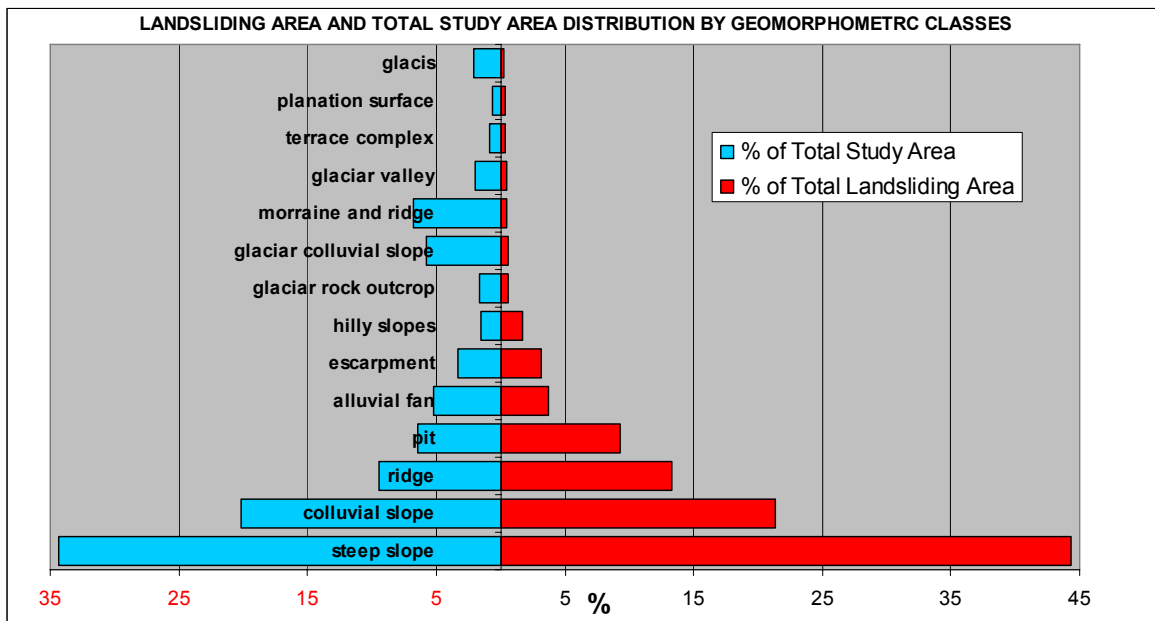


Figure 5.15. Landsliding area and total study area distribution (%) by geomorphometric units.



### 5.10 Landslide area – Holdridge's life zone system relationship

Landcover is a very important factor for landsliding process because of the protective character of the vegetation on the soil profile. It is generally accepted that a densely vegetated area is less prone to mass movements than an bare area. In order to define the average status of the landcover in this study area, a classification based in the Holdridge system was applied.

The Holdridge System defines relatively equal and comparable ecological units called life zones (Holdridge, 1967; Lugo et al., 1996). These life zones are identified using a triangular matrix whose axes represent the variables of biotemperature, precipitation, and potential evapotranspiration ratio; basic variables as temperature and precipitation per station from the study area for a 30 years period were available, allowing the application of this system in the study area. Later, a NDVI product from the same Landsat TM imagery used for the contrast-widening procedure was added to the final classification in order to improve the modeling and representation of the study area life zones. Hence, that the Holdridge's life zones product obtained in this analysis can be considered not only as climatic divisions that define conditions for ecosystem functioning but also as a landcover product. Appendix 7.6 illustrates the procedure followed to delineate the Holdridge life's zones in this study.

Figure 5.16 displays the relationship between the classes of the Holdridge's life zones factor map with the landslide inventory map. At a first glance it is very noticeable the concentration of landsliding process along the subtropical-premontane-dry-shrubland and subtropical-premontane-dry-woodland classes as well as the decisive presence of landslides in the subtropical-premontane-bare-soil class. On the other hand, the subalpine-rain-wooded-grassland instead of its considerable distribution on the whole area, shows an almost absence in the landsliding process. Temperate-montane-cloud-forest considered in this classification the most extensive life zone class, encloses a moderate incidences of landslides, which confirm the protective character of the vegetation cover.

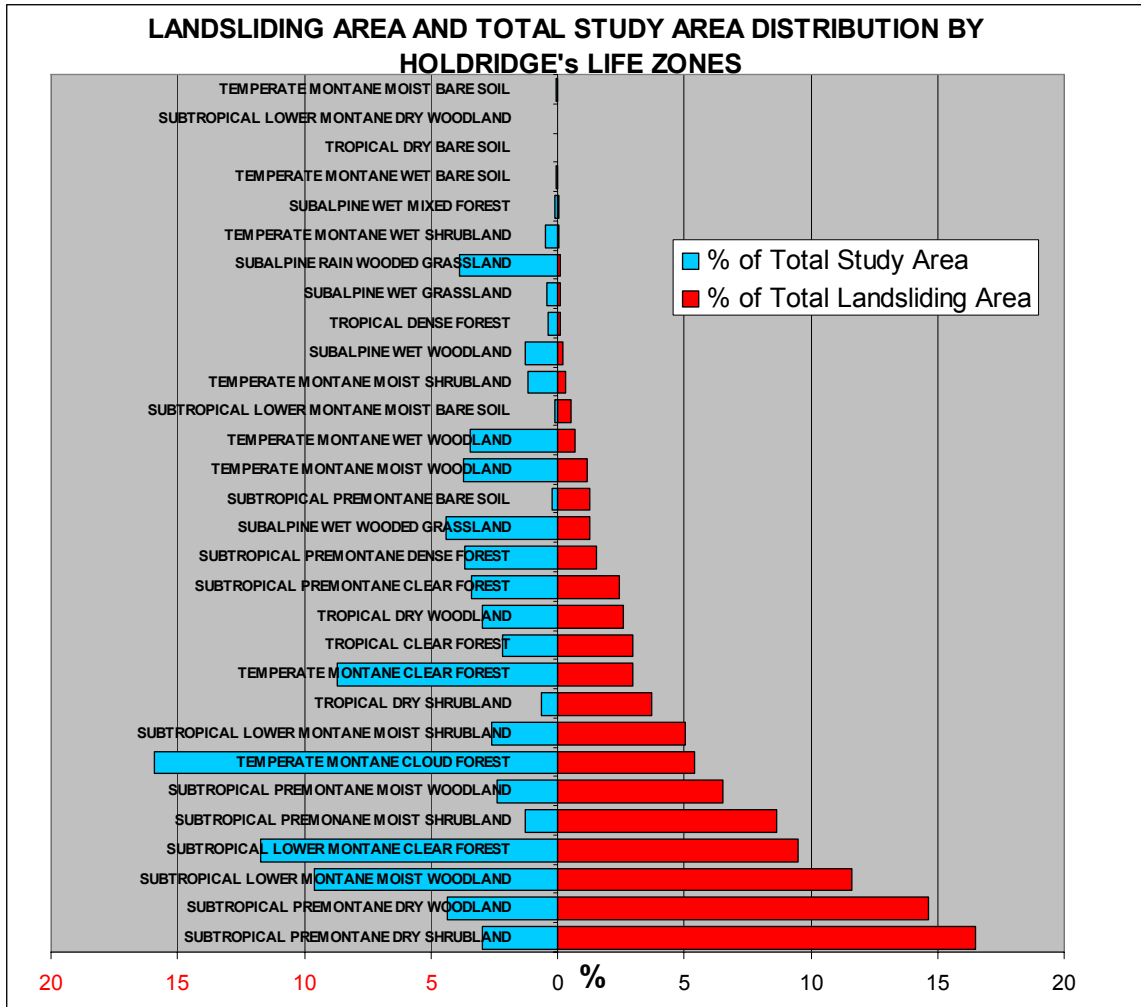


Figure 5.16. Landsliding area and total study area distribution (in %) by Holdridge's Life Zones.

### 5.11 Landslide area – Geomorphological units relationship

The main difference between the geomorphometric and the geomorphological factor maps generated for this study is that the first represents a more static landscape whereas the second includes not only geo-forms but its genetic origin (associated to the lithological map), the weathering process affecting them (associated to the Holdridge's life zones), and the topographical position (associated to altitude ranges and DEM). A description about how was made the geomorphological factor map is found in the Chapter 6 of this study. Figure 5.17, shows the distribution of the landsliding area and total study area over the classes extracted from the geomorphological factor map generated for this study and as expected, the classes moderate-denudational-ridges-and-

tops, moderate-denudational-hills, denudational-steep-slopes, escarpment and denudational-hills; concentrate most of the landslides incidences.

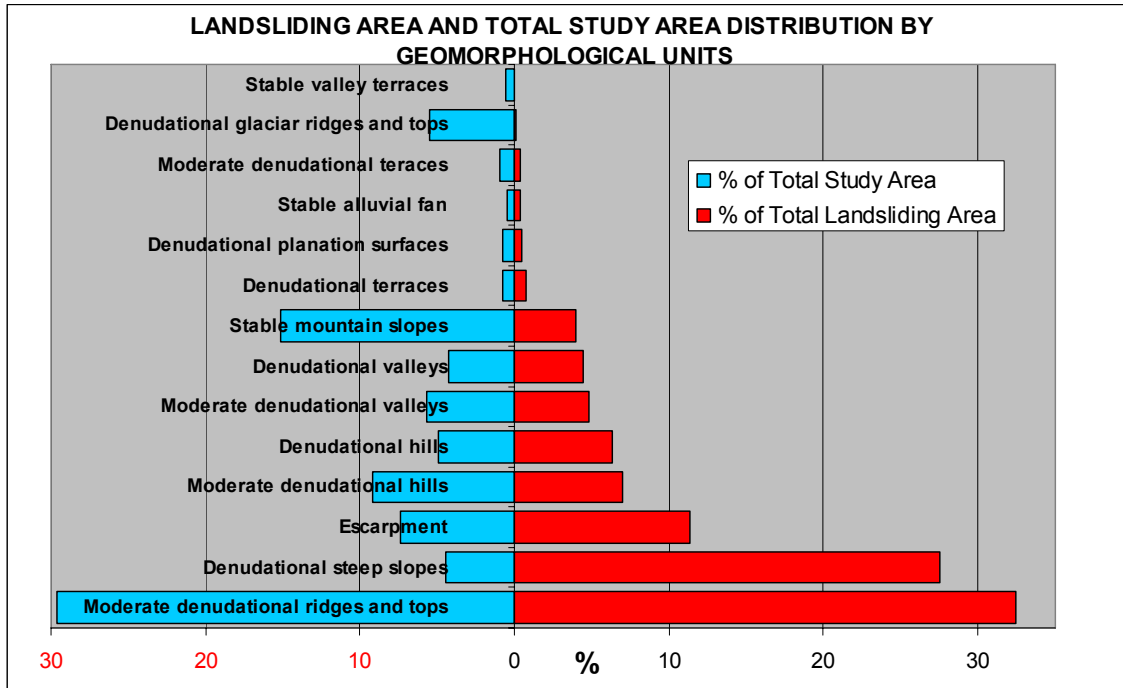


Figure 5.17. Landsliding area and total study area distribution (%) by geomorphological units.

Conversely the stable-mountain-slopes class displays a moderate concentration of landsliding area in spite of its stable character, which could be explained because this geomorphological class encloses most of the temperate-mountain-cloud-forest class (Figure 5.17), considered a priori a stable environment but however affected by spots of landsliding process.

### 5.12 Landslide – factor maps analysis by area density

A density analysis index provides the researcher with a preliminary approach about the role played by every factor/class map in landslide generation over the study area based in the overall landslide density of the study area as a common denominator. Products expected from this density analysis are: A distribution curve of cumulative density analysis values per number of classes and subsequent tables describing the factor maps, and classes sorted in descending order following its importance in landslide incidences. All the 118 classes contained within the 11 factor maps used in the previous statistical relationship analysis were used to compute the density analysis. Those factors map are

the layers related to: Slope angle, shape and aspect classes, altitude ranges classes, lithology classes, drainage and lineaments buffer distance classes, geomorphological units, geomorphometric classes, internal relief classes and Holdridge life's zones map. This factor analyses index measures whether landslides within a class are over or under represented and it is expressed in percentages. The formula for this index is:

$$Da = 100 \left( \frac{N_{\text{pix}}(sxi)}{N_{\text{pix}}(xi)} \right) - 100 \left( \frac{N_{\text{pix}}(\text{total landslide area})}{N_{\text{pix}}(\text{total study area})} \right)$$

where:

$Da$  = Density analyses index

$N_{\text{pix}}(sxi)$  = Amount of pixels with landslides in class  $i$

$N_{\text{pix}}(xi)$  = Total amount of pixels in class  $i$

$N_{\text{pix}}(\text{total landslide area})$  = Total amount of pixels with landslides in the study area

$N_{\text{pix}}(\text{total study area})$  = Total amount of pixels of the study area

A  $Da$  positive with higher values indicate an overestimation of the landsliding process in the evaluated class, which means that the class is an important key in the generation of landslides. On the other hand, negative  $Da$  values indicate that the landsliding process is under represented in the assessed class, suggesting that that class is not important in the generation of landslides. In order to facilitate the interpretation of the factor analyses index along the classes, a cumulative curve of those values per class number was built (Figure 5.18), then points of inflexion in the curve were inferred as thresholds to classify the 118 classes in four new classes (Very high, High, Moderate, Low) following the level of influence or relevancy of these classes as landslide prone. Appendices 5.4 to 5.7 describe the ranked classes and factor maps involved. The Density analysis index here performed allowed:

1.- The computation of the level of influence of each class in the landsliding process of the study area based in the density of the landslide occurrences and correlated to the whole study area. Following these results, it was found that the zones classified with an internal relief between 150 to 200 m, have the highest influence in landslide generation, while the class denudational ridges and tops, belonging to the geomorphological units factor map, displays the lowest level of influence.

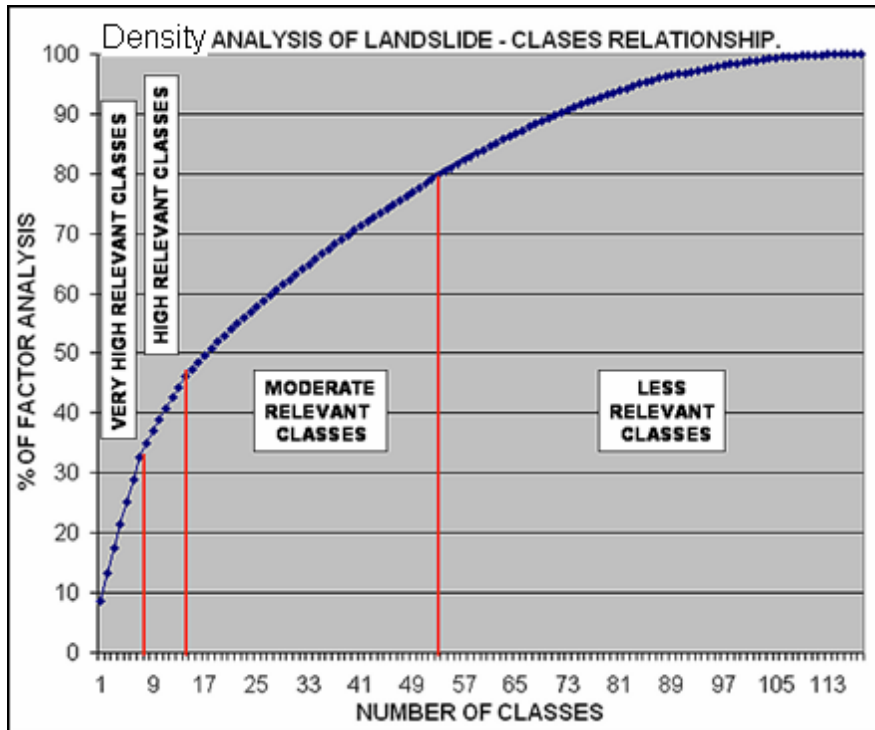


Figure 5.18. Distribution of the cumulative density analysis values per class number. The classes have been previously arranged by its factor analyze value in descending order.

However certain geomorphological classes as denudational steep slopes, was considered as the third class associated with the landsliding process. Hence, the importance of the computing of every class instead of factor maps to determine levels of influence related to the landslide occurrences. From these results is noticeable the dominance of classes from the Holdridge's life zone map among the classes considered as high to very high relevancy in the landslide occurrences, particularly life zones featured to have low vegetation covers.

2.- The aggregation of the classes into a new four level classes following the level of association to landslide occurrences as depicted in Appendixes 5.4. to 5.7.

3.- The weighing and ranking of the factor maps following a total density analysis index obtained from the algebraic summation of the class indices aggregated per original factor map. In that way, the level of association of each factor map to landslide occurrences is defined. These values are described in Table 5.1 and depicted in Figure 5.19. The highest level of influence of the classes belonging to the Holdridge's life zone and internal relief factor maps in the landsliding process contrast with the poor association of the landslide

occurrences and the lithology classes, except for the Meta-conglomeratic-sandy-matrix class which is ranked as a high relevant class.

Table 5.1. Density analysis index aggregated per factor map

RANK	FACTOR MAPS	$\Sigma(DA)$	RANK	FACTOR MAPS (cont.)	$\Sigma(DA)$
1	HOLDRIDGE LIFE'S ZONES	64.2	7	DRAINAGE BUFFER	1.1
2	INTERNAL RELIEF	28.9	8	SLOPE SHAPE	0.1
3	ALTITUDE RANGES	7.2	9	SLOPE ASPECT	-0.1
4	GEOMORPHOLOGICAL UNITS	3.7	10	LITHOLOGY	-7.4
5	LINEAMENTS BUFFER	3.2	11	GEOMORPHOMETRIC	-11.8
6	SLOPE CLASSES	2.6			

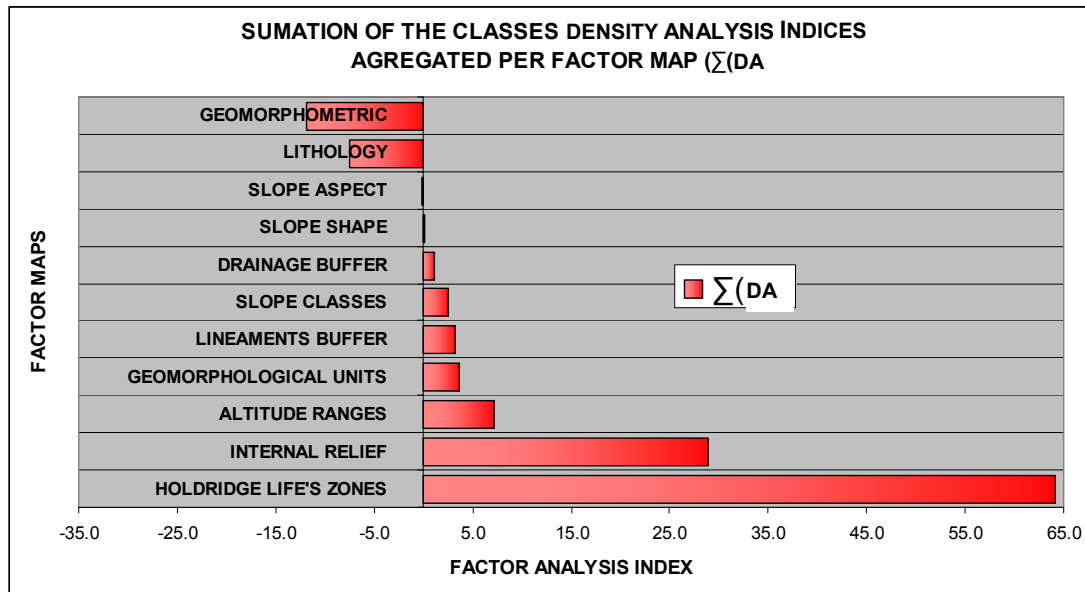


Figure 5.19. Distribution of the aggregated class indices per factor map.

Although the performing of the density analysis index allows a helpful exploration on the relationship between the landsliding process and the set of available geographical factors in the study area; this analysis cannot be considered definitive since it is largely based in descriptive statistics, so it can be suitable only as a first approaching since the complexity of the geomorphological processes generally asks for more refined techniques as those to be developed in the incoming chapters.

## Chapter 6: The Geomorphological, Multicriteria evaluation (MCE) and the Probabilistic approaches

### 6.1 The Geomorphological approach. Hierarchical structure and diagnostic factors

In a general overview, the geomorphological approach to landslide hazard zonation is the reclassification of a previous and very detailed geomorphological map or fieldwork survey within different landslide hazard classes (van Westen, 2003). To construct this detailed geomorphological legend the first thing to do is to separate the landscape and the landforms into several classes or domains, dividing it into smaller terrain units with similar properties. Methods proposed to achieve a suitable landscape partition for landslide hazard zonation vary following the space-mapping concept, in that sense Huabin et al., (2005), recognizes grid cells, unique- condition units, slope units, topographic units and terrain mapping units.

Given that each unit has a set of ground conditions that are different from its adjacent units (Hansen, 1984), a mapping unit represents a landscape portion that maximizes intra-unit homogeneity and inter-unit heterogeneity, representing a geomorphologic hierarchical classification as proposed by Meijerink (1998). Table 6.1.1, summarizes the geomorphological hierarchical structure and the diagnostic factors applied in this analysis and Figure 6.1.1 a flowchart of the procedure.

Table 6.1.1. Hierarchical structure of the TMU and TMsU and diagnostic factor applied. After Meijerink (1998).

<b>LEVEL OF COMPLEXITY</b>	<b>DIAGNOSTIC FACTORS</b>
Terrain Mapping Complexes	Morphogenesis
	Main Relief
	Main Landform
Geomorphological Units	Morphogenesis
	Lithology
	Overall Geomorphic Process
Terrain Mapping Units (TMU)	Internal Relief
	Detailed Geomorphological Settings
	Geomorphological Process
Terrain Mapping Subunits (TMsU)	Geomorphometry
	Detailed Geomorphic Process
	Landuse

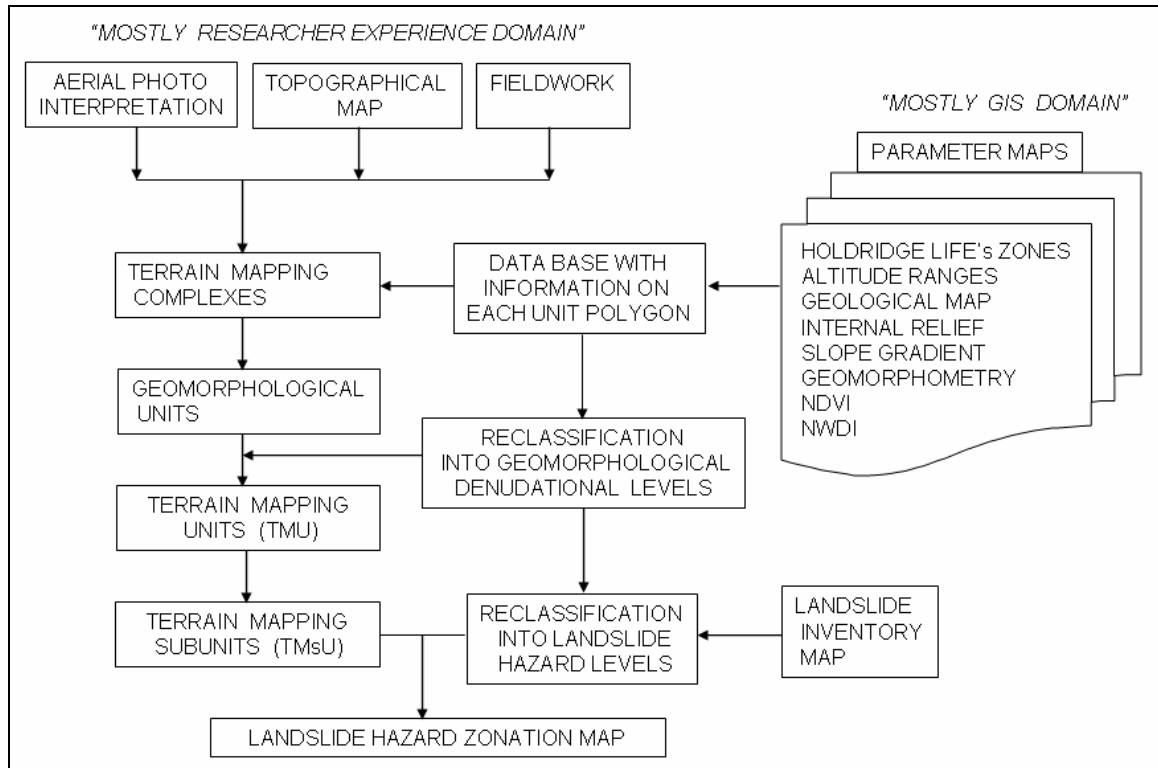


Figure 6.1.1. Landslide hazard zonation heuristic geomorphological approach methodological flowchart.

### 6.1.1 The Terrain Mapping Complexes

Basically, the physiographical settings of the study area are given primarily by the structural orientation of its geological units, which were lately reshaped by the accumulation / denudation processes related to past climatic events and the present high rates of tropical weathering. The NW-SE orientation of the Cordillera de Mérida is geographically expressed not only in the trends of the mountain ranges but in the main longitudinal valleys where the accumulation process is permanently nourished by the high erosive rates that takes place in the transversal intramountain valleys. By overlaying and combining of the factor maps, a classification of the study area in five main terrain complexes was derived which are described in Table 6.1.2 and displayed in Figure 6.1.2.



Table 6.1.2. Source data and criteria layers used to map the diagnostic factors involved in the definition of the study area terrain mapping complexes.

LEVEL OF COMPLEXITY	DIAGNOSTIC FACTORS	CRITERION MAP	SOURCE DATA
Terrain Mapping Complexes	Morphogenesis	- Altitude ranges - Holdridge Life's zones	- Field work - DEM - Temperature and precipitation distribution - Landsat imagery
	Main relief	- Internal relief	- Field work - DEM
	Main landform	- Slope	- Field work - DEM

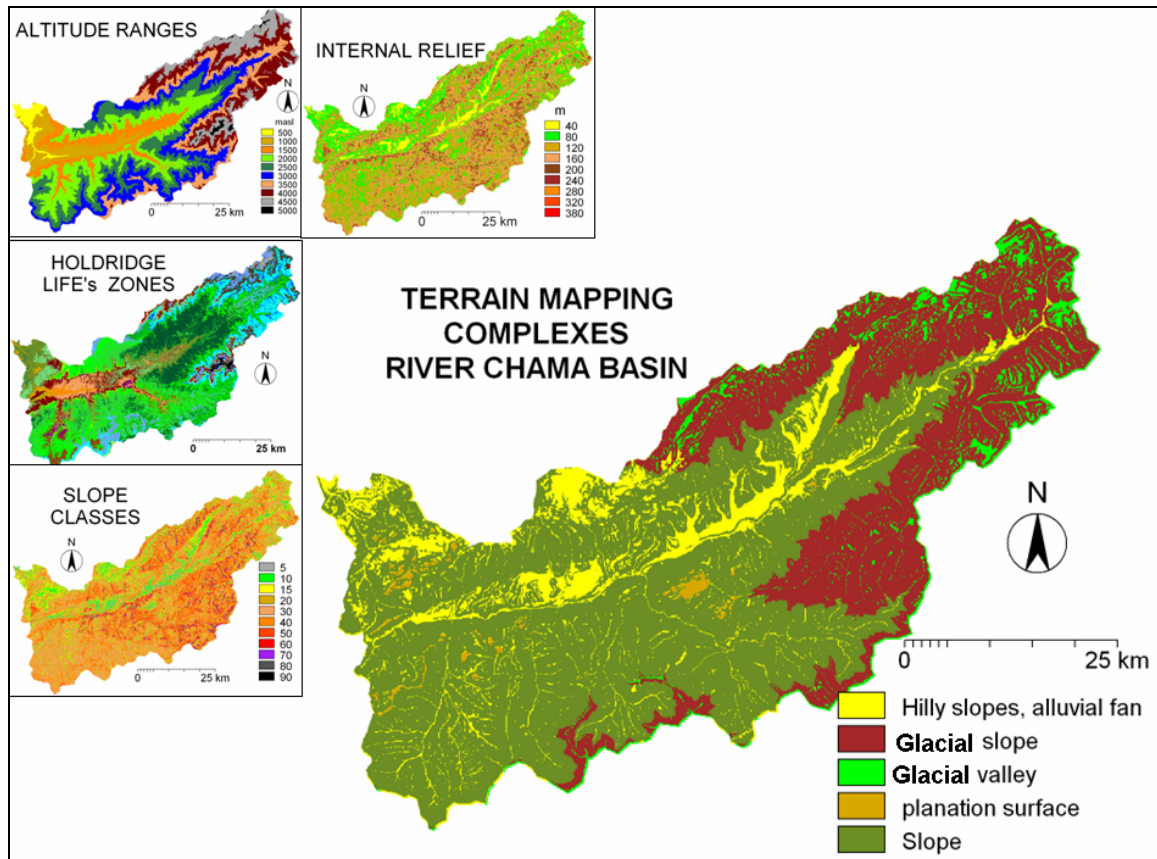


Figure 6.1.2. Study area final terrain mapping complexes classification and related layers used in the process.

### 6.1.2 The Geomorphological units. Factors

The most important map in the landslide hazard assessment, besides the landslide inventory map, is a geomorphological map. This type of map figures prominently in many of the analytical techniques (van Westen, 1994), and it also offers a more generalized perspective than the TMsU layer; thus, included in the statistical approach given its lesser subjectivity and higher potential for lending itself to extrapolation.

The geomorphological evolution of the study area has been influenced first by the climate changes during the Quaternary glacial age and lately by neo-tectonic activity (Schubert, 1980). Past processes have been characterized by successive cycles of accumulation and strong denudation, particularly concentrated along the river valleys, where it is possible to define different topographic levels of terraces which are related to also different periods of accumulation / denudation. The former terrain complexes layer is the first input to define geomorphological units, together with the altitude ranges, slope and Holdridge life's zones layers. However the level of analysis increases with the adding of new layers as the geological and the landslide inventory map. Table 6.1.3 describes the criteria layers representing the geomorphological diagnostic factors used to define the geomorphological units layer (Figure 6.1.3).

Table 6.1.3. Source data and criteria layers used to map the diagnostic factors involved in the definition of the study area geomorphological units.

<b>LEVEL OF COMPLEXITY</b>	<b>DIAGNOSTIC FACTORS</b>	<b>CRITERION MAP</b>	<b>SOURCE DATA</b>
Geomorphological Units	Main physiographic units	-Terrain mapping complexes	- Field work - DEM - Temperature and precipitation distribution - Landsat imagery
	Detailed morphogenesis	- Altitude ranges - Holdridge life's zones	- Field work - DEM - Landsat imagery
	Lithology	- Geological map	- National atlases - Field work - DEM - Aerial photographs
	Overall geomorphic process	- Slope - Geological map - Landslide inventory map	- Field work - DEM - Landsat imagery - Aerial photographs

### 6.1.3 The Terrain Mapping Units (TMU)

The physical aspect of a TMU can be summarized following its main features. When working with a GIS with the overlaying of several thematic data layers, two main types of TMU can be created: the typical feature and the unique-condition feature (Lawrence et al., 1993). A typical feature TMU is that one with predictable properties and position over the landscape, such as the slope and topographical units. A unique-condition feature represents isolated, unusual and often very small landscape features, however very

important when it contains attributes which could be desirable or undesirable to a project.

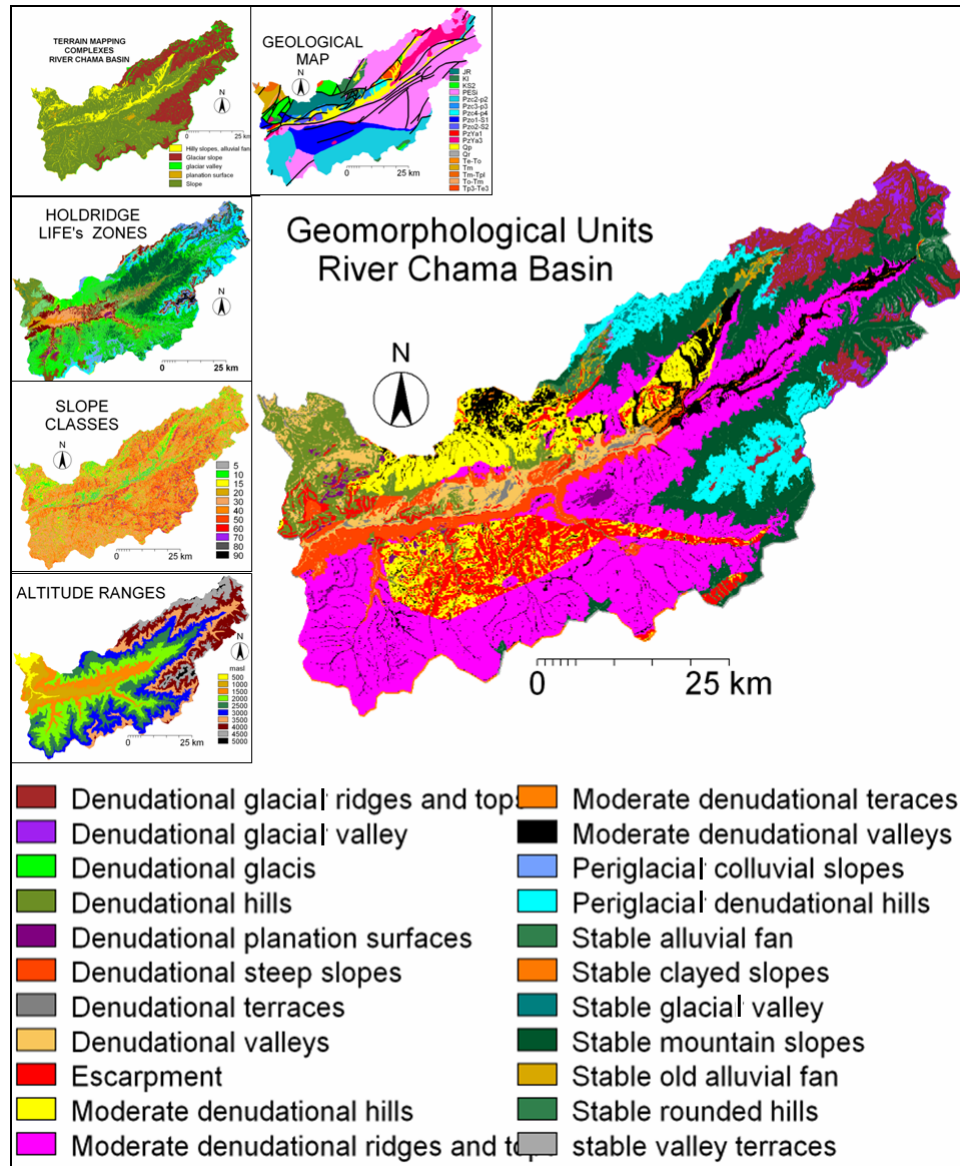


Figure 6.1.3. Study area final geomorphological units classification and related layers used in the process.

Because the procedure to outline TMU in this analysis was largely based in map overlaying and aggregation techniques, the terrain units obtained here are considered to be not only physically based TMU but also functional units aggregated following the researcher's criteria on slope instability, thus these TMU and subunits respond to the unique-condition criterion. The TMU outlined here also contain useful information about the current geomorphological dynamic of every unit (Appendix 6.1), which can be

considered a preliminary assessment of their landslide susceptibility. Figure 6.1.4 depicts the final TMU layer obtained by the use of the criteria layers outlined in Table 6.1.4. Due to the technical impossibility to represent the 253 computed TMU; these are comprised in 30 categories attending their denudational character.

Table 6.1.4 Source data and criteria layers used to map the diagnostic factors involved in the definition of the study area terrain mapping units (TMU).

LEVEL OF COMPLEXITY	DIAGNOSTIC FACTORS	CRITERION MAP	SOURCE DATA
Terrain Mapping Units (TMU)	Geomorphological Units	- Geomorphological units	- Field work - DEM - Temperature and precipitation distribution - Landsat imagery - National atlases - Aerial photographs
	Detailed Geomorphological Settings	- Geomorphic units - Geological map - Slope	- National atlases - Field work - DEM - Aerial photographs
	Geomorphological processes	- Geomorphic units - Landslide inventory map - Slope - Geological map - Holdridge Life's Zones	- National atlases - Field work - DEM - Aerial photographs - Landsat imagery - Temperature and precipitation distribution

#### 6.1.4 DEM and geomorphometry. An Empirical procedure for geomorphometric classification.

A better achievement of the geomorphological approach, asks for the improving of the data input, and this improvement can be reached increasing the quantity and quality of this data. Nowadays, GIS procedures and remotely sensed data, play a crucial role in the updating of the traditional geomorphological approach (Coelho-Netto et al., 2006) for instance, the computing of new algorithms on the study area DEM (Table 6.1.5), allowed the generation of a more consistent geomorphometric factor map, to obtain the Terrain Mapping Subunits (TMsU), key layer in achieving the geomorphological landslide hazard zonation map. The geomorphometric classification produced in this section is still experimental, since it has been applied only to the study area and is largely controlled by the previous fieldwork survey and photo-interpretation analyses discussed earlier.

Geomorphometric forms defined here are described in 13 different classes. Table 6.1.5 describes the factors and criteria used to define the geomorphometric forms and Figure 6.1.5 displays the final geomorphometric map.

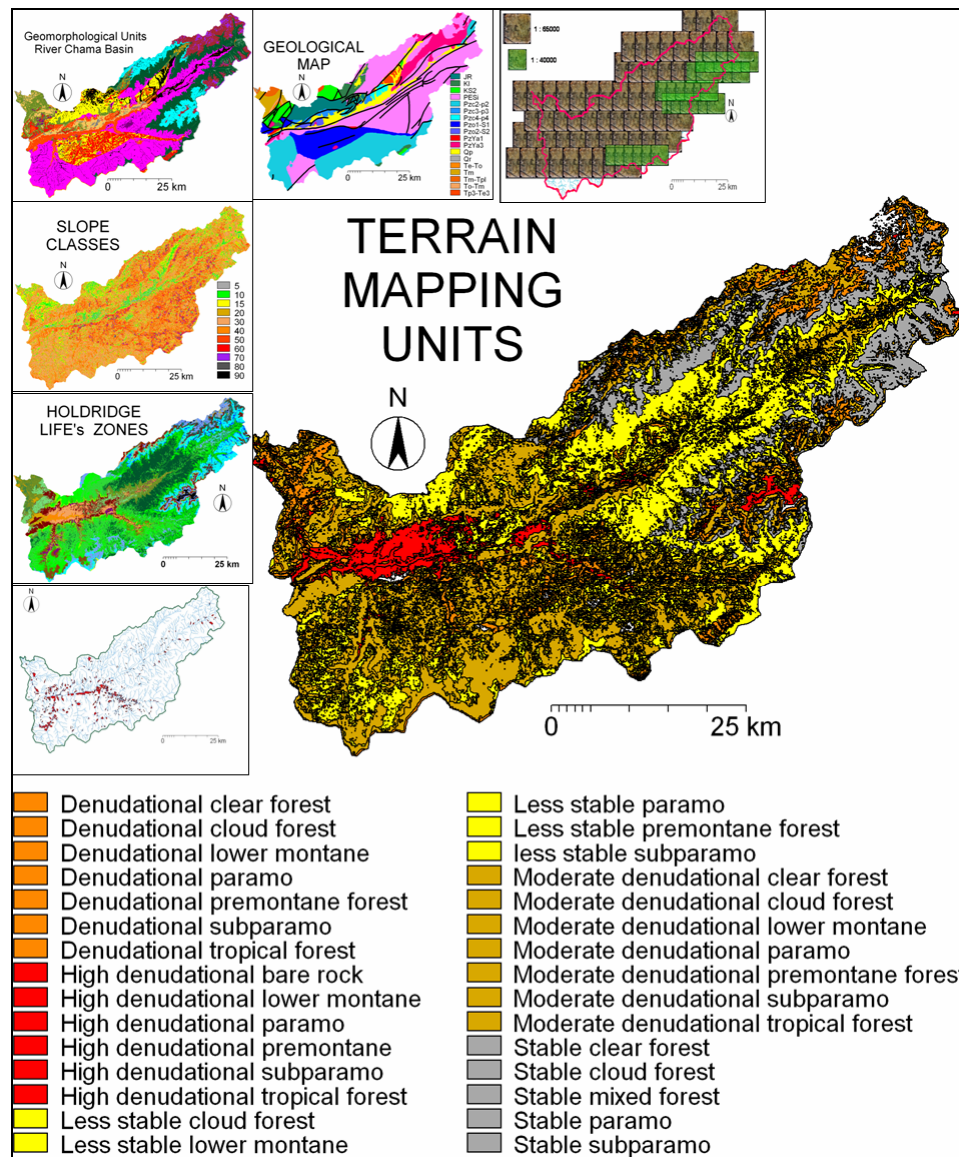



Figure 6.1.4. Study area final TMU classification and related layers used in the process. In order to circumvent the complex representation of the actual 253 TMU polygons, the legend in this figure deals only with the 30 main categories. Appendix 6.1 describes the subcategories used in creating the categories displayed above.

Figure 6.1.6 illustrates the matching between the geomorphometric classification achieved via DEM processing and the ground geofoms as displayed in an aerial-photograph for a periglacial valley in the study area.

Table 6.1.5 Factors and criteria used in the segmentation, delineation, extraction and final overlaying of the geomorphometric forms computed from DEM of the study area (STD = standard deviation, MEAN = mean of the sample, AND - OR connectors = intersection and union respectively).

	FORM	FACTOR	CRITERION	OVER-LAYING ORDER
Glacial forms	Rock outcrops	- Slope angle - Internal relief	Slope $x \geq 40$ AND Inrelief $x \geq \text{mean} + \text{STD}$	UPPER LAYER  LOWER LAYER
	Glacial valley	- Slope angle - Slope shape	Slope $x \leq 12$ AND Long Convex $x \leq \text{mean} + \text{STD}$	
	Glacis	- Slope angle	Slope $12 \leq x \leq 16$	
	Moraine	- Slope shape	Plain Curvature $x \leq \text{mean} + \text{STD}$	
	Glacial colluvial slope	- Slope angle	Slope $16 < x < 24$	
Slope forms	Steep slope	- Slope angle	Slope $x \geq 24$	
	Colluvial slope	- Slope angle	Slope $12 < x < 24$	
	Ridge	- Slope shape	Long Convexity $x \geq \text{mean} + \text{STD}$ OR Plan Convexity $x \leq \text{mean} - \text{STD}$ OR Profile Convexity $x \geq \text{mean} + 2\text{STD}$ OR Cross Convexity $x \geq \text{mean} + \text{STD}$	
	Pit / gully	- Slope shape	Cross Convexity $x \leq \text{mean} - 2\text{STD}$ OR Plan Convexity $x \geq \text{mean} + 2\text{STD}$ OR Profile Convexity $x \leq \text{mean} - 2\text{STD}$	
	Escarpment	- Slope shape - Internal relief	Profile Convex $x \geq \text{mean} + 2\text{STD}$ OR Long Convex $x \geq \text{mean} + 2\text{STD}$ OR Internal relief $x \geq \text{mean} + 2\text{STD}$	
Valley forms	Terrace complex	- Slope angle	Slope $x \leq 4$	
	Alluvial fan	- Slope angle	Slope $4 < x \leq 12$	
	Valley bottom	- Slope angle - Slope shape	Slope $x \leq 4$ AND Profile Convexity $x \leq \text{mean} - 2\text{STD}$	

### 6.1.5 The Terrain Mapping Subunits (TMsU)

Given the unique-condition feature considered for the landscape partition of the study area, there is not a rigorous connection between the units from the TMU layer, to those outlined in the TMsU layer, because at this level the legend of the new units is based on the functional relationship of the factors involved. In that sense, the TMsU procedure could be considered not scientifically consistent but pragmatically useful since its application is directed to a more practical use: How to divide a terrain into homogeneous units for practical applications (van Westen, 1993). From this procedure was possible to get 286 TMsU aggregated in 90 categories (Appendix 6.2). Table 6.1.6, describes the diagnostic factors and criterion maps used to outline the TMsU which are depicted in Figure 6.1.7.

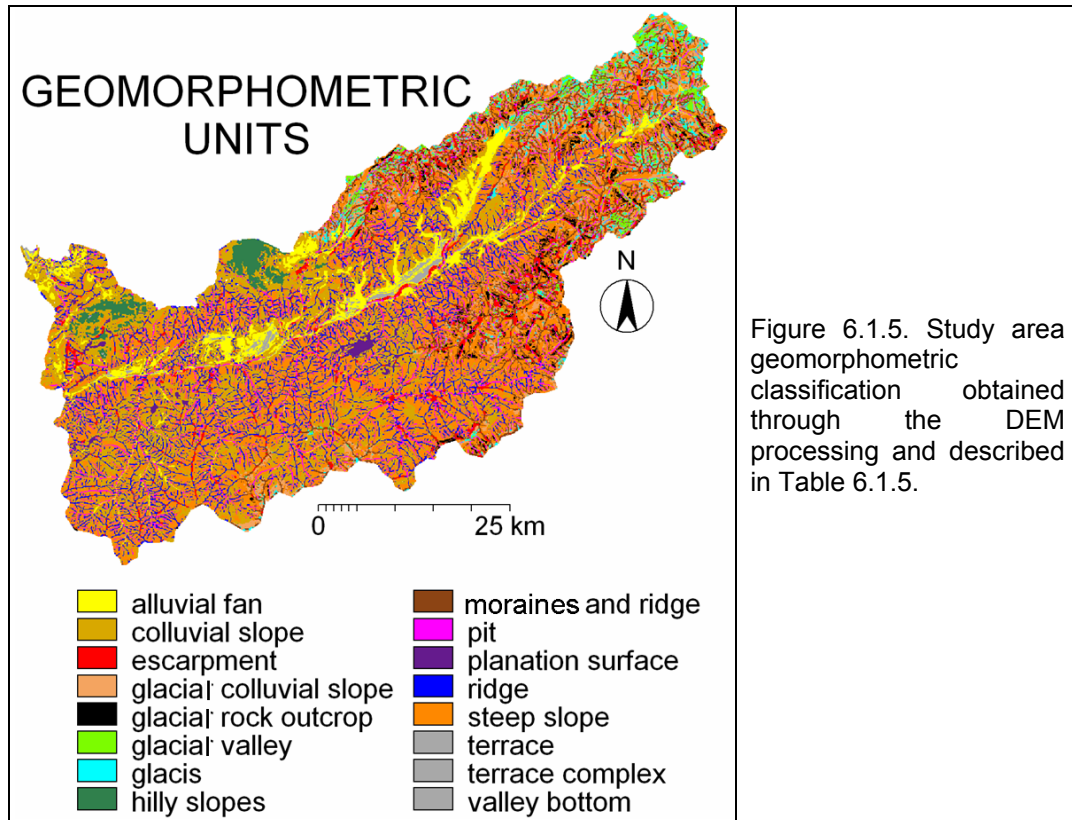


Figure 6.1.5. Study area geomorphometric classification obtained through the DEM processing and described in Table 6.1.5.

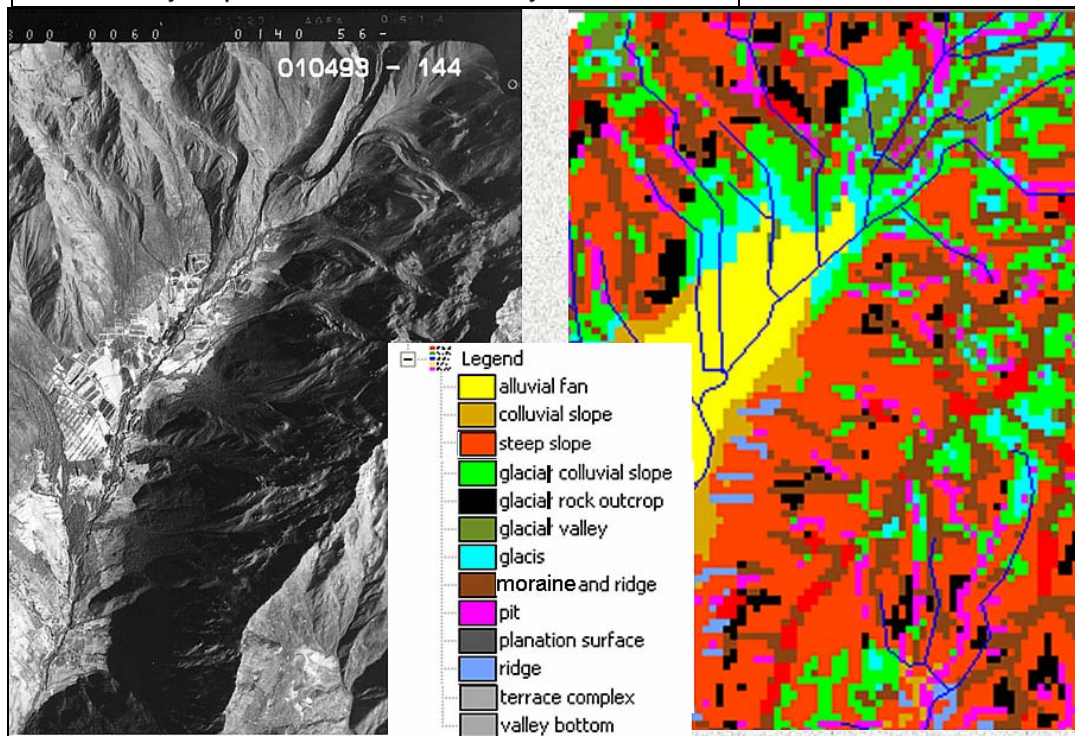
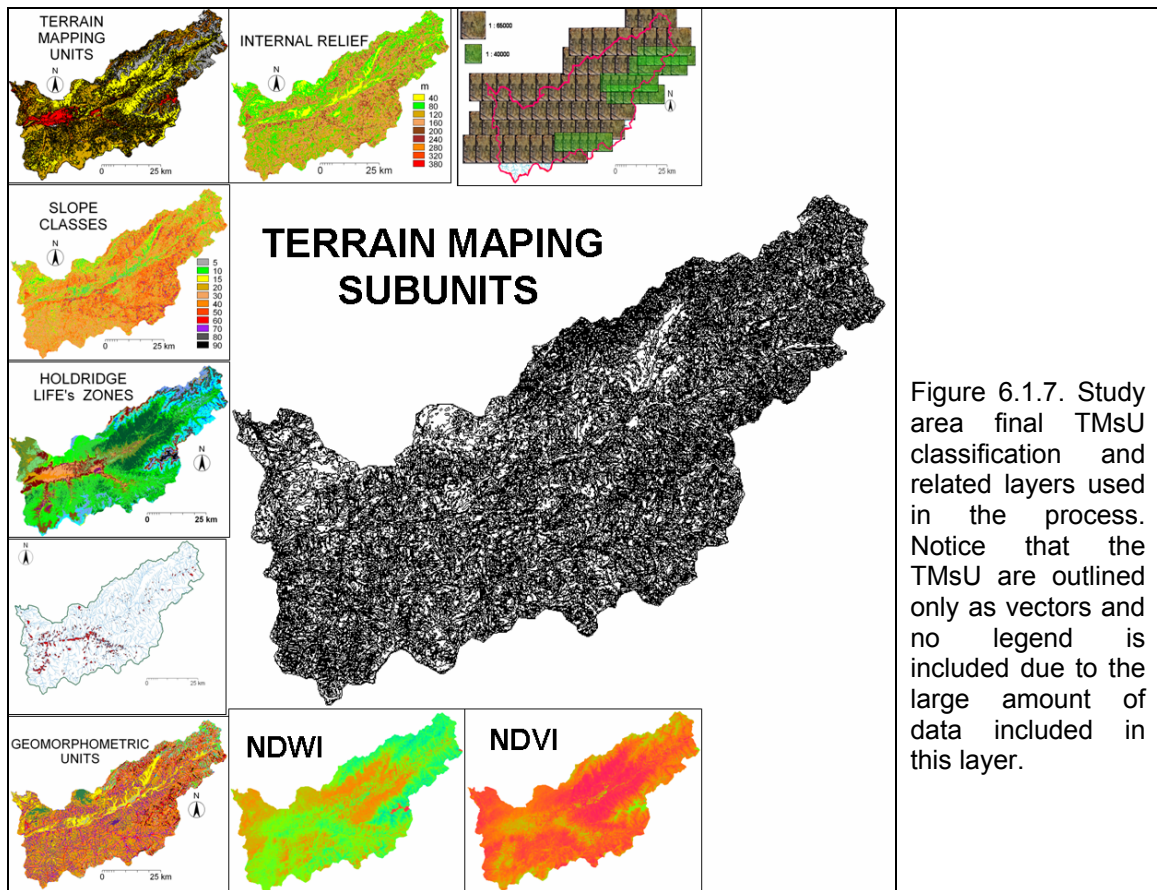


Figure 6.1.6. Visual comparison between the ground geofoms as displayed in an aerial-photograph (left) and their classification in geomorphometric forms (right) achieved through the proposed algorithm (Table 6.1.5) applied to the 90 m study area DEM; notice the delineation of the moraine located at the upper right corner.

Table 6.1.6. Source data and criteria layers used to map the diagnostic factors involved in the definition of the study area terrain mapping subunits (TMsU).

LEVEL OF COMPLEXITY	DIAGNOSTIC FACTORS	CRITERION MAP	SOURCE DATA
Terrain Mapping Subunits (TMsU)	Terrain Mapping Units (TMU)	- Terrain Mapping units (TMU)	- Field work - DEM - Temperature and precipitation distribution - Landsat imagery - National atlases - Aerial photographs
	Detailed Geomorphological Forms	- Slope - Internal relief - Geomorphometry	- National atlases - Field work - DEM - Aerial photographs - Landsat imagery - Temperature and precipitation distribution
	Landcover	- Holdridge Life's Zones - Landslide inventory map - NDVI - NDWI	- Field work - Temperature and precipitation distribution - Landsat imagery - Aerial photographs





### 6.1.6 Classification of the Terrain Mapping Subunits into a landslide hazard zonation map

As explained throughout this section, the partition of the landscape following the hierarchical structure described in Table 6.1.1, and subsequently under a raster GIS platform; allowed the researcher to discern better on the characteristics, spatial distribution and functional relationship of every TMsU becomes clearer in terms of its propensity to landsliding process (Appendix 6.2). Then, is necessary to confirm the “very high hazard” character of the subunits affected by slope instability by the overlaying of the landslide’s scars point map (which is extracted from the landslide inventory map) onto the TMsU layer (Figure 6.1.8). At this point of the procedure, the aggregation of the TMsU into four landslide hazard classes is a simple reclassification of the TMsU categories and subcategories (Appendix 6.2), given its landslide prone character. This procedure is broadly illustrated in Figure 6.1.8 and the final geomorphological landslide hazard map is illustrated in Appendix 7.1.

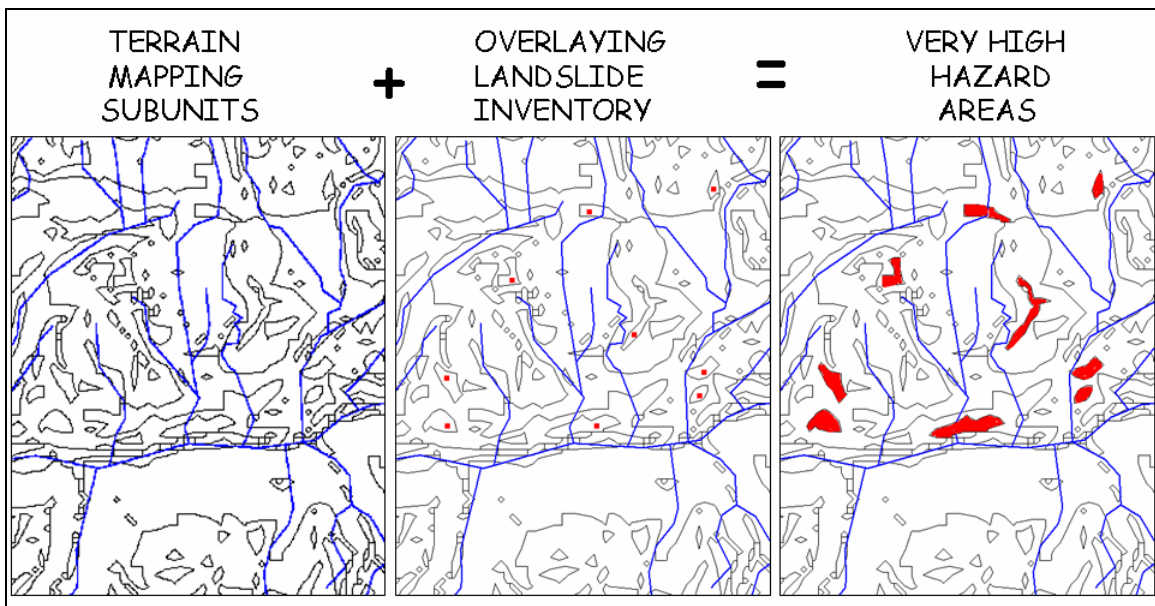


Figure 6.1.8. Ideal illustration of the final step carried out to classify the TMsU into a landslide hazard zonation map. Landslide scars are overlaid on the TMsU layer to define which polygon units encompass what is assumed to be the most susceptible terrain to landsliding process. Surrounding terrain polygons would keep the already classification achieved in the TMU process (high denudational, denudational, moderate denudational, low denudational and stable). The importance of this overlaying is - in most of the cases- the confirmation and/or update of the high denudational character of the terrain subunit under analyses.

Even with the use of GIS, the new information resulting from the map overlaying and aggregation, overwhelms the analytical perception of the researcher, resulting in the

potential to overestimate the hazard classes. For example, Figure 6.1.9 illustrates an emblematic landslide (La Trujillana), from the western part of the study area. In this illustration is observed that not only the actual landslide polygon is classified as a very high hazard class but also the surrounding slopes. This is explained because, although this mass movement is taking place on very defined slopes, the landslide scar occurs within an extensive TMsU which has been already defined as high denudational and landslide prone unit.

To conclude Van Westen et al., (2006), stated, in spite of the increasing popularity of GIS procedures in landslide hazard analyses, data collection by experts remains necessary because of the generally non-availability of landslide inventories as well as thematic geographical information plus the inconsistency and uncertainty encompassed in the current data input.

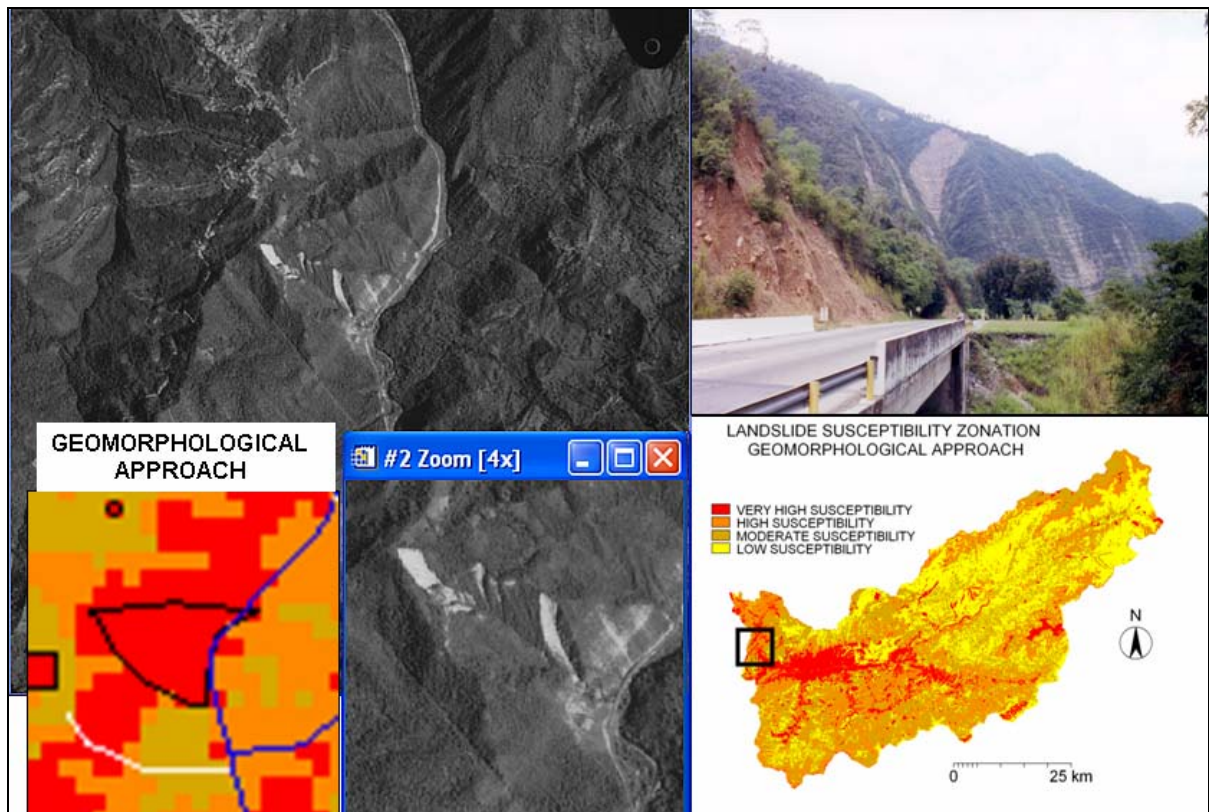


Figure 6.1.9. Overview of La Trujillana landslide and how it is depicted in the aerial photograph and classified at the geomorphological landslide hazard map. A potential over estimation is observed along side the main landslide.

### 6.2 The MCE paradigm. Justification of the MCE for this study. Background

The multicriteria evaluation (MCE) is part of the Decision Theory approach which is oriented in two main frameworks: The descriptive and the normative (Hansson, 1994). The first one rests on the use of logical and theoretical constructions in order to explain and predict the behavior of the criteria involved in a decision process. The normative tries to define the optimal behavior of the analyzed criteria based in a previous “rationality”, which was assumed intuitively from the observed patterns of every criteria involved in a decision process (Harish et al., 2007). Whereas the descriptive framework seeks to define “How does the criteria behave?” the normative one seeks to establish “How they should behave” (Gómez et al., 2005). Since in any geomorphological survey, the perceived importance of each criterion in the landsliding process, directly affects the weighing of all the criteria considered and subsequently the decision-process, a process to determine the relative importance of criteria is required and this process known as the multicriteria evaluation (MCE) (Atkinson et al., 2005). The MCE can be achieved using the Analytical Hierarchy Process (AHP) method.

Jankowski (1995) classifies the multicriteria evaluation methods based on the aggregation procedures used to integrate the assigned values of the criteria and priorities considered in a case study. In that way, the AHP is considered a normative, additive and compensatory technique, which matches the heuristic approach generally applied in geomorphological assessments. Decision theory approach and the MCE methods have not been adapted fully to geomorphological research (Gomez et al., 2005). Moreover, maps can only play a limited role as decision support tools in such analyses (Jankowski, 2001). Hence, any justification and outcomes of its applicability and success must be found in empirical analyses like those performed in Eastman et al., (1995), Barredo (1996), Malczewski (1999), Huang et al., (2003), Jiang et al., (2000), and Atkinson et al., (2005).

#### 6.2.1 Integrating MCE into GIS

The analytical gaps found in the GIS related to the integration of MCE into them have been circumvented at some level by GIS prototypes. Examples are as those ILWIS and IDRISI packages from the ITC and Clark University respectively, which already have modules to address MCE.

Since inductive and deductive analyses in geomorphological surveys have been widely accepted, generally the geomorphological evaluation of a landslide problem begins with the discrimination and definition of the geographical variables involved into the process, and then, the modeling of the found patterns becomes a matter of the researcher's expertise, technical availability and methodological tools to process the data collected. In that sense, taking into account the recommended general trend to apply in MCE for geographical analyses elaborated by Gomez (2005) after Malczewski (1999) in this analysis the MCE-GIS integration is applied following Table 6.2.1.

Table 6.2.1. Comparison between MCE – GIS integration steps in a geographical case of study.

<b>Gomez (2005) (general trend)</b>	<b>This study</b>	
Definition of the problem	Description of the landslide event	Discrimination of the process involved in the event
Definition of alternatives and criteria modeling		Selection of the environmental factors related to the process
Elaboration of the Decision Matrix	MCE modeling of the landslide susceptibility and hazard	Selection and production of the cartography representing those factors
Selection of the evaluation methods		Normalizing of the cartographic layers
Selection of alternatives		Weighing of those layers
Sensitivity analysis	Validation	Layer integration
Explanation and recommendations on the products		Consistency index (CI) and consistency ratio (CR)
		Map comparison: actual landslide distribution vs. predicted hazard areas

### 6.2.3 The Analytical Hierarchy Process (AHP)

The AHP is a logical and structural framework that allows the identification and modeling of the factors implicated in the landsliding in a way that facilitates the detection of mass movement prone areas and final classification of the study area into different landslide hazard levels. This process is carried out by the:

- Identification of the criteria involved in the landsliding process.
- Decomposing the problem into a hierarchical structure of factors, processes and criteria.
- Normalization of the criteria data layers. The method to use in this analysis is the Maximum Value Ranking method (Jiang et al., 2000).

- Ranking the importance of the criteria. In this analysis this step is carried out by pairwise comparison, which is explained later in this chapter.
- Computing and aggregation of the reciprocal and normalized matrices to calculate the Priority Eigen Vector (PEV), which is used to compensate the value of every criterion layer prior to its final integration in the final landslide susceptibility map.
- Validation of the statistical procedure via Consistency Index (CI) and Consistency Ratio (CR). This last step requires computing the Maximum Eigen Value (MaxEV) from the normalized matrix, and is a measure of the consistency and reliability of the judgments applied in the pairwise comparison.

#### 6.2.4 Definition of the processes involved in the landsliding process

Intensive rainfall, seismic shaking, volcanic eruption and basal erosion, are considered triggering factors and their occurrences over certain areas can generate any of the three main landslide processes (Cruden et al., 1996), such: 1) landsliding by the increasing of the shear stresses; 2) landsliding by the lowering of the strength and; 3) landsliding by reducing the material strength.

Several researches (Ferrer et al., 1999, 2003, 2005a,b), in the Venezuelan Andes and other tropical mountain environments (Coelho-Netto, 2006), associate the landsliding process to the increasing of the shear stresses via removal of support and uplift due to the basal erosion and neotectonic processes respectively. Ferrer, (2005a) recognizes the main role played by the lowering of the strength in the material and mass characteristics caused by the schistose texture of the metamorphic rocks outcropping in the study area. Together with the lithological aspect and steep slopes, these factors are favoring the mechanical and chemical weathering and subsequent generation of extensive layers of saprolite susceptible to slope failure. Precipitation is likely the main triggering factor in the landsliding process for the study area.

The mass movement events in the study area can be analyzed in factors, processes and criterion. Factors represent the main parameters and properties contributing to the landsliding process while processes describe different stages of the event. Processes become the interaction framework of the factors previously defined. Criteria are the pragmatic unity to indirectly evaluate the process magnitudes. Table 6.2.2, describes the

factors –conceptually defined-, the observed processes and the associated criteria. The criteria definition is narrowly related to the data availability for instance, this analysis is largely spatial and remote sensed oriented, then most of the considered criteria were obtained through this kind of source.

Table 6.2.2. Main factors, processes and criterion involved in the study area landsliding process.

		FACTORS		PROCESSES	CRITERION
RUPTURE ZONE		PRECIPITATION	Intensity, Duration, Frequency.		
			Seasonality		
		BASIN HYDROLOGY	Area	RUNNOFF	ALTITUDE RANGES
			Infiltration		
	TRANSPORT ZONE	SUSCEPTIBILITY TO LANDSLIDE AND EROSION	Morphology	ROCK FALL	GEOMORPHOLOGY
			Slopes		GULLY, RILL EROSION
			Geology	CREEPING	SLOPE GRADIENT
			Saprolite		LITHOLOGY
			Land cover		
			DETRITUS SOURCE AND PROPERTIES	Material size and mobility	DEEP LANDSLIDES
				SHALLOW LANDSLIDE	HOLDRIDGE LIFE's ZONES
ACCUMULATION ZONE	FLOW CORRIDORS	Geometry	DEBRIS FLOW	LINEAMENTS BUFFER	
		Blocking potential		DRAINAGE BUFFER	
	FINAL ACCUMULATIONS	Alluvial fans	BASAL EROSION	GEOMORPHOMETRY	
Banks, Levees		SEDIMENTATION			

#### 6.2.5 Normalizing factor maps to criteria maps

Given that original factor maps have different measure units, scales and meaning related to the landsliding process analyzed; it is necessary to standardize the values of every factor map to a same scale which at the same time replicates the landslide potentiality found in them. For instance, in a 0 to 1 scale, 0 represents the lowest potentiality of the criterion properties to develop landslides while 1 is representing the highest potentiality.

Some authors (Castellanos et al., 2005; Jiang and Eastman, 2000; Malczewski, 1999), recommend the maximum value method to normalize factor maps, which is easy when the factor map has a value domain as those found in slope gradient, internal relief, altitude, and buffer distance maps. However given that many of the factor maps used in

this analysis are expressed in nominal scale or classes (i.e. lithology, holdridge life's zones, geomorphological, geomorphometry, and slope shape), those classes in every map should be ordered following its susceptibility to landsliding process, then assigned values between 0 (less susceptible) to 1 (more susceptible). Table 6.2.3 outlines the original scale and values contained in the factor maps, and the resulting minimum and maximum normalized values of the subsequent criterion map; a more complete explanation on the source of these values can be found in Appendix 6.3 and Chapter 5. In this way, factor maps values are normalized and converted to criteria maps.

Table 6.2.3. Description of the original data range contained in the factor maps, and the resulting minimum and maximum normalized values of the subsequent criterion map.

FACTOR MAP	DATA RANGE	Original Values		Criterion map	
		Min value	Max value	Min value	Max value
HOLDRIDGE LIFE'S ZONES	NOMINAL	classes		0.02	1
INTERNAL RELIEF	RATIO	0m	376.7m	0.13	1
ALTITUDE RANGES	INTERVAL	<500m	<5000m	0.10	1
GEOMORPHOLOGICAL UNITS	NOMINAL	classes		0.05	1
LINEAMENTS BUFFER	RATIO	0m	500m	0.17	1
SLOPE GRADIENT	RATIO	0°	80°	0	1
DRAINAGE BUFFER	RATIO	0m	90m	0.50	1
SLOPE SHAPE	NOMINAL	classes		0.33	1
SLOPE ASPECT	INTERVAL	0°	360°	0.11	1
LITHOLOGY	NOMINAL	classes		0.06	1
GEOMORPHOMETRIC	NOMINAL	classes		0.07	1

#### 6.2.6 Compensating weights via pairwise procedure

In order to combine the criteria maps into a final landslide hazard map, it is necessary to assign weights to each of them to compensate for their contribution to the landsliding process. Saaty (2004) outlined the pairwise procedure where the importance of a criterion map is rated through a comparison to every other criterion map using a nine points reciprocal scale. Table 6.2.4 describe those nine levels of importance in terms of the contribution to landsliding process then, factor maps are compared and later, those values are transposed to a reciprocal matrix, which is described in the next section.

Table 6.2.4. Levels of importance used to qualify / quantify the pairwise comparison of the criteria involved in the study area landsliding process.

LEVEL OF IMPORTANCE	DEFINITION	DESCRIPTION
1	Equal preference	Each criterion ( <b>x,j</b> ), contribute almost equally to the landsliding process
2	Equal to moderate preference	
3	Moderate preference	Former experiences slightly privileged the importance of criterion <b>x</b> over <b>j</b> in the landsliding process
4	Moderate to strong preference	
5	Strong preference	Practically the dominance of criterion <b>x</b> over <b>j</b> in the landsliding process can be demonstrated
6	Strong to very strong preference	
7	Very strong preference	There is evidence determining the supremacy of criterion <b>x</b> over <b>j</b> in the landsliding process
8	Very to extremely preference	
9	Extremely preference	The absolute dominance of criterion <b>x</b> over <b>j</b> in the landsliding process has been already confirmed

#### 6.2.7 Computing the Analytical Hierarchy matrices for the criteria maps

The computing of the Analytical Hierarchy Matrix for the criterion maps deals with the following steps:

- Construction of the reciprocal matrix following the parameters obtained from the pairwise procedure (Table 6.2.5).
- Normalization of the reciprocal matrix and subsequent calculation of the maximum eigen vector or priority eigen vector (PEV), the normalized priority eigen vector (NPEV) and the maximum eigen value (MaxEV) (Table 6.2.6).
- Validation via the consistency index (CI) and consistency ratio (CI) (equation 1 and 2).



Table 6.2.5. Reciprocal Matrix

	j										
x	HOLDRIDGE LIFE'S ZONES	INTERNAL RELIEF	ALTITUDE RANGES	GEOMORPHOLOGICAL UNITS	LINEAMENTS BUFFER	SLOPE CLASSES	DRAINAGE BUFFER	SLOPE SHAPE	SLOPE ASPECT	LITHOLOGY	GEOMORPHOMETRY
HOLDRIDGE LIFE'S ZONES	1	2	2	3	4	5	6	7	7	8	9
INTERNAL RELIEF	0.5	1	2	2	3	4	5	6	7	7	8
ALTITUDE RANGES	0.5	0.5	1	2	2	3	4	5	6	7	7
GEOMORPHOLOGICAL UNITS	0.33	0.5	0.5	1	2	2	3	4	5	6	7
LINEAMENTS BUFFER	0.25	0.33	0.5	0.5	1	2	2	3	4	5	6
SLOPE CLASSES	0.2	0.25	0.33	0.5	0.5	1	2	2	3	4	5
DRAINAGE BUFFER	0.17	0.20	0.25	0.33	0.5	0.5	1	2	2	3	4
SLOPE SHAPE	0.14	0.17	0.20	0.25	0.33	0.5	0.5	1	2	2	3
SLOPE ASPECT	0.14	0.14	0.17	0.20	0.25	0.33	0.5	0.5	1	2	2
LITHOLOGY	0.13	0.14	0.14	0.17	0.20	0.25	0.33	0.5	0.5	1	2
GEOMORPHOMETRY	0.11	0.13	0.14	0.14	0.17	0.20	0.25	0.33	0.5	0.5	1
$\Sigma (j)$	<b>3.47</b>	<b>5.36</b>	<b>7.24</b>	<b>10.09</b>	<b>13.95</b>	<b>18.78</b>	<b>24.58</b>	<b>31.33</b>	<b>38.0</b>	<b>45.5</b>	<b>54</b>

Table 6.2.6. Normalized Matrix

	jN												
xN	HOLDRIDGE LIFE'S ZONES	INTERNAL RELIEF	ALTITUDE RANGES	GEOMORPHOLOGICAL UNITS	LINEAMENTS BUFFER	SLOPE CLASSES	DRAINAGE BUFFER	SLOPE SHAPE	SLOPE ASPECT	LITHOLOGY	GEOMORPHOMETRY	PRIORITY EIGEN VECTOR (PEV)	NORMALIZED P EV
HOLDRIDGE LIFE'S ZONES	0.288	0.373	0.276	0.297	0.287	0.266	0.244	0.223	0.184	0.176	0.167	0.253	0.878
INTERNAL RELIEF	0.144	0.187	0.276	0.198	0.215	0.213	0.203	0.191	0.184	0.154	0.148	0.192	1.030
ALTITUDE RANGES	0.144	0.093	0.138	0.198	0.143	0.160	0.163	0.160	0.158	0.154	0.130	0.149	1.079
GEOMORPHOLOGICAL UNITS	0.096	0.093	0.069	0.099	0.143	0.106	0.122	0.128	0.132	0.132	0.130	0.114	1.147
LINEAMENTS BUFFER	0.072	0.062	0.069	0.050	0.072	0.106	0.081	0.096	0.105	0.110	0.111	0.085	1.185
SLOPE CLASSES	0.058	0.047	0.046	0.050	0.036	0.053	0.081	0.064	0.079	0.088	0.093	0.063	1.184
DRAINAGE BUFFER	0.048	0.037	0.035	0.033	0.036	0.027	0.041	0.064	0.053	0.066	0.074	0.047	1.145
SLOPE SHAPE	0.041	0.031	0.028	0.025	0.024	0.027	0.020	0.032	0.053	0.044	0.056	0.035	1.081
SLOPE ASPECT	0.041	0.027	0.023	0.020	0.018	0.018	0.020	0.016	0.026	0.044	0.037	0.026	1.002
LITHOLOGY	0.036	0.027	0.020	0.017	0.014	0.013	0.014	0.016	0.013	0.022	0.037	0.021	0.944
GEOMORPHOMETRY	0.032	0.023	0.020	0.014	0.012	0.011	0.010	0.011	0.013	0.011	0.019	0.016	0.861
												MaxEV	11.54

- Where:
- Priority Eigen Vector (PEV) =  $\sum(xN_jjN)/n$
  - Normalized Priority Eigen Vector (NPEV) =  $PEV * \sum(j)$
  - Maximum Eigen Value (MaxEV) =  $\sum(NPEV)$

Consistency index (CI) and consistency ratio (CR)

$$CI = \frac{MaxEV - n}{n - 1} = \frac{11.54 - 11}{10} = 0.054 \quad \text{(Equation 1)}$$

$$CR = \frac{CI}{RI} \quad \text{Where RI} = 1.51, \text{ then } CR = \frac{0.054}{1.51} = 0.036 \quad \text{(Equation 2)}$$

The upper triangular section of the reciprocal matrix (Table 6.2.5) is filled using the values obtained from the pairwise comparison; then, the lower triangular section is completed with the reciprocal values by  $r_{(jx)} = \frac{1}{r_{(xj)}}$ , where  $r_{(xj)}$  is the value of row x and column j. The criteria maps in both matrices were ordered following the ranking obtained from the density analysis index (Table 5.1, Chapter 5). In this way the subjective values assigned through the pairwise comparison are transformed in a set of linear weights (Malczewski, 1996). The priority eigen values (PEV) obtained through the reciprocal matrix (Table 6.2.6) are later used to compensate the corresponding criterion map, which are finally combined in an algebraic overlaying sum to reproduce the landslide susceptibility map resulting from the MCE-AHP approach. The consistency index (CI) and consistency ratio (CR) are statistical indices applied to test the consistency and reliability of the judgment carried out during the pairwise comparison procedure, in that sense the maximum eigen value (MaxEV) resulting from the normalized matrix (Table 6.2.6) should be equal to the number of factors (n) compared. However Saaty (1990), cited by Atkinson et al., (2005), stated that a consistency ratio (CR) of 0.10 or less is considered acceptable given the subjectivity of the pairwise procedure in geographical assessments, and recommended the use of the CR as a measure of the level of inconsistency found in CI. For this purpose, the CI value is compared to the Ratio Index Consistency (RI), which can be obtained from several experimental researches as those described in Alonso et al., (2006) (Appendix 6.4). Since the pairwise procedure carried out in this AHP has a deviation of only 3.6%, then it is considered acceptable.

#### 6.2.8 Data output integration and final classification. The landslide susceptibility and hazard maps

After the converting of original factor maps to criteria maps, these are combined into a landslide susceptibility map, taken into account the weights provided by the priority eigen value (PEV), as described in Equation 3:

$$\text{LSM} = \text{HLZ}(0.253) + \text{IR}(0.192) + \text{AR}(0.149) + \text{GU}(0.114) + \text{LB}(0.085) + \text{SC}(0.063) + \text{DB}(0.047) + \text{SS}(0.035) + \text{SA}(0.026) + \text{L}(0.021) + \text{GM}(0.016) \quad (\text{Equation 3})$$

Where: LSM = Landslide susceptibility map

	CRITERION LAYER	PEV		CRITERION LAYER (cont.)	PEV
HLZ	HOLDRIDGE LIFE'S ZONES	0.253	DB	DRAINAGE BUFFER	0.047
IR	INTERNAL RELIEF	0.192	SS	SLOPE SHAPE	0.035
AR	ALTITUDE RANGES	0.149	SA	SLOPE ASPECT	0.026
GU	GEOMORPHOLOGICAL UNITS	0.114	L	LITHOLOGY	0.021
LB	LINEAMENTS BUFFER	0.085	GM	GEOMORPHOMETRIC	0.016
SC	SLOPE CLASSES	0.063			

Figure 6.2.1 illustrates the distribution of the MCE landslide susceptibility index across the study area. Higher index values represent areas with a higher susceptibility to develop landsliding processes, while lower index values state are for areas with a lower to null potentiality to landslide occurrences. Landslides polygons outlined in black were overlaid on the MCE landslide susceptibility to depict the landslide distribution along the susceptibility index patterns.

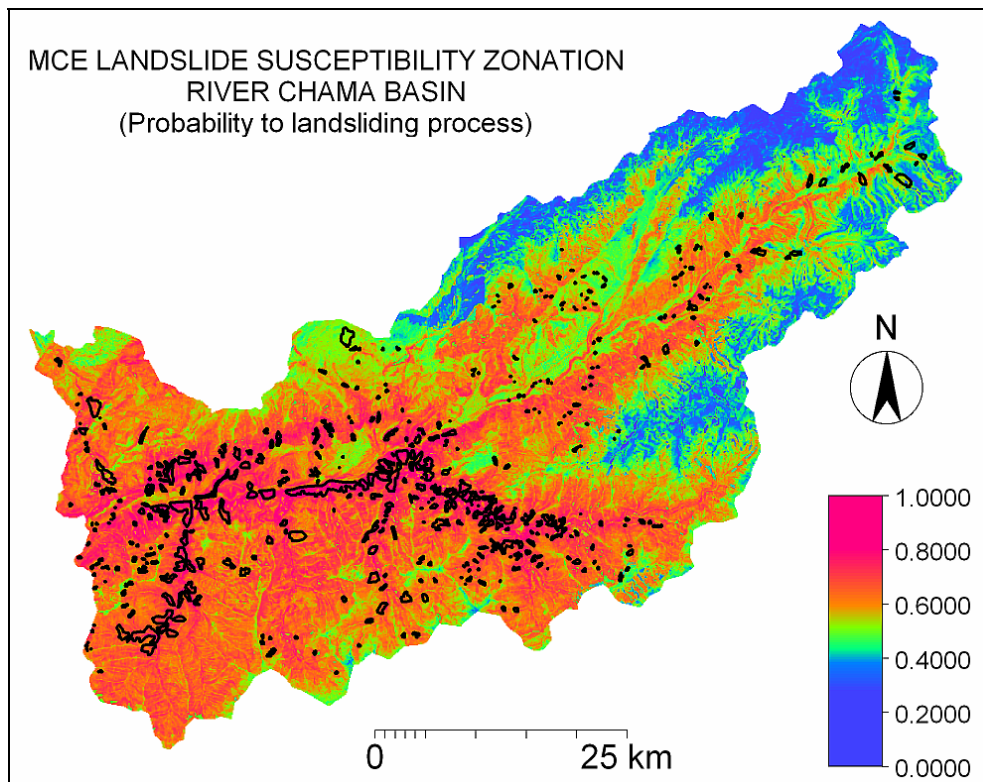


Figure 6.2.1. Study area MCE landslide susceptibility zonation. Landslides outlined in black are from the landslide inventory map.

Finally, the MCE landslide susceptibility zonation was subsequently reclassified into the traditional four landslide hazard levels (Low, Moderate, High, and Very High landslide hazard), using a cumulative frequency rate curve (Figure 6.2.2). This curve which is the result of a map-comparison between the MCE susceptibility map and the landslide inventory map and it provides the thresholds required for slicing operation (Table 6.2.7). Appendix 7.3 depicts the reclassified MCE landslide susceptibility map into the MCE landslide hazard zonation map.

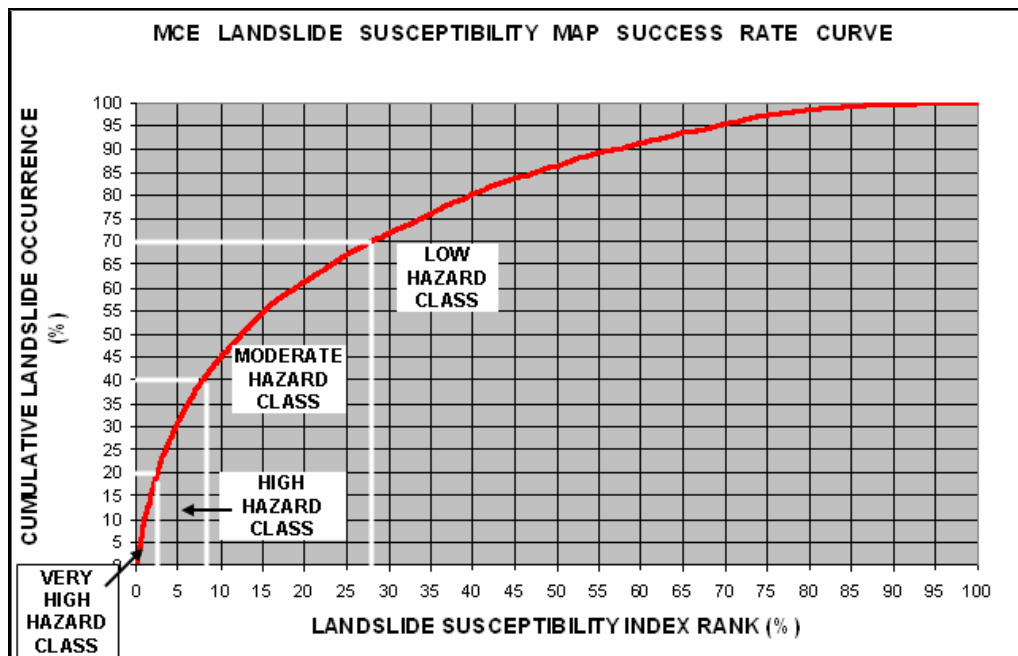


Figure 6.2.2. Landslide occurrence / MCE landslide susceptibility index relationship cumulative frequency distribution.

Table 6.2.7. MCE thresholds used to classify the MCE index susceptibility into landslide hazard classes with corresponding cumulative landslide occurrences and cumulative landslide susceptibility index values.

Cumulative landslide occurrence (%)	Potential % of the landsliding area to be predicted	Top cumulative landslide susceptibility Index (%)	Threshold at index value	Assigned class
20	80 (100-20)	2.31	over 0.7466	VERY HIGH HAZARD
40	60 (100-40)	7.95	up to 0.7466	HIGH HAZARD
70	30 (100-70)	28.08	up to 0.6782	MODERATE HAZARD
> 70	≤ 30	+ 28.08	up to 0.6204	LOW HAZARD

### 6.3 Probabilistic landslide hazard zonation through the Weights of Evidence model

Probabilistic approaches applied to landslide hazard zonation are mainly based in the Bayes theorem which is a mathematical method used for decision-making under conditions of uncertainty (Aspinall et al., 1993). However, it has the potential of converting knowledge of predictive correlations from multiclass factor maps, in combination with a landslide inventory map, to landslide hazard probabilities (Gorsevski et al., 2003). Hence, that in every probabilistic approach the role of each factor or parameter map contributing to the landsliding process is determined on the basis of the observed relations with the past/present landslide distribution (Bonham- Carter, 1996).

The Weights of Evidence index, allows the assessment of the landsliding probability of each class of a parameter map by assessing a value (weight) for the presence but also for the absence of landslide occurrence within the class, defining a degree of probability of having a future landsliding process in the considered class. This model has been applied in quantitative medical diagnosis, mineral potential mapping (Bonham –Carter et al., 1989; Agterberg et al., 1990, 2002), and also landslide hazard analysis (Van Westen et al., 2003; Lee et al., 2004; Neuhauser et al., 2006).

Briefly, the weights of evidence are provided by (van Westen et al., 2003):

$$C = W_i^+ - W_i^-$$

where,

$C$  = Weight of evidence, or also considered as the contrast factor, it is a quantitative approach to describe the spatial association between the landslide occurrences and the represented class from the parameter map under consideration. In this analysis, this value is considered to be the final probabilistic weight of an assessed class to turn out into landsliding process.

$W_i^+$  = Presence of the factor for the occurrence of landslides, is the difference between the prior or unconditional probability and the posterior or conditional probability to landsliding process of a single class.

$W_i^-$  = Absence of the factor for the occurrence of landslides. It is the difference between the prior or unconditional probability and the posterior or conditional probability to landsliding process of a single class, given a landslide absence. In a raster GIS platform this method is applied using the resulting contingency tables generated by the

map comparison procedure between the landslide inventory map and each of the parameter maps. Since in this analysis the parameter maps include several classes, Table 6.3.1 shows the possible combination and the weights of evidence computed for each of the classes and written in number of pixels (Npix).

Table 6.3.1. Map comparison and possible combinations from the landslide inventory and a parameter map single class.

		PARAMETER MAP CLASS(j)	
		PRESENT	ABSENT
LANDSLIDE OCCURRENCES	PRESENT	Npix 1	Npix 2
	ABSENT	Npix 3	Npix 4

Where:

$$W_i^+ = \log_e = \frac{\frac{Npix1}{Npix1 + Npix2}}{\frac{Npix3}{Npix3 + Npix4}} \quad \text{(Equation 1)}$$

$$W_i^- = \log_e = \frac{\frac{Npix2}{Npix1 + Npix2}}{\frac{Npix4}{Npix3 + Npix4}} \quad \text{(Equation 2)}$$

Details of the mathematical background are discussed in Bonham –Carter (1996). This method is objective, and avoids the subjective choice of weighting factors by subjective considerations; however, in the combination of input maps it is assumed that the maps are conditionally independent of each other respect to landslide occurrence.

### 6.3.1 Data entry. Test of conditional independence

Due to the comparative nature of this analysis, the parameter maps used in the weights of evidence procedure are practically the same of those considered in the MCE and geomorphological approaches and described in Table 5.1. The TMU and TMsU were excluded from the analysis since those layers already express the interaction of the parameter maps and the landslide occurrences then, any weight computed from these layers will be favoring the represented units in detriment of the remaining data set. The weights of evidence procedure followed over here is illustrated in Figure 6.3.1 and outlined as follow:

- 1.- Classification of each parameter map into a number of relevant classes
- 2.- Selection of the parameter maps via test of independence.

- 2.- Combination of the selected parameter maps with the landslide inventory map via map comparison procedure.
- 3.- Calculation of weighting values for the classes belonging to the parameter maps used.
- 4.- Reclassification of the parameter maps into weight of evidence layers
- 5.- Combination of the resulting weight of evidence layers into a final probability map named landslide susceptibility map.
- 6.- Computing the success rate curve and definition of the thresholds to reclassify the landslide susceptibility map into a four hazard classes landslide hazard zonation map.

#### Test of conditional independence

Since the most important assumption in weights of evidence procedure comes from the application of Bayesian probability theory in the model, it is assumed that the parameter maps considered are conditionally independent from each other respect to the landslide occurrences (Neuhauser et al., 2006); hence, only the independent parameter maps should be considered in the final weights of evidence combination. Nowadays when using weights of evidence, the literature offers two ways to circumvent the problem related to the violation of conditional independence among a set of parameter layers. One of them is related to the introduction of a new input layer (Thiart et al., 2003; Thiery et al., 2007), which should be the reclassification of the former “dependent” layer via the aggregation of its classes or as result of its combination with another layer, but keeping its geomorphological significance (van Westen et al., 2003).

The other way to avoid this drawback, particularly when workings with landslide occurrences, is converting the multiclass parameter maps into simple binary maps (Bonham –Carter, 1996; Lee et al., 2004; Neuhauser et al., 2006). This procedure was also followed by Gorsevski et al., (2003), for using an integration of Fuzzi K- Bayesian approaches to classify landslide hazard in central Idaho, and by Franca-Rochali et al., (2003), this last in a modeling of mineral potential mapping in Brazil.



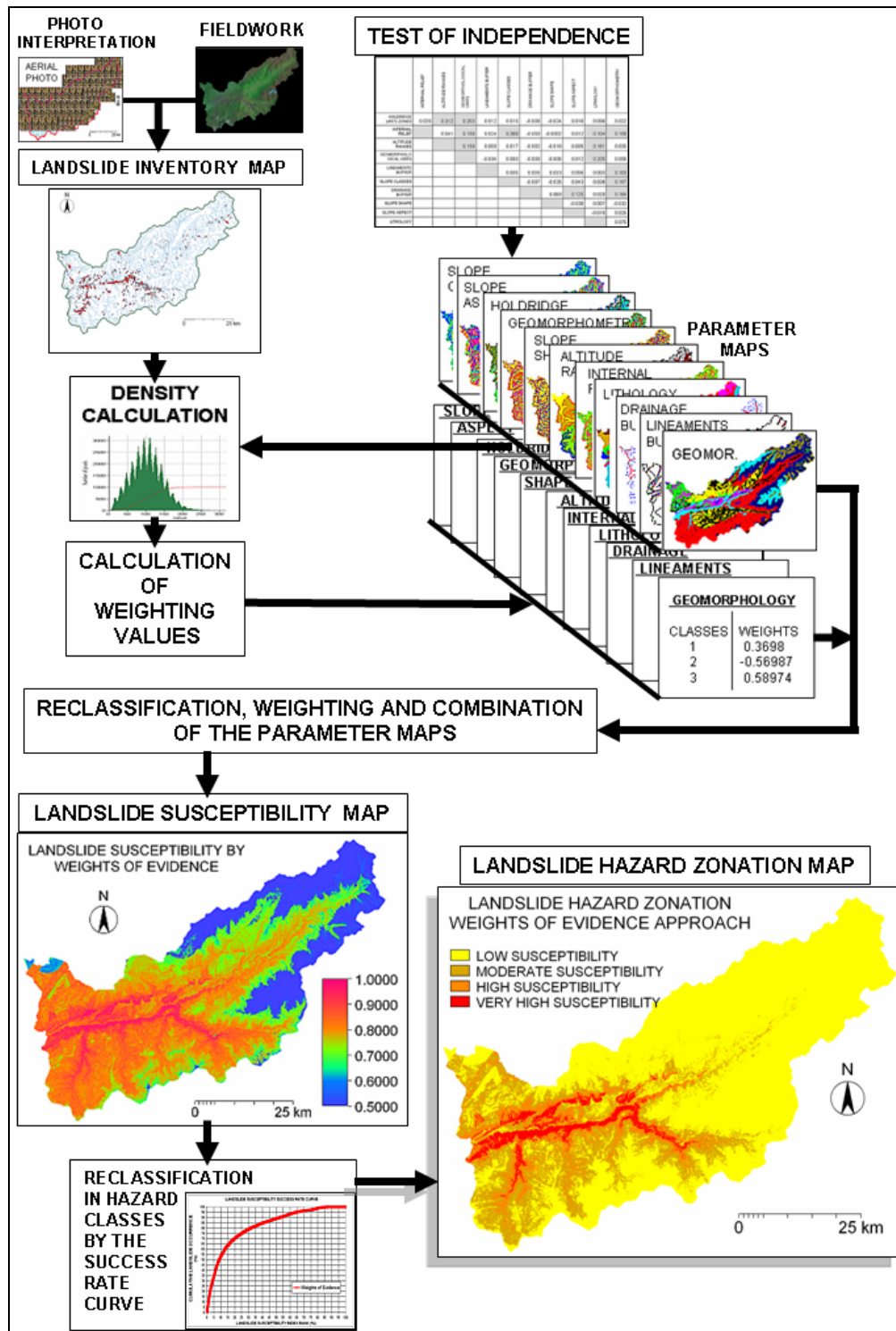


Figure 6.3.1. Illustrative chart about the weights of evidence procedure

However, the both above mentioned procedures lay in an arbitrary manipulation of the geographical data set, which could affect the consistency of the preliminary conception of a landslide hazard zonation by putting too much emphasis in the data processing and a

less attention to the spatial interaction of the available data. In this analysis two methods: Chi square test and Kappa index, are used to perform the testing of conditional independence since both statistics can measure the degree of association of a pair of parameter layers based in a pairwise comparison and subsequent contingency table and it can be applicable only to locations at which landslides occur (Neuhauser et al., 2006). The steps carried out to compute the Chi square test and the Kappa index are illustrated in Figures 6.3.2 and 6.3.3, and outlined as follow:

#### Chi Square test

- 1.- Selection of the layer data set
- 2.- Reclassification of each layer from the data set into binary layers, giving its propensity to landsliding processes. To perform this step every parameter layer was reclassified following the preliminary factor analyses classification performed in Chapter 5 and described in Appendixes 5.4. to 5.7. In brief, 118 classes incorporating the 11 parameter layers were categorized in four landslide prone classes, from here the very high, high, and moderate relevant classes were aggregated into a single landslide prone class. The less relevant class was treated a non-landslide prone class, accomplishing by this way the binary reclassification of the data set.
- 3.- Extraction of the landsliding area from each of the binary layer
- 4.- Comparison of these new binary parameter layers and compute of the related pairwise contingency table
- 5.- Computing of the Chi square test for every contingency table and selection of the possible layer combinations giving the conditional independence criteria. This criteria is given by the critical value of the Chi square distribution which is determined here at 99% of significance level and to a degree of freedom computed from the equation:  $df = (r-1)(c-1)$ . In this case, because the data provided from binary layers have two classes in rows (  $r$  ) and columns (  $c$  ), the degree of freedom is 1 which account for a Chi square critical value of 6.6349. This threshold is interpreted whether a Chi square value from a contingency table is below 6.6349 the pairwise of binary parameter layer considered is independent, otherwise values over this threshold are to describe dependent pairwise.

## Kappa index

- 1.- Selection of the layer data set
- 2.- Reclassification of each layer from the data set into the four prone landslide classes already categorized following the density analysis categorization in Chapter 5 and described in Appendixes 5.4. to 5.7.
- 3.- Extraction of the landsliding area from each of the new four classes parameter layers
- 4.- Pairwise comparison of these new four classes parameter layers and computing of the related contingency table
- 5.- Computing of the Kappa index for every contingency table and selection of the possible layer combinations giving the conditional independence criteria. The Kappa index takes on the value 1 if there is a perfect agreement of the spatial association between the pairwise of parameter layers considered, and becomes -1 if there is a perfect disagreement. Given that Kappa values lower than 0.4 represent poor agreement (Congalton, 2004), in this analysis three different groups following different Kappa thresholds are considered from the several computed Kappa indices: pairwise combinations with a computed Kappa index  $\leq 0$ , which means that all pairwise combination with Kappa values lower / equal to 0 are considered conditional independent; pairwise combinations with Kappa values  $\leq 0.01$ , were pairwise combinations lower / equal to 0.01 are considered independent and pairwise combinations with Kappa index lower / equal  $\leq 0.1$  to be considered also independent. Tables 6.3.2 to 6.3.5, show the results obtained from the application of the Chi square test and Kappa index, as well as the possible combinations given the conditional independence criteria before described.

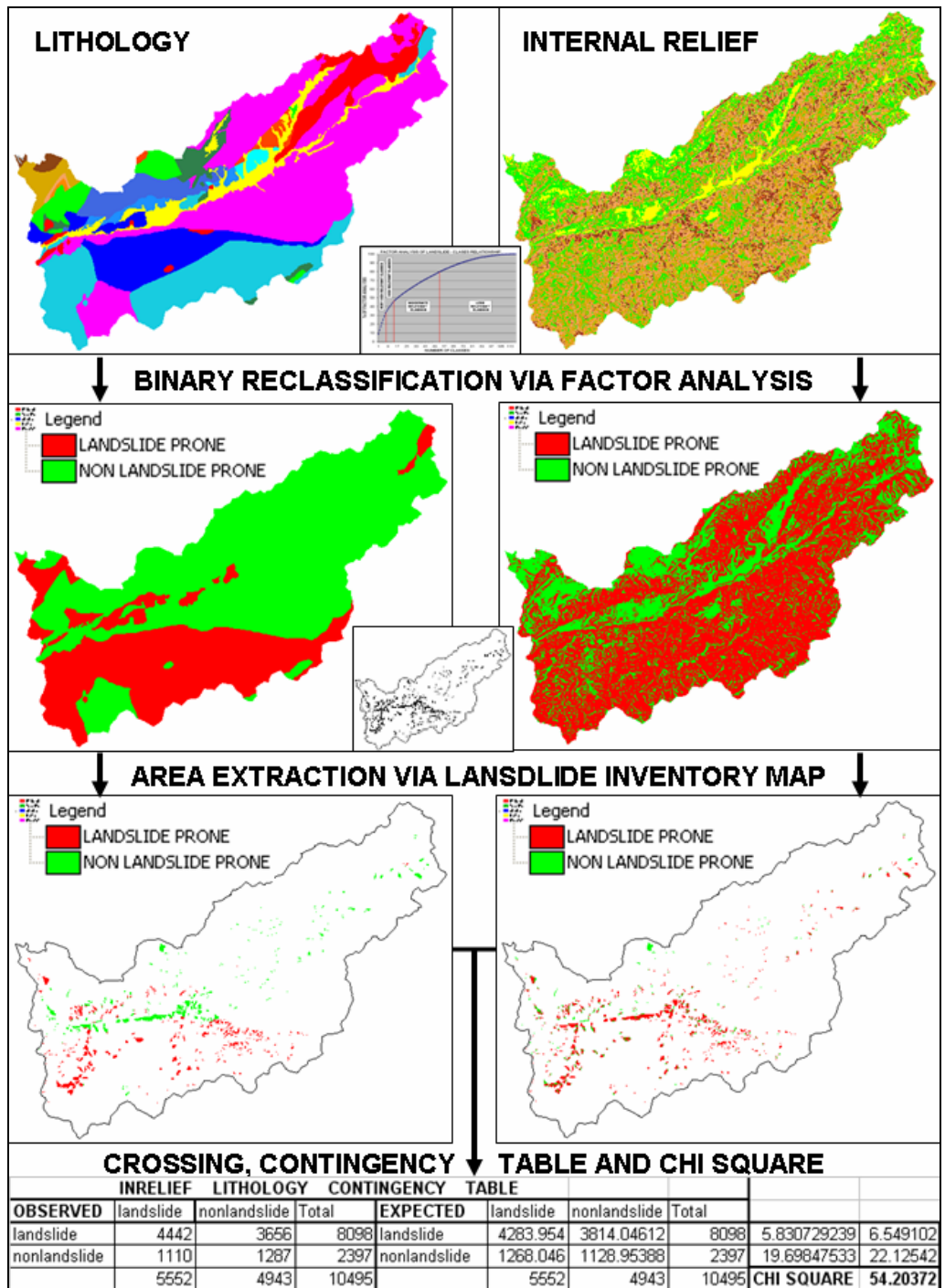


Figure 6.3.2. Test of conditional independence procedures using Chi square test for lithology and internal relief.

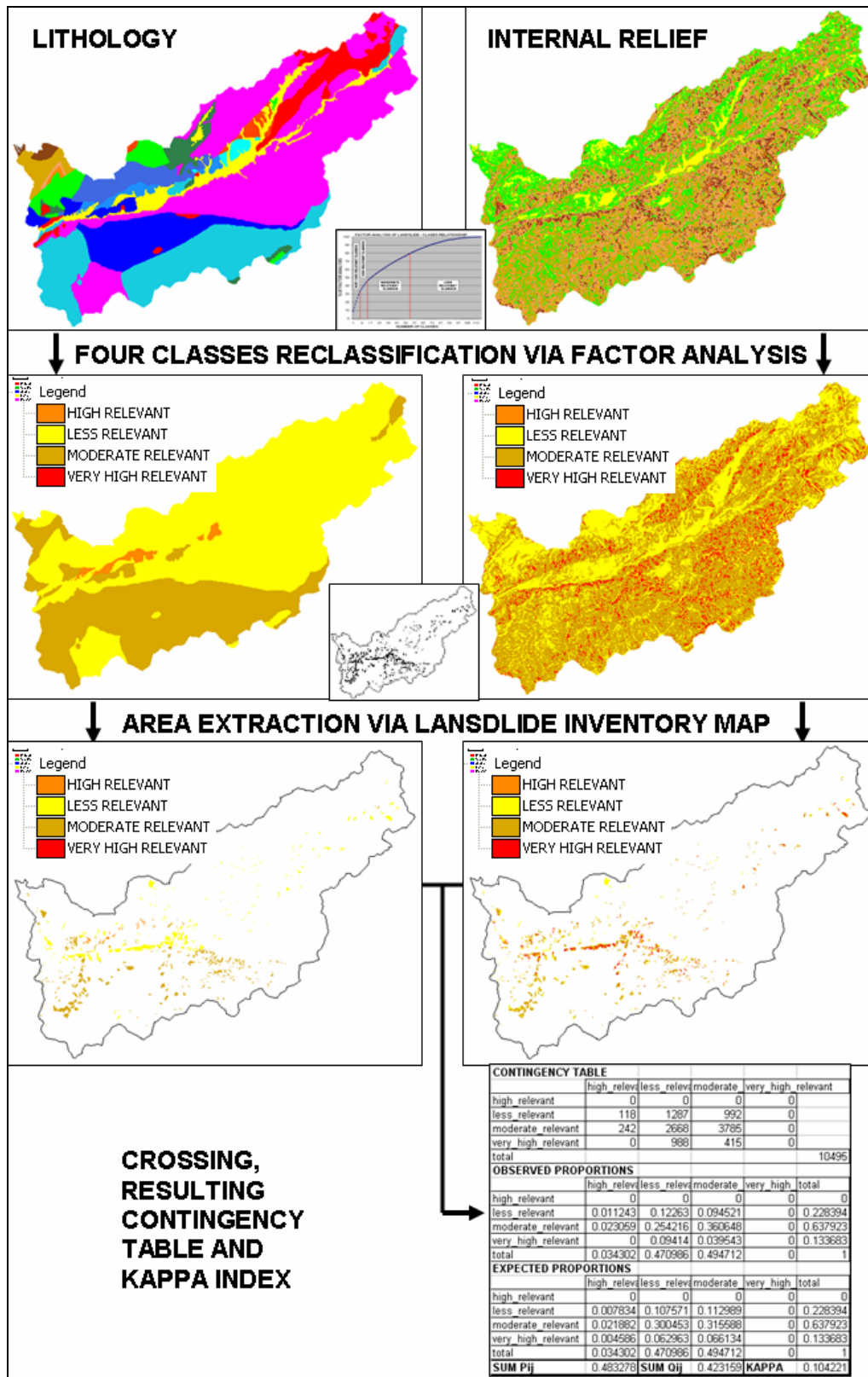


Figure 6.3.3. Test of conditional independence procedures using Kappa index for lithology and internal relief.

### 6.3.2 Computing the weights of evidence. Selection of scenarios

The Weights of Evidence were computed for all the classes and parameter maps following the Equations 1 and 2. These weights of evidence were used to reclassify the parameter maps into a new set of layers which should be combined to generate a landslide susceptibility map and eventually the probabilistic landslide hazard map. Following the assumption of conditional independence –in this case from 55 possible parameter map combinations– 27 met the requirements of conditional independence (actually 31 combinations but 4 of them are repeated).

Because each of the combinations generate a potential landslide susceptibility map, it was necessary to test the predictive capacity of each of these new susceptibility layers. In regard, those new layers were compared with the landslide inventory map and the resulting frequency plotted in a success rate curve (Chung et al., 1999); a better explanation on the success rate curve is displayed later in Chapter 7. Following the success rate curves (Appendixes 6.7 to 6.10), as in Chi square as well as in Kappa index testing, the first combination proved to be the most suitable in all of the scenarios at predicting the landsliding patterns in the study area, fulfilling the Bayesian requirement of independence. These combinations are:

- Holdridge life's zones + lineament buffers + slope shape (from the Chi square scenario)
- Holdridge life's zones + drainage buffers + slope shape (from Kappa  $\leq 0$  scenario)
- Holdridge life's zones + drainage buffers + slope shape + slope aspect (from Kappa  $\leq 0.01$  scenario)
- Holdridge life's zones + internal relief + lineaments buffers + slope classes + drainage buffers + slope shape + slope aspect + lithology + geomorphometry (from Kappa  $\leq 0.1$  scenario).

Table 6.3.2. Contingency table with CHI SQUARE values from the pairwise test of conditional independence. Degrees of freedom = 1 and 99% significance level (6.6349). Excluded combination values are shaded)

	INTERNAL RELIEF	ALTITUDE RANGES	GEOMORPHOLOGICAL UNITS	LINEAMENTS BUFFER	SLOPE CLASSES	DRAINAGE BUFFER	SLOPE SHAPE	SLOPE ASPECT	LITHOLOGY	GEOMORPHOMETRY
HOLDRIDGE LIFE'S ZONES	44.6749	3234.456	925.1592	3.680697	72.71359	30.95166	5.317432	19.34848	32.63307	45.95958
INTERNAL RELIEF		30.49585	433.3923	4.939136	3030.467	5.511486	0.004438	8.262328	54.20372	746.8704
ALTITUDE RANGES			1292.151	2.404956	35.1815	98.468	0.92073	3.572862	47.40241	110.43
GEOMORPHOLOGICAL UNITS				2.433324	292.9208	10.58314	0.440219	52.76321	102.71	504.853
LINEAMENTS BUFFER					0.059652	0.886231	8.000257	14.55046	0.04437	504.853
SLOPE CLASSES						9.723332	16.01998	26.30112	11.54403	331.5028
DRAINAGE BUFFER							5.655959	16.8488	1.106003	68.04438
SLOPE SHAPE								4.796998	0.491603	57.11065
SLOPE ASPECT									8.836326	17.8802
LITHOLOGY										186.4222
<p>Combinations of parameter maps considered to be conditionally independent following the Chi square test:</p> <ol style="list-style-type: none"> <li>1- Holdridge life's zones + lineament buffers + slope shape</li> <li>2- Internal relief + lineament buffers + drainage buffers + slope shape</li> <li>3- Altitude ranges + lineament buffers + slope shape + slope aspect</li> <li>4- Geomorphological units + lineament buffers + slope shape</li> <li>5- Lineament buffers + slope classes + drainage buffers + lithology</li> <li>6- Drainage buffers + slope shape + lithology</li> <li>7- Slope shape + slope aspect + lithology</li> </ol>										

Table 6.3.3. Contingency table with Kappa values  $\leq 0$ , from the pairwise test of conditional independence (excluded combinations in shade).

	INTERNAL RELIEF	ALTITUDE RANGES	GEOMORPHOLOGICAL UNITS	LINEAMENTS BUFFER	SLOPE CLASSES	DRAINAGE BUFFER	SLOPE SHAPE	SLOPE ASPECT	LITHOLOGY	GEOMORPHOMETRY
HOLDRIDGE LIFE'S ZONES	0.035	0.312	0.203	0.012	0.015	-0.008	-0.024	0.010	0.096	0.022
INTERNAL RELIEF		0.041	0.158	0.024	0.369	-0.050	-0.0002	0.012	0.104	0.159
ALTITUDE RANGES			0.159	0.008	0.017	-0.082	-0.010	0.005	0.161	0.035
GEOMORPHOLOGICAL UNITS				-0.004	0.060	-0.008	-0.006	0.012	0.205	0.066
LINEAMENTS BUFFER					0.005	0.036	0.033	0.056	0.003	0.103
SLOPE CLASSES						-0.087	-0.026	0.043	0.036	0.157
DRAINAGE BUFFER							0.068	0.125	0.020	0.184
SLOPE SHAPE								-0.020	0.007	-0.032
SLOPE ASPECT									-0.015	0.025
LITHOLOGY										0.075
<p>Combinations of parameter maps considered to be conditionally independent following Kappa values <math>\leq 0</math>:</p> <ol style="list-style-type: none"> <li>1- Holdridge life's zones + drainage buffers + slope shape</li> <li>2- Internal relief + drainage buffers + slope shape</li> <li>3- Altitude ranges + drainage buffers + slope shape</li> <li>4- Geomorphological units + lineament buffers + slope shape</li> <li>5- Slope classes + drainage buffers + slope shape</li> <li>6- Slope shape + slope aspect + geomorphometry</li> <li>7- Slope aspect + lithology</li> </ol>										



Table 6.3.4. Contingency table with Kappa values  $\leq 0.01$ , from the pairwise test of conditional independence (excluded combinations in shade).

	INTERNAL RELIEF	ALTITUDE RANGES	GEOMORPHOLOGICAL UNITS	LINEAMENTS BUFFER	SLOPE CLASSES	DRAINAGE BUFFER	SLOPE SHAPE	SLOPE ASPECT	LITHOLOGY	GEOMORPHOMETRY
HOLDRIDGE LIFE'S ZONES	0.035	0.312	0.203	0.012	0.015	-0.008	-0.024	0.010	0.096	0.022
INTERNAL RELIEF		0.041	0.158	0.024	0.369	-0.050	-0.0002	0.012	0.104	0.159
ALTITUDE RANGES			0.159	0.008	0.017	-0.082	-0.010	0.005	0.161	0.035
GEOMORPHOLOGICAL UNITS				-0.004	0.060	-0.008	-0.006	0.012	0.205	0.066
LINEAMENTS BUFFER					0.005	0.036	0.033	0.056	0.003	0.103
SLOPE CLASSES						-0.087	-0.026	0.043	0.036	0.157
DRAINAGE BUFFER							0.068	0.125	0.020	0.184
SLOPE SHAPE								-0.020	0.007	-0.032
SLOPE ASPECT									-0.015	0.025
LITHOLOGY										0.075

Combinations of parameter maps considered to be conditionally independent following Kappa values  $\leq 0.01$ :

- 1- Holdridge life's zones + drainage buffers + slope shape + slope aspect
- 2- Internal relief + drainage buffers + slope shape (already second combination at the Chi square test)
- 3- Altitude ranges + lineament buffers + drainage buffers + slope shape + slope aspect
- 4- Geomorphological units + lineament buffers + drainage buffers + slope shape
- 5- Lineaments buffers + slope classes + lithology
- 6- Slope classes + drainage buffers + slope shape (already fifth combination at the Chi square test)
- 7- Slope shape + slope aspect + lithology + geomorphometry
- 8- Slope aspect + lithology (already seventh combination at the Chi square test)

Table 6.3.5. Contingency table with Kappa values  $\leq 0.1$ , from the pairwise test of conditional independence (excluded combinations in shade).

	INTERNAL RELIEF	ALTITUDE RANGES	GEOMORPHOLOGICAL UNITS	LINEAMENTS BUFFER	SLOPE CLASSES	DRAINAGE BUFFER	SLOPE SHAPE	SLOPE ASPECT	LITHOLOGY	GEOMORPHOMETRY
HOLDRIDGE LIFE'S ZONES	0.035	0.312	0.203	0.012	0.015	-0.008	-0.024	0.010	0.096	0.022
INTERNAL RELIEF		0.041	0.158	0.024	0.369	-0.050	-0.0002	0.012	0.104	0.159
ALTITUDE RANGES			0.159	0.008	0.017	-0.082	-0.010	0.005	0.161	0.035
GEOMORPHOLOGICAL UNITS				-0.004	0.060	-0.008	-0.006	0.012	0.205	0.066
LINEAMENTS BUFFER					0.005	0.036	0.033	0.056	0.003	0.103
SLOPE CLASSES						-0.087	-0.026	0.043	0.036	0.157
DRAINAGE BUFFER							0.068	0.125	0.020	0.184
SLOPE SHAPE								-0.020	0.007	-0.032
SLOPE ASPECT									-0.015	0.025
LITHOLOGY										0.075

Combinations of parameter maps considered to be conditionally independent following Kappa values  $\leq 0.1$ :

- 1- Holdridge life's zones + internal relief + lineaments buffers + slope classes + drainage buffers + slope shape + slope aspect + lithology + geomorphometry
- 2- Internal relief + altitude ranges + lineaments buffers + drainage buffers + slope shape + slope aspect
- 3- Altitude ranges + lineament buffers + slope classes + drainage buffers + slope shape + slope aspect + geomorphometry
- 4- Geomorphological units + lineament buffers + slope classes + drainage buffers + slope shape + slope aspect + geomorphometry
- 5- Lineaments buffers + slope classes + drainage buffers + slope shape + slope aspect + lithology
- 6- Slope classes + drainage buffers + slope shape + slope aspect + lithology
- 7- Slope shape + slope aspect + lithology + geomorphometry (already seventh combination at the Kappa  $\leq 0.01$  index)
- 8- Slope aspect + lithology + geomorphometry
- 9- Lithology + geomorphometry

Then a new success rate curve computed for these four most suitable scenarios (Figure 6.3.4) in order to define which of these is more precise for landslide prediction under the probabilistic approach. The scenario built on the first combination of the Kappa  $\leq 0.1$  criterion is assumed to be the best selection and arrangement of parameter layers to predict landslide areas in the study area following the weights of evidence procedure. The area under the success rate curves provides an estimation of the overall accuracy about how powerful can be each of the landslide predictive scenarios (Lee et al., 2004). Table 6.3.6 outlines these values for the curves represented in Figure 6.3.4. Boham-Carter (1994) states that an accuracy over 80% can be considered successful.

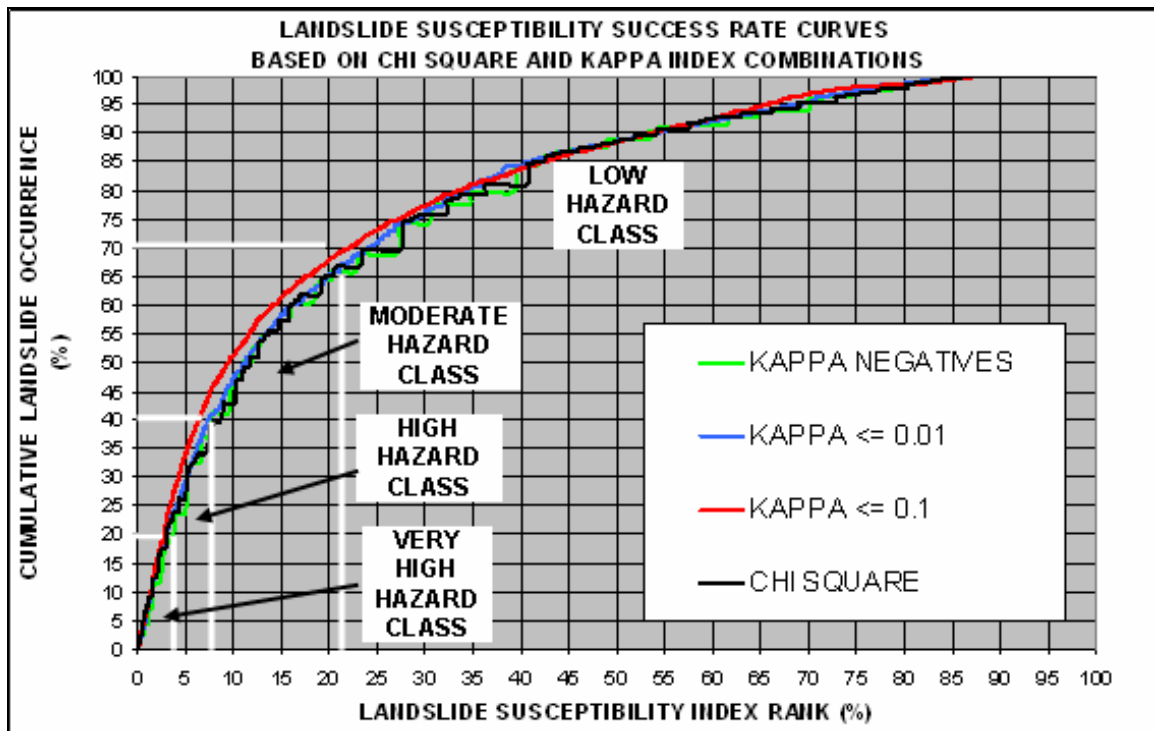


Figure 6.3.4. Success rate curve based on the most suitable combinations obtained from the four scenarios analyzed.

Table 6.3.6. Overall accuracy of the four weights of evidence combination scenarios, computed as the area under the curve.

Weights of Evidence Scenarios by criterion	Overall accuracy (%)
Kappa $\leq 0$	79.94
Chi square	80.06
Kappa $\leq 0.01$	80.70
Kappa $\leq 0.1$	81.66

### 6.3.3 Data integration, classification and interpretation

Each of the selected four scenarios plus the all of the weights combinations were integrated in subsequent layers which express the spatial probability of landsliding process across the study area, then these layers should be reclassified in the four hazard classes used throughout all this study. The four hazard classes were assigned following the cumulative landslide occurrence to be predicted, as described in Table 6.3.7 and already illustrated in Figure 6.3.4. The Figure 6.3.5 show the reclassification in four hazard levels of the selected four weights of evidence scenarios.

The probabilistic landslide hazard map based in the Kappa  $\leq 0.1$  scenario (Appendix 7.2) is considered the most suitable weights of evidence hazard map to predict landslides in the study area and reveals a similar pattern related to the distribution of the landslide hazard zones, if compared to the very preliminary zonation found density analysis of Chapter 5, to the geomorphological approach (Appendix 7.1), and MCE (Appendix 7.3), landslide hazard zonation maps. From a visual point this weights of evidence landslide hazard map, shows straightforwardly the River Chama middle section as the most landslide hazardous area, however fails in the assignation of higher landslide hazard classes in areas with fewer landslide occurrences like those in the very upper basin. This failure is associated in the case of weights of evidence procedure, to the reduced number of landslides reported in a very compact and uniform geographical area as the páramo is, then given as a result a much lower probability to landsliding.

Although the main advantage of weights of evidence procedure is that the parameter factor and / or parameter layers used in the assessment can be determined by the researcher (van Westen et al., 2003), the application of a test of conditional independence improves the selection process to a better combination of layers, avoiding the over representation of hazard classes, a common gap particularly in regional studies where the scale of the study is more generalized.

Table 6.3.7. Susceptibility rank index thresholds used to classify the selected weight of evidence layers into landslide hazard classes following the cumulative predicted landslide occurrences

Cumulative landslide occurrence (%)	Potential % of the landsliding area to be predicted	Approximately top cumulative landslide susceptibility Index (%)	Assigned class
20	80 (100-20)	4	VERY HIGH HAZARD
40	60 (100-40)	7.8	HIGH HAZARD
70	30 (100-70)	22	MODERATE HAZARD
> 70	≤ 30	+ 21.5	LOW HAZARD

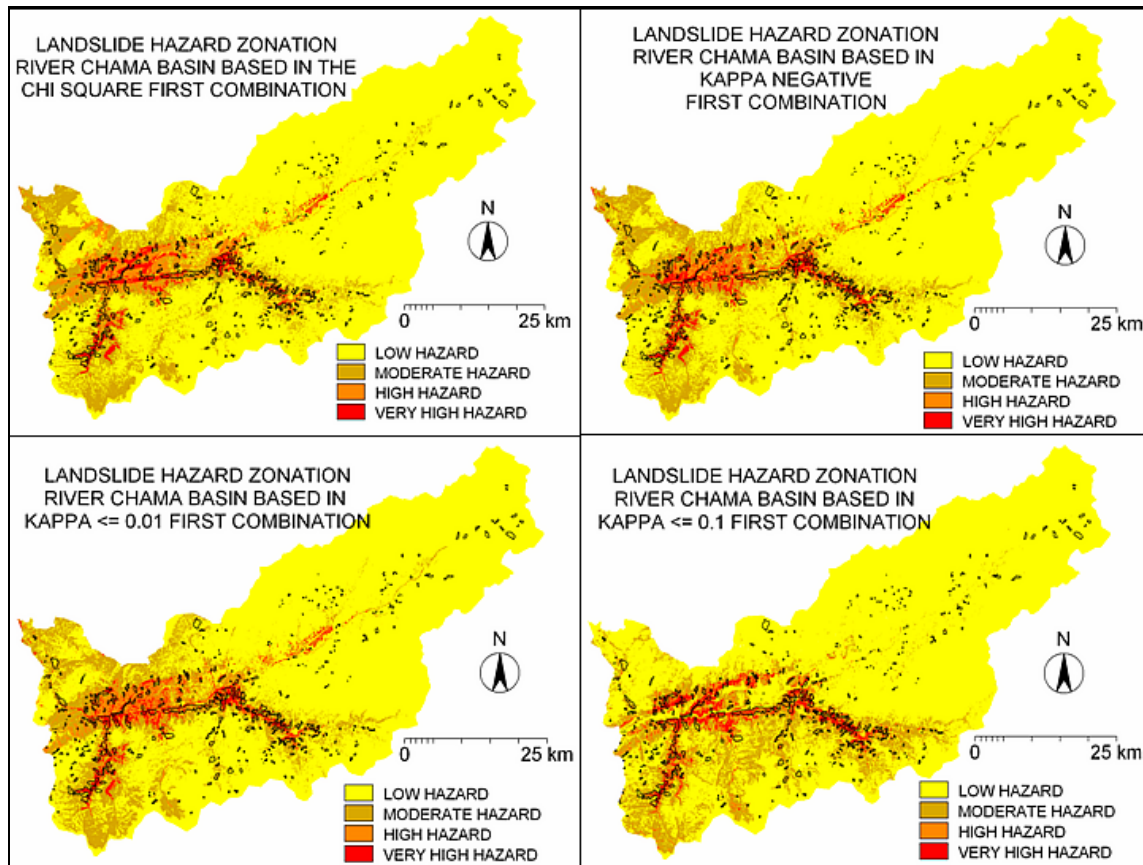


Figure 6.3.5. Landslide hazard zonation scenarios following the Chi square, Kappa negative, Kappa <= 0.01 and Kappa <= 0.1, weights of evidence combination (Actual landslides from the landslide inventory map outlined in black).

However, the tendency to reclassify a multiclass map to a binary one in order to apply a test of conditional independence like Chi square, reduces the integral character of any geographical factor (Thiery et al., 2007), therefore to circumvent this conceptual problem, in this analysis was successfully applied the Kappa index at different thresholds. These different Kappa thresholds allowed to increase the number of parameter layers to

an optimum, since it was proved that over and misrepresentation of potential hazard classes, are associated to a very basic combination of layers as well as with the arbitrary use of all of them. These associated gaps are associated to over and misclassification of the hazard classes across the study area as well as untrue classification of certain geographical features. At first glance, taken into account the weights of evidence displayed by classes in Appendix 6.5 and sorted in descendent order in Appendix 6.6, it is possible to detect which parameter layer is playing a more influence in the spatial definition of the hazard classes. For example Figure 6.3.6, show the patterns to be found across the study area most western part related to the landslide hazard classes distribution, in this figure scenarios related to the Chi square, Kappa  $\leq 0$  and Kappa  $\leq 0.01$  criteria describe a similar distribution and concentration of the moderate and low hazard classes in the represented section, which is noticeably different respect to the patterns found in the Kappa  $\leq 0.1$  scenario.

This feature can be explained in the fact that Chi square, Kappa  $\leq 0$  and Kappa  $\leq 0.01$  scenarios, are combinations where the Holdridge life's zones parameter layer through its classes: *Tropical dry woodland* and *tropical clear forest*; are playing a major role in the definition of this areas as of moderate hazard given its relative higher positive C values (Table 6.3.8.).

Table 6.3.8. Weights of evidence of selected classes (taken from Appendix 6.6)

RANK	PARAMETER LAYER	CLASSES	C
8	ALTITUDE RANGES	< 1000	1.1625
11		< 1500	1.0337
13	HOLDRIDGE LIFE'S ZONES	tropical dry woodland	0.9933
28		tropical clear forest	0.3137
31	ALTITUDE RANGES	< 500	0.2981
39	LITHOLOGY	claystone	0.1978
69		oil shales, limestone	-0.27
72	HOLDRIDGE LIFE'S ZONES	subtropical premontane clear forest	-0.3451
96		tropical dense forest	-1.1394
108	LITHOLOGY	clayey sand, shales	-1.7964
116		clayey sandstone	-3.1471
119		alluvion	-8.016
120		massive conglomerate	-8.016

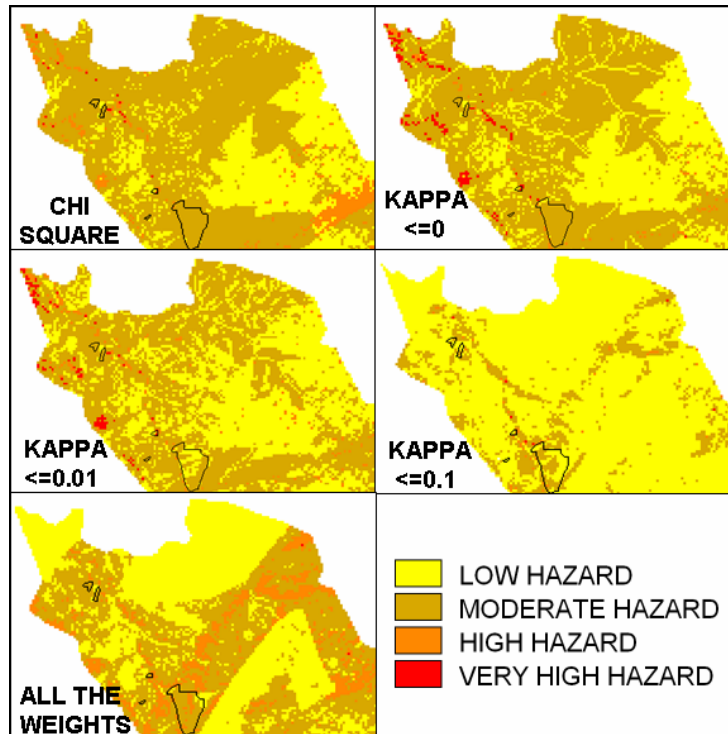


Figure 6.3.6. Landslide hazard distribution across the study area most western part, following the four possible scenarios given the test of conditional independence plus the all the weights combination (actual landslides are outlined in black).

Given the improvements experienced from the Chi square to Kappa $\leq 0.1$  scenarios, related to the landslide predictive capacity as illustrated in Figure 6.3.4; seems at this point of the analyses that the more inclusion of parameter layers, the better landslide hazard product, however Figure 6.3.7 illustrates an over representation of one parameter layer when the landslide hazard map is built with a combination of all the weights of evidence. This landslide hazard map, shows an unusual strip and triangle like features, of moderate and low hazard classes respectively. This phenomenon probably reflects the over representation of the classes from the lithological layer (C), which is over estimated by the Holdridge life's zones (A) and altitude ranges (B) classes in this section. Nevertheless, in this analysis, the combination of Holdridge life's zones and altitude ranges layers is not allowed neither under Chi square test nor Kappa index combinations, because it violates the assumption of conditional independence.

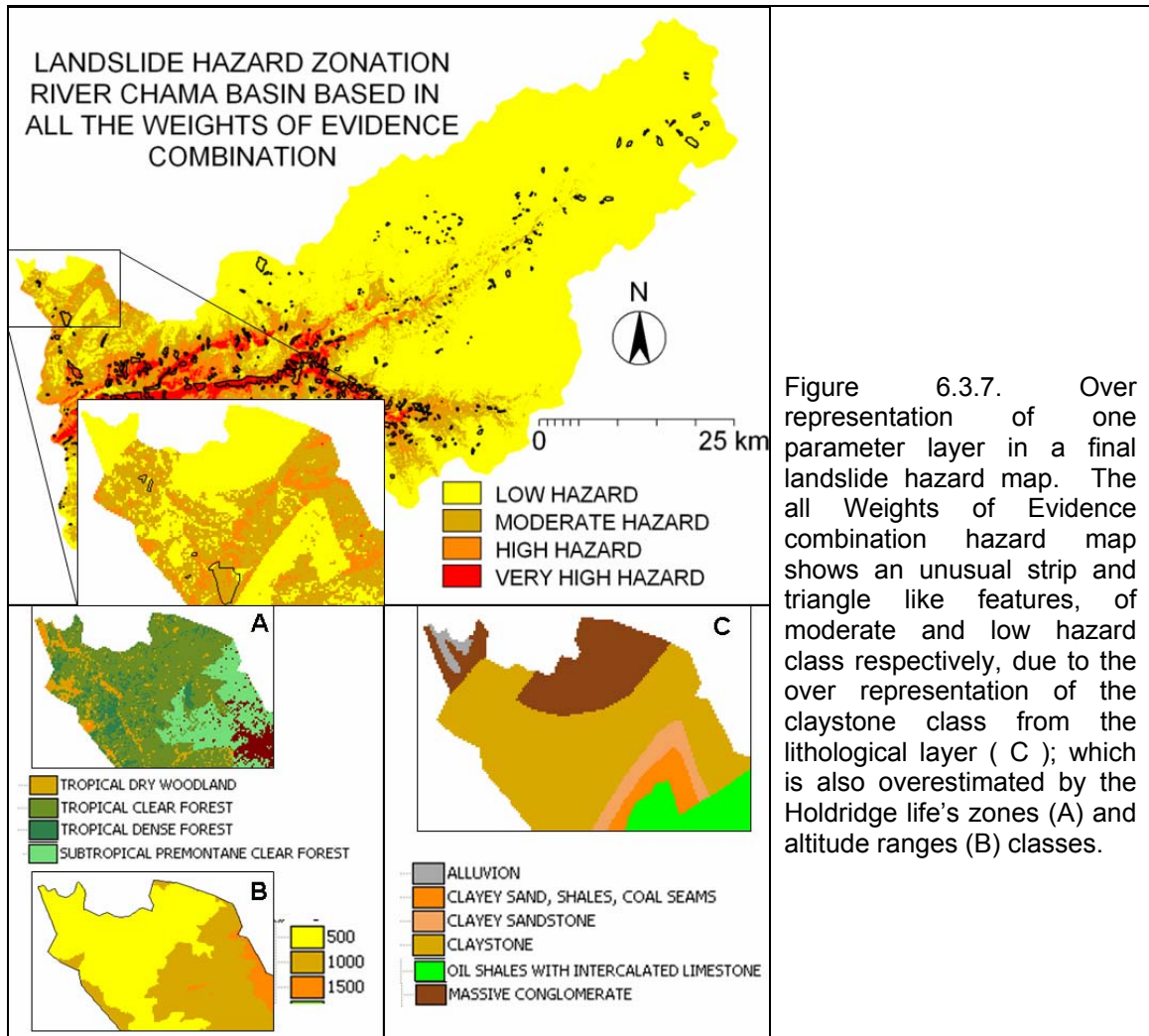


Figure 6.3.7. Over representation of one parameter layer in a final landslide hazard map. The all Weights of Evidence combination hazard map shows an unusual strip and triangle like features, of moderate and low hazard class respectively, due to the over representation of the claystone class from the lithological layer ( C ); which is also overestimated by the Holdridge life's zones (A) and altitude ranges (B) classes.



## Chapter 7: Summary of the three landslide methodologies and conclusions

The aim of this chapter is to compare and validate the three different final landslide hazard maps obtained through also different methodological approaches as those are: The heuristic geomorphological approach, the Multicriteria Evaluation (MCE) approach via the Analytical hierarchy procedure, and the Statistical approach represented by the Weights of Evidence procedure. These methods are assessed with respect to their accuracy and correctness in classification of landslide hazard classes.

To achieve this goal, a map comparison procedure between the three hazard maps and the landslide inventory map, allows a preliminary spatial visualization and assessment of the distribution of the hazard classes through the total area, and by this way it enables the computing of different levels of uncertainties and matching by each of the hazard maps. This technique are helpful in order to address the general performance of the landslide hazard maps generated in this study, however, given the complexity involved in any hazard predictive analysis, a contingency matrix procedure is applied to be evaluated statistically for the accuracy and error rate of the hazard maps. The contingency matrix is used for checking the accuracy of the landslide hazard classification on the basis of its comparison to the landslide inventory map, resulting in a tabulation of occurrences per frequency and in a number of accuracy measurements. Given that the weakness in any landslide hazard classification is partly explained by the quantity and quality of data input (Remondo et al, 2003), the accuracy and error rate are also computed for the factor maps used throughout this analysis.

Since the error rate and uncertainty procedures generally allow only the disclosing of landslide pixel misclassification, a validation of the landslide hazard maps predictive power is necessary (Chung et al , 2003), then a success rate curve is computed and is outlined for all the three hazard maps. The success rate curve is sketched out for each of the predictive hazard maps and it is based in the comparison between them and the landslide occurrences contained in the study area's landslide inventory map, describing the model's goodness of fit. Finally, given that the validation via success rate curve may potentially define the most accurate landslide hazard zonation map, an identification and

quantification of the correlation between the three hazard maps was carried out in order to assess their spatial association. In all of the former testing procedures the landslide inventory map is the fundamental key and point of reference since the landsliding area is the basic feature to be outlined in any landslide predictive map.

The uncertainty in this study is defined as the experimental inaccuracy with which a pixel is classified or not as a landslide prone pixel given the relationship between the landslide occurrences outlined in the inventory map, and the landslide hazard classes predicted by the landslide hazard maps. The uncertainty can be linked to the accuracy of the prediction (ACP) obtained from a contingency matrix and interpreted at three levels: No-uncertainty, low-moderate uncertainty and moderate high-uncertainty. In the same sense, the error misclassification (EM) can be interpreted as a: Matched, subestimated and overestimated classification of a pixel into a landslide hazard class. Concepts related to ACP and EM are full described in the next section. Table 7.1 describes a qualitative interpretation of uncertainty and matching from the landslide hazard classes / landslide occurrences relationship whereas Figures 7.1 to 7.3, display its spatial distribution.

Table 7.1. Uncertainty and matching following the landslide hazard classes / landslide occurrences relationship

<b>Landslide hazard classes</b>	<b>Landslide occurrences</b>	<b>Uncertainty</b>	<b>Matching</b>
Low hazard	Non-landslide	No-uncertainty	Matched
	Landslide	Low - moderate	Subestimated
Moderate hazard	Non-landslide		Overestimated
	Landslide	No-uncertainty	Matched
High hazard	Non-landslide	Moderate - high	Overestimated
	Landslide	No-uncertainty	Matched
Very high hazard	Non-landslide	Moderate - high	Overestimated
	Landslide	No-uncertainty	Matched

At first glance (see Figures 7.3 to 7.5), the Weights of evidence could be considered as more successful than the MCE and Geomorphological procedures, given its higher rate in the matching and no-uncertainty reached in the classification of the actual landslide areas as hazardous; however it can not be considered conclusive because the predictive power of the models is potentially encompassed within the moderate-high uncertainty and overestimation of landsliding areas found on them. Therefore, it is necessary to test the accuracy, error and precision of these predictive models.

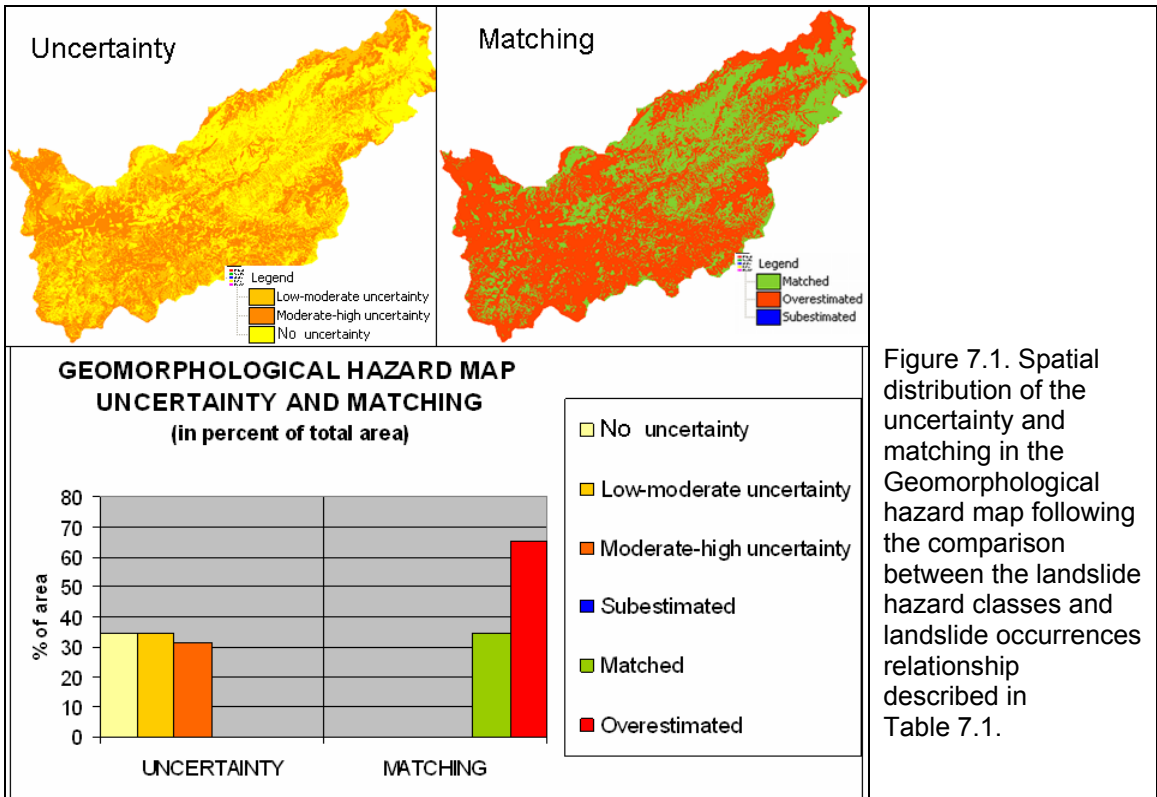


Figure 7.1. Spatial distribution of the uncertainty and matching in the Geomorphological hazard map following the comparison between the landslide hazard classes and landslide occurrences relationship described in Table 7.1.

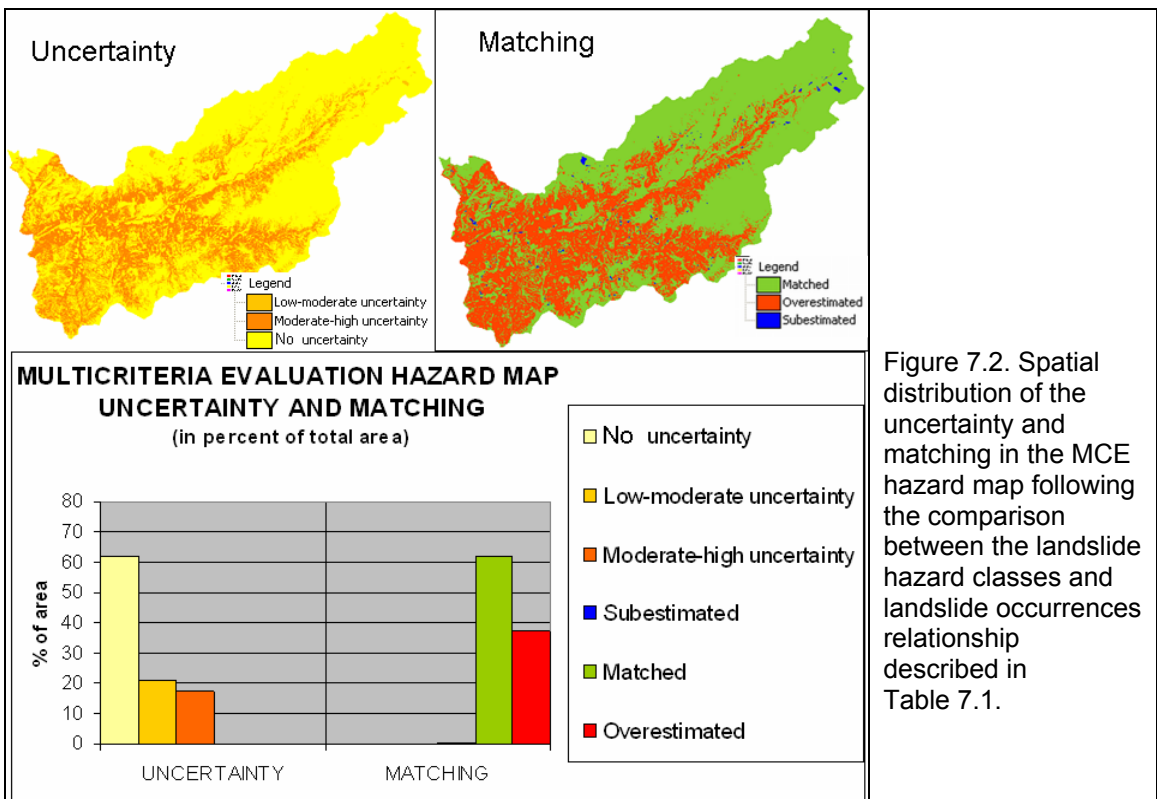
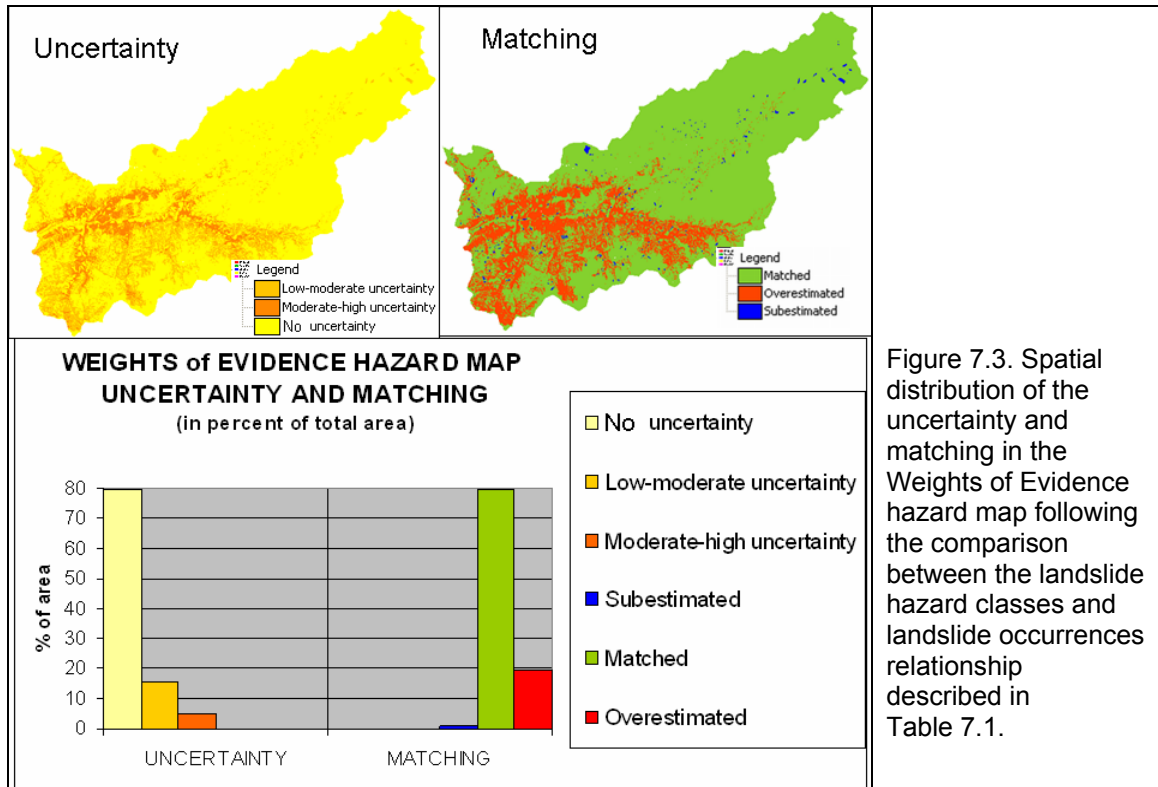


Figure 7.2. Spatial distribution of the uncertainty and matching in the MCE hazard map following the comparison between the landslide hazard classes and landslide occurrences relationship described in Table 7.1.



### 7.1 Evaluation of the accuracy and error rate

The distribution, uncertainty and matching of the landslide hazard classes by the three hazard zonation procedures over the whole and landsliding area, can be used only as a preliminary description of the performance of these approaches, however once a classification procedure is applied, it is vital to check out the accuracy of the method in assigning hazard classes to a particular area, which is often done using a contingency matrix (Jensen, 1998). A contingency matrix is a visualization tool called also a matching or error matrix, where each column of the matrix represents the predicted classes, while each row represents the actual classes (Burrough et al., 1998).

Generally, the two main measurements can be obtained from the contingency matrix as those are: The accuracy of the prediction and the error for misclassification. Error rates are used to compare the predictive power of landslide hazard maps being the primary quantitative measure for evaluating the predictive power of a classification rule (Brenning, 2005). Table 7.2 describes the parameters of measuring derived from a contingency matrix procedure which are better illustrated in Appendix 7.4.

Table 7.2. Landslide hazard classes distribution over the landsliding area per methodological approach.

Symbol	Measuring	Description
<i>AC</i>	Overall Accuracy	Proportion of pixels <b>correctly</b> predicted as non-landslide occurrences
<i>TP</i>	True Positive Rate	Proportion of pixels <b>correctly</b> predicted as landslide occurrences
<i>TN</i>	True Negative Rate	Proportion of pixels <b>correctly</b> predicted as non-landslide occurrences
<i>FP</i>	False Positive Rate	Proportion of pixels <b>incorrectly</b> predicted as landslide occurrences
<i>FN</i>	False Negative Rate	Proportion of pixels <b>incorrectly</b> predicted as non-landslide occurrences
<i>P</i>	Precision	Proportion of pixels <b>correctly</b> predicted as landslide occurrences

In this study the accuracy of the prediction (ACP), and the error for misclassification (EM) are given by the geometric mean in the following equations:

$$ACP = \left( \prod (AC, TP, TN, P) \right)^{1/4}$$

$$EM = \left( \prod (FP, FN) \right)^{1/2}$$

### 7.2 Accuracy and error rate within landslide hazard maps

In order to compare the three landslide hazard zonation maps to the landslide inventory map it was necessary to aggregate the landslide hazard classes to two main domains: one related to a significant landslide predictive class as that made out by the aggregation of all the pixels belonging to the high and very hazard classes, and a second domain considered as a non-significant hazard class which was conformed by the pixels classified within the moderate and low hazard classes. These new reclassified landslide hazard maps are then compared to the also two classes (landslide, non-landslide) landslide inventory map, getting a two entries contingency matrix (Appendix 7.4). Following Figure 7.4, the Weights of Evidence procedure map is assumed to have the best accuracy over all the accuracy parameters except in the true positive rate, where the geomorphological procedure reaches a full score. However, this accuracy of the Weights of evidence procedure is actually supported by the matching in classifying the non-

landslide pixels rather than the non-landslide ones, as is shown by the differences between True positive and True negative rates.

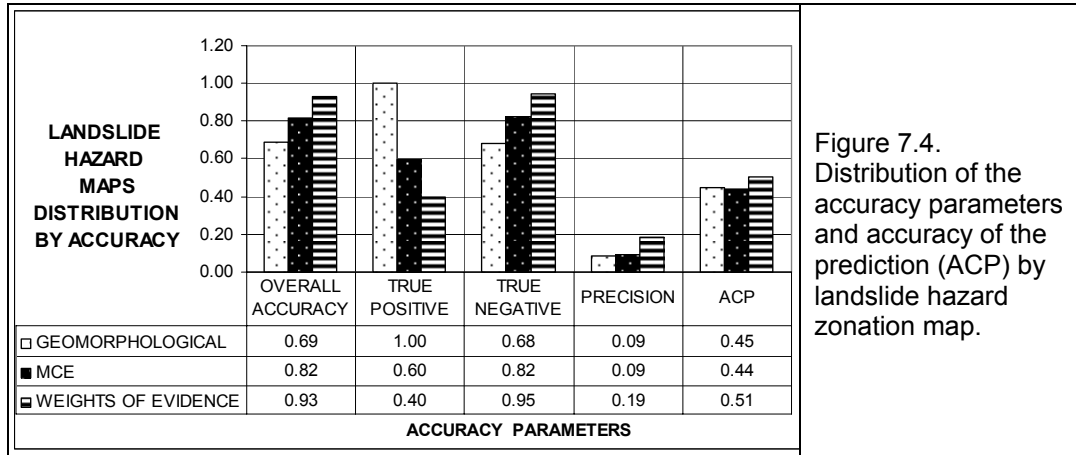


Figure 7.4. Distribution of the accuracy parameters and accuracy of the prediction (ACP) by landslide hazard zonation map.

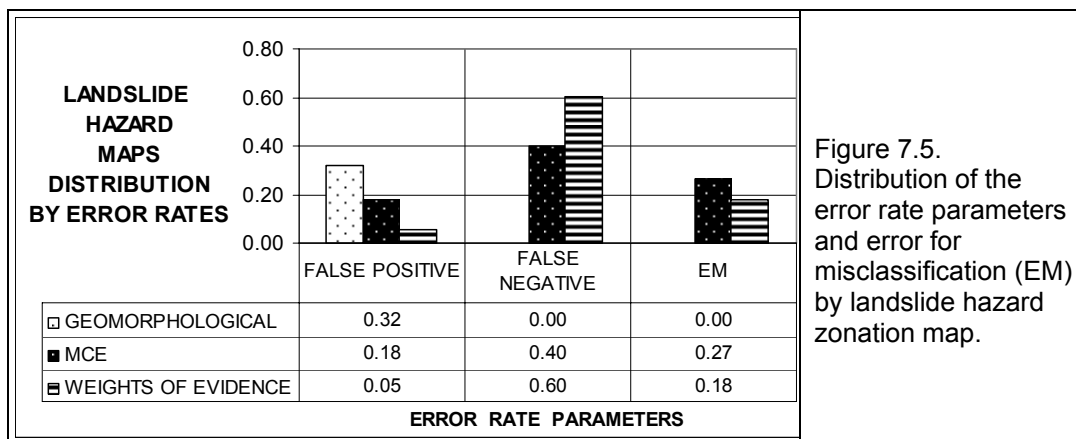


Figure 7.5. Distribution of the error rate parameters and error for misclassification (EM) by landslide hazard zonation map.

Such the high matching of non-landslide pixels allows the Weights of Evidence procedure to show a better precision; however, some of those non-landslide pixels are actually landslides as it is shown in Figure 7.5, as a false negative rate. A false positive rate is always preferred than a false negative because a non-landslide pixel classified as a landslide hazard class is a potential prediction. The interpretation of the contingency matrix parameters demonstrates that, although the ACP (Figure 7.4) of the Weights of Evidence procedure is slightly more significant than the geomorphological and MCE procedures, respectively, the EM (Figure 7.5), found in the MCE and Weights of Evidence affect negatively the reliability of these procedures comparing to the

geomorphological procedure. In this regard, from the contingency matrix assessment the geomorphological procedure hazard map can be considered a better achievement, followed by the Weights of evidence and later the MCE.

### 7.3 Accuracy and error rate within factor maps

A healthy practice in the landslide hazard zonation is the identification of the sources of error which can influence the reliability of the landslide hazard models, since it provides the only way to improve the methodological procedure. In this analysis, the factor maps used for the performance of the three landslide hazard models, were compared to the landslide inventory map via also a contingency matrix procedure, in order to determine the role played of the data input in the hazard classes final classification: in other words, how helpful were these factor maps in the accomplish of the three different landslide hazard zonations carried out and which of them need to be improved. To apply the two entries contingency matrix (Appendix 7.4), the factor maps were reclassified following the classes defined in the density analysis index (Chapter 5), and later aggregated into two single classes, one considered as landsliding prone and the second as a non landslide prone. The results are presented graphically in Figures 7.8 and 7.9.

If it can be assumed that the reliability of the ACP (Figure 7.6) is indirectly proportional to the EM rates (Figure 7.7), it is possible to define two main groups of factor maps. The first group incorporates the geomorphological units, Holdridge life's zones, altitude ranges, lithology, drainage buffers and internal relief maps. These factors were considered in this study as the more consistent factor maps for the hazard zonation practice.

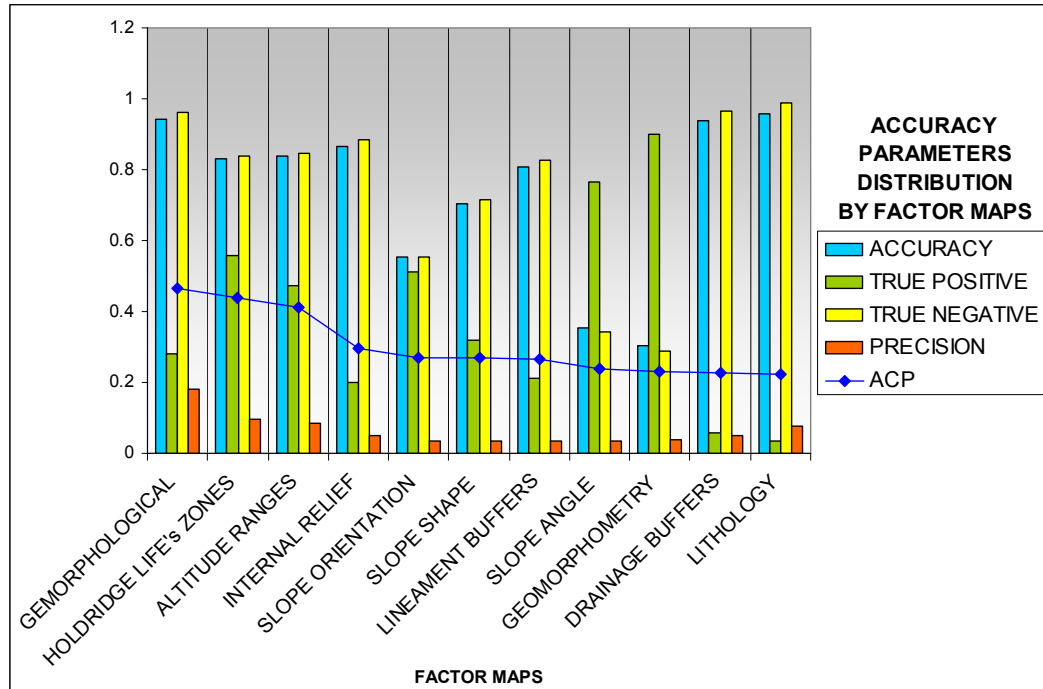


Figure 7.6. Accuracy parameters distribution by factor maps.

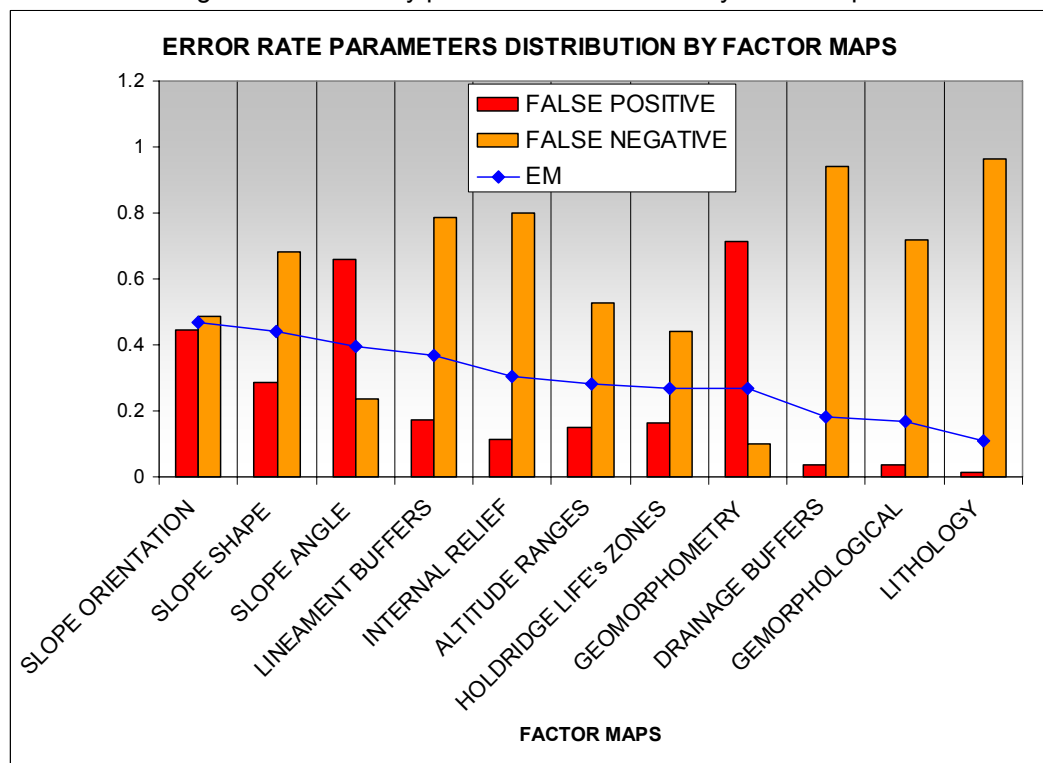


Figure 7.7 Error rate parameters distribution by factor maps.

The second group, comprising the geomorphometric units, lineament buffers, slope angle, slope shape and slope orientation maps, was considered less consistent. The first



group guarantees an enhancement of the accuracy and precision of the compared landslide hazard models, while the second group required improvement. For example, there is not doubt that the slope angle is may be the most important element in slope instability; however, not all the areas with steep slopes are landslide prone, and misclassification of these areas can reflect the previous reclassification of the raw data into a slope angle classes map. Another example is given by the internal relief map which is at some point a reclassification of the terrain slope angle. As shown in Figures 7.8 and 7.9, it scores better than the slope angle map as a landslide predictor, probably because of the different range and scale used in its reclassification into classes.

The study area's geomorphological evolution is largely founded upon climatic processes; hence, landsliding processes are particularly linked to the interaction precipitation-lithology-climatic zones. These are better represented in the geomorphological units, Holdridge life's zones and altitude ranges factor maps. Together, they were found more consistent in the landslide hazard zonation, suggesting that the better quantity and integration of the geographical settings, the better is the association with the slope instability process. For example, factor maps like the geomorphological units and Holdridge life's zones, are based on the interrelationship between by other geographical variables such as lithology and landforms for the first instance and climate and landcover in the second. On the other hand, factor maps as the slope orientation and shape, which represent solely features of the terrain as the geometric shape and aspect, show a lesser descriptive link with slope instability.

#### 7.4 Validation

Whether the contingency matrix procedure allows the assessment of the model's performance, providing important insights to improve the data input and its final calibration in prediction modeling, the most important and the absolutely essential component is to carry out a validation of the prediction results (Chung et al., 2003). At the same time, field validation must guide further data collection and field practice for landslide hazard mapping. In this section the validation of the landslide hazard maps is addressed through two procedures: the success rate curve and the coefficient of correlation.

#### 7.4.1 Success rate curve

The success rate curve illustrates how well the hazard maps perform with respect to the left-side landslide accumulated distribution (Lee, 2005), in the sense that indicates the percentage of all landslides that occur in the classes with the highest values for the delineation of landslide hazard by the different methods (van Westen et al., 2003). These susceptibility indices values are ranked from high to low along the X-axis, this being the analytical technique for assessing and empirically comparing the results of the different landslide hazard predictions (Chung et al., 2003). Figure 7.8 describes the success rate curves calculated for the three different landslide hazard maps compared in this study. Assuming that an ideal success rate curve, with perfect prediction accuracy should include the total area of the Cartesian diagram, the areas under the different success rate curves can be of use to estimate the overall prediction accuracy of every procedure discussed here.

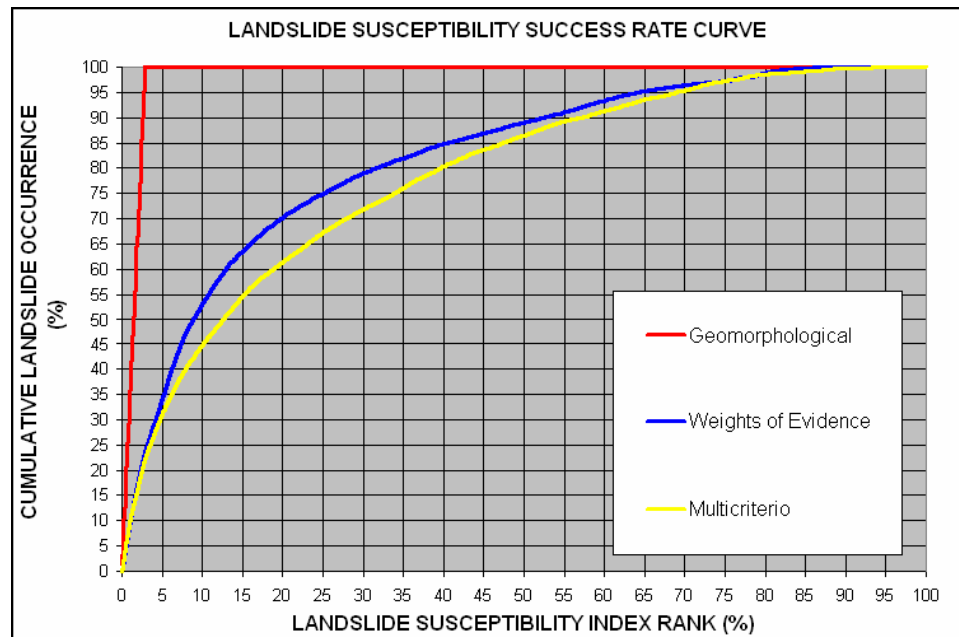


Figure 7.8. Success rate curves calculated for the three landslide hazard zonation maps. The Y-axis indicates the cumulative percentage of the all landsliding occurrences in the study area, and the X-axis indicates the landslide susceptibility indices ranked from high to low values based on the frequency observed from the histogram. As an example, when the landslide susceptibility rank is 5%, it is representing the top 5% of the landslide hazard classes or landslide probabilities, and in this case that 5% is able to predict the 100%, 35% and 32% of the landslide occurrences following the Geomorphological, Weights of evidence and Multicriteria evaluation (MCE) respectively.

Given a value of 1 for the total area, the following areas are recalculated as ratio values. In this way the area ratio value of the geomorphological approach success rate curve is 0.984, the statistical approach 0.82 and the MCE approach 0.785, which could be interpreted as the analyzed approaches have respectively 98.4%, 82% and 78.5% of prediction accuracy on the landsliding processes of the study area. Though Figure 7.8 clearly indicates the dominance of the geomorphological approach over the statistical and the MCE approaches, the predictive power of all the landslide hazard maps can be considered successful since the prediction accuracy for each exceeds 75%.

#### 7.4.2 Correlation

A correlative analysis is a statistical tool that, in the case of a spatial data, characterizes the distribution of pixel values in two raster maps, in order to obtain the degree of accuracy of their spatial association (Boham-Carter, 1996). In this correlative analysis, the main goal is to define which pixels in a tested map are correctly classified with respect to another map, assuming this last as the base map. As indicated the success rate curve, the geomorphological hazard map is the more reliable with respect to the Weights of Evidence and MCE hazard maps; therefore, it is used as a base map for this correlative analysis. Main reason for this comparison is to set how close are the analyzed hazard maps, since they are representing the same topic with the same parameter and classes, therefore this correlation is considered only for illustrative purposes.

- Accuracy: the probability that classes as in a tested map are classified as the same classes as in the base map
- Reliability: the probability that classes in the base map correspond to the same classes as in the tested map.
- Overall accuracy: probability given by the product of total amount of correctly classified areas within the total study area.

A better description on the background and use of the correlative statistics in spatial data can be reached at Hagen (2002), Foody et al., (2002), and Boham-Carter (1996).

Table 7.3, describes the correlative analysis applied to the Geomorphological, Weights of Evidence and MCE hazard maps. The following conclusions can be drawn for this table:

- The three landslide hazard maps in general show a low to moderate level of spatial association, which is expected because they were generated under different procedures.
- The highest level of spatial association is found between the Weights of Evidence and the MCE hazard maps, followed by the correlation between the geomorphological and MCE maps. The lowest level of association is found between the geomorphological and the Weights of Evidence maps, which can be explained not only on the differences of data processing but also because of the difference in the data representation; the geomorphological map uses a unique-condition mapping unit, whereas the Weights of Evidence is a full pixel unit based procedure.
- The moderate association described between MCE and the Weights of Evidence hazard maps at first can be explained by the fact that both methods are based on the basis of pixel-based data weighting procedures. However, this moderate level of spatial association is also found between the MCE and the Geomorphological hazard maps, which reflects the fact that the weighting of the factor maps in the MCE is mostly heuristic.
- The Low hazard class described the highest accuracy in the correlation between the hazard classes in the three maps, which is expected since 97% of the total area is landslide free.
- The reliability of the Very high hazard class among the analyzed maps is higher in all the correlations except at the low hazard class between the Weights of Evidence and MCE maps. This is a clear sign of the reliability of the landslide hazard zonation provided through the geomorphological procedure, since it was selected as the base map in this correlative analysis.

Table 7.3. Matrix of correlative analysis of the landslide hazard zonation maps.

<b>GEOMORPHOLOGICAL / WEIGHTS OF EVIDENCE. CORRELATION (pixels)</b>					
HAZARD CLASSES	LOW HAZARD	MODERATE HAZARD	HIGH HAZARD	VERY HIGH HAZARD	ACCURACY
LOW HAZARD	105399	5343	208	19	0.95
MODERATE HAZARD	96472	19544	2973	1073	0.16
HIGH HAZARD	56424	19225	3635	1927	0.04
VERY HIGH HAZARD	15544	10151	6138	6391	0.17
RELIABILITY	0.28	0.36	0.38	0.68	
AVERAGE ACCURACY = 33.11%					
AVERAGE RELIABILITY = 42.62%					
OVERALL ACCURACY = 38.51%					
<b>GEOMORPHOLOGICAL / MCE. CORRELATION (pixels)</b>					
HAZARD CLASSES	LOW HAZARD	MODERATE HAZARD	HIGH HAZARD	VERY HIGH HAZARD	ACCURACY
LOW HAZARD	93708	14518	3985	145	0.83
MODERATE HAZARD	70707	31773	17109	2282	0.26
HIGH HAZARD	39252	19826	17940	5245	0.22
VERY HIGH HAZARD	10274	7818	11432	9087	0.24
RELIABILITY	0.44	0.43	0.36	0.54	
AVERAGE ACCURACY = 38.70%					
AVERAGE RELIABILITY = 44.14%					
OVERALL ACCURACY = 42.95%					
<b>WEIGHTS OF EVIDENCE / MCE. CORRELATION (pixels)</b>					
HAZARD CLASSES	LOW HAZARD	MODERATE HAZARD	HIGH HAZARD	VERY HIGH HAZARD	ACCURACY
LOW HAZARD	206875	52396	14083	485	0.76
MODERATE HAZARD	2653	19719	27715	4176	0.36
HIGH HAZARD	363	925	6252	5414	0.48
VERY HIGH HAZARD	244	400	2142	6624	0.70
RELIABILITY	0.98	0.27	0.12	0.40	
AVERAGE ACCURACY = 57.64%					
AVERAGE RELIABILITY = 44.36%					
OVERALL ACCURACY = 68.33%					

Because the three landslide hazard models compared here were built with the same factor maps and under a preliminary basis provided by the Density analysis (Chapter 5), a higher level of spatial association could be expected than what was achieved. However, the low to moderate spatial association measured between the three landslide hazard maps demonstrates that in this case, different approaches in the landslide hazard zonation practice, play a more important role in the final hazard maps rather than the quantity and quality of the data input. The role of the quantity and quality of the data input to improve any landslide hazard zonation practice depends more on the level of integration of the

geographical variables and processes within the factor maps, as documented by van Westen et al., (2006). By comparison, the addition of more detailed geomorphological data increased the overall accuracy of a series of landslide hazard zonation maps built on the basis of a bivariate statistical analysis. These results do not invalidate the landslide predictive power of the landslide hazard maps here already demonstrated through the success rate curve, because inter-map correlation measures are generally useful for exploring relationship rather than to confirm them (Boham-Carter, 1996).

Differences in the boundaries of the hazard classes can also ruin the correlation between the three hazard maps (Ardizzone et al., 2002). For instance, in the case of the geomorphological hazard map, the class boundaries are sharp and closed to natural-physical features, but in the case of the MCE and the Weights of Evidence, the class boundaries are delineated by just the grouping of pixels with a same value. This gap can be traced back into the factor maps and the procedure applied to process them. Suzen et al., (2004), in a comparison between bivariate and multivariate procedures for landslide hazard zonation, found that most of the errors were dependent on the class boundaries of the factor maps, which probably is later enhanced or lessened during the processing of the data. For example, whether the geomorphological approach tends to overestimate landslide hazard areas given the subjectivity in the definition of the terrain mapping units, in the statistical approach there is a tendency to simplify the factors that condition landslides (van Westen, 2006).

### 7.8 Conclusions

In this study, three main landslide hazard zonation procedures which represent a gradation between the heuristic and the probabilistic approaches – the geomorphological, the Multicriteria evaluation (MCE) and the Statistical (Weights of Evidence) –, were applied to a single tropical mountain basin, that was characterized by large scale landsliding processes. The resulting landslide hazard zonation maps were assessed, compared, and validated in order to outline the main differences between the approaches in terms of accuracy and reliability. Accomplishing of this main goal required the following other steps:

- The building of a landslide inventory map by the use of high resolution aerial photographs and hyperspectral information from LANDSAT imagery.
- The generation of a more consistent DEM from remotely sensed data with the merging of ground control points with the SRTM data and the ASTER stereo-image satellite data.
- Designing of all the procedures and data format to work within a GIS data base.
- The testing of each approach using the same factor map data set, and based on a comparable relationship as obtained from the density analysis procedure in Chapter 5.
- Evaluation of the uncertainty, accuracy, and error within the final and within the used factor maps.

Since the landslide inventory map is probably the most important data input for landslide hazard zonation practice, such maps could be improved as well in spatial as in temporal and spectral resolution using remote sensing information. At present time, it is possible to get high resolution imagery by the use of the Quick Bird and Ikonos satellite systems. It is likely that the incoming improvement of the spatial resolution in the Moderate Resolution Imaging Spectroradiometer (MODIS) system will allow a more consistent monitoring of world-wide areas affected by landslides, by generating landcover products that are an important data inputs for the estimation of landslide susceptibility. This improvement together with data remotely sensed data on precipitation can be the starting point of a new prediction system for rainfall triggered landslides as that described in Yang et al. (2007), and reinforces the necessity for a global data base that address the passive factors involved in landsliding process.

This study also demonstrated the practical use of the LANDSAT imagery, not only to detect landslide's scars but also to update and complement previous information or that one provided through different source. Moreover, satellite imagery obviates the time consuming task of digitizing and orthorectifying aerial photographs, permitting faster transposing of information between the manual photointerpretation to the GIS data base. A landslide inventory map should contain as much information as possible including a temporal dimension, although for general and regional scale analyses the occurrences and

dimension of the landslides is often the only information required. In tropical mountain areas the rapid regrowth of vegetation on surfaces after landslides, makes difficult their detection using satellite imagery; therefore, fieldwork is always required.

A DEM provides either directly or indirectly more than 40% of the total data input in a landslide susceptibility analysis and, a reliable DEM is therefore fundamental to the accuracy of final landslide hazard maps. In this analysis, the DEM obtained through remote sensing data as that provided by the SRTM and ASTER imagery systems was improved with the input of over 200 GCPs taken during fieldwork. In this regard, the accuracy or consistency of SRTM base DEM versus one derived from ASTER data is moot, as both DEM sources were able to reproduce a useful topographic model of the study area, particularly because the rationale of this analysis matches the regional scope.

The diffusion of GIS is allowing earth science data to be efficiently and cost-effectively processed for geomorphological surveys (Carrara, 1989; Soeters et al., 1996; Carrara et al., 1991). However, besides a few exceptions (Wang and Unwin, 1992; van Westen, 1993; van Westen, N. Rengers and R. Soeters, 2003), this issue has not received adequate attention in the literature, and highlights the importance of bridging this methodological gap between the traditional geomorphological and probabilistic landslide hazard zonation approaches, through the use of GIS for data base construction and general routines. Probably one of the challenges for landslide hazard zonation with GIS environment will be the effective incorporation of the landslide triggering factors within the final hazard map and a 3D dynamic to improve the prediction on the scope, speed and dimension of the landslide body. This latter task is particularly crucial as the hazards posed by any landslide are obviously related to its mass and speed, the lethality being disproportionately greater for large slides than for small ones.

The only way to enhance the objectivity and reliability of any landslide hazard zonation mapping approach is reducing the uncertainty in the data input. This issue deals with the generation of better factor maps, which involves the generation of a more integrated data. For example, in this study some factors maps such as the Holdridge life's zones and the geomorphological units, were determined to be the most accurate parameters for landslide prediction, as they are the product of several geographical variables rather than the solely arbitrary partition of a variable domain (as in the case of the slope orientation



where slope aspect is classified just upon azimuth's intervals and not associated to another related geographical variable as wind/precipitation distribution and solar radiation). Probably the generalization of the low hazard class in the weights of evidence procedure in clear contrast with the overestimation of the higher hazard classes in the geomorphological approach, has an initial point in the use of different units of analysis; the pixel-based feature used in the first and the unique-condition feature for the second. In that sense, the weights of evidence procedure can be substantially improved if the factor maps to put into the model are preliminary reclassified under a unique-condition feature basis.

To be sure, the landslide hazard zonation practice clearly requires the knowledge of the causal factors and the ability to represent them in a map, as a previous step to construct the GIS data base and subsequent processing under any hazard zonation approach. Thus, a better conceptualization of the landsliding process in a selected area can considerably reduce the uncertainty of the input factor maps

Finally, although the results over here obtained are only valid for this area, the validity of the traditional geomorphological approach over the statistical and the MCE procedures does not disqualify the achievement of these hazard maps. The MCE procedure is faster and does not need a previous landslide inventory map, which makes it very adaptable to situations where such information may not be available. It also can serve as a basis for improving a subsequent geomorphological as it will identify likely sites of mass wasting activity, and simplify fieldwork and other aspects in the geomorphological analysis.

Further research must be addressed to:

- Circumvent the concept of conditional independence in geographical data processed under classical statistical assumptions. In this study, the use of the Kappa index instead of the Chi Square to test the level of association of the factor maps used in the probabilistic approach, was proved to be more convenient.
- Develop multiple levels of analysis in the MCE procedure to ensure the evaluation of the membership of the classes contained in the factor maps. Following the density analysis was demonstrated that in certain factor maps the low membership to landsliding process of the most of the classes, averages the

membership of the few landslide-prone classes, reducing their contribution into the model.

- Explore the relationship between temporal NDVI, NWDI, wetness indices, etc; provided by remote sensing imagery and precipitation records with landsliding process as a way to establish at regional scope, thresholds to predict landslide triggering mechanism.
- Incorporate soil profiles data into landslide hazard modeling via the extrapolation of point data together with remotely sensed information.

### 7.8 Summary

Three main landslide hazard zonation procedures representing a gradation between the heuristic and the probabilistic approaches: The Geomorphological, the Multicriteria evaluation (MCE) and the Statistical (Weights of Evidence), which were assessed, compared and validated in order to outline differences terms of accuracy and reliability.

The accomplishing of this main goal required the following other steps:

- The building of a landslide inventory map via aerial photographs, fieldwork and LANDSAT imagery.
- A more consistent DEM from remotely sensed data ASTER – SRTM and GCP
- The design of all the procedures and data format within a GIS data base.
- The testing of each approach using the same factor map data set and based in a previous density analysis.
- Evaluation of the uncertainty, accuracy and error within the final maps and within the used factor maps.

Following the results showed in this study, the three landslide hazard zonation approaches are not exclusive and these can be used successfully under different condition of accuracy of prediction power, objectivity and reproducibility, and versatility in cases of lack of data input and rapid assessment demand. This conditions and the suggested use of landslide hazard approaches are described in table 7.4.

Table 7.4. Suggested uses of different landslide hazard zonation approaches following different condition and purposes.

	LHZ approaches
In terms of accuracy and predictive power	Geomorphological
	Weights of evidence
	MCE
Reproduction capability and objectivity	Weights of evidence
	MCE
	Geomorphological
Following its versatility and response to a rapid environmental assessment	MCE
	Geomorphological
	Weights of evidence

#### Contribution

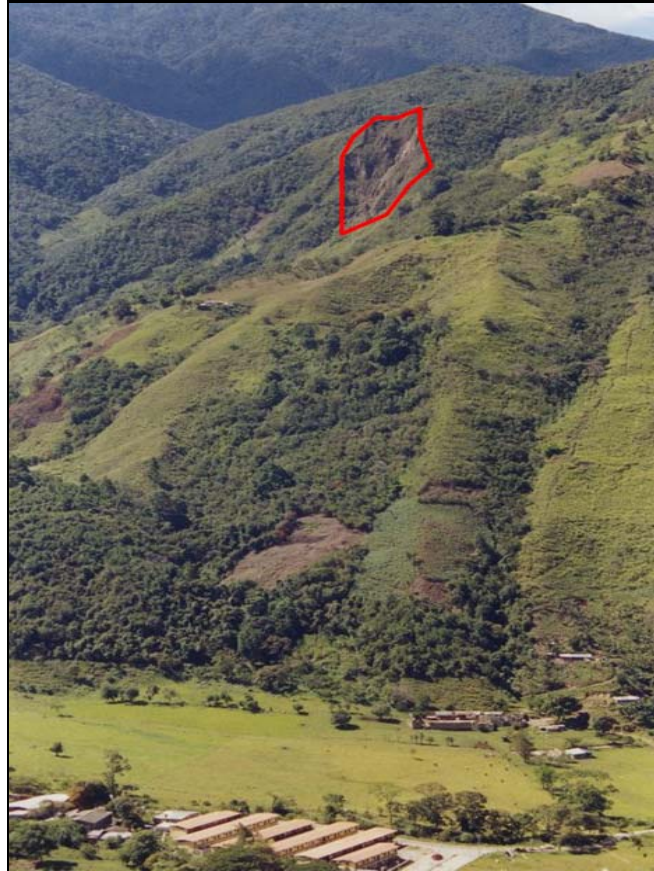
- Bridging the gap between the heuristic and statistical approaches in landslide hazard zonation practice, through the use of GIS routines and remote sensing data.
- Introducing the MCE as a versatile and reliable procedure for landslide hazard zonation.
- Improving the testing of conditional independence between the factor maps in the weights of evidence procedure by the use more “geographical” indices
- Evidencing the need of more “geographically” integral factor maps for landslide hazard zonation practice.
- Illustrating the feasibility of remote sensing data for landslide susceptibility practice.
- Demonstrating that different landslide approaches are inclusive since it can be used under different conditions of data availability, processing and necessity.

#### Future developing and career’s plans

- Developing of regional data bases on landslide susceptibility based in remote sensing sources.
- A better definition of concepts related to natural hazards and risks, as well as a clear understanding of the target of these analyses.
- Increasing of the modeling of geographical landslide prone variables to more integrated approaches.
- Adaptation of traditional geomorphology to a more dynamic approach supported by remote sensing data as a way to increase consistency, quantity and quality of data.
- To bring the gap between landslide triggering factors and passive factors.

## APPENDICES

	<p><b>Appendix 2.1.</b> Although some lithological units as those as Fm. Aguardiente and Fm. La Quinta, could be considered softer than Fm. Mucuchachi; landsliding processes may take place on this last as the result of the construction of a road (2003, photo by José Roa).</p>
	<p><b>Appendix 2.2.</b> Recent alluvial fans can push rivers and streams against weak geomorphological units, activating basal erosive process and subsequent slope instabilization. (2006, photo by José Roa)</p>
	<p><b>Appendix 2.3.</b> River and stream incision on very steep slopes is clearly recognizable in dry environments, illustrating the dynamic of the accumulative / erosive process in the study area. (2006, photo by José Roa)</p>



**Appendix 2.4.** Probably human intervention could be associated with the developing of located major landslides, which are later enlarged given the retrogressive character of shallow landslides developed on very steep and longitudinal slopes (2004, photo by José Roa).

**Appendix 2.6.** Landsliding process under different ecological areas. 1- Under dry climatic conditions as those found at the Lagunillas's badlands, the highly weathered meta- sandy rock losses cohesion and generates a rapid spontaneous landslide helped by the steep slope. 2- A better vegetation cover contributes with slope stabilization, however very slow mass movements as creeping, can reveal focal slope instabilization which under a potential extreme rainfall or earthquake could develop into a major landslide (2006, photo by José Roa).



### Appendix 3.1 DEFINITIONS OF TERMS

Standard terms suggested by UNDRO (United Nations Disaster Relief Organization), Sassa (2001), and Varnes (1984) related to landslide hazard zonation.

**Natural Hazard (H):** The probability of occurrence, within a specified period of time and within a given area, of a potentially damaging phenomenon.

**Vulnerability (V):** The degree of loss to a given element or set of elements at risk resulting from the occurrence of a natural phenomenon of a given magnitude. It is expressed on a scale from 0 (no damage) to 1 (total loss).

**Specific risk (Rs):** The expected degree of loss due to a particular natural phenomenon. It may be expressed by the product of H and V.

**Elements at risk (E):** The population, properties, economic activities, including public services, etc; at risk in a given area.

**Total risk (Rt):** The expected number of lives lost, persons injured, damages to property, or disruptions of economic activity due to a particular natural phenomenon. It is therefore the product of the specific risk (Rs) and the elements at risk (E).  $R_t = E * R_s = E * (H * V)$ .

**Zonation:** The division of the land surface into areas and the ranking of these areas according to degrees of actual or potential hazard. Hence landslide hazard zonation shows potential hazard of landslides or other mass movements on a map, displaying the spatial distribution of hazard classes.



**Appendix 5.1.** La Trujillana landslide seen from a S-N perspective. (2006, photo by José Roa).



**Appendix 5.2.** Lagunillas's badlands (2000, photo by Carlos Ferrer).



**Appendix 5.3.** El Palón flowslide from a N-S perspective (2003, photo by José Roa).



**Appendix 5.4.** Density analysis. Very high relevant factor map classes for landsliding process

<b>FACTOR MAP</b>	<b>CLASSES</b>	<b>FACTOR ANALYSIS</b>	<b>FACTOR % ACCUM.</b>	<b>CLASS NUMBER</b>
INTERNAL RELIEF	<200	34.71	8.70	1
HOLDRIDGE LIFE'S ZONES	SUBTROPICAL PREMONTANE MOIST SHRUBLAND	17.21	13.35	2
GEOMORPHOLOGICAL UNITS	DENUATIONAL STEEP SLOPES	15.33	17.56	3
HOLDRIDGE LIFE'S ZONES	TROPICAL DRY SHRUBLAND	14.10	21.49	4
HOLDRIDGE LIFE'S ZONES	SUBTROPICAL PREMONTANE BARE SOIL	13.40	25.25	5
HOLDRIDGE LIFE'S ZONES	SUBTROPICAL PREMONTANE DRY SHRUBLAND	13.37	29.01	6
HOLDRIDGE LIFE'S ZONES	SUBTROPICAL LOWER MONTANE MOIST BARE SOIL	12.65	32.61	7

**Appendix 5.5.** Density analysis. High relevant factor map classes for landsliding process

<b>FACTOR MAP</b>	<b>CLASSES</b>	<b>FACTOR ANALYSIS</b>	<b>FACTOR % ACCUM.</b>	<b>CLASS NUMBER</b>
HOLDRIDGE LIFE'S ZONES	SUBTROPICAL PREMONTANE DRY WOODLAND	6.95	34.88	8
ALTITUDE RANGES	<=1000	6.35	37.02	9
HOLDRIDGE LIFE'S ZONES	SUBALPINE WET WOODED GRASSLAND	5.32	38.92	10
ALTITUDE RANGES	<=1500	5.22	40.80	11
HOLDRIDGE LIFE'S ZONES	SUBTROPICAL PREMONTANE MOIST WOODLAND	5.06	42.63	12
LITHOLOGY	META-CONGLOMERATIC SANDY MATRIX	4.63	44.37	13
HOLDRIDGE LIFE'S ZONES	TROPICAL DRY WOODLAND	4.61	46.11	14

**Appendix 5.6.** Density analysis.Moderate relevant factor map classes for landsliding process

<b>FACTOR MAP</b>	<b>CLASSES</b>	<b>FACTOR ANALYSIS</b>	<b>FACTOR % ACCUM.</b>	<b>CLASS NUMBER</b>
HOLDRIDGE LIFE'S ZONES	SUBTROPICAL LOWER MONTANE MOIST SHRUBLAND	2.79	47.42	15
SLOPE CLASSES	80	2.11	48.58	16
LITHOLOGY	PHYLLITES, SCHISTS, SHALES	1.98	49.70	17
DRAINAGE BUFFER	RIVERBUFFER<90M	1.94	50.82	18
ALTITUDE RANGES	<=2000	1.89	51.93	19
GEOMORPHOLOGICAL UNITS	ESCARPMENT	1.59	52.96	20
SLOPE CLASSES	50	1.49	53.97	21
LITHOLOGY	PHYLLITES, SHALES	1.47	54.98	22
GEOMORPHOMETRIC	PIT	1.33	55.96	23
GEOMORPHOMETRIC	RIDGE	1.24	56.92	24
ALTITUDE RANGES	<= 500	1.19	57.86	25
SLOPE CLASSES	60	1.08	58.78	26
HOLDRIDGE LIFE'S ZONES	TROPICAL CLEAR FOREST	1.02	59.68	27
LINEAMENTS BUFFER	<200m	0.97	60.58	28
GEOMORPHOMETRIC	STEEP SLOPE	0.89	61.45	29
GEOMORPHOLOGICAL UNITS	DENUATIONAL HILLS	0.87	62.32	30
LINEAMENTS BUFFER	<50m	0.86	63.19	31
LINEAMENTS BUFFER	<100m	0.81	64.04	32
SLOPE CLASSES	40	0.80	64.89	33
SLOPE CLASSES	70	0.76	65.74	34
SLOPE ASPECT	N	0.70	66.57	35
HOLDRIDGE LIFE'S ZONES	SUBTROPICAL LOWER MONTANE MOIST WOODLAND	0.62	67.38	36
LITHOLOGY	CLAYSTONE	0.60	68.19	37
SLOPE ASPECT	NE	0.55	68.98	38
LINEAMENTS BUFFER	<300m	0.54	69.77	39
INTERNAL RELIEF	<150	0.46	70.55	40
SLOPE ASPECT	E	0.36	71.30	41
SLOPE SHAPE	CONCAVE	0.34	72.05	42
GEOMORPHOLOGICAL UNITS	MODERATE DENUATIONAL RIDGES AND TOPS	0.27	72.78	43
GEOMORPHOMETRIC	HILLY SLOPES	0.25	73.50	44
GEOMORPHOMETRIC	COLLUVIAL SLOPE	0.19	74.21	45
GEOMORPHOLOGICAL UNITS	DENUATIONAL VALLEYS	0.16	74.92	46
INTERNAL RELIEF	<125	0.12	75.62	47
SLOPE ASPECT	SW	0.11	76.31	48
HOLDRIDGE LIFE'S ZONES	TROPICAL DRY BARE SOIL	0.09	77.00	49
LINEAMENTS BUFFER	<400m	0.09	77.69	50
SLOPE CLASSES	30	0.02	78.36	51

**Appendix 5.7.** Density analysis. Less relevant factor map classes for landsliding process

FACTOR MAP	CLASSES	FACTOR ANALYSIS	FACTOR % ACCUM.	CLASS NUMBER
SLOPE ASPECT	S	-0.02	79.02	52
GEOMORPHOMETRIC	ESCARPMENT	-0.08	79.67	53
SLOPE SHAPE	CONVEX	-0.10	80.32	54
LINEAMENTS BUFFER	<500m	-0.11	80.96	55
GEOMORPHOLOGICAL UNITS	DENUATIONAL TERRACES	-0.11	81.61	56
SLOPE SHAPE	STRAIGHT	-0.16	82.24	57
INTERNAL RELIEF	<100	-0.25	82.85	58
SLOPE ASPECT	SE	-0.30	83.45	59
SLOPE ASPECT	FLAT	-0.40	84.02	60
GEOMORPHOLOGICAL UNITS	MODERATE DENUDATIONAL VALLEYS	-0.47	84.58	61
SLOPE ASPECT	W	-0.51	85.13	62
LITHOLOGY	GRANITIC GNEISS, MICA SCHISTS	-0.52	85.68	63
HOLDRIDGE LIFE'S ZONES	SUBTROPICAL LOWER MONTANE CLEAR FOREST	-0.56	86.22	64
SLOPE ASPECT	NW	-0.62	86.75	65
SLOPE CLASSES	20	-0.64	87.27	66
LITHOLOGY	OIL SHALES WITH INTERCALATED LIMESTONE	-0.69	87.77	67
GEOMORPHOLOGICAL UNITS	MODERATE DENUDATIONAL HILLS	-0.69	88.28	68
DRAINAGE BUFFER	STREAMBUFFER<45M	-0.80	88.77	69
GEOMORPHOMETRIC	ALLUVIAL FAN	-0.83	89.24	70
HOLDRIDGE LIFE'S ZONES	SUBTROPICAL PREMONTANE CLEAR FOREST	-0.84	89.72	71
SLOPE CLASSES	15	-0.85	90.19	72
INTERNAL RELIEF	<75	-0.89	90.65	73
ALTITUDE RANGES	<=2500	-0.93	91.10	74
SLOPE CLASSES	5	-1.01	91.54	75
LITHOLOGY	CONGLOMERATIC RED SANDS	-1.01	91.97	76
SLOPE CLASSES	10	-1.17	92.37	77
LITHOLOGY	UNCONSOLIDATED CONGLOMERATIC SEDIMENTS	-1.18	92.76	78
HOLDRIDGE LIFE'S ZONES	TEMPERATE MONTANE WET BARE SOIL	-1.21	93.15	79
HOLDRIDGE LIFE'S ZONES	SUBTROPICAL LOWER MONTANE DRY WOODLAND	-1.27	93.52	80
LITHOLOGY	PEBBLE TO FINE CLAYEY CONSOLIDATED CONGLOMERATE	-1.27	93.90	81
GEOMORPHOLOGICAL UNITS	DENUATIONAL PLANATION SURFACES	-1.28	94.27	82
GEOMORPHOMETRIC	PLANATION SURFACE	-1.29	94.64	83
INTERNAL RELIEF	<50	-1.36	95.00	84

(cont.)

<b>FACTOR MAP</b>	<b>CLASSES</b>	<b>FACTOR ANALYSIS</b>	<b>FACTOR % ACCUM.</b>	<b>CLASS NUMBER</b>
GEOMORPHOMETRIC	TERRACE COMPLEX	-1.41	95.34	85
LITHOLOGY	GRANITES, PEGMATITES	-1.52	95.65	86
HOLDRIDGE LIFE'S ZONES	SUBTROPICAL PREMONTANE DENSE FOREST	-1.71	95.93	87
INTERNAL RELIEF	<25	-1.82	96.17	88
GEOMORPHOMETRIC	GLACIAL ROCK OUTCROP	-1.90	96.40	89
ALTITUDE RANGES	<=3000	-1.91	96.63	90
GEOMORPHOLOGICAL UNITS	MODERATE DENUDATIONAL TERRACES	-1.92	96.85	91
HOLDRIDGE LIFE'S ZONES	TEMPERATE MONTANE CLEAR FOREST	-1.93	97.07	92
HOLDRIDGE LIFE'S ZONES	TEMPERATE MONTANE CLOUD FOREST	-1.94	97.29	93
HOLDRIDGE LIFE'S ZONES	TROPICAL DENSE FOREST	-1.98	97.50	94
HOLDRIDGE LIFE'S ZONES	TEMPERATE MONTANE MOIST WOODLAND	-2.00	97.71	95
LITHOLOGY	SILTSTONE SHALE LIMESTONE INTERCALATED LAYERS	-2.02	97.91	96
HOLDRIDGE LIFE'S ZONES	SUBALPINE WET MIXED FOREST	-2.03	98.11	97
INTERNAL RELIEF	>200	-2.10	98.29	98
GEOMORPHOLOGICAL UNITS	STABLE MOUNTAIN SLOPES	-2.16	98.46	99
ALTITUDE RANGES	<=3500	-2.18	98.62	100
HOLDRIDGE LIFE'S ZONES	SUBALPINE WET GRASSLAND	-2.19	98.78	101
GEOMORPHOLOGICAL UNITS	STABLE ALLUVIAL FAN	-2.23	98.94	102
GEOMORPHOMETRIC	GLACIAL VALLEY	-2.26	99.08	103
HOLDRIDGE LIFE'S ZONES	TEMPERATE MONTANE WET WOODLAND	-2.37	99.20	104
HOLDRIDGE LIFE'S ZONES	TEMPERATE MONTANE MOIST BARE SOIL	-2.37	99.32	105
LITHOLOGY	CLAYEY SAND, SHALES, COAL SEAMS	-2.44	99.43	106
ALTITUDE RANGES	<=4000	-2.47	99.52	107
HOLDRIDGE LIFE'S ZONES	SUBALPINE WET WOODLAND	-2.51	99.61	108
HOLDRIDGE LIFE'S ZONES	TEMPERATE MONTANE MOIST SHRUBLAND	-2.57	99.68	109
GEOMORPHOMETRIC	GLACIS	-2.60	99.75	110
LITHOLOGY	MARINE SHALES, MARLS, LIMESTONE	-2.64	99.81	111
HOLDRIDGE LIFE'S ZONES	TEMPERATE MONTANE WET SHRUBLAND	-2.64	99.87	112
GEOMORPHOMETRIC	GLACIAL COLLUVIAL SLOPE	-2.66	99.92	113
GEOMORPHOMETRIC	MORaine AND RIDGE	-2.71	99.96	114
GEOMORPHOLOGICAL UNITS	STABLE VALLEY TERRACES	-2.79	99.98	115
LITHOLOGY	CLAYEY SANDSTONE	-2.81	100.00	116
HOLDRIDGE LIFE'S ZONES	SUBALPINE RAIN WOODED GRASSLAND	-2.87	100.01	117
GEOMORPHOLOGICAL UNITS	DENUDATIONAL GLACIAL RIDGES AND TOPS	-2.89	100.01	118

**Appendix 6.1. Terrain mapping units categories and subcategories**

TERRAIN MAPPING UNITS		
TMU CATEGORY	TMU SUBCATEGORY	AREA (m <sup>2</sup> )
Denudational clear forest	Escarpment * TEMPERATE MONTANE CLEAR FOREST	9477000
	Escarpment * TEMPERATE MONTANE WET SHRUBLAND	437400
	Escarpment * TEMPERATE MONTANE MOIST WOODLAND	3653100
	Denudational planation surfaces * TEMPERATE MONTANE MOIST WOODLAND	170100
	Moderate denudational terraces * TEMPERATE MONTANE MOIST SHRUBLAND	5119200
	Denudational planation surfaces * TEMPERATE MONTANE MOIST SHRUBLAND	24300
	Escarpment * TEMPERATE MONTANE MOIST SHRUBLAND	988200
	Moderate denudational valleys * TEMPERATE MONTANE MOIST BARE SOIL	40500
	Moderate denudational terraces * TEMPERATE MONTANE MOIST BARE SOIL	704700
	Moderate denudational ridges and tops * TEMPERATE MONTANE MOIST BARE SOIL	688500
Denudational cloud forest	Escarpment * TEMPERATE MONTANE CLOUD FOREST	24842700
	Escarpment * TEMPERATE MONTANE WET WOODLAND	4835700
Denudational lower montane	Escarpment * SUBTROPICAL LOWER MONTANE MOIST WOODLAND	29767500
	Denudational planation surfaces * SUBTROPICAL LOWER MONTANE CLEAR FOREST	7217100
	Denudational steep slopes * SUBTROPICAL LOWER MONTANE DRY WOODLAND	380700
	Denudational valleys * SUBTROPICAL LOWER MONTANE DRY WOODLAND	72900
	Denudational terraces * SUBTROPICAL LOWER MONTANE DRY WOODLAND	32400
	Denudational valleys * SUBTROPICAL LOWER MONTANE DRY SHRUBLAND	16200
	Moderate denudational valleys * SUBTROPICAL LOWER MONTANE MOIST BARE SOIL	210600
	Moderate denudational ridges and tops * SUBTROPICAL LOWER MONTANE MOIST BARE SOIL	1782000
	Moderate denudational hills * SUBTROPICAL LOWER MONTANE MOIST BARE SOIL	210600
Denudational páramo	Denudational glacial valley * NIVAL RAIN SHRUBLAND	1838700
	Denudational glacial ridges and tops * ALPINE PÁRAMO RAIN GRASSLAND	36514800
	Denudational glacial ridges and tops * NIVAL RAIN SHRUBLAND	5410800
	Denudational glacial ridges and tops * ALPINE PÁRAMO RAIN SHRUBLAND	26260200
	Periglacial denudational hills * ALPINE PÁRAMO RAIN SHRUBLAND	30771900
	Periglacial denudational hills * NIVAL RAIN SHRUBLAND	1741500
Denudational premontane forest	Escarpment * SUBTROPICAL PREMONTANE DENSE FOREST	13057200
	Escarpment * SUBTROPICAL PREMONTANE MOIST WOODLAND	8739900

TERRAIN MAPPING UNITS (cont.)		
TMU CATEGORY	TMU SUBCATEGORY	AREA (m <sup>2</sup> )
Denudational premontane forest	Escarpment * SUBTROPICAL PREMONANE MOIST SHRUBLAND	2835000
	Escarpment * SUBTROPICAL PREMONTANE CLEAR FOREST	8707500
	Escarpment * SUBTROPICAL PREMONTANE DRY WOODLAND	11453400
	Denudational planation surfaces * SUBTROPICAL PREMONTANE DRY SHRUBLAND	348300
	Moderate denudational valleys * SUBTROPICAL PREMONTANE BARE SOIL	567000
	Moderate denudational ridges and tops * SUBTROPICAL PREMONTANE BARE SOIL	1433700
	Moderate denudational hills * SUBTROPICAL PREMONTANE BARE SOIL	81000
Denudational subpáramo	Escarpment * SUBALPINE RAIN WOODLAND	24300
	Escarpment * SUBALPINE RAIN WOODED GRASSLAND	137700
	Escarpment * SUBALPINE WET WOODED GRASSLAND	688500
	Escarpment * SUBALPINE WET WOODLAND	170100
	Periglacial denudational hills * SUBALPINE RAIN SHRUBLAND	21238200
	Escarpment * SUBALPINE WET GRASSLAND	89100
	Escarpment * SUBALPINE RAIN SHRUBLAND	48600
Denudational tropical forest	Escarpment * TROPICAL DENSE FOREST	486000
	Denudational hills * TROPICAL CLEAR FOREST	37057500
	Denudational planation surfaces * TROPICAL CLEAR FOREST	421200
	Denudational steep slopes * TROPICAL CLEAR FOREST	2600100
	Denudational valleys * TROPICAL DRY WOODLAND	9104400
	Denudational planation surfaces * TROPICAL DRY WOODLAND	48600
High denudational bare rock	Denudational glacial ridges and tops * BARE ROCK	8602200
	Denudational glacial ridges and tops * ALPINE PÁRAMO RAIN BARE SOIL	1433700
	Denudational glacial valley * BARE ROCK	2154600
	Periglacial denudational hills * BARE ROCK	7476300
	Periglacial colluvial slopes * SUBALPINE RAIN BARE SOIL	8100
High denudational lower montane	Denudational steep slopes * SUBTROPICAL LOWER MONTANE DRY SHRUBLAND	194400
	Escarpment * SUBTROPICAL LOWER MONTANE MOIST BARE SOIL	704700
High denudational páramo	Denudational glacial valley * ALPINE PÁRAMO RAIN BARE SOIL	486000
	Periglacial denudational hills * ALPINE PÁRAMO RAIN BARE SOIL	1271700
High denudational premontane	Denudational terraces * SUBTROPICAL PREMONTANE DRY SHRUBLAND	2948400
	Denudational valleys * SUBTROPICAL PREMONTANE DRY SHRUBLAND	20484900
	Denudational hills * SUBTROPICAL PREMONTANE DRY SHRUBLAND	14693400
	Denudational steep slopes * SUBTROPICAL PREMONTANE DRY SHRUBLAND	38904300
	Escarpment * SUBTROPICAL PREMONTANE DRY SHRUBLAND	8650800
	Escarpment * SUBTROPICAL PREMONTANE BARE SOIL	826200
	Moderate denudational terraces * SUBTROPICAL PREMONTANE BARE SOIL	891000
	Denudational valleys * SUBTROPICAL PREMONTANE BARE SOIL	1125900
	Denudational hills * SUBTROPICAL PREMONTANE BARE SOIL	97200

TERRAIN MAPPING UNITS (cont.)		
TMU CATEGORY	TMU SUBCATEGORY	AREA (m <sup>2</sup> )
High denudational premontane	Denudational terraces * SUBTROPICAL PREMONTANE BARE SOIL	421200
	Denudational steep slopes * SUBTROPICAL PREMONTANE BARE SOIL	1053000
High denudational subpáramo	Denudational glacial ridges and tops * SUBALPINE RAIN BARE SOIL	291600
	Periglacial denudational hills * SUBALPINE RAIN BARE SOIL	1077300
	Denudational glacial valley * SUBALPINE RAIN BARE SOIL	259200
High denudational tropical forest	Escarpment * TROPICAL CLEAR FOREST	2405700
	Denudational hills * TROPICAL DRY WOODLAND	9525600
	Denudational terraces * TROPICAL DRY WOODLAND	1782000
	Escarpment * TROPICAL DRY WOODLAND	3402000
	Denudational steep slopes * TROPICAL DRY WOODLAND	5516100
	Denudational terraces * TROPICAL DRY SHRUBLAND	1385100
	Denudational valleys * TROPICAL DRY SHRUBLAND	7346700
	Denudational hills * TROPICAL DRY SHRUBLAND	2835000
	Denudational hills * TROPICAL DRY BARE SOIL	16200
	Escarpment * TROPICAL DRY SHRUBLAND	2721600
	Denudational steep slopes * TROPICAL DRY SHRUBLAND	4293000
	Denudational terraces * TROPICAL DRY BARE SOIL	64800
	Denudational valleys * TROPICAL DRY BARE SOIL	137700
	Escarpment * TROPICAL DRY BARE SOIL	40500
	Denudational steep slopes * TROPICAL DRY BARE SOIL	8100
Less stable cloud forest	Moderate denudational ridges and tops * TEMPERATE MONTANE CLOUD FOREST	226273500
	Moderate denudational valleys * TEMPERATE MONTANE CLOUD FOREST	45878400
	Moderate denudational terraces * TEMPERATE MONTANE CLOUD FOREST	4268700
	Moderate denudational hills * TEMPERATE MONTANE CLOUD FOREST	48235500
	Stable mountain slopes * TEMPERATE MONTANE CLEAR FOREST	114363900
	Stable alluvial fan * TEMPERATE MONTANE WET WOODLAND	8375400
	Stable mountain slopes * TEMPERATE MONTANE WET WOODLAND	70899300
	stable valley terraces * TEMPERATE MONTANE WET WOODLAND	3337200
	Stable rounded hills * SUBALPINE WET MIXED FOREST	40500
	Stable rounded hills * TEMPERATE MONTANE WET WOODLAND	6957900
	Stable clayed slopes * TEMPERATE MONTANE WET WOODLAND	145800
	Stable mountain slopes * TEMPERATE MONTANE WET SHRUBLAND	7662600
	Stable alluvial fan * TEMPERATE MONTANE WET SHRUBLAND	1020600
	stable valley terraces * TEMPERATE MONTANE WET SHRUBLAND	2745900
	Stable old alluvial fan * TEMPERATE MONTANE WET SHRUBLAND	477900
	Stable rounded hills * TEMPERATE MONTANE WET SHRUBLAND	1109700
Stable clayed slopes * TEMPERATE MONTANE WET SHRUBLAND	299700	
Less stable lower montane	Moderate denudational valleys * SUBTROPICAL LOWER MONTANE MOIST WOODLAND	28908900
	Moderate denudational ridges and tops * SUBTROPICAL LOWER MONTANE MOIST WOODLAND	151210800
	Moderate denudational hills * SUBTROPICAL LOWER MONTANE MOIST WOODLAND	61867800
	Stable mountain slopes * SUBTROPICAL LOWER MONTANE CLEAR FOREST	40500

TERRAIN MAPPING UNITS (cont.)		
TMU CATEGORY	TMU SUBCATEGORY	AREA (m <sup>2</sup> )
Less stable páramo	Denudational glacial valley * ALPINE PÁRAMO RAIN CLOSED SHRUBLAND	704700
	Denudational glacial valley * NIVAL RAIN CLOSE SHRUBLAND	97200
	Stable glacial valley * NIVAL RAIN GRASSLAND	1393200
	Stable glacial valley * ALPINE PÁRAMO RAIN SHRUBLAND	5443200
	Stable glacial valley * NIVAL RAIN SHRUBLAND	72900
Less stable premontane forest	Moderate denudational valleys * SUBTROPICAL PREMONTANE DENSE FOREST	14839200
	Moderate denudational ridges and tops * SUBTROPICAL PREMONTANE DENSE FOREST	25725600
	Moderate denudational terraces * SUBTROPICAL PREMONTANE DENSE FOREST	2754000
	Denudational planation surfaces * SUBTROPICAL PREMONTANE DENSE FOREST	542700
	Moderate denudational hills * SUBTROPICAL PREMONTANE DENSE FOREST	23846400
	Denudational valleys * SUBTROPICAL PREMONTANE CLEAR FOREST	24478200
	Denudational valleys * SUBTROPICAL PREMONTANE DRY WOODLAND	29759400
less stable subpáramo	Denudational glacial valley * SUBALPINE RAIN WOODLAND	494100
	Denudational glacial valley * SUBALPINE RAIN MIXED FOREST	8100
	Periglacial colluvial slopes * SUBALPINE RAIN WOODED GRASSLAND	955800
	Stable alluvial fan * SUBALPINE WET GRASSLAND	1134000
	Stable mountain slopes * SUBALPINE WET GRASSLAND	10173600
	stable valley terraces * SUBALPINE WET GRASSLAND	866700
	Stable glacial valley * SUBALPINE RAIN SHRUBLAND	3102300
	Stable old alluvial fan * SUBALPINE WET GRASSLAND	170100
	Stable rounded hills * SUBALPINE WET GRASSLAND	502200
Moderate denudational clear forest	Denudational planation surfaces * TEMPERATE MONTANE CLEAR FOREST	850500
	Moderate denudational hills * TEMPERATE MONTANE CLEAR FOREST	6123600
	Denudational terraces * SUBTROPICAL PREMONTANE CLEAR FOREST	5127300
	Moderate denudational hills * TEMPERATE MONTANE MOIST WOODLAND	7962300
	Moderate denudational hills * TEMPERATE MONTANE MOIST SHRUBLAND	866700
	Stable mountain slopes * TEMPERATE MONTANE WET BARE SOIL	518400
Moderate denudational cloud forest	Denudational planation surfaces * TEMPERATE MONTANE CLOUD FOREST	4390200
	Moderate denudational ridges and tops * TEMPERATE MONTANE CLEAR FOREST	90898200
	Moderate denudational valleys * TEMPERATE MONTANE MOIST WOODLAND	11445300
	Moderate denudational valleys * TEMPERATE MONTANE MOIST SHRUBLAND	2081700
	Moderate denudational ridges and tops * TEMPERATE MONTANE MOIST WOODLAND	80991900
	Moderate denudational terraces * TEMPERATE MONTANE MOIST WOODLAND	3215700
	Moderate denudational ridges and tops * TEMPERATE MONTANE MOIST SHRUBLAND	24567300



TERRAIN MAPPING UNITS (cont.)		
TMU CATEGORY	TMU SUBCATEGORY	AREA (m <sup>2</sup> )
Moderate denudational cloud forest	Stable alluvial fan * TEMPERATE MONTANE WET BARE SOIL	72900
Moderate denudational lower montane	Moderate denudational terraces * SUBTROPICAL LOWER MONTANE MOIST WOODLAND	3102300
	Denudational planation surfaces * SUBTROPICAL LOWER MONTANE MOIST WOODLAND	2195100
	Denudational steep slopes * SUBTROPICAL LOWER MONTANE CLEAR FOREST	24300
	Denudational valleys * SUBTROPICAL LOWER MONTANE CLEAR FOREST	40500
	Denudational terraces * SUBTROPICAL LOWER MONTANE CLEAR FOREST	8100
	Moderate denudational valleys * SUBTROPICAL LOWER MONTANE CLEAR FOREST	34886700
	Escarpment * SUBTROPICAL LOWER MONTANE MOIST SHRUBLAND	4730400
	Moderate denudational ridges and tops * SUBTROPICAL LOWER MONTANE CLEAR FOREST	148594500
	Escarpment * SUBTROPICAL LOWER MONTANE CLEAR FOREST	68736600
	Moderate denudational ridges and tops * SUBTROPICAL LOWER MONTANE MOIST SHRUBLAND	59470200
	Moderate denudational terraces * SUBTROPICAL LOWER MONTANE CLEAR FOREST	1960200
	Moderate denudational valleys * SUBTROPICAL LOWER MONTANE MOIST SHRUBLAND	4365900
	Moderate denudational hills * SUBTROPICAL LOWER MONTANE CLEAR FOREST	77387400
	Moderate denudational terraces * SUBTROPICAL LOWER MONTANE MOIST SHRUBLAND	639900
	Moderate denudational hills * SUBTROPICAL LOWER MONTANE MOIST SHRUBLAND	5418900
	Denudational planation surfaces * SUBTROPICAL LOWER MONTANE MOIST SHRUBLAND	315900
Moderate denudational terraces * SUBTROPICAL LOWER MONTANE MOIST BARE SOIL	105300	
Moderate denudational páramo	Denudational glacial ridges and tops * ALPINE PÁRAMO RAIN CLOSED SHRUBLAND	2162700
	Denudational glacial ridges and tops * NIVAL RAIN CLOSE SHRUBLAND	558900
	Denudational glacial ridges and tops * SUBALPINE RAIN WOODLAND	3086100
	Periglacial denudational hills * ALPINE PÁRAMO RAIN WOODLAND	72900
	Periglacial denudational hills * NIVAL RAIN CLOSE SHRUBLAND	24300
	Denudational glacial ridges and tops * NIVAL RAIN GRASSLAND	32910300
	Denudational glacial valley * NIVAL RAIN GRASSLAND	14515200
	Denudational glacial ridges and tops * ALPINE PÁRAMO RAIN WOODED GRASSLAND	48600
	Periglacial denudational hills * ALPINE PÁRAMO RAIN WOODED GRASSLAND	1247400
	Periglacial denudational hills * NIVAL RAIN GRASSLAND	16718400
	Denudational glacial valley * ALPINE PÁRAMO RAIN GRASSLAND	11510100
	Denudational glacial valley * ALPINE PÁRAMO RAIN SHRUBLAND	8861400
	Stable glacial valley * ALPINE PÁRAMO RAIN BARE SOIL	234900

TERRAIN MAPPING UNITS (cont.)		
TMU CATEGORY	TMU SUBCATEGORY	AREA (m <sup>2</sup> )
Moderate denudational páramo	Stable glacial valley * BARE ROCK	396900
Moderate denudational premontane forest	Denudational terraces * SUBTROPICAL PREMONTANE DENSE FOREST	2535300
	Denudational hills * SUBTROPICAL PREMONTANE DENSE FOREST	5848200
	Denudational valleys * SUBTROPICAL PREMONTANE DENSE FOREST	9954900
	Denudational steep slopes * SUBTROPICAL PREMONTANE DENSE FOREST	6204600
	Moderate denudational valleys * SUBTROPICAL PREMONTANE MOIST WOODLAND	6066900
	Moderate denudational valleys * SUBTROPICAL PREMONANE MOIST SHRUBLAND	4398300
	Moderate denudational ridges and tops * SUBTROPICAL PREMONANE MOIST SHRUBLAND	20468700
	Moderate denudational terraces * SUBTROPICAL PREMONTANE MOIST WOODLAND	1790100
	Moderate denudational terraces * SUBTROPICAL PREMONANE MOIST SHRUBLAND	2162700
	Moderate denudational ridges and tops * SUBTROPICAL PREMONTANE MOIST WOODLAND	25903800
	Denudational hills * SUBTROPICAL PREMONTANE CLEAR FOREST	38815200
	Denudational hills * SUBTROPICAL PREMONTANE DRY WOODLAND	26519400
	Moderate denudational hills * SUBTROPICAL PREMONANE MOIST SHRUBLAND	6552900
	Denudational terraces * SUBTROPICAL PREMONTANE DRY WOODLAND	4479300
	Denudational steep slopes * SUBTROPICAL PREMONTANE DRY WOODLAND	52309800
	Denudational steep slopes * SUBTROPICAL PREMONTANE CLEAR FOREST	16799400
	Denudational planation surfaces * SUBTROPICAL PREMONTANE CLEAR FOREST	4446900
	Denudational planation surfaces * SUBTROPICAL PREMONTANE DRY WOODLAND	1555200
	Denudational planation surfaces * SUBTROPICAL PREMONTANE MOIST WOODLAND	753300
	Denudational planation surfaces * SUBTROPICAL PREMONANE MOIST SHRUBLAND	121500
Moderate denudational subpáramo	Denudational glacial ridges and tops * SUBALPINE RAIN MIXED FOREST	48600
	Periglacial denudational hills * SUBALPINE RAIN WOODLAND	9598500
	Periglacial denudational hills * SUBALPINE RAIN MIXED FOREST	664200
	Denudational glacial valley * SUBALPINE RAIN WOODED GRASSLAND	10764900
	Periglacial denudational hills * SUBALPINE RAIN WOODED GRASSLAND	55501200
	Denudational glaciis * SUBALPINE RAIN WOODED GRASSLAND	16200
	Periglacial colluvial slopes * SUBALPINE RAIN SHRUBLAND	332100
	Stable mountain slopes * SUBALPINE WET BARE SOIL	826200
	Stable alluvial fan * SUBALPINE WET BARE SOIL	340200
	stable valley terraces * SUBALPINE WET BARE SOIL	388800
	stable valley terraces * TEMPERATE MONTANE WET BARE SOIL	348300
	Stable glacial valley * SUBALPINE RAIN BARE SOIL	664200

TERRAIN MAPPING UNITS (cont.)		
TMU CATEGORY	TMU SUBCATEGORY	AREA (m <sup>2</sup> )
Moderate denudational subpáramo	Stable rounded hills * SUBALPINE WET BARE SOIL	16200
Moderate denudational tropical forest	Denudational hills * TROPICAL DENSE FOREST	6885000
	Denudational terraces * TROPICAL DENSE FOREST	591300
	Denudational valleys * TROPICAL DENSE FOREST	2948400
	Moderate denudational hills * SUBTROPICAL PREMONTANE MOIST WOODLAND	26195400
	Denudational planation surfaces * TROPICAL DENSE FOREST	24300
	Denudational steep slopes * TROPICAL DENSE FOREST	40500
	Denudational valleys * TROPICAL CLEAR FOREST	17406900
	Denudational terraces * TROPICAL CLEAR FOREST	3515400
Stable clear forest	Stable alluvial fan * TEMPERATE MONTANE CLEAR FOREST	9574200
	stable valley terraces * TEMPERATE MONTANE CLEAR FOREST	1887300
	Stable old alluvial fan * TEMPERATE MONTANE CLEAR FOREST	3912300
	Moderate denudational valleys * TEMPERATE MONTANE CLEAR FOREST	10967400
	Moderate denudational terraces * TEMPERATE MONTANE CLEAR FOREST	2016900
	Stable rounded hills * TEMPERATE MONTANE CLEAR FOREST	2251800
	Stable mountain slopes * TEMPERATE MONTANE CLOUD FOREST	95085900
	Stable alluvial fan * TEMPERATE MONTANE CLOUD FOREST	7006500
	stable valley terraces * TEMPERATE MONTANE CLOUD FOREST	534600
	Stable old alluvial fan * TEMPERATE MONTANE CLOUD FOREST	1790100
	Stable rounded hills * TEMPERATE MONTANE CLOUD FOREST	1377000
	Stable clayed slopes * TEMPERATE MONTANE CLOUD FOREST	631800
	Stable old alluvial fan * TEMPERATE MONTANE WET WOODLAND	4957200
	Stable glacial valley * SUBALPINE RAIN MIXED FOREST	81000
	Stable alluvial fan * SUBALPINE WET MIXED FOREST	218700
	Stable mountain slopes * SUBALPINE WET MIXED FOREST	3240000
	stable valley terraces * SUBALPINE WET MIXED FOREST	72900
	Stable páramo	Stable glacial valley * ALPINE PÁRAMO RAIN CLOSED SHRUBLAND
Periglacial denudational hills * ALPINE PÁRAMO RAIN CLOSED SHRUBLAND		16791300
Stable glacial valley * NIVAL RAIN CLOSE SHRUBLAND		8100
Stable glacial valley * ALPINE PÁRAMO RAIN WOODED GRASSLAND		89100
Stable subpáramo	Stable glacial valley * SUBALPINE RAIN WOODLAND	648000
	Periglacial colluvial slopes * SUBALPINE RAIN WOODLAND	234900
	Periglacial colluvial slopes * SUBALPINE RAIN MIXED FOREST	8100
	Denudational glacial ridges and tops * SUBALPINE RAIN WOODED GRASSLAND	40248900
	Stable alluvial fan * SUBALPINE WET WOODED GRASSLAND	14004900
	Stable mountain slopes * SUBALPINE WET WOODED GRASSLAND	103979700
	stable valley terraces * SUBALPINE WET WOODED GRASSLAND	4835700
	Stable alluvial fan * SUBALPINE WET WOODLAND	3855600
	Stable mountain slopes * SUBALPINE WET WOODLAND	30707100
	stable valley terraces * SUBALPINE WET WOODLAND	891000

TERRAIN MAPPING UNITS (cont.)		
<b>TMU CATEGORY</b>	<b>TMU SUBCATEGORY</b>	<b>AREA (m<sup>2</sup>)</b>
Stable subpáramo	Stable glacial valley * SUBALPINE RAIN WOODDED GRASSLAND	4698000
	Stable old alluvial fan * SUBALPINE WET WOODLAND	761400
	Stable old alluvial fan * SUBALPINE WET WOODDED GRASSLAND	1911600
	Stable rounded hills * SUBALPINE WET WOODDED GRASSLAND	2203200
	Stable rounded hills * SUBALPINE WET WOODLAND	980100
	Stable old alluvial fan * SUBALPINE WET MIXED FOREST	8100

**Appendix 6.2. Terrain mapping subunits categories and subcategories**

TERRAIN MAPPING SUBUNITS		
TMsU CATEGORY	TMsU SUBCATEGORY	AREA m <sup>2</sup>
Denudational escarpment	Moderate denudational premontane forest	4884300
	Moderate denudational clear forest	348300
	Moderate denudational lower montane	9857700
	Moderate denudational tropical forest	356400
Denudational alluvial fan	Denudational temperate forest	8100
	Denudational premontane forest	324000
	Denudational clear forest	8100
	Moderate denudational lower montane	11210400
	Moderate denudational tropical forest	11672100
Denudational clear forest steep slope	Moderate denudational clear forest	1344600
Denudational colluvial slope	Denudational temperate forest	550800
	Denudational clear forest	1012500
	Denudational tropical forest	26592300
Denudational glacial colluvial slope	Denudational temperate forest	105300
	Denudational subpáramo	2721600
	Denudational clear forest	518400
	Denudational páramo	24802200
	Denudational premontane forest	1976400
	Denudational lower montane	818100
Denudational glacial valley	Denudational temperate forest	194400
	Denudational subpáramo	364500
	Denudational clear forest	64800
	Denudational páramo	1903500
Denudational glacia	Denudational subpáramo	550800
	Denudational clear forest	186300
	Denudational páramo	11534400
Denudational hillslopes	Denudational lower montane	105300
	Denudational tropical forest	2308500
Denudational lower montane forest steep slope	Moderate denudational lower montane	176304600
Denudational moraine and ridge	Denudational temperate forest	656100
	Denudational subpáramo	4568400
	Denudational clear forest	1166400
	Denudational páramo	24826500
Denudational páramo escarpment	Moderate denudational páramo	3904200
	Moderate denudational subpáramo	7654500
	Denudational páramo	6658200
Denudational páramo steep slope	Moderate denudational subpáramo	24405300
	Denudational subpáramo	6334200
	Denudational páramo	30334500

TERRAIN MAPPING SUBUNITS (cont.)		
TM <sub>SU</sub> CATEGORY	TM <sub>SU</sub> SUBCATEGORY	AREA m <sup>2</sup>
Denudational pit	Denudational temperate forest	1125900
	Moderate denudational premontane forest	17633700
	Moderate denudational clear forest	372600
	Denudational lower montane	826200
	Moderate denudational lower montane	29970000
	Moderate denudational tropical forest	2835000
	Denudational páramo	5572800
Denudational planation surface	Denudational premontane forest	226800
	Denudational clear forest	56700
	Denudational lower montane	6569100
	Denudational tropical forest	502200
Denudational premontane forest steep slope	Moderate denudational premontane forest	73653300
Denudational ridge	Denudational temperate forest	2033100
	Denudational premontane forest	5694300
	Denudational clear forest	1854900
	Denudational lower montane	3069900
	Denudational tropical forest	5232600
Denudational rock outcrop	Moderate denudational páramo	2041200
	Less stable páramo	64800
	Less stable subpáramo	186300
	Moderate denudational subpáramo	5694300
	Less stable temperate forest	14895900
	Moderate denudational temperate forest	1709100
	Moderate denudational lower montane	8100
Denudational temperate forest escarpment	Moderate denudational temperate forest	4795200
Denudational temperate forest steep slope	Moderate denudational temperate forest	92615400
Denudational terrace complex	Denudational tropical forest	194400
	High denudational tropical forest	1960200
Denudational tropical forest steep slope	Moderate denudational tropical forest	7476300
High denudational alluvial fan	Denudational lower montane	32400
	Denudational tropical forest	4479300
	High denudational tropical forest	5807700
	High denudational premontane	12522600
High denudational bare rock steep slope	High denudational bare rock	6463800
High denudational clear forest steep slope	Denudational clear forest	10918800
High denudational colluvial slope	High denudational tropical forest	12077100
	High denudational premontane	22744800
	High denudational lower montane	32400

TERRAIN MAPPING SUBUNITS (cont.)		
TMsU CATEGORY	TMsU SUBCATEGORY	AREA m <sup>2</sup>
High denudational escarpment	Denudational premontane forest	3110400
	Denudational clear forest	1231200
	Denudational lower montane	866700
	Denudational tropical forest	1474200
	High denudational tropical forest	2300400
	High denudational premontane	3896100
	High denudational lower montane	72900
High denudational glacial colluvial slope	High denudational bare rock	2551500
	High denudational páramo	24300
	High denudational subpáramo	81000
High denudational glacial valley	High denudational bare rock	396900
	High denudational páramo	113400
	High denudational subpáramo	121500
High denudational glacis	High denudational bare rock	226800
	High denudational páramo	8100
	High denudational subpáramo	32400
High denudational hillslopes	High denudational tropical forest	153900
	High denudational premontane	48600
High denudational lower montane forest steep slope	Denudational lower montane	18500400
	High denudational lower montane	396900
High denudational moraine and ridge	High denudational bare rock	3061800
	High denudational páramo	64800
	High denudational subpáramo	105300
High denudational páramo escarpment	Denudational subpáramo	1652400
	High denudational páramo	178200
	High denudational subpáramo	226800
High denudational páramo steep slope	High denudational páramo	121500
	High denudational subpáramo	89100
High denudational pit	Denudational premontane forest	2624400
	Denudational clear forest	777600
	Denudational tropical forest	2106000
	High denudational tropical forest	3507300
	High denudational premontane	6731100
	High denudational lower montane	32400
	High denudational bare rock	558900
	High denudational páramo	97200
High denudational subpáramo	89100	

TERRAIN MAPPING SUBUNITS (cont.)		
<b>TMsU CATEGORY</b>	<b>TMsU SUBCATEGORY</b>	<b>AREA m<sup>2</sup></b>
High denudational planation surface	High denudational premontane	89100
High denudational premontane forest steep slope	Denudational premontane forest	31428000
	High denudational premontane	27021600
High denudational ridge	High denudational tropical forest	3863700
	High denudational premontane	11988000
	High denudational lower montane	8100
High denudational rock outcrop	Denudational temperate forest	623700
	Denudational subpáramo	526500
	Denudational clear forest	372600
	Denudational páramo	2972700
	High denudational bare rock	955800
	High denudational páramo	72900
	High denudational subpáramo	16200
High denudational temperate forest escarpment	Denudational temperate forest	1174500
High denudational temperate forest steep slope	Denudational temperate forest	17115300
High denudational tropical forest steep slope	Denudational tropical forest	8067600
	High denudational tropical forest	11493900
Less stable glacial colluvial slope	Less stable páramo	202500
	Less stable subpáramo	1555200
	Less stable temperate forest	33704100
	Less stable lower montane	8100
Less stable alluvial fan	Less stable temperate forest	34206300
	Less stable premontane forest	34506000
	Less stable lower montane	2818800
Less stable clear forest steep slope	Stable clear forest	534600
Less stable colluvial slope	Less stable temperate forest	100221300
	Less stable premontane forest	35105400
	Less stable lower montane	74204100
Less stable escarpment	Stable clear forest	259200
Less stable glacial valley	Less stable páramo	2162700
	Less stable subpáramo	1223100
	Less stable temperate forest	5815800
Less stable glacia	Less stable páramo	251100
	Less stable subpáramo	437400
	Less stable temperate forest	8958600
	Less stable lower montane	8100
Less stable hillslopes	Less stable temperate forest	486000
	Less stable premontane forest	9136800
	Less stable lower montane	12441600



TERRAIN MAPPING SUBUNITS (cont.)		
TM <sub>s</sub> U CATEGORY	TM <sub>s</sub> U SUBCATEGORY	AREA m <sup>2</sup>
Less stable moraine and ridge	Less stable páramo	1247400
	Less stable subpáramo	2114100
	Less stable temperate forest	46040400
	Less stable lower montane	16200
Less stable páramo escarpment	Stable páramo	1725300
	Stable subpáramo	12417300
Less stable páramo steep slope	Less stable páramo	291600
	Less stable subpáramo	1717200
	Stable páramo	5710500
	Stable subpáramo	63414900
Less stable pit	Less stable páramo	388800
	Less stable subpáramo	826200
	Less stable temperate forest	38483100
	Stable subpáramo	16370100
	Stable mixed forest	105300
	Stable clear forest	1377000
Less stable planation surface	Less stable temperate forest	810000
	Less stable premontane forest	170100
	Less stable lower montane	162000
Less stable ridge	Less stable temperate forest	52253100
	Less stable premontane forest	11040300
	Less stable lower montane	37357200
Less stable temperate forest escarpment	Stable temperate forest	2211300
	Stable mixed forest	105300
Less stable temperate forest steep slope	Stable temperate forest	44963100
	Stable mixed forest	437400
Less stable terrace complex	Less stable lower montane	32400
	Moderate denudational tropical forest	1773900
Moderate denudational alluvial fan	Moderate denudational temperate forest	5564700
	Moderate denudational premontane forest	14426100
	Moderate denudational clear forest	1125900
Moderate denudational colluvial slope	Moderate denudational temperate forest	50932800
	Moderate denudational premontane forest	88128000
	Moderate denudational clear forest	11072700
	Moderate denudational lower montane	118665000
	Moderate denudational tropical forest	21124800
Moderate denudational escarpment	Less stable premontane forest	1838700
	Less stable lower montane	4333500
Moderate denudational glacial colluvial slope	Moderate denudational páramo	16904700
	Moderate denudational subpáramo	10278900
	Moderate denudational temperate forest	17058600

TERRAIN MAPPING SUBUNITS (cont.)		
<b>TMsU CATEGORY</b>	<b>TMsU SUBCATEGORY</b>	<b>AREA m<sup>2</sup></b>
Moderate denudational glacial colluvial slope	Moderate denudational clear forest	64800
	Moderate denudational lower montane	40500
Moderate denudational glacial valley	Moderate denudational páramo	17107200
	Moderate denudational subpáramo	5832000
	Moderate denudational temperate forest	769500
Moderate denudational glacis	Moderate denudational páramo	10141200
	Moderate denudational subpáramo	3337200
	Moderate denudational temperate forest	2324700
	Moderate denudational clear forest	40500
	Moderate denudational lower montane	40500
Moderate denudational hillslopes	Moderate denudational temperate forest	696600
	Moderate denudational premontane forest	4714200
	Moderate denudational clear forest	105300
	Moderate denudational lower montane	10886400
	Moderate denudational tropical forest	3175200
Moderate denudational lower montane forest steep slope	Less stable lower montane	87407100
Moderate denudational moraine and ridge	Moderate denudational páramo	20946600
	Moderate denudational subpáramo	17593200
	Moderate denudational temperate forest	11761200
	Moderate denudational clear forest	129600
	Moderate denudational lower montane	97200
Moderate denudational páramo escarpment	Less stable páramo	186300
	Less stable subpáramo	275400
Moderate denudational páramo steep slope	Moderate denudational páramo	14531400
Moderate denudational pit	Moderate denudational páramo	3636900
	Moderate denudational subpáramo	7929900
	Moderate denudational temperate forest	8999100
	Denudational subpáramo	1036800
	Less stable premontane forest	6334200
	Less stable lower montane	14353200

TERRAIN MAPPING SUBUNITS (cont.)		
TM <sub>SU</sub> CATEGORY	TM <sub>SU</sub> SUBCATEGORY	AREA m <sup>2</sup>
Moderate denudational planation surface	Moderate denudational temperate forest	3045600
	Moderate denudational premontane forest	3450600
	Moderate denudational clear forest	688500
	Moderate denudational lower montane	3175200
	Moderate denudational tropical forest	16200
Moderate denudational premontane forest steep slope	Less stable premontane forest	17018100
Moderate denudational ridge	Moderate denudational temperate forest	23271300
	Moderate denudational premontane forest	34570800
	Moderate denudational clear forest	2170800
	Moderate denudational lower montane	63876600
	Moderate denudational tropical forest	5321700
Moderate denudational rock outcrop	Stable temperate forest	3547800
	Stable páramo	1782000
	Stable subpáramo	10254600
	Stable mixed forest	234900
	Stable clear forest	162000
Moderate denudational temperate forest escarpment	Less stable temperate forest	14563800
Moderate denudational temperate forest steep slope	Less stable temperate forest	205715700
Moderate denudational terrace complex	Moderate denudational clear forest	1944000
	Denudational clear forest	8100
	Moderate denudational lower montane	988200
Stable alluvial fan	Stable temperate forest	4560300
	Stable clear forest	6390900
Stable colluvial slope	Stable temperate forest	11655900
	Stable clear forest	1482300
Stable glacial colluvial slope	Stable temperate forest	6682500
	Stable páramo	1911600
	Stable subpáramo	43197300
	Stable mixed forest	121500
	Stable clear forest	2575800
Stable glacial valley	Stable temperate forest	1498500
	Stable páramo	1101600

TERRAIN MAPPING SUBUNITS (cont.)		
TMsU CATEGORY	TMsU SUBCATEGORY	AREA m <sup>2</sup>
Stable glacial valley	Stable subpáramo	14466600
	Stable mixed forest	81000
	Stable clear forest	3037500
Stable glacis	Stable temperate forest	2114100
	Stable páramo	793800
	Stable subpáramo	16410600
	Stable mixed forest	56700
	Stable clear forest	2065500
Stable moraine and ridge	Stable temperate forest	10675800
	Stable páramo	2883600
	Stable subpáramo	45457200
	Stable mixed forest	97200
Stable pit	Stable clear forest	1992600
	Stable temperate forest	9072000
Stable planation surface	Stable páramo	1611900
	Stable temperate forest	97200
Stable ridge	Stable clear forest	56700
	Stable temperate forest	6771600
Stable terrace complex	Stable clear forest	672300
	Stable temperate forest	8100
	Less stable temperate forest	1628100
	Moderate denudational temperate forest	210600
	Less stable premontane forest	3628800
	Denudational premontane forest	16200
	Moderate denudational premontane forest	7848900
Stable clear forest	170100	
	High denudational premontane	2956500

**Appendix 6.3.** Ordering and ranking of the factor map classes. Density analysis values used for this ranking are taken from Appendixes 5.4 to 5.7.

#### HOLDRIDGE LIFE'S ZONES

CLASSES	DENSITY ANALYSIS	RANK
SUBTROPICAL PREMONANE MOIST SHRUBLAND	17.21	1.00
TROPICAL DRY SHRUBLAND	14.10	0.98
SUBTROPICAL PREMONTANE BARE SOIL	13.40	0.96
SUBTROPICAL PREMONTANE DRY SHRUBLAND	13.37	0.93
SUBTROPICAL LOWER MONTANE MOIST BARE SOIL	12.65	0.91
SUBTROPICAL PREMONTANE DRY WOODLAND	6.95	0.89
SUBALPINE WET WOODED GRASSLAND	5.32	0.87
SUBTROPICAL PREMONTANE MOIST WOODLAND	5.06	0.85
TROPICAL DRY WOODLAND	4.61	0.83
SUBTROPICAL LOWER MONTANE MOIST SHRUBLAND	2.79	0.80
TROPICAL CLEAR FOREST	1.02	0.78
SUBTROPICAL LOWER MONTANE MOIST WOODLAND	0.62	0.76
TROPICAL DRY BARE SOIL	0.09	0.74
SUBTROPICAL LOWER MONTANE CLEAR FOREST	-0.56	0.72
SUBTROPICAL PREMONTANE CLEAR FOREST	-0.84	0.70
TEMPERATE MONTANE WET BARE SOIL	-1.21	0.67
SUBTROPICAL LOWER MONTANE DRY WOODLAND	-1.27	0.65
SUBTROPICAL PREMONTANE DENSE FOREST	-1.71	0.63
TEMPERATE MONTANE CLEAR FOREST	-1.93	0.61
TEMPERATE MONTANE CLOUD FOREST	-1.94	0.59
TROPICAL DENSE FOREST	-1.98	0.57
TEMPERATE MONTANE MOIST WOODLAND	-2.00	0.54
SUBALPINE RAIN MIXED FOREST	-2.03	0.52

HOLDRIDGE LIFE'S ZONES (cont)

CLASSES	DENSITY ANALYSIS	RANK
SUBALPINE WET GRASSLAND	-2.19	0.50
TEMPERATE MONTANE WET WOODLAND	-2.37	0.48
TEMPERATE MONTANE MOIST BARE SOIL	-2.37	0.46
SUBALPINE WET WOODLAND	-2.51	0.43
TEMPERATE MONTANE MOIST SHRUBLAND	-2.57	0.41
TEMPERATE MONTANE WET SHRUBLAND	-2.64	0.39
SUBALPINE RAIN WOODED GRASSLAND	-2.87	0.37
SUBTROPICAL LOWER MONTANE DRY SHRUBLAND	n/a	0.35
SUBALPINE RAIN BARE SOIL	n/a	0.33
SUBALPINE RAIN SHRUBLAND	n/a	0.30
SUBALPINE WET BARE SOIL	n/a	0.28
SUBALPINE WET MIXED FOREST	n/a	0.26
SUBALPINE RAIN WOODLAND	n/a	0.24
ALPINE PARAMO RAIN BARE SOIL	n/a	0.22
ALPINE PARAMO RAIN SHRUBLAND	n/a	0.20
ALPINE PARAMO RAIN CLOSED SHRUBLAND	n/a	0.17
ALPINE PARAMO RAIN WOODED GRASSLAND	n/a	0.15
ALPINE PARAMO RAIN WOODLAND	n/a	0.13
ALPINE PARAMO RAIN GRASSLAND	n/a	0.11
BARE ROCK	n/a	0.09
NIVAL RAIN GRASSLAND	n/a	0.07
NIVAL RAIN CLOSE SHRUBLAND	n/a	0.04
NIVAL RAIN SHRUBLAND	n/a	0.02

INTERNAL RELIEF

CLASSES	DENSITY ANALYSIS	RANK
<200	34.71	1.00
<150	0.46	0.88
<125	0.12	0.75
<100	-0.25	0.63
<75	-0.89	0.50
<50	-1.36	0.38
<25	-1.82	0.25
>200	-2.10	0.13

ALTITUDE RANGES

CLASSES	DENSITY ANALYSIS	RANK
<=1000	6.35	1
<=1500	5.22	0.9
<=2000	1.89	0.8
<= 500	1.19	0.7
<=2500	-0.93	0.6
<=3000	-1.91	0.5
<=3500	-2.18	0.4
<=4000	-2.47	0.3
<=4500	n/a	0.2
<=5000	n/a	0.1

### GEOMORPHOLOGICAL UNITS

CLASSES	DENSITY ANALYSIS	RANK
Denudational steep slopes	15.33	1.00
Escarpment	1.59	0.95
Denudational hills	0.87	0.90
Moderate denudational ridges and tops	0.27	0.86
Denudational valleys	0.16	0.81
Denudational terraces	-0.11	0.76
Moderate denudational valleys	-0.47	0.71
Moderate denudational hills	-0.69	0.67
Denudational planation surfaces	-1.28	0.62
Moderate denudational terraces	-1.92	0.57
Stable mountain slopes	-2.16	0.52
Stable alluvial fan	-2.23	0.48
stable valley terraces	-2.79	0.43
Denudational glacial ridges and tops	-2.89	0.38
Denudational glacial valley	n/a	0.33
Periglacial colluvial slopes	n/a	0.29
Periglacial denudational hills	n/a	0.24
Stable clayed slopes	n/a	0.19
Stable glacial valley	n/a	0.14
Stable old alluvial fan	n/a	0.10
Stable rounded hills	n/a	0.05

### LINEAMENTS BUFFER

CLASSES	DENSITY ANALYSIS	RANK
<200m	0.97	1.00
<50m	0.86	0.83
<100m	0.81	0.67
<300m	0.54	0.50
<400m	0.09	0.33
<500m	-0.11	0.17

### SLOPE GRADIENT

CLASSES	DENSITY ANALYSIS	RANK
80	2.11	1
50	1.49	0.81
60	1.08	0.69
40	0.80	0.60
70	0.76	0.59
30	0.02	0.36
20	-0.64	0.16
15	-0.85	0.10
5	-1.01	0.05
10	-1.17	0

### DRAINAGE BUFFER

CLASSES	DENSITY ANALYSIS	RANK
riverbuffer<90m	1.94	1
streambuffer<45m	-0.80	0.5

### SLOPE SHAPE

CLASSES	DENSITY ANALYSIS	RANK
CONCAVE	0.34	1.00
CONVEX	-0.10	0.67
STRAIGHT	-0.16	0.33

### SLOPE ASPECT

CLASSES	DENSITY ANALYSIS	RANK
N	0.70	1.00
NE	0.55	0.89
E	0.36	0.78
SW	0.11	0.67
S	-0.02	0.56
SE	-0.30	0.44
FLAT	-0.40	0.33
W	-0.51	0.22
NW	-0.62	0.11

### LITHOLOGY

CLASSES	DENSITY ANALYSIS	RANK
META-CONGLOMERATIC SANDY MATRIX	4.63	1.00
PHYLLITES, SCHISTS, SHALES	1.98	0.94
PHYLLITES, SHALES	1.47	0.88
CLAYSTONE	0.60	0.81
GRANITIC GNEISS, MICA SCHISTS	-0.52	0.75
OIL SHALES WITH INTERCALATED LIMESTONE	-0.69	0.69
CONGLOMERATIC RED SANDS	-1.01	0.63
UNCONSOLIDATED CONGLOMERATIC SEDIMENTS	-1.18	0.56
PEBBLE TO FINE CLAYEY CONSOLIDATED CONGLOMERATE	-1.27	0.50
GRANITES, PEGMATITES	-1.52	0.44
SILTSTONE SHALE LIMESTONE INTERCALATED LAYERS	-2.02	0.38
CLAYEY SAND, SHALES, COAL SEAMS	-2.44	0.31
MARINE SHALES, MARLS, LIMESTONE	-2.64	0.25
CLAYEY SANDSTONE	-2.81	0.19
ALLUVION	0.00	0.13
MASSIVE CONGLOMERATE	0.00	0.06

### GEOMORPHOMETRY

CLASSES	DENSITY ANALYSIS	RANK
pit	1.33	1.00
ridge	1.24	0.93
steep slope	0.89	0.86
hilly slopes	0.25	0.79
colluvial slope	0.19	0.71
escarpment	-0.08	0.64
alluvial fan	-0.83	0.57
planation surface	-1.29	0.50
terrace complex	-1.41	0.43
glaciar rock outcrop	-1.90	0.36
glaciar valley	-2.26	0.29
glacis	-2.60	0.21
glaciar colluvial slope	-2.66	0.14
moraine and ridge	-2.71	0.07



**Appendix 6.4.** Random Index (RI) values obtained from various authors per number of factors compared.

	Oak Ridge	Wharton	Golden Wang	Lane, Verdini	Forman	Noble	Tumala, Wan	Aguaron et al	Alonso, Lamata
	100	500	1000	2500		500		100000	100000
3	0.382	0.58	0.5799	0.52	0.5233	0.49	0.500	0.525	0.5245
4	0.946	0.90	0.8921	0.87	0.8860	0.82	0.834	0.882	0.8815
5	1.220	1.12	1.1159	1.10	1.1098	1.03	1.046	1.115	1.1086
6	1.032	1.24	1.2358	1.25	1.2539	1.16	1.178	1.252	1.2479
7	1.468	1.32	1.3322	1.34	1.3451	1.25	1.267	1.341	1.3417
8	1.402	1.41	1.3952	1.40		1.31	1.326	1.404	1.4056
9	1.350	1.45	1.4537	1.45		1.36	1.369	1.452	1.4499
10	1.464	1.49	1.4882	1.49		1.39	1.406	1.484	1.4854
11	1.576	1.51	1.5117			1.42	1.433	1.513	1.5141
12	1.476		1.5356	1.54		1.44	1.456	1.535	1.5365
13	1.564		1.5571			1.46	1.474	1.555	1.5551
14	1.568		1.5714	1.57		1.48	1.491	1.570	1.5713
15	1.586		1.5831			1.49	1.501	1.583	1.5838

Source: Alonso et al, 2006, p449

**Appendix 6.5.** Weights of evidence by factor / classes

<b>FACTOR MAP</b>	<b>CLASSES</b>	<b>C</b>
INRELIEF	40	-0.7717
	80	-0.3837
	120	-0.0316
	160	0.1721
	200	0.6217
	240	0.8019
	280	0.4824
	320	1.0515
	380	0.7969
	ALTITUDE	500
1000		1.1625
1500		1.0337
2000		0.5316
2500		-0.4158
3000		-1.119
3500		-1.119
4000		-8.0369
4500		-8.0369
5000		-8.0369
GEOMORPHOMETRY	alluvial fan	-0.3472
	colluvial slope	0.0576
	escarpment	-0.0354
	glacial colluvial slope	-2.3854
	glacial rock outcrop	-1.0656
	glacial valley	-1.4941
	glacis	-2.1906
	hilly slopes	0.0772
	moraine and ridge	-2.5826
	pit	0.3825
	planation surface	-0.5978
	ridge	0.3578
	steep slope	0.2667
	terrace complex	-0.6745

<b>FACTOR MAP</b>	<b>CLASSES</b>	<b>C</b>
LITHOLOGY	ALLUVION	-8.016
	CLAYEY SAND, SHALES, COAL SEAMS	-1.7964
	CLAYEY SANDSTONE	-3.1471
	CLAYSTONE	0.1978
	CONGLOMERATIC RED SANDS	-0.4313
	GRANITES, PEGMATITES	-0.7433
	GRANITIC GNEISS, MICA SCHISTS	-0.1999
	MARINE SHALES, MARLS, LIMESTONE	-2.3432
	MASSIVE CONGLOMERATE	-8.016
	META-CONGLOMERATIC SANDY MATRIX	0.9947
	OIL SHALES WITH INTERCALATED LIMESTONE	-0.27
	PEBBLE TO FINE CLAYEY CONSOLIDATED CONGLOMERATE	-0.5786
	PHYLLITES, SCHISTS, SHALES	0.5355
	PHYLLITES, SHALES	0.4231
	SILTSTONE SHALE LIMESTONE INTERCALATED LAYERS	-1.1824
	UNCONSOLIDATED CONGLOMERATIC SEDIMENTS	-0.531
SLOPE ANGLE	5	-0.4487
	10	-0.5426
	15	-0.3673
	20	-0.2695
	30	-0.0104
	40	0.2316
	50	0.4081
	60	0.3067
	70	0.2204
	80	0.5456
	90	-8.0334
LINEAMENTS BUFFER	<50m	0.2674
	<100m	0.2555
	<200m	0.3036
	<300m	0.1907
	<400m	0.0549
	<500m	-0.0066

<b>FACTOR MAP</b>	<b>CLASSES</b>	<b>C</b>
DRAINAGE BUFFER	<140m	0.5271
	<90m	-0.3258
FLOW	E	0.1192
	FLAT	-0.1503
	N	0.2208
	NE	0.1772
	NW	-0.2432
	S	-0.0035
	SE	-0.1068
	SW	0.0412
	W	-0.1915
SLOPE SHAPE	concave	0.1129
	straight	-0.0539
	convex	-0.0356
GEOMORPHOLOGY	Denudational glacial ridges and tops	-4.1034
	Denudational glacial valley	-8.016
	Denudational glacia	-8.016
	Denudational hills	0.2682
	Denudational planation surfaces	-0.5847
	Denudational steep slopes	1.9994
	Denudational terraces	-0.0248
	Denudational valleys	0.0546
	Escarpment	0.4488
	Moderate denudational hills	-0.2746
	Moderate denudational ridges and tops	0.0907
	Moderate denudational terraces	-1.0684
	Moderate denudational valleys	-0.179
	Periglacial colluvial slopes	-8.016
	Periglacial denudational hills	-8.016
	Stable alluvial fan	-1.4436
	Stable clayed slopes	-8.016
	Stable glacial valley	-8.016
	Stable mountain slopes	-1.3489
	Stable old alluvial fan	-8.016
Stable rounded hills	-8.016	
stable valley terraces	-3.0038	

<b>FACTOR MAP</b>	<b>CLASSES</b>	<b>C</b>
HOLDRIDGE ZONES	SUBTROPICAL PREMONTANE DRY SHRUBLAND	1.8616
	SUBTROPICAL PREMONTANE BARE SOIL	1.863
	TROPICAL CLEAR FOREST	0.3137
	TROPICAL DENSE FOREST	-1.1394
	TROPICAL DRY BARE SOIL	0.0311
	TROPICAL DRY SHRUBLAND	1.9142
	TROPICAL DRY WOODLAND	0.9933
	SUBTROPICAL PREMONTANE DRY WOODLAND	1.2885
	SUBTROPICAL PREMONTANE CLEAR FOREST	-0.3451
	SUBTROPICAL PREMONTANE DENSE FOREST	-0.8889
	SUBTROPICAL PREMONANE MOIST SHRUBLAND	2.12
	SUBTROPICAL PREMONTANE MOIST WOODLAND	1.0559
	SUBTROPICAL LOWER MONTANE DRY SHRUBLAND	-8.016
	SUBTROPICAL LOWER MONTANE DRY WOODLAND	-0.5786
	SUBTROPICAL LOWER MONTANE CLEAR FOREST	-0.2171
	SUBTROPICAL LOWER MONTANE MOIST BARE SOIL	1.8078
	SUBTROPICAL LOWER MONTANE MOIST SHRUBLAND	0.6965
	SUBTROPICAL LOWER MONTANE MOIST WOODLAND	0.1978
	TEMPERATE MONTANE MOIST BARE SOIL	-1.6824
	TEMPERATE MONTANE MOIST SHRUBLAND	-1.2985
	TEMPERATE MONTANE MOIST WOODLAND	-1.1607
	TEMPERATE MONTANE CLOUD FOREST	-1.0982
	TEMPERATE MONTANE WET BARE SOIL	-0.5486
	TEMPERATE MONTANE WET SHRUBLAND	-2.3092
	TEMPERATE MONTANE WET WOODLAND	-1.6646
	SUBALPINE RAIN BARE SOIL	-8.016
	SUBALPINE RAIN SHRUBLAND	-8.016
	SUBALPINE RAIN MIXED FOREST	-8.016
	SUBALPINE WET BARE SOIL	-8.016
	SUBALPINE WET GRASSLAND	-1.375
	SUBALPINE WET WOODED GRASSLAND	-1.2742
	SUBALPINE WET WOODLAND	-1.9479
	SUBALPINE WET MIXED FOREST	-1.2046
	SUBALPINE RAIN WOODED GRASSLAND	-3.921
	SUBALPINE RAIN WOODLAND	-8.016
	ALPINE PARAMO RAIN BARE SOIL	-8.016
	ALPINE PARAMO RAIN SHRUBLAND	-8.016
	ALPINE PARAMO RAIN CLOSED SHRUBLAND	-8.016
	ALPINE PARAMO RAIN WOODED GRASSLAND	-8.016
	ALPINE PARAMO RAIN WOODLAND	-8.016
	ALPINE PARAMO RAIN GRASSLAND	-8.016
	BARE ROCK	-8.016
	NIVAL RAIN GRASSLAND	-8.016
	NIVAL RAIN CLOSE SHRUBLAND	-8.016
NIVAL RAIN SHRUBLAND	-8.016	
TEMPERATE MONTANE CLEAR FOREST	-1.0882	

**Appendix 6.6.** Weights of evidences of factor / classes ordered in descendent sort

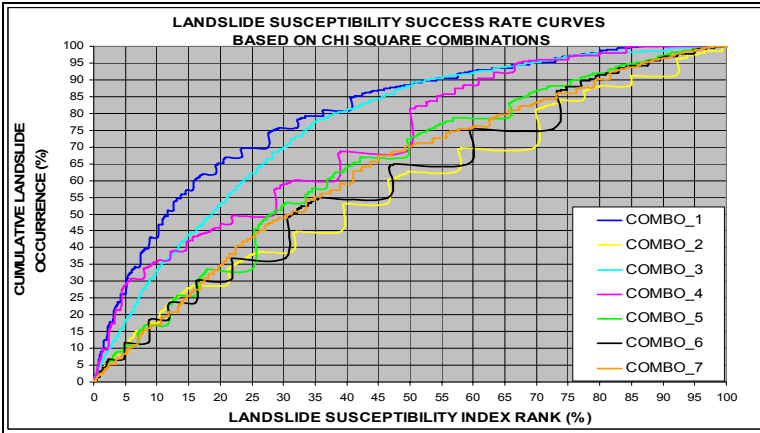
	<b>FACTOR MAP</b>	<b>CLASSES</b>	<b>C</b>
1	HOLDRIDGE ZONES	SUBTROPICAL PREMONANE MOIST SHRUBLAND	2.12
2	GEOMORPHOLOGY	Denudational steep slopes	1.9994
3	HOLDRIDGE ZONES	TROPICAL DRY SHRUBLAND	1.9142
4	HOLDRIDGE ZONES	SUBTROPICAL PREMONTANE BARE SOIL	1.863
5	HOLDRIDGE ZONES	SUBTROPICAL PREMONTANE DRY SHRUBLAND	1.8616
6	HOLDRIDGE ZONES	SUBTROPICAL LOWER MONTANE MOIST BARE SOIL	1.8078
7	HOLDRIDGE ZONES	SUBTROPICAL PREMONTANE DRY WOODLAND	1.2885
8	ALTITUDE	1000	1.1625
9	HOLDRIDGE ZONES	SUBTROPICAL PREMONTANE MOIST WOODLAND	1.0559
10	INRELIEF	320	1.0515
11	ALTITUDE	1500	1.0337
12	LITHOLOGY	META-CONGLOMERATIC SANDY MATRIX	0.9947
13	HOLDRIDGE ZONES	TROPICAL DRY WOODLAND	0.9933
14	INRELIEF	240	0.8019
15	INRELIEF	380	0.7969
16	HOLDRIDGE ZONES	SUBTROPICAL LOWER MONTANE MOIST SHRUBLAND	0.6965
17	INRELIEF	200	0.6217
18	SLOPE ANGLE	80	0.5456
19	LITHOLOGY	PHYLLITES, SCHISTS, SHALES	0.5355
20	ALTITUDE	2000	0.5316
21	DRAINAGE BUFFER	<140m	0.5271
22	INRELIEF	280	0.4824
23	GEOMORPHOLOGY	Escarpment	0.4488
24	LITHOLOGY	PHYLLITES, SHALES	0.4231
25	SLOPE ANGLE	50	0.4081
26	GEOMORPHOMETRY	pit	0.3825
27	GEOMORPHOMETRY	ridge	0.3578
28	HOLDRIDGE ZONES	TROPICAL CLEAR FOREST	0.3137
29	SLOPE ANGLE	60	0.3067
30	LINEAMENTS	<200m	0.3036
31	ALTITUDE	500	0.2981
32	GEOMORPHOLOGY	Denudational hills	0.2682
33	LINEAMENTS	<50m	0.2674
34	GEOMORPHOMETRY	steep slope	0.2667
35	LINEAMENTS	<100m	0.2555
36	SLOPE ANGLE	40	0.2316
37	FLOW	N	0.2208
38	SLOPE ANGLE	70	0.2204

	<b>FACTOR MAP</b>	<b>CLASSES</b>	<b>C</b>
39	LITHOLOGY	CLAYSTONE	0.1978
40	HOLDRIDGE ZONES	SUBTROPICAL LOWER MONTANE MOIST WOODLAND	0.1978
41	LINEAMENTS	<300m	0.1907
42	FLOW	NE	0.1772
43	INRELIEF	160	0.1721
44	FLOW	E	0.1192
45	SLOPE SHAPE	concave	0.1129
46	GEOMORPHOLOGY	Moderate denudational ridges and tops	0.0907
47	GEOMORPHOMETRY	hilly slopes	0.0772
48	GEOMORPHOMETRY	colluvial slope	0.0576
49	LINEAMENTS	<400m	0.0549
50	GEOMORPHOLOGY	Denudational valleys	0.0546
51	FLOW	SW	0.0412
52	HOLDRIDGE ZONES	TROPICAL DRY BARE SOIL	0.0311
53	FLOW	S	-0.0035
54	LINEAMENTS	<500m	-0.0066
55	SLOPE ANGLE	30	-0.0104
56	GEOMORPHOLOGY	Denudational terraces	-0.0248
57	INRELIEF	120	-0.0316
58	GEOMORPHOMETRY	escarpment	-0.0354
59	SLOPE SHAPE	convex	-0.0356
60	SLOPE SHAPE	straight	-0.0539
61	FLOW	SE	-0.1068
62	FLOW	FLAT	-0.1503
63	GEOMORPHOLOGY	Moderate denudational valleys	-0.179
64	FLOW	W	-0.1915
65	LITHOLOGY	GRANITIC GNEISS, MICA SCHISTS	-0.1999
66	HOLDRIDGE ZONES	SUBTROPICAL LOWER MONTANE CLEAR FOREST	-0.2171
67	FLOW	NW	-0.2432
68	SLOPE ANGLE	20	-0.2695
69	LITHOLOGY	OIL SHALES WITH INTERCALATED LIMESTONE	-0.27
70	GEOMORPHOLOGY	Moderate denudational hills	-0.2746
71	DRAINAGE BUFFER	<90m	-0.3258
72	HOLDRIDGE ZONES	SUBTROPICAL PREMONTANE CLEAR FOREST	-0.3451
73	GEOMORPHOMETRY	alluvial fan	-0.3472
74	SLOPE ANGLE	15	-0.3673
75	INRELIEF	80	-0.3837
76	ALTITUDE	2500	-0.4158
77	LITHOLOGY	CONGLOMERATIC RED SANDS	-0.4313

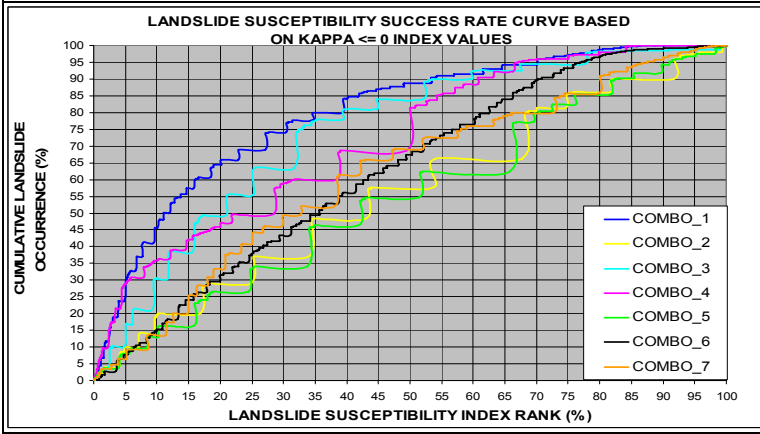
	<b>FACTOR MAP</b>	<b>CLASSES</b>	<b>C</b>
78	SLOPE ANGLE	5	-0.4487
79	LITHOLOGY	UNCONSOLIDATED CONGLOMERATIC SEDIMENTS	-0.531
80	SLOPE ANGLE	10	-0.5426
81	HOLDRIDGE ZONES	TEMPERATE MONTANE WET BARE SOIL	-0.5486
82	LITHOLOGY	PEBBLE TO FINE CLAYEY CONSOLIDATED CONGLOMERATE	-0.5786
83	HOLDRIDGE ZONES	SUBTROPICAL LOWER MONTANE DRY WOODLAND	-0.5786
84	GEOMORPHOLOGY	Denudational planation surfaces	-0.5847
85	GEOMORPHOMETRY	planation surface	-0.5978
86	GEOMORPHOMETRY	terrace complex	-0.6745
87	LITHOLOGY	GRANITES, PEGMATITES	-0.7433
88	INRELIEF	40	-0.7717
89	HOLDRIDGE ZONES	SUBTROPICAL PREMONTANE DENSE FOREST	-0.8889
90	GEOMORPHOMETRY	glacial rock outcrop	-1.0656
91	GEOMORPHOLOGY	Moderate denudational teraces	-1.0684
92	HOLDRIDGE ZONES	TEMPERATE MONTANE CLEAR FOREST	-1.0882
93	HOLDRIDGE ZONES	TEMPERATE MONTANE CLOUD FOREST	-1.0982
94	ALTITUDE	3000	-1.119
95	ALTITUDE	3500	-1.119
96	HOLDRIDGE ZONES	TROPICAL DENSE FOREST	-1.1394
97	HOLDRIDGE ZONES	TEMPERATE MONTANE MOIST WOODLAND	-1.1607
98	LITHOLOGY	SILTSTONE SHALE LIMESTONE INTERCALATED LAYERS	-1.1824
99	HOLDRIDGE ZONES	SUBALPINE WET MIXED FOREST	-1.2046
100	HOLDRIDGE ZONES	SUBALPINE WET WOODED GRASSLAND	-1.2742
101	HOLDRIDGE ZONES	TEMPERATE MONTANE MOIST SHRUBLAND	-1.2985
102	GEOMORPHOLOGY	Stable mountain slopes	-1.3489
103	HOLDRIDGE ZONES	SUBALPINE WET GRASSLAND	-1.375
104	GEOMORPHOLOGY	Stable alluvial fan	-1.4436
105	GEOMORPHOMETRY	glacial valley	-1.4941
106	HOLDRIDGE ZONES	TEMPERATE MONTANE WET WOODLAND	-1.6646
107	HOLDRIDGE ZONES	TEMPERATE MONTANE MOIST BARE SOIL	-1.6824
108	LITHOLOGY	CLAYEY SAND, SHALES, COAL SEAMS	-1.7964
109	HOLDRIDGE ZONES	SUBALPINE WET WOODLAND	-1.9479
110	GEOMORPHOMETRY	glacis	-2.1906
111	HOLDRIDGE ZONES	TEMPERATE MONTANE WET SHRUBLAND	-2.3092
112	LITHOLOGY	MARINE SHALES, MARLS, LIMESTONE	-2.3432
113	GEOMORPHOMETRY	glacial colluvial slope	-2.3854
114	GEOMORPHOMETRY	moraine and ridge	-2.5826
115	GEOMORPHOLOGY	stable valley terraces	-3.0038
116	LITHOLOGY	CLAYEY SANDSTONE	-3.1471



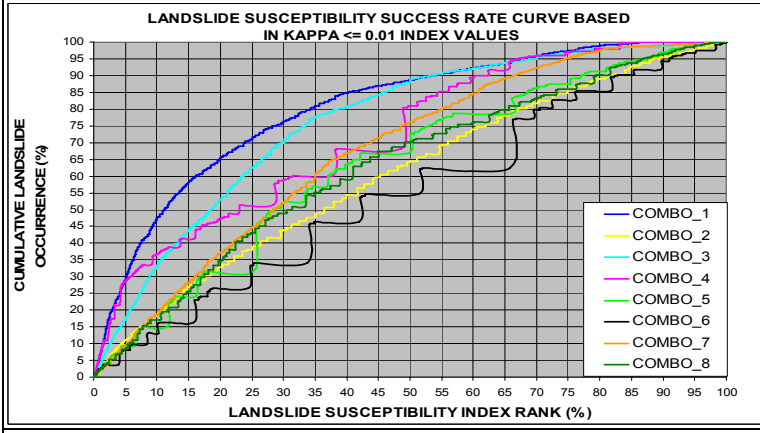
	<b>FACTOR MAP</b>	<b>CLASSES</b>	<b>C</b>
117	HOLDRIDGE ZONES	SUBALPINE RAIN WOODED GRASSLAND	-3.921
118	GEOMORPHOLOGY	Denudational glacial ridges and tops	-4.1034
119	LITHOLOGY	ALLUVION	-8.016
120	LITHOLOGY	MASSIVE CONGLOMERATE	-8.016
121	GEOMORPHOLOGY	Denudational glacial valley	-8.016
122	GEOMORPHOLOGY	Denudational glacis	-8.016
123	GEOMORPHOLOGY	Periglacial colluvial slopes	-8.016
124	GEOMORPHOLOGY	Periglacial denudational hills	-8.016
125	GEOMORPHOLOGY	Stable clayed slopes	-8.016
126	GEOMORPHOLOGY	Stable glacial valley	-8.016
127	GEOMORPHOLOGY	Stable old alluvial fan	-8.016
128	GEOMORPHOLOGY	Stable rounded hills	-8.016
129	HOLDRIDGE ZONES	SUBTROPICAL LOWER MONTANE DRY SHRUBLAND	-8.016
130	HOLDRIDGE ZONES	SUBALPINE RAIN BARE SOIL	-8.016
131	HOLDRIDGE ZONES	SUBALPINE RAIN SHRUBLAND	-8.016
132	HOLDRIDGE ZONES	SUBALPINE RAIN MIXED FOREST	-8.016
133	HOLDRIDGE ZONES	SUBALPINE WET BARE SOIL	-8.016
134	HOLDRIDGE ZONES	SUBALPINE RAIN WOODLAND	-8.016
135	HOLDRIDGE ZONES	ALPINE PARAMO RAIN BARE SOIL	-8.016
136	HOLDRIDGE ZONES	ALPINE PARAMO RAIN SHRUBLAND	-8.016
137	HOLDRIDGE ZONES	ALPINE PARAMO RAIN CLOSED SHRUBLAND	-8.016
138	HOLDRIDGE ZONES	ALPINE PARAMO RAIN WOODED GRASSLAND	-8.016
139	HOLDRIDGE ZONES	ALPINE PARAMO RAIN WOODLAND	-8.016
140	HOLDRIDGE ZONES	ALPINE PARAMO RAIN GRASSLAND	-8.016
141	HOLDRIDGE ZONES	BARE ROCK	-8.016
142	HOLDRIDGE ZONES	NIVAL RAIN GRASSLAND	-8.016
143	HOLDRIDGE ZONES	NIVAL RAIN CLOSE SHRUBLAND	-8.016
144	HOLDRIDGE ZONES	NIVAL RAIN SHRUBLAND	-8.016
145	SLOPE ANGLE	90	-8.0334
146	ALTITUDE	4000	-8.0369
147	ALTITUDE	4500	-8.0369
148	ALTITUDE	5000	-8.0369



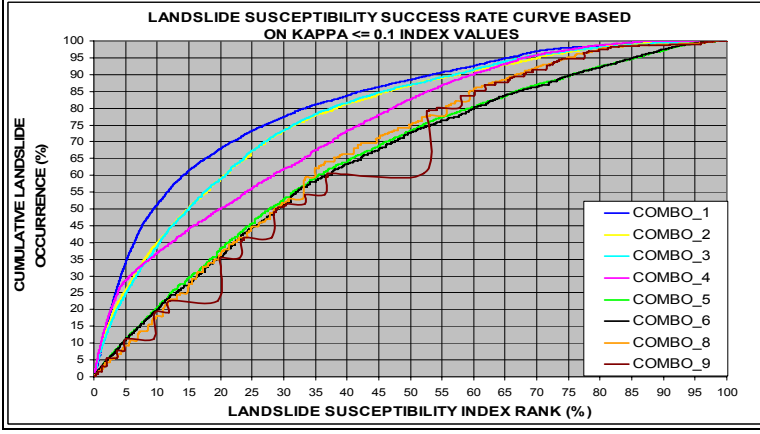
**Appendix 6.7.** Success rate curve based on the accumulated frequency of susceptibility probabilities against the study area cumulative landslide occurrences from the seven combinations obtained with the Chi square test.



**Appendix 6.8.** Success rate curve based on the accumulated frequency of susceptibility probabilities against the study area cumulative landslide occurrences from the seven combinations obtained with the Kappa <= 0 criteria.

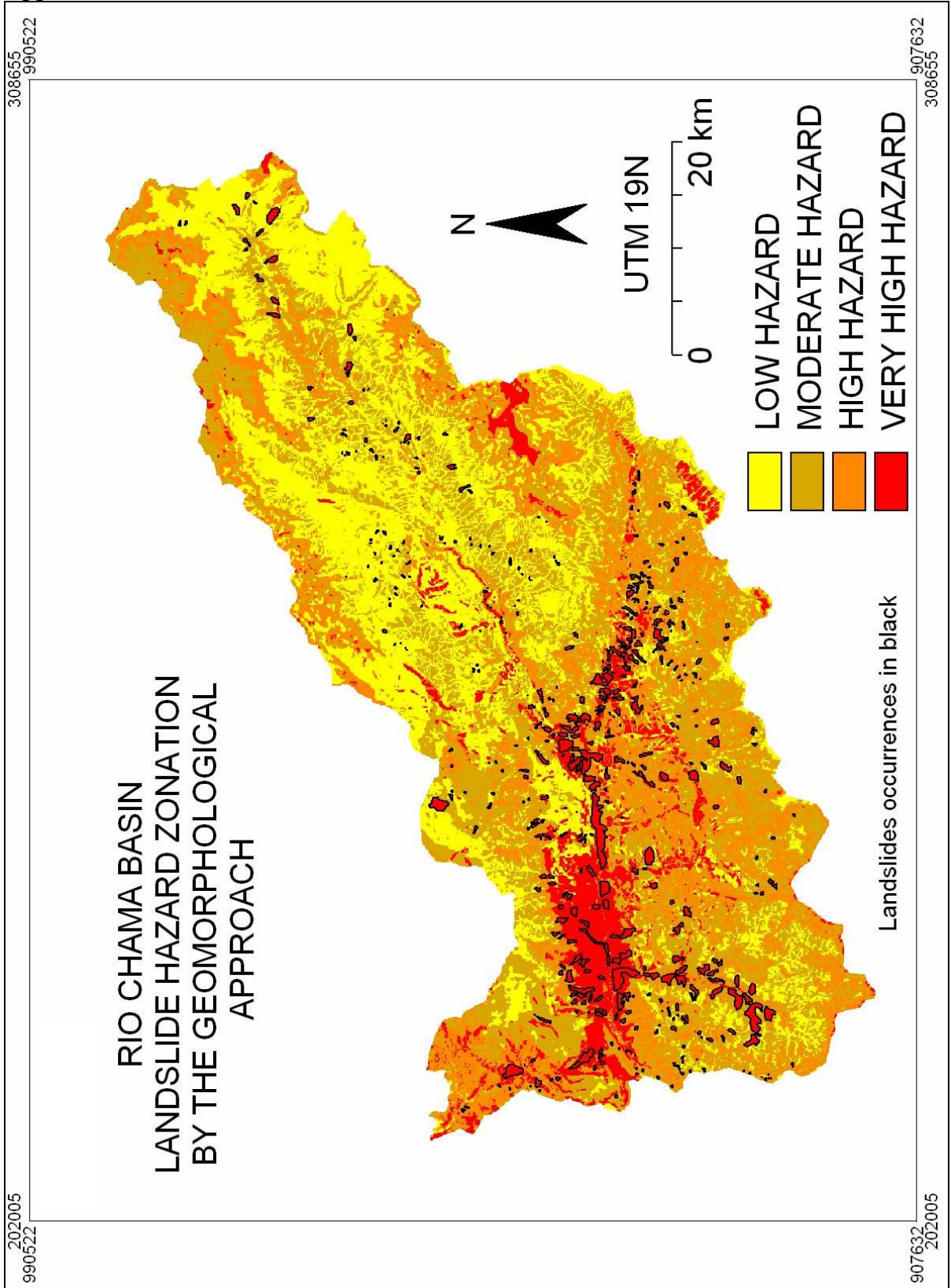


**Appendix 6.9.** Success rate curve based on the accumulated frequency of susceptibility probabilities against the study area cumulative landslide occurrences with the Kappa <= 0.01 criteria.

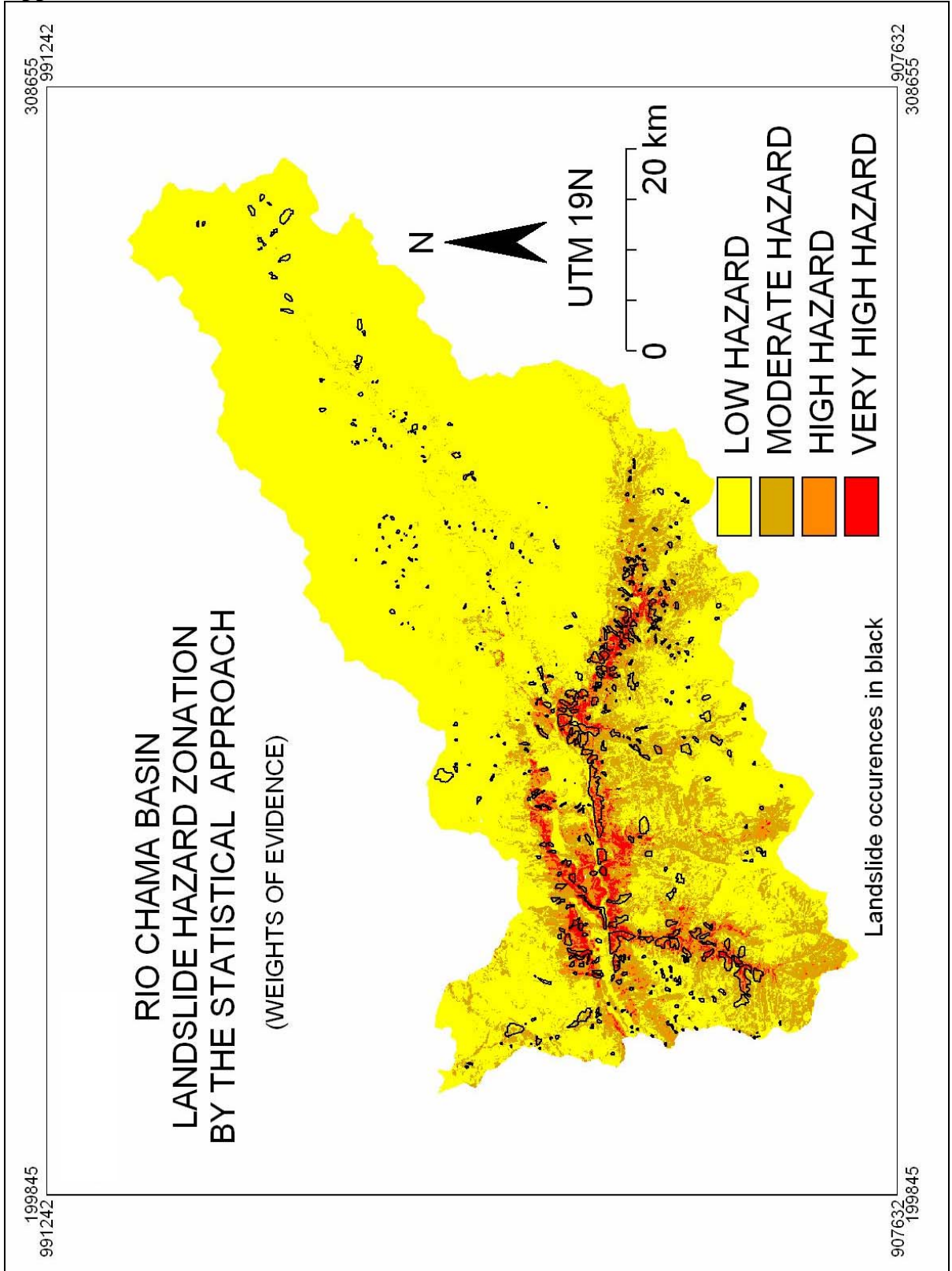


**Appendix 6.10.** Success rate curve based on the accumulated frequency of susceptibility probabilities against the study area cumulative landslide occurrences with the Kappa <= 0.1 criteria.

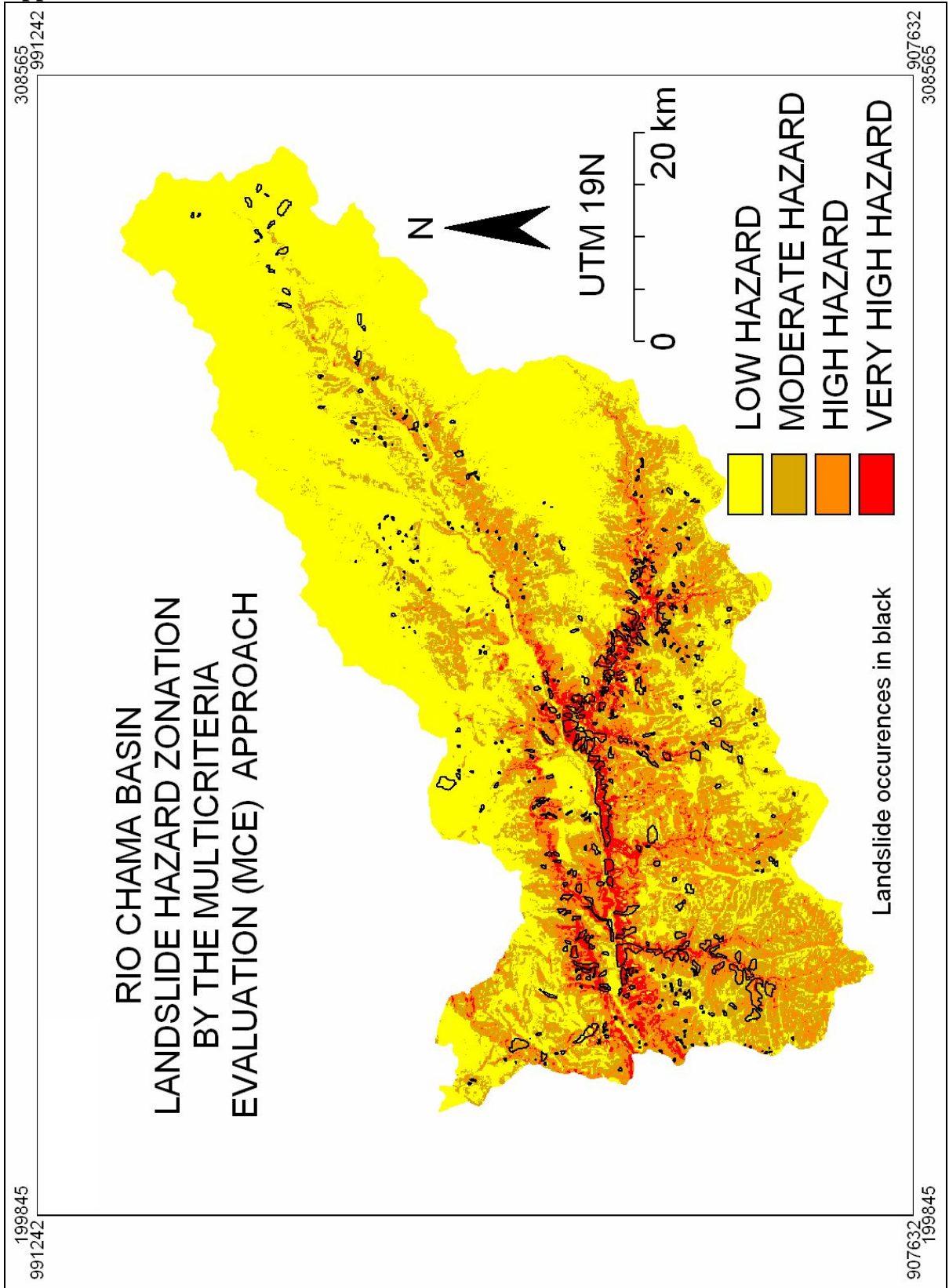
Appendix 7.1



Appendix 7.2



Appendix 7.3



## Appendix 7.4

### Accuracy and error Rates via Contingency Matrix

A contingency matrix (Kohavi and Provost, 1998) applied to landslide hazard zonation contains information about actual and predicted landslide hazard classes done by a hazard approach or methodology. These predictions are compared to an actual landslide inventory map of the assessed area. The following example describes the concepts and measures used in the contingency matrix to compute error rates. Since the landslide inventory map used in this study provides only information about the occurrence or absence of landslides, the maps to be analyzed should be aggregated to also only two hazard classes: low / absence of landslides or high / presence of landslides. The following exemplifies the arrangement of the contingency matrix followed by an explanation of its measures and concepts.

Contingency Matrix		Landslide hazard map prediction domains	
		NON-LANDSLIDE	LANDSLIDE
Landslide inventory map	NON-LANDSLIDE	a	b
	LANDSLIDE	c	d

- a is the number of pixels **correctly** predicted as non-landslide occurrences,
- b is the number of pixels **incorrectly** predicted as landslide occurrences,
- c is the number of pixels **incorrectly** predicted as non-landslide occurrences, and
- d is the number of pixels **correctly** predicted as landslide occurrences.

Where:

- The *overall accuracy* (AC) is the proportion of the total number of pixels **correctly** predicted as non-landslide occurrences. It is determined using the equation:

$$AC = \frac{a + d}{a + b + c + d}$$

- The *true positive rate* (TP) is the proportion of the number of pixels **correctly** predicted as landslide occurrences, as calculated using the equation:

$$TP = \frac{d}{c + d}$$

- The *true negative rate* (TN) is the proportion of number of pixels **correctly** predicted as non-landslide occurrences, as calculated using the equation:

$$TN = \frac{a}{a + b}$$

- The *false positive rate* (FP) is the proportion of the number of pixels **incorrectly** predicted as landslide occurrences, as calculated using the equation:

$$FP = \frac{b}{a + b}$$

- The *false negative rate* (FN) is the proportion of number of pixels **incorrectly** predicted as non-landslide occurrences, as calculated using the equation:

$$FN = \frac{c}{c + b}$$

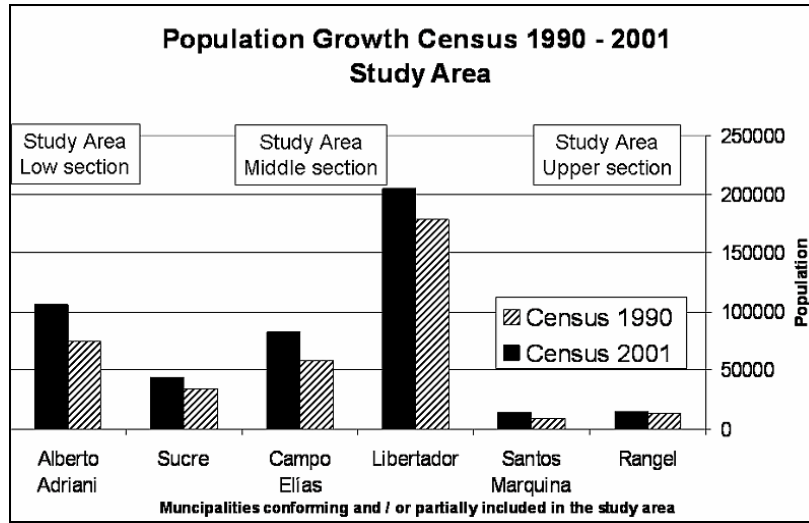
- Finally, *precision* (P) is the proportion of the number of pixels **correctly** predicted as landslide occurrences, as calculated using the equation:

$$P = \frac{d}{b + d}$$

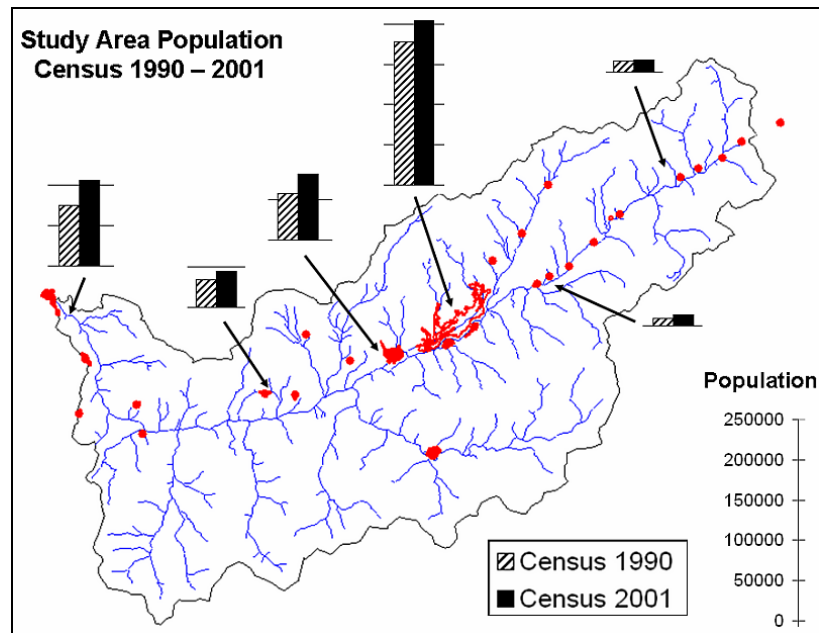
## Appendix 7.5

Population of the municipalities involved in the study area from census 1990 and 2000.

Municipalities	Population					
	Census 1990		Census 2001		Annual geometric growth (%)	Relative growth (%)
	Total	%	Total	%		
<b>TOTAL STUDY AREA</b>	<b>368640</b>	<b>100,0</b>	<b>466779</b>	<b>100,0</b>	<b>2.1</b>	<b>25.4</b>
<b>Rangel</b>	13232	6.4	15206	3.3	1.3	14.9
<b>Santos Marquina</b>	9232	4.4	13795	3.0	3.7	49.4
<b>Libertador</b>	178580	85.9	204879	43.9	1.3	14.,7
<b>Campo Elias</b>	58671	28.2	82397	17.7	3.1	40.4
<b>Sucre</b>	33928	16.3	44418	9.5	2.5	30.9
<b>Alberto Adriani</b>	74997	36.1	106084	22.7	3.2	41.5



Study area population growth by municipalities from 1990 and 2000 census.



Study area main human settlements as provided by municipalities 1990 and 2000 census.



## Appendix 7.6.

Holdridge's life zones are definite vegetation types given a range of temperature, humidity and precipitation. This physical features are given by the following indices: bio-temperature (BT), mean annual precipitation (P) and potential evapotranspiration rate (PER); and their plotting in the Holdridge's triangular classification scheme constructed by BT, P and PER.

$$\begin{aligned} BT &= \sum T / 12 \\ PET &= BT \times 58.93 \\ PER &= PET / P \end{aligned}$$

Where: BT = Mean annual bio-temperature ( $^{\circ}\text{C}$ ),  
T = mean monthly temperature ( $0^{\circ}\text{C} < t < 30^{\circ}\text{C}$ ),  
PET = Potential evapotranspiration  
PER = Potential evapotranspiration rate  
P = Annual precipitation (mm).

The mean annual BT varies from  $0^{\circ}\text{C}$  to  $30^{\circ}\text{C}$ . Mean monthly temperature lower than  $0^{\circ}\text{C}$  and higher than  $30^{\circ}\text{C}$ , are settled to these boundaries. In this study the spatial data input is reclassified following the boundaries proposed in the Holdridge's triangular chart (1967). An NDVI of the study area, derived from two set of Landsat imagery (path/row 006/054 on the 08-13-1996 and path/row 007/054 on the 09-05-1996), is used as additional layer in order to confirm and sharp the classes obtained by the traditional procedure. The reclassification of each of the data layers in Holdridge's zones, facilitates the comparing, overlaying and tabulation of them in a common domain. This reclassification is performed following the class's range given in the Holdridge's triangular chart (Figure A.7.6.1) and illustrated in Figure A.7.6.2. Given that the NDVI histogram describes a character of normal distribution, this layer is classified following the Standard deviation classification method, which calculates the mean value and then divides the NDVI range by several deviations above and below the mean, generating new classes representing different vegetation units assuming that NDVI index is representing, in some way, vegetation conditions as density (Pan et al, 2003).

Table A.7.6.1, describes the overlaying procedure followed so in the reclassification as in the aggregation of reclassified layers. Tables A.7.6.2 to A.7.6.4 describes the aggregation procedure, these tables are the result and the source of the linked data layers. A better illustration of this procedure is displayed in Figure A.7.6.3.

Table A.7.6.1. Overlaying of the reclassified data layers to obtain the final Zone3 or Holdridge classes.

DATA INPUT	RECLASSIFICATION	TABLE OVERLAYING PROCEDURE		
Annual precipitation	Precipitation classes	Zone1	Zone2	Zone3. Holdridge life's zones
PER	PER classes			
BT (°C)	Altitudinal classes			
NDVI	NDVI classes			

Table A.7.6.2. Table overlaying and aggregation of the Annual precipitation data and Potential evapotranspiration rate (PER), to a new reclassified layer named Zone1.

	PETrclasses	ppclasses	NPix	Area	ZONES1
0.25 * 1000	0.25	<=1000	25855	209425500	RAIN TUNDRA
0.25 * 2000	0.25	<=2000	22849	185076900	RAIN FOREST
0.50 * 1000	0.50	<=1000	20979	169929900	WET FOREST
0.50 * 2000	0.50	<=2000	45837	371279700	WET FOREST
1.00 * 1000	1.00	<=1000	25866	209514600	MOIST FOREST
1.00 * 2000	1.00	<=2000	158442	1283380200	MOIST FOREST
2.00 * 1000	2.00	<=1000	40839	330795900	DRY FOREST
2.00 * 2000	2.00	<=2000	16487	133544700	DRY FOREST
Min			16487	133544700	
Max			158442	1283380200	
Avg			44644	361618425	
Std			47055	381147782	
Sum			357154	2892947400	

Table A.7.6.3. Table overlaying and aggregation of the Altitudinal classes and Zone1, to a new reclassified layer named Zone2.

	ALTITUDINAL	ZONES1	NPix	Area	ZONES2
NIVAL * RAIN NIVAL	NIVAL	RAIN TUNDRA	8171	66185100	Nival rain shrubland
NIVAL * RAIN NIVAL	NIVAL	RAIN FOREST	3436	27831600	Nival rain woodland
ALPINE PARAM ALPINE PARAMO	ALPINE PARAMO	RAIN TUNDRA	10867	88022700	Alpine paramo rain shrubland
ALPINE PARAM ALPINE PARAMO	ALPINE PARAMO	RAIN FOREST	7187	58214700	Alpine paramo rain woodland
SUBALPINE * SUBALPINE	SUBALPINE	RAIN TUNDRA	6817	55217700	Subalpine rain shrubland
SUBALPINE * SUBALPINE	SUBALPINE	WET FOREST	22608	183124800	Subalpine wet woodland
SUBALPINE * SUBALPINE	SUBALPINE	RAIN FOREST	12226	99030600	Subalpine rain woodland
TEMPERATE MOI TEMPERATE MONTANE	TEMPERATE MONTANE	WET FOREST	44195	357979500	Temperate montane wet forest
TEMPERATE MOI TEMPERATE MONTANE	TEMPERATE MONTANE	MOIST FOREST	41229	333954900	Temperate montane moist forest
SUBTROPICAL SUBTROPICAL LOWER MONTANE	SUBTROPICAL LOWER MONTANE	WET FOREST	13	105300	Subtropical lower montane wet forest
SUBTROPICAL SUBTROPICAL LOWER MONTANE	SUBTROPICAL LOWER MONTANE	MOIST FOREST	119924	971384400	Subtropical lower montane moist forest
SUBTROPICAL SUBTROPICAL LOWER MONTANE	SUBTROPICAL LOWER MONTANE	DRY FOREST	95	769500	Subtropical lower montane dry forest
SUBTROPICAL SUBTROPICAL PREMONTANE	SUBTROPICAL PREMONTANE	MOIST FOREST	23155	187555500	Subtropical premontane moist forest
SUBTROPICAL SUBTROPICAL PREMONTANE	SUBTROPICAL PREMONTANE	DRY FOREST	42066	340734600	Subtropical premontane dry forest
TROPICAL * TROPICAL	TROPICAL	DRY FOREST	15165	122836500	Tropical dry forest
Min			13	105300	
Max			119924	971384400	
Avg			23810	192863160	
Std			30498	247035159	
Sum			357154	2892947400	

Table A.7.6.4. Table overlaying and aggregation of the NDVI classes and Zone2, to a final reclassified layer named Zone3 (Figure 7.6.4), which represents the Holdridge zones.

ZONES2	NDVI classes	ZONES3	NPix	Area
Tropical dry forest	BARE SOIL	TROPICAL DRY BARE SOIL	33	267300
Tropical dry forest	SHRUB	TROPICAL DRY SHRUBLAND	2295	18589500
Tropical dry forest	WOODLAND	TROPICAL DRY WOODLAND	3628	29386800
Tropical dry forest	CLEAR FOREST	TROPICAL CLEAR FOREST	7850	63585000
Tropical dry forest	DENSE FOREST	TROPICAL DENSE FOREST	1359	11007900
Subtropical premontane dry forest	BARE SOIL	SUBTROPICAL PREMONTANE BARE SOIL	371	3005100
Subtropical premontane dry forest	SHRUB	SUBTROPICAL PREMONTANE DRY SHRUBLAND	10621	86030100
Subtropical premontane dry forest	WOODLAND	SUBTROPICAL PREMONTANE DRY WOODLAND	15565	1.26E+08
Subtropical premontane dry forest	CLEAR FOREST	SUBTROPICAL PREMONTANE CLEAR FOREST	12145	98374500
Subtropical premontane dry forest	DENSE FOREST	SUBTROPICAL PREMONTANE DENSE FOREST	3364	27248400
Subtropical premontane moist forest	BARE SOIL	SUBTROPICAL PREMONTANE BARE SOIL	431	3491100
Subtropical premontane moist forest	SHRUB	SUBTROPICAL PREMONTANE MOIST SHRUBLAND	4511	36539100
Subtropical premontane moist forest	WOODLAND	SUBTROPICAL PREMONTANE MOIST WOODLAND	8576	69465600
Subtropical premontane moist forest	CLEAR FOREST	SUBTROPICAL PREMONTANE DENSE FOREST	5437	44039700
Subtropical premontane moist forest	DENSE FOREST	SUBTROPICAL PREMONTANE DENSE FOREST	4200	34020000
Subtropical lower montane dry forest	SHRUB	SUBTROPICAL LOWER MONTANE DRY SHRUBLAND	26	210600
Subtropical lower montane dry forest	WOODLAND	SUBTROPICAL LOWER MONTANE DRY WOODLAND	60	486000
Subtropical lower montane dry forest	CLEAR FOREST	SUBTROPICAL LOWER MONTANE CLEAR FOREST	9	72900
Subtropical lower montane moist forest	BARE SOIL	SUBTROPICAL LOWER MONTANE MOIST BARE SOIL	372	3013200
Subtropical lower montane moist forest	SHRUB	SUBTROPICAL LOWER MONTANE MOIST SHRUBLAND	9254	74957400
Subtropical lower montane moist forest	WOODLAND	SUBTROPICAL LOWER MONTANE MOIST WOODLAND	34205	2.77E+08
Subtropical lower montane moist forest	CLEAR FOREST	SUBTROPICAL LOWER MONTANE CLEAR FOREST	41826	3.39E+08
Subtropical lower montane moist forest	DENSE FOREST	TEMPERATE MONTANE CLOUD FOREST	34267	2.78E+08
Subtropical lower montane wet forest	CLEAR FOREST	SUBTROPICAL LOWER MONTANE CLEAR FOREST	5	40500
Subtropical lower montane wet forest	DENSE FOREST	TEMPERATE MONTANE CLOUD FOREST	8	64800
Temperate montane moist forest	BARE SOIL	TEMPERATE MONTANE MOIST BARE SOIL	177	1433700
Temperate montane moist forest	SHRUB	TEMPERATE MONTANE MOIST SHRUBLAND	4158	33679800
Temperate montane moist forest	WOODLAND	TEMPERATE MONTANE MOIST WOODLAND	13277	1.08E+08
Temperate montane moist forest	CLEAR FOREST	TEMPERATE MONTANE CLEAR FOREST	14453	1.17E+08
Temperate montane moist forest	DENSE FOREST	TEMPERATE MONTANE CLOUD FOREST	9164	74228400
Temperate montane wet forest	BARE SOIL	TEMPERATE MONTANE WET BARE SOIL	116	939600
Temperate montane wet forest	SHRUB	TEMPERATE MONTANE WET SHRUBLAND	1700	13770000
Temperate montane wet forest	WOODLAND	TEMPERATE MONTANE WET WOODLAND	12286	99516600
Temperate montane wet forest	CLEAR FOREST	TEMPERATE MONTANE CLEAR FOREST	16700	1.35E+08
Temperate montane wet forest	DENSE FOREST	TEMPERATE MONTANE CLOUD FOREST	13393	1.08E+08
Subalpine rain woodland	BARE SOIL	SUBALPINE RAIN BARE SOIL	216	1749600
Subalpine rain woodland	SHRUB	SUBALPINE RAIN SHRUBLAND	3052	24721200
Subalpine rain woodland	WOODLAND	SUBALPINE RAIN WOODED GRASSLAND	7568	61300800
Subalpine rain woodland	CLEAR FOREST	SUBALPINE RAIN WOODLAND	1297	10505700
Subalpine rain woodland	DENSE FOREST	SUBALPINE RAIN MIXED FOREST	93	753300
Subalpine wet woodland	BARE SOIL	SUBALPINE WET BARE SOIL	194	1571400
Subalpine wet woodland	SHRUB	SUBALPINE WET GRASSLAND	1598	12943800
Subalpine wet woodland	WOODLAND	SUBALPINE WET WOODED GRASSLAND	15761	1.28E+08
Subalpine wet woodland	CLEAR FOREST	SUBALPINE WET WOODLAND	4613	37365300
Subalpine wet woodland	DENSE FOREST	SUBALPINE WET MIXED FOREST	442	3580200
Subalpine rain shrubland	BARE SOIL	SUBALPINE RAIN BARE SOIL	68	550800
Subalpine rain shrubland	SHRUB	SUBALPINE RAIN WOODED GRASSLAND	1400	11340000
Subalpine rain shrubland	WOODLAND	SUBALPINE RAIN WOODED GRASSLAND	4900	39690000
Subalpine rain shrubland	CLEAR FOREST	SUBALPINE RAIN WOODLAND	442	3580200
Subalpine rain shrubland	DENSE FOREST	SUBALPINE RAIN MIXED FOREST	7	56700
Alpine paramo rain woodland	BARE SOIL	ALPINE PARAMO RAIN BARE SOIL	186	1506600
Alpine paramo rain woodland	SHRUB	ALPINE PARAMO RAIN SHRUBLAND	4471	36215100
Alpine paramo rain woodland	WOODLAND	ALPINE PARAMO RAIN CLOSED SHRUBLAND	2356	19083600
Alpine paramo rain woodland	CLEAR FOREST	ALPINE PARAMO RAIN WOODED GRASSLAND	165	1336500
Alpine paramo rain woodland	DENSE FOREST	ALPINE PARAMO RAIN WOODLAND	9	72900
Alpine paramo rain shrubland	BARE SOIL	ALPINE PARAMO RAIN BARE SOIL	237	1919700
Alpine paramo rain shrubland	SHRUB	ALPINE PARAMO RAIN GRASSLAND	5934	48065400
Alpine paramo rain shrubland	WOODLAND	ALPINE PARAMO RAIN SHRUBLAND	4336	35121600
Alpine paramo rain shrubland	CLEAR FOREST	ALPINE PARAMO RAIN CLOSED SHRUBLAND	354	2867400
Alpine paramo rain shrubland	DENSE FOREST	ALPINE PARAMO RAIN WOODED GRASSLAND	6	48600
Nival rain woodland	BARE SOIL	BARE ROCK	972	7873200
Nival rain woodland	SHRUB	NIVAL RAIN GRASSLAND	2236	18111600
Nival rain woodland	WOODLAND	NIVAL RAIN SHRUBLAND	224	1814400
Nival rain woodland	CLEAR FOREST	NIVAL RAIN CLOSE SHRUBLAND	4	32400
Nival rain shrubland	BARE SOIL	BARE ROCK	1328	10756800
Nival rain shrubland	SHRUB	NIVAL RAIN GRASSLAND	5860	47466000
Nival rain shrubland	WOODLAND	NIVAL RAIN SHRUBLAND	900	7290000
Nival rain shrubland	CLEAR FOREST	NIVAL RAIN CLOSE SHRUBLAND	82	664200

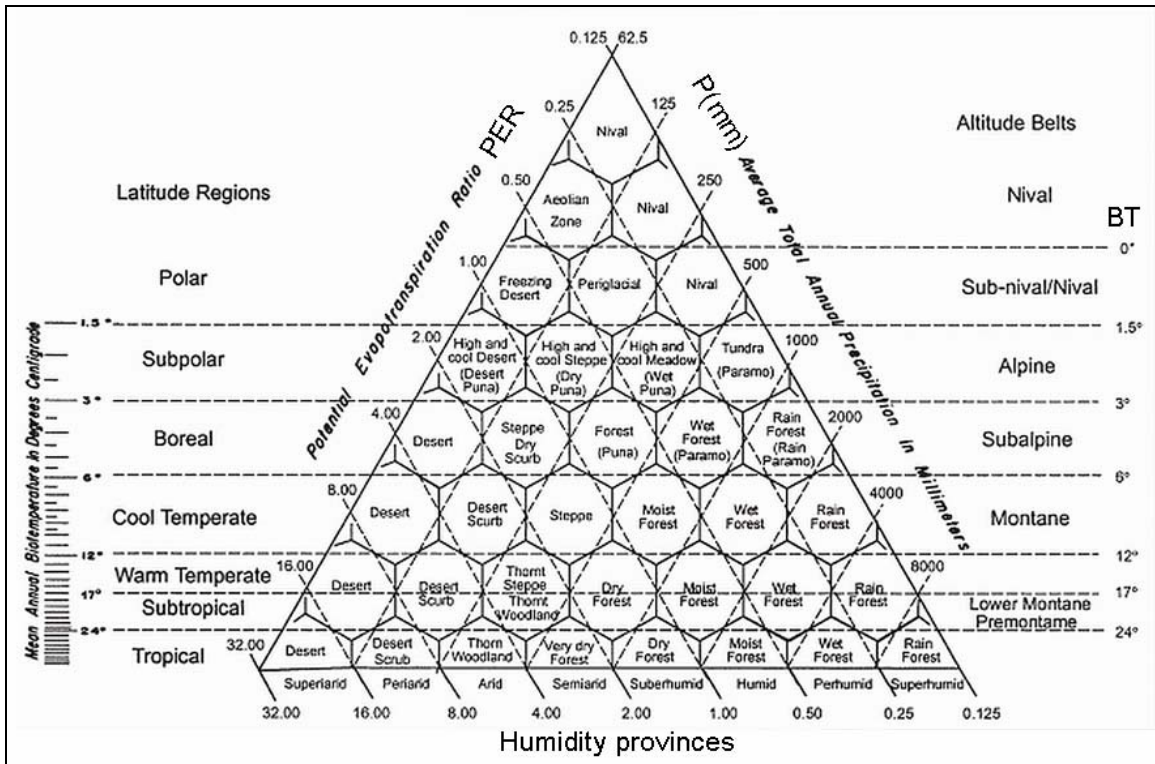


Figure A.7.6.1. Holdridge classification chart (After Holdridge, 1967)

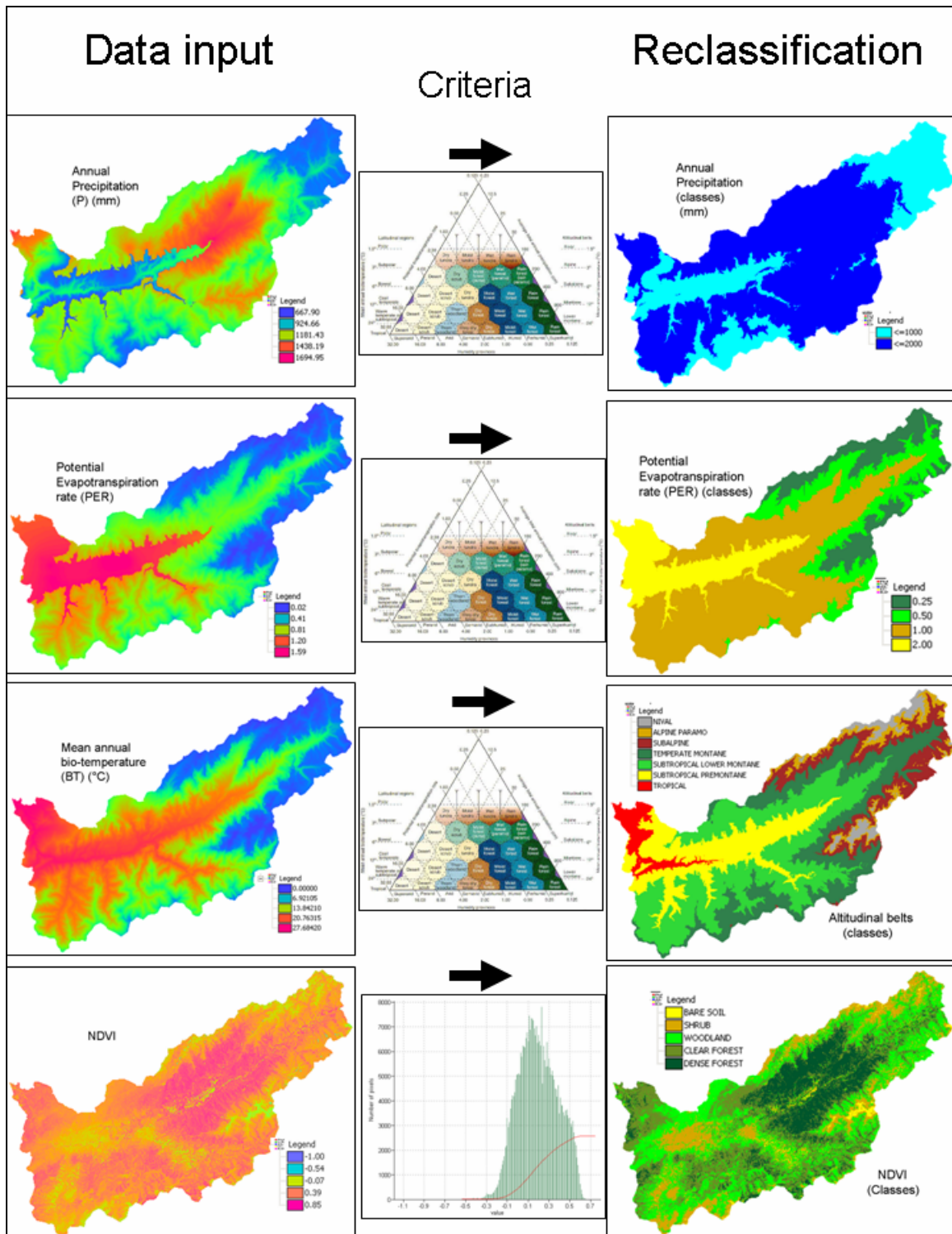


Figure A.7.6.2. Illustration on the data input and subsequently reclassified layers following either the Holdridge classification chart or the Standard deviation classification method applied on the NDVI layer.

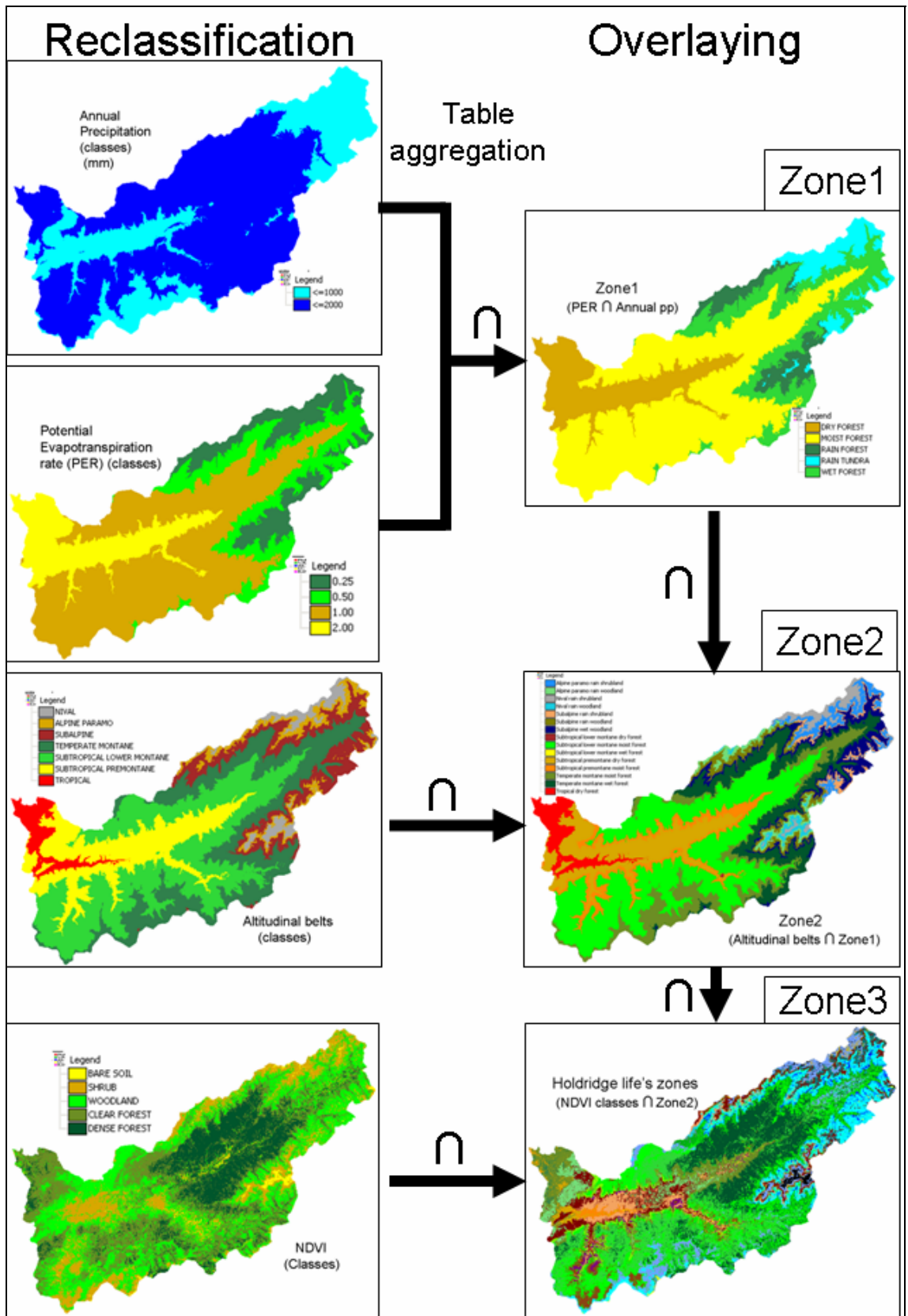
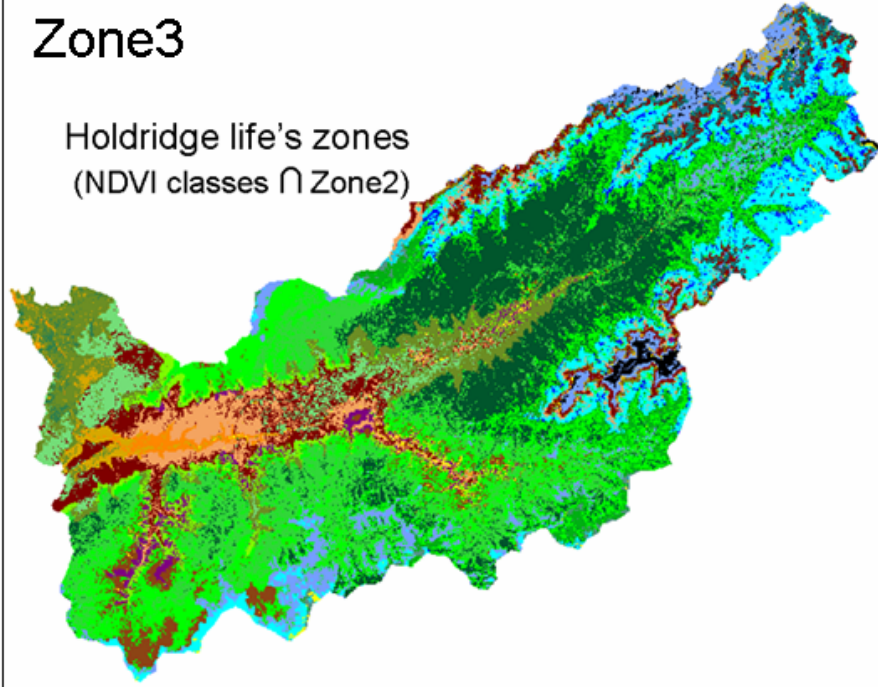


Figure A.7.6.3. Overlaying of the reclassified layers by table aggregation procedure.

# Zone3

Holdridge life's zones  
(NDVI classes  $\cap$  Zone2)



## Holdridge life's zones legend

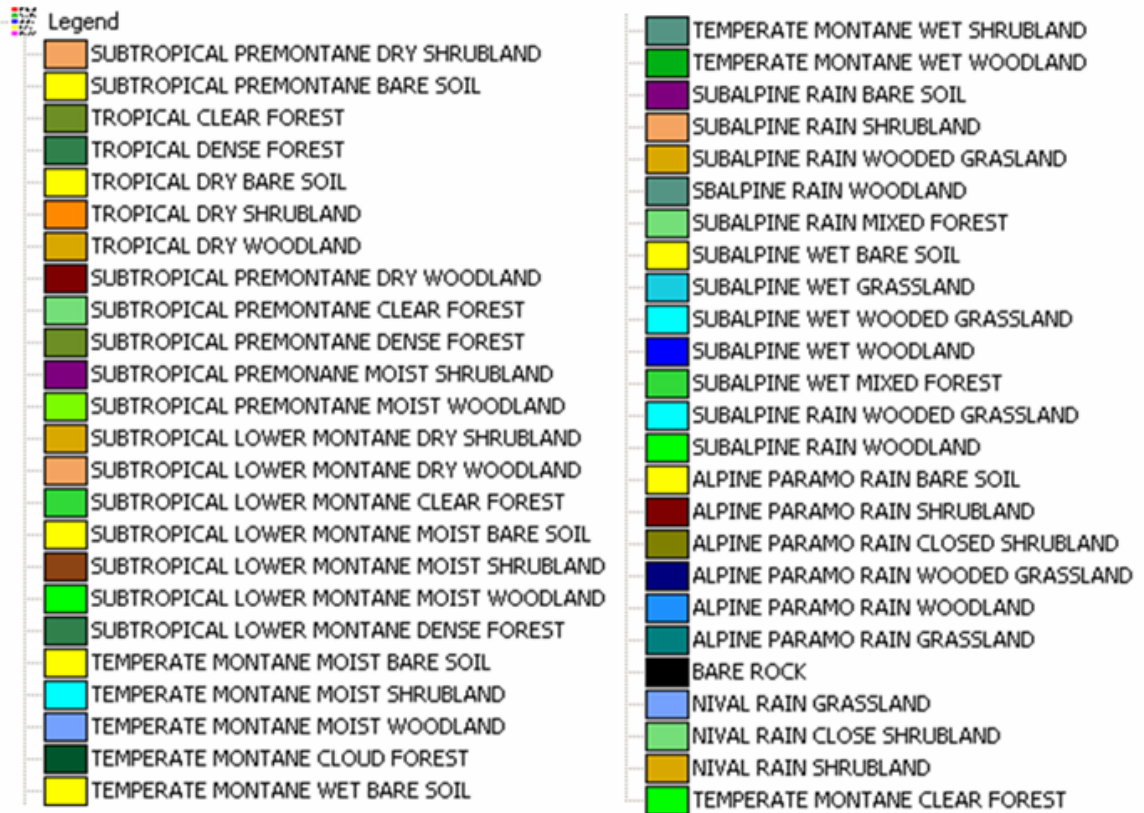


Figure A.7.6.4. Final Holdridge life's zones layer.

## Bibliography

- AGTERBERG, F. P., BONAM-CARTER, G.F. AND WRIGHT, D. F., 1990, Statistical pattern integration for mineral exploration. In: Computer applications in resource estimation, prediction and assessment for metals and petroleum, Editors: G. Gaal, G. and Merriam, D. F. Merriam, Pergamon Press, Toronto, pp. 1-21.
- AGTERBERG, F.P. AND CHENG Q., 2002, Conditional independence test for weights of evidence modeling. *Natural Resources Research* **11**, 249-255.
- ALEOTTI, P. AND R. CHOWDHURY., 1999, Landslide hazard assessment: summary review and new perspectives. *Journal Bulletin of Engineering Geology and the Environment*, **58**, 21- 44.
- ALONSO, J. A. AND LAMATA M. T., 2006, Consistency in the analytic Hierarchy Process: A new Approach, *International Journal of Uncertainty, Fuzziness and Knowledge-Based Systems*, **14**, 4, 445-459. Available online at: <http://hera.ugr.es/doi/16515833.pdf> (last visit December 1/2007).
- ANABALAGAN, R., 1992, Landslide hazard evaluation and zonation mapping in mountainous terrain. *Engineering Geology*. **32**, 269-277.
- ARDIZZONE, F., CARDINALI, M., CARRARA, A., GUZZETTI, F., AND REICHENBACH P., 2002, Impact of mapping errors on the reliability of landslide hazard maps. *Natural Hazards and Earth System Sciences*, **2**, 3-14.
- ASPINALL, R. AND VEITCH N., 1993, Habitat mapping from satellite imagery and wildlife survey data using a bayesian modeling procedure in a GIS. *Photogrammetric Engineering and Remote Sensing*, **59**, 537-543.
- ATKINSON, D., DEADMAN, P., DUDYCHA, D., AND TRAYNOR S., 2005, Multicriteria evaluation and least cost path analysis for an arctic all-weather road. *Applied Geography*, **25**, 287-307.
- AUDEMARD, F., MACHETTE, M., COX, J., DART, R., AND HALLER, K., 2000, Map and Database of Quaternary Faults in Venezuela and its Offshore Regions, USGS, Open-File Report 00-018.
- BARREDO, J.L., 1996, *Sistemas de Información Geográfico y Evaluación Multicriterio en la ordenación del Territorio*. Ra-ma (ed), Madrid, España, 279p.
- BELLIZZIA, A., PIMENTEL, N. AND BAJO, R., 1976, Mapa geológico-estructural de Venezuela, escala 1:500000, Ministerio de Minas e Hidrocarburos, Dirección de Geología, Caracas.
- BOLCH, T., AND KAMP, U., 2006, Glacier Mapping in High Mountains Using DEMs, ASTER and Landsat Data. In *Proceedings 8th International Symposium on High Mountain Remote Sensing Cartography*, 20-27 March 2005, La Paz, Bolivia, *Grazer Schriften der Geographie und Raumforschung*, **41**, Graz, 13-24.
- BONHAM-CARTER, G., 1994, *Geographic information systems for geoscientists: modeling with GIS*, Pergamon Press, Oxford, Ottawa, 398p
- BONHAM-CARTER, G.F., 1996, *Geographic information systems for geoscientists, modeling with GIS*. *Computer Methods in the Geosciences*, vol. **13**, 414p, Pergamon/Elseiver
- BONAM-CARTER, G.F., AGTERBERG, F. P., AND WRIGHT, D. F., 1989, Weights of evidence modeling: A new approach to mapping mineral potential, In: Agterberg, F.P., and Bonham-Carter, G.F., (eds.), *Statistical application in Earth Sciences: Geological Survey of Canada*, Paper 89-9, pp. 171-183.
- BRABB, E.E., 1984, Innovative approaches to landslide hazard mapping. In *Proceedings 4th International Symposium on Landslides*, Toronto, 1: 307-324.
- BRENNING, A., 2005, Spatial prediction models for landslide hazards: review, comparison and evaluation. *Natural Hazards and Earth System Sciences*, **5**, 853-862.
- BURROUGH, P.A. AND MCDONNELL, R.A., 1998, *Principles of Geographical Information Systems*, Oxford University Press, New York.



- CARRARA, A., 1983, A multivariate model for landslide hazard evaluation. *Mathematical Geology*, **15**: 403-426.
- CARRARA, A., 1989, Landslide hazard mapping by statistical methods: a “black–box” model approach. In *International Workshop on Natural Disasters in European–Mediterranean Countries*, Siccardi, F. and Bras, R. (eds.) pp. 427-445, Perugia, 27 June-1 July 1989, CNR–US NFS.
- CARRARA, A., CARDINALI, M., DETTI, R., GUZZETTI F., PASQUID V. AND REICHENBACH P., 1991, GIS Techniques and statistical models in evaluating landslide hazard. *Earth Surface Processes and Landform*, **16**, 5, 427-445.
- CARRARA, A., CARDINALI, M., GUZZETTI, F. AND REICHENBACH, P., 1995, GIS technology in mapping landslide hazard. In *Geographical Information Systems in Assessing Natural Hazards*, Carrara, A. and Guzzetti, F. (eds.), pp. 135-175, Kluwer Academic Publisher, Dordrecht, The Netherlands.
- CASTELLANOS ABELLA, E.A. AND VAN WESTEN, C.J., 2005, Development of a system for landslide risk assessment for Cuba. In *Proceedings of the international conference on landslide risk management*, O. Hungr, R. Fell, R. Couture and E. Eberhardt (eds) pp. 1-10 (31 May - 3 June, Vancouver. London: Balkema.
- CHANDER G. AND MARKHAM B., 2003, Revised Landsat-5 TM Radiometric Calibration Procedures and Postcalibration Dynamic Ranges. *IEEE Transactions on Geoscience and Remote Sensing*, **41**, 11, 2674-2677.
- CHARVÉRIAT, CÉLINE, 2000, *Natural Disaster in Latin America and the Caribbean: An Overview of Risk*. Working Paper #434, Research Department, Inter-American Development Bank, Washington, DC.
- CHOWDHURY, R.N., 1988, Special lecture: Analysis methods of assessing landslide risk - recent developments. In, *Proceedings of the 5th International Symposium on Landslides*, C. Bonnard (ed) pp. 515-524, Rotterdam.
- CHUNG, C.F., AND FABBRI, A.G., 1999, Probabilistic prediction models for landslide hazard mapping, *Photogrammetric Engineering and Remote Sensing*, **65**, 12, 1389-1399
- CHUNG, C.F. AND FABBRI, A.G., 2001, Prediction models for landslide hazard zonation using a fuzzy set approach. In *Geomorphology and Environmental Impact Assessment*, M. Marchetti and V. Rivas (eds) pp. 31-47, Balkema Publishers, The Netherlands.
- CHUNG C.J. AND FABBRI, A.G., 2003, Validation of Spatial Prediction Models for Landslide Hazard Mapping. *Natural Hazards*, **30**, 3, 451-472.
- CHUNG, C.J., FABBRI, A.G. AND VAN WESTEN, C.J., 1995, Multivariate regression analysis for landslide hazard zonation. In *Geographical Information Systems in Assessing Natural Hazards*, Carrara, A. and Guzzetti, F. (eds.) Kluwer Academic Publisher, Dordrecht, The Netherlands, pp.107-142
- COELHO-NETTO, A. L., AVELAR, A.S., FERNANDES, M., AND LACERDA, W., 2006, Landslide susceptibility in a mountainous geocosystem, Tijuca Massif, Rio de Janeiro: The role of morphometric subdivision of the terrain. *Geomorphology*, vol. 87, 3, 120-131
- CONGALTON, R., 2004, Putting the map back in map accuracy assessment. In: *Remote Sensing and GIS accuracy assessment*, chapter 1, Ross S. Lunetta; John G. Lyon (eds.), pp. 1-12 Routledge press, USA, 304p
- COTECCHIA, V., 1978, Systematic reconnaissance mapping and registration of slope movements. *Bulletin International Association Engineering Geology*, **17**, 5-37.
- CROZIER, M.J., 1986, Landslides: causes, consequences & environment. Croom Helm Pub., London, 252p.
- CRUDEN, D. AND VARNES, D., 1996, Landslide Types and Processes. In: *Landslides, Investigation and Mitigation*. A.K. Turner and R.L. Schuster (eds.), pp. 36-75, Transportation Research Board Special Report 247, Washington, D.C. National Academy of Sciences.
- DEGRAFF, J.V. AND CANUTI, P., 1988, Using isopleth mapping to evaluate landslide activity in relation to agricultural practices. *International Association Engineering Geology Bulletin*, **36**, 61-71.

- DELAUNAY, J., 1981, *Carte de France des zones vulnérables a des glissements, écroulements, affaissements et effondrements de terrain*, Bureau de Recherches Géologiques et Minières, 81 SGN 567 GEG, 23 p. (in French).
- DUNCAN, M. J., 1996, Slope stability analysis. In *Landslides investigation and mitigation*, Turner AK, Shuster RL (eds), Transportation Research Board – National Research Council, Special Report 247. pp. 337-371.
- EASTMAN, J. R., JIN, W., KYEM, P. A. K. AND J. TOLEDANO, 1995, Raster procedures for multi-criteria/multiobjective decisions. *Photogrammetry and Remote Sensing*, **61**, 5, 539- 547.
- EVANS, I.S., 1981, General geomorphometry. In *Geomorphological Techniques*, Goudie, A.S. (ed.) pp.31-37.
- FABBRI, A.G., CHUNG, C.J., CENDRERO, C, AND REMONDO, J., 2003, Is Prediction of Future Landslides Possible with a GIS? *Natural Hazards*, **30**, 3 487-503.
- FERRER, C., 1991, *Características geomorfológicas y neotectónicas de un segmento de la falla de Boconó entre la ciudad de Mérida y la Laguna de Mucubají, Estado Mérida*. Guía de la excursión. Escuela Latinoamericana de Geofísica, Universidad de Los Andes, Merida, 25p.
- FERRER, C., 1999, Dammed and failure of natural dams and its relations with coseismic events: Some examples from the Venezuelan Andes. *Revista Geográfica Venezolana*, **40**, 1, 119-131.
- FERRER, C. AND LAFFAILLE, J., 2003, A physical zoning analysis for the outfitting of slums in the Venezuelan Andes. *Revista Geográfica Venezolana*, **44**, 2, 247-267.
- FERRER, C. AND LAFFAILLE, J., 2005a. A study about multiple hazards in the basin of the Chama River (Venezuelan Central Andes): The case of El Paraíso torrent. *Revista Geográfica Venezolana*, volumen extraordinario, 93 - 117.
- FERRER, C., LAFFAILLE, J. AND RINCÓN, J., 2005b, An evidence about the formation and rupture of a natural dam in the middle basin of the Chama River (Venezuelan central Andes), the limitations of the historical catalogues. *Revista Geográfica Venezolana*, volumen extraordinario, 69-92.
- FRANCA-ROCHALI, W., BONHAM-CARTER, G. AND MISI, A., 2003, GIS modeling for mineral potential mapping of carbonate-hosted PB-ZN deposits. *Revista Brasileira de Geociências*, **33**, 2, 191-196.
- FOODY, G. M., AND ATKINSON, P., 2002, *Uncertainty in Remote Sensing and GIS*, John Wiley & Sons, New York, 307p.
- GAO, B-C., 1996, NDWI a Normalized Difference Water Index for remote sensing of vegetation liquid water from space. *Remote Sensing of Environment*, **58**, 257-266.
- GERRARD, J. AND GADNER R., 2002, Relationships Between Landsliding and Land Use in the Likhu Khola Drainage Basin, Middle Hills, Nepal. *Mountain Research and Development*, **22**, 1, 48-55.
- GLADE T., 1998, Establishing the frequency and magnitude of landslide-triggering rainstorm events in New Zealand. *Environ. Geol.*, **35**, 160–174.
- GLOBAL LAND COVER FACILITY-GLCF. UNIVERSITY OF MARYLAND, 2005, LANDSAT ETM+ and SRTM data. Web site: [www.landcover.org](http://www.landcover.org) (ultima visita 25 de Agosto del 2007).
- GÓMEZ, M. AND BARREDO, J., 2005, *Sistemas de Informacion Geográfica y evaluación multicriterio en la ordenación del territorio*, RA-MA(ed.), 2da edicion, Madrid, 276p.
- GOND, V., BARTHOLOME, E., OUATTARA, F., NONGUIERMA, A., AND BADO, L., 2004, Surveillance et cartographie des plan d'eau et des zones humides et inondables en régions arides avec l'instrument VEGETATION embarqué sur SPOT 4, *International Journal of Remote Sensing*, **25**, 987-1004.
- GORSEVSKI, P., GESSLER, P. AND JANKOWSKI, P., 2003, Integrating a fuzzy k-means classification and a Bayesian approach for spatial prediction of landslide hazard. *Journal of Geographical Systems*, **5**, 223-251.
- GUZZETTI, F., CARRARA, A., CARDINALI, M. AND REICHENBACH P., 1999, Landslide hazard evaluation: a review of current techniques and their application in a multi-scale study, Central Italy. *Geomorphology*, **31**, 181-216.

- HAGEN, A., 2002, *Comparison of maps containing nominal data*. Technical report commissioned by RIVM – National Institute for Public Health and the Environment, Project: MAP-SOR S/550002/01/RO. Research Institute for Knowledge Systems. Available online at: [www.riks.nl/RiksGeo/Projects/MapComparison/RIVM\\_Map%20comparison.pdf](http://www.riks.nl/RiksGeo/Projects/MapComparison/RIVM_Map%20comparison.pdf) (last visit 09/07/07)
- HANSEN, A., 1984, Landslide Hazard Analysis. In *Slope Instability*, Brunsten, D. and Prior, D.B. (eds), pp. 523-602, Wiley & Sons, New York.
- HANSSON, SVEN O., 1994, Decision Theory: A Brief Introduction. Available online at: <http://www.infra.kth.se/~soh/decisiontheory.pdf> (last visit: May-2007)
- HARISH, K., SAMEER, S., KARAMJIT, B., AND ROY, P., 2007. Multicriteria Spatial Decision Analysis in Web GIS Environment. *GeoInformatica*, **11**, 4, 407-429.
- HOLDRIDGE, L., 1967, Life Zone Ecology, San Jose, Costa Rica: Tropical Science Center.
- HUABIN, W., GANGJUN, L., WEIYA, X., AND WANG, G., 2005, GIS-based landslide hazard assessment: an overview, *Progress in Physical Geography*, **29**, 4, 548-567.
- HUANG, B., CHEU, R., AND LIEW, Y., 2003, GIS-AHP Model for HAZMAT Routing with security considerations. In *IEEE 6<sup>th</sup> International Conference of Intelligent Transportation Systems*, 10-12 Oct. 2003. Shanghai, China. Vol 2, 1644 - 1649
- JANKOWSKI, P. AND NYERGES, T., 2001, GIS-Supported Collaborative Decision Making: Results of an Experiment, *Annals of the Association of American Geographers*, **91**, 1, 48–70.
- JANKOWSKI, P., 1995, Integrating GIS and multiple criteria decision-making methods. *International Journal of Geographical Information System*, **3**, 251-273.
- JENSEN, J.R., 1998, *Introductory Digital Image Processing: a Remote Sensing Approach* (2nd ed). Prentice Hall, 316p.
- JIANG, H. AND EASTMAN, J. R., 2000, Application of fuzzy measures in multi-criteria evaluation in GIS. *International Journal of Geographical Information Systems*, **14**, 2, 173-184.
- JOHNSON, R.B., AND DEGRAFF, J.V., 1988, *Principles of Engineering Geology*. John Wiley and Sons, New York, 497p.
- KAMP, U., BOLCH, T. AND OLSENHOLLER, J., 2003, DEM Generation from ASTER Satellite Data for Geomorphometric Analysis of Cerro Sillajhuay, Chile/Bolivia. In *Proceedings Annual Meeting Imaging and Geospatial Information Society (ASPRS)*, 5-9.5.2003, Anchorage, U.S.A., 9 pp. CD-ROM
- KAMP, U., BOLCH, T. AND OLSENHOLLER, J., 2005, Geomorphometry of Cerro Sillajhuay, Chile/Bolivia: Comparison of DEMs Derived from ASTER Remote Sensing Data and Contour Maps. *Geocarto International*, **20**, 23-34.
- KIENHOLZ, H., SCHNEIDER, G., BICHSEL, M., GRUNDER, M. AND MOOL, P., 1984, Mapping of mountain hazards and slope stability. *Mountain Research and Development*, **4**, 3, 247-266.
- KWANG-HOON CHI, KIWON LEE, AND NO-WOOK PARK, 2002, Landslide Stability Analysis and Prediction Modeling with Landslide Occurrences on KOMPSAT EOC Imagery. *Korean Journal of Remote Sensing*, **18**, 1, pp.1-12
- LA MARCA, E., 1993, *Origen y Evolución Geológica de La Cordillera de Mérida*. Publicaciones del Museo de Ciencia y Tecnología de Mérida.
- LAWRANCE, C. J., BYARD R. J., AND P. J. BEAVEN, 1993, Terrain Evaluation Manual. Transport Research Laboratory, ISBN 0 11 551109 1. Available online at: [http://www.transport-links.org/transport\\_links/publications/publications\\_v.asp?id=689&title=TERRAIN+EVALUATION+MANUAL](http://www.transport-links.org/transport_links/publications/publications_v.asp?id=689&title=TERRAIN+EVALUATION+MANUAL).
- LEE, S., 2005, Application and cross validation of spatial logistic multiple regression for landslide susceptibility analysis. *Geosciences Journal*, **9**, 1, 63-71.

- LEE, S., AND CHOI, J., 2004, Landslide susceptibility mapping using GIS and the weight of evidence model. *International journal geographical information science*, **18**, 8, 789-814.
- LEROI, E., 1996, Landslide hazard-risk maps at different scales: Objectives, tools and developments. In *Landslides*, Senneset (ed.), Balkema Publisher, Rotterdam, pp 35-51.
- LIN, C.W., LEE, S.Y. AND HUANG, M.L., 2006, The empirical rainfall thresholds to trigger in Central Taiwan after 1999 Chi-Chi earthquake debris flows. *Geophysical Research Abstracts*, **8**. Available online at: <http://www.cosis.net/abstracts/EGU06/02775/EGU06-J-02775.pdf>
- LUGO A. E., MOLINA, S., SCATENA, F., VÉLEZ-RODRÍGUEZ, LL., 1996, *A Fifty-three Year Record of Land Use Change in the Guánica Forest Biosphere Reserve and Its Vicinity. Río Piedras, Puerto Rico*, International Institute of Tropical Forestry.
- MALCZEWSKI, J., 1996, A GIS-based approach to multiple criteria group decision making. *International Journal of Geographical Information Systems* **10**, 8, 955-971.
- MALCZEWSKI, J., 1999, *GIS and Multiple-criteria Decision Analysis*. John Wiley & Sons (ed), Toronto.
- MARNR., 1983, *Proyecto sistemas ambientales venezolanos*. Caracas, 219p.
- MARNR-Division de Meteorología y Climatología, 2004, Datos de precipitación de las estaciones ubicadas en el Estado Merida (Archivos internos) Caracas.
- MEIJERINK, A.M.J., 1998, Data acquisition and data capture through terrain mapping unit. *International Computer Journal*, **1**, 23-44.
- MEIJERINK, A.M.J., DE BROUWER A.H., MANNAETS, C. AND VALENZUELA, C., 1994, *Introduction to the use of geographic information system for practical hydrology*, UNESCO-ITC, 243p.
- MILES, S.B. AND HO, C.L., 1999, Rigorous landslide hazard zonation using Newmark's method and stochastic ground motion simulation. *Soil Dynamics and Earthquake Engineering*, **18**, 4 305-323.
- MILIARESIS, G.CH., 2001, Extraction of Bajadas from Digital Elevation Models and Satellite Imagery. *Computers & Geosciences*, **27**, 10, 1159-1169.
- MYERS, N., R. A. MITTERMEIER, C. G. MITTERMEIER, DA FONSECA, G. A. B. AND KENT, J., 2000, Biodiversity hotspots for conservation priorities. *Nature*, **403**, 853-858
- NEUHAUSER, B. AND TERHORST, B., 2006, Landslide susceptibility assessment using weights-of-evidence applied to a study area at the Jurassic escarpment (SW-Germany). *Geomorphology*, **86**, 12-24.
- ORTIGAO, A. AND SAYAO, A., (eds.), 2004, *Handbook of slope stabilization*, Springer Berlin / Heidelberg, 465p.
- PAN, Y. LI, X., GONG, P., HE, C., SHI, P., AND PU, R., 2003, An integrative classification of vegetation in China based on NOAA AVHRR and vegetation-climate indices of the Holdridge life zone, *International Journal of Remote Sensing*, **24**, 5, 1009-1027.
- PASUTO, A. AND SOLDATI, M., 1999, The use of landslide units in geomorphological mapping: an example in the Italian Dolomites. *Geomorphology*, **30**,1-2 53-64.
- PDVSA-INTEVEP, 2007, Stratigraphical Lexicon of Venezuela. Available on line at: <http://www.pdv.com/lexico/lexicohi.htm> (last visit: Feb, 2007).
- POMEROY, J.S., 1978, Isopleth maps of landslide deposits, Washington county, Pennsylvania a guide to comparative slope stability. U.S. Geological Survey Miscellaneous Field Investigation Map, MF-1010.
- REICHENBACH, P., GALLI, M., CARDINALI, M., GUZZETTI, F. AND ARDIZZONE, F., 2005, Geomorphologic mapping to assess landslide risk: concepts, methods and applications in the Umbria Region of central Italy. In: *Landslide risk assessment*, Glade, T., Anderson, M.G. and Crozier, M.J. (eds.) Wiley-New York, pp. 429-468

- REMONDO, J., GONZÁLEZ-DÍEZ, A., DE TERÁN, J.R.D., CENDRERO, A., FABBRI, A. AND CHUNG, C.F., 2003, Validation of Landslide Susceptibility Maps; Examples and Applications from a Case Study in Northern Spain. *Natural Hazards*, **30**, 437-449.
- ROA, J., 2007, The use of satellite data and imagery for landslide susceptibility mapping in the river Mocoties basin, Merida – Venezuela. *Revista Geográfica Venezolana*, **48**, (in press).
- ROUSE, J., HASS, R., SCHELL, J., DEERING, D. AND HARLAN, Y J., 1974, Monitoring the vernal advancement of retrogradation of natural vegetation. NASA/GSFC, type III, final report, 371p.
- SAATY, T.L., 1990, *Multicriteria Decision Making - The Analytic Hierarchy Process*. McGrawHill, New York, NY. Volume I, AHP Series.
- SAATY, T.L., 2004, The analytic network process: dependence and feedback in decision making (Part 1): theory and validation examples, Session 4B: Theory and development of the analytic hierarchy process/analytic network process. In *Proceedings of the 17th International Conference on Multiple Criteria Decision Making*, August 6-11, 2004, the Whistler Conference Centre, Whistler, BC, Canada. CD-ROM
- SASSA, K., 2001, Landslide risk mitigation and protection of cultural and natural heritage. *Proceedings of the UNESCO / IGCP Symposium on Landslide Risk Mitigation and Protection of Cultural and Natural Heritage*; Tokyo, 268p.
- SCHUBERT, C., 1980, Late Cenozoic pull-apart basins, Boconó fault zone, Venezuelan Andes. *Journal of Structural Geology*, **2**, 4, 463-468.
- SELBY, RICHARD, 2007, Creating Digital Elevation Models and Orthoimages from ASTER Imagery. PCI Geomatics, United Kingdom. Available online at: [http://www.pcigeomatics.com/services/support\\_center/tech\\_papers/grsg\\_aster\\_article.pdf](http://www.pcigeomatics.com/services/support_center/tech_papers/grsg_aster_article.pdf) (last visit: July 15, 2007)
- SOETERS, R. AND VAN WESTEN, C., 1996, Slope instability recognition, analysis and zonation. In *Landslides Investigation and Mitigation*, A.K. Turner and R.L. Schuster (eds.), Transportation Research Board Special Report, 247. Washington, D.C.: National Academy of Sciences, pp. 129-177.
- STRAHLER, A. AND STRAHLER, A., 1997, *Physical Geography, Science and Systems of the Human Environment*,. John Wiley and Sons, New York.
- SÜZEN, M.L. AND DOYURAN, V., 2004, Data driven bivariate landslide susceptibility assessment using geographical information systems: a method and application to Asarsuyu catchment, Turkey. *Engineering Geology*, **71**, 3-4, 303-321.
- TERLIEN, M.T.J., 1998, The determination of statistical and deterministic hydrological landslide-triggering thresholds. *Environmental Geology* **35**, 124–130.
- TERLIEN, M.T.J., VAN WESTEN, C.J. AND VAN ASCH, TH.W.J., 1995, Deterministic modelling in GIS-based landslide hazard assessment. In *Geographical Information Systems in Assessing Natural Hazard*, Carrara, A. and Guzzetti, F. (eds.), pp. 57-77, Kluwer Academic Publisher, Dordrecht, The Netherlands.
- THIART, C.; BONHAM-CARTER, G.F. AND AGTERBERG F.P., 2003, Conditional independence in weights of evidence: Application of an improved test. *Proceedings of the International Association for Mathematical Geology*, IAMG 2003 Portsmouth, UK, September 7-12. CD-ROM
- THIERY, Y., MALET, J.P., STERLACCHINI, S., PUISSANT, A., AND MAQUAIRE, O., 2007, Landslide susceptibility assessment by bivariate methods at large scales: Application to a complex mountainous environment, *Geomorphology*, **92**, 38-59.
- TUCKER, G.E., CATANI, F., RINALDO, A. AND BRAS, R.L., 2001, Statistical analysis of drainage density from digital terrain data. *Geomorphology*, **36**, 187-202.
- USGS, 2006, Landslide Hazard Program. Available on line at: <http://landslides.usgs.gov/learningeducation/glossary.php#1> (last visit 11/11/06)

- VAN WESTEN C., 1994, GIS in landslide hazard zonation: a review, with examples from the Andes of Colombia. In: *Mountain Environments and GIS*, Price, M.F. and Heywood, D.I (eds.), Basingstoke, UK, 135-165.
- VAN WESTEN, C., RENGERS, N. AND SOETERS, R., 2003, Use of geomorphological information in indirect landslide susceptibility assessment. *Natural hazards* **30**, 399-419.
- VAN WESTEN, C.J., VAN ASCH, T.W.J. AND SOETERS R., 2006, Landslide hazard and risk zonation –why is it still so difficult?. *Bulletin of Engineering Geology of the Environment*. **65**, 167-184.
- VAN WESTEN, C.J., VAN DUREN, I.C., KRUSE, H.M.G. AND TERLIEN, M.T.J., 1993, *GISSIZ : training package for Geographic Information Systems in slope instability zonation*. ITC Publication 15, 245 p., 359 p. ISBN: 90-6164-078-4, Enschede, The Netherlands.
- VARNES, D. J., 1978, Landslide types and processes. In *Landslides and engineering practice*. E.B. Eckel (ed). Special report 29, Highway Research Board pp. 20-47.
- VARNES, D. J., 1984, Landslide hazard zonation: a review of principles and practice. Commission on landslides of the IAEG, UNESCO, *Natural Hazard*, **3**, 61p.
- VARNES, D. AND CRUDEN, D., 1996, *Landslide types and processes*. In Landslides investigation and mitigation, special report 247, Transportation Research Board, National Research Council, pp. 36-75
- VERSTAPPEN, H. AND ZUIDMAN, R., 1991, *Le système ITC de levées géomorphologiques*, ITC publication #10, Enschede, The Netherlands.
- VIVAS, L., 1992, *Los Andes Venezolanos*, Academia Nacional de la Historia. Caracas. 300 p.
- WANG, S.-Q., AND UNWIN, D.J., 1992, Modelling landslide distribution on loess soils in China: an investigation. *International Journal of Geographical Information Systems*, **6**, 391-405.
- WIECZOREK, G., 1996, Landslide Triggering Mechanisms. In *Landslides Investigation and Mitigation* A.K. Turner and R.L. Schuster (eds.), Transportation Research Board Special Report 247, pp. 36-75, Washington, D.C
- WIECZOREK, G., 2001, Debris-flow and flooding hazards associated with the December 1999 storm in coastal Venezuela and strategies for mitigation. U.S. Dept. of the Interior, U.S. Geological Survey. Available online at: <http://pubs.usgs.gov/of/2001/ofr-01-0144/>
- WRIGHT, R.H., CAMPBELL, R.H. AND NILSEN, T.H., 1974, Preparation and use of isopleth maps of landslide deposits. *Geology*, **2**, 483-485.
- YANG, HONG, Y., ADLER, R. AND HUFFMAN, G., 2007, An experimental global prediction system for rainfall-triggered landslides using satellite remote sensing and geospatial datasets. *IEEE Transactions on Geoscience and Remote Sensing*, **45**, 6, pp. 1671 – 1680.
- ZEZERE, J. L., REIS, E., GARCIA R., OLIVEIRA, S., RODRIGUES, M.L., VIEIRA, G., AND FERREIRA, A. B., 2004, Integration of spatial and temporal data for the definition of different landslide hazard scenarios in the area north of Lisbon (Portugal). *Natural Hazards and Earth System Sciences*, **4**, 133–146.